



HAL
open science

Localization of the source of large silicic ignimbrites through magnetic techniques: applications in Turkey

Alessandro Agro

► **To cite this version:**

Alessandro Agro. Localization of the source of large silicic ignimbrites through magnetic techniques: applications in Turkey. Earth Sciences. Université Blaise Pascal - Clermont-Ferrand II, 2014. English. NNT : 2014CLF22445 . tel-00999468

HAL Id: tel-00999468

<https://theses.hal.science/tel-00999468>

Submitted on 3 Jun 2014

HAL is a multi-disciplinary open access archive for the deposit and dissemination of scientific research documents, whether they are published or not. The documents may come from teaching and research institutions in France or abroad, or from public or private research centers.

L'archive ouverte pluridisciplinaire **HAL**, est destinée au dépôt et à la diffusion de documents scientifiques de niveau recherche, publiés ou non, émanant des établissements d'enseignement et de recherche français ou étrangers, des laboratoires publics ou privés.

N° d'Ordre : D.U. 2445

UNIVERSITÉ BLAISE PASCAL – CLERMONT-FERRAND II
(U.F.R. Sciences et Technologies)

ÉCOLE DOCTORALE DES SCIENCES FONDAMENTALES
E.D. ° 785

THÈSE

Présentée pour obtenir le grade de
DOCTEUR D'UNIVERSITÉ
Spécialité : Volcanologie - Géophysique

Par

Alessandro AGRÒ

Master

**Localization of the source of large silicic ignimbrites
through magnetic techniques: applications in Turkey**

Soutenue publiquement à Turin le 14 mars 2014, devant la commission d'examen composée de :

M. Guido GIORDANO	Université de Rome III, Italie	Examineur
Mme Lucia GURIOLI	Université Blaise Pascal, Clermont-Fd	Examinatrice
M. Jean-Luc LE PENNEC	IRD, Univ. Blaise Pascal, Clermont-Fd	Directeur de thèse
M. Michael ORT	Université d'Arizona, USA	Rapporteur
M. Roberto SULPIZIO	Université de Bari, Italie	Rapporteur-Président
Mme Elena ZANELLA	Université de Turin, Italie	Directrice de thèse

CONTENTS

1	INTRODUCTION AND BACKGROUND.....	1
	<i>1.1 - Ignimbrite volcanism: from eruptions to calderas</i>	<i>4</i>
1.1.1	Classification of explosive eruptions and eruptive processes.....	4
1.1.2	Pyroclastic deposits and Pyroclastic Density Currents (PDCs): generalities.....	5
1.1.3	Pyroclastic fall deposits.....	8
1.1.4	PDCs deposits.....	9
	<i>1.1.4.1 Depositional processes in PDCs.....</i>	<i>9</i>
	<i>1.1.4.2 Fluidization and elutriation.....</i>	<i>10</i>
	<i>1.1.4.3 Architecture of ignimbrite deposits.....</i>	<i>11</i>
	<i>1.1.4.4 Structure and texture of ignimbrite deposits.....</i>	<i>12</i>
1.1.5	Origin and formation of calderas.....	17
	<i>1.1.5.1 Classification of calderas.....</i>	<i>17</i>
	<i>1.1.5.2 Caldera development.....</i>	<i>19</i>
1.2	<i>Vent location: field indicators and fabric development in ignimbrites.....</i>	<i>21</i>
1.2.1	Origin of grain fabric in ignimbrites and implications for flow directions.....	21
1.2.2	Field evidence for constraining the eruptive vent.....	23
1.2.3	The magnetic fabric: an effective tool to resolve the problem of source location.....	24
1.3	<i>The ignimbrite volcanism of Anatolia: features, challenges and outlook.....</i>	<i>29</i>
1.3.1	Geotectonic outline.....	29
1.3.2	Anatolian volcanism.....	30
	<i>1.3.2.1 Cappadocia region.....</i>	<i>31</i>
	<i>1.3.2.2 Afyon-Eskişehir region.....</i>	<i>36</i>
2	FIELD AND LABORATORY METHODS.....	42
	<i>2.1 Field investigation.....</i>	<i>42</i>
2.1.1	Stratigraphic measurements.....	42
2.1.2	Field directional structures.....	43
2.1.3	Isopach and isopleth maps.....	44
2.1.4	Volume estimation and calculation of the eruption magnitude.....	44
2.2	<i>Paleomagnetic sampling and laboratory methods.....</i>	<i>45</i>
2.2.1	Paleomagnetic sampling.....	45

2.2.2	Rock-magnetic methods	46
2.2.2.1	<i>Magnetic mineralogy</i>	47
2.2.2.2	<i>Natural Remanent Magnetization (NRM)</i>	48
2.2.2.3	<i>Magnetic fabric</i>	49
2.2.3	Geochronologic datings	52
3	AFYON-ESKIŞEHİR IGNIMBRITES: FIELD DATA	54
3.1	Stratigraphy	54
3.1.1	The Incik ignimbrite	58
3.1.1.1	<i>Type section</i>	59
3.1.1.2	<i>Lateral facies variations</i>	64
3.1.2	The Sabuncu ignimbrite	75
3.1.2.1	<i>Type section</i>	76
3.1.2.2	<i>Lateral facies variations</i>	78
3.1.3	The Seydiler ignimbrite	82
3.1.3.1	<i>Type section</i>	83
3.1.3.2	<i>Lateral facies variations</i>	85
3.2	Isopach and isopleth maps	93
4	PALEOMAGNETIC SAMPLING AND MAGNETIC MINERALOGY	106
4.1	<i>Kızilkaya ignimbrite</i>	106
4.2	<i>Afyon-Eskişehir ignimbrites</i>	111
5	MAGNETIC FABRIC	118
5.1	<i>Kızilkaya ignimbrite</i>	118
5.1.1	Density and bulk susceptibility	118
5.1.2	AMS and magnetic fabric	119
5.1.3	AIRM, AARM and magnetic fabric	123
5.2	<i>Afyon-Eskişehir ignimbrites</i>	128
5.2.1	Density and bulk susceptibility	128
5.2.2	AMS and magnetic fabric	129
5.2.3	AIRM and magnetic fabric	141
6	MAGNETIC REMANENCE	142

7 DATA INTERPRETATION.....	146
7.1 Kızulkaya ignimbrite.....	146
7.1.1 Magnetic fabric.....	146
7.1.2 Magnetic remanence.....	148
7.2 Afyon-Eskişehir ignimbrites.....	152
7.2.1 Considerations about eruption dynamics and paleogeography.....	152
7.2.2 Ignimbrites volume and eruption magnitude determination.....	155
7.2.3 Locating the source of the Afyon-Eskişehir ignimbrites: reconciling field evidence with magnetic fabric data.....	160
7.2.3.1 Isopach and isopleth maps.....	160
7.2.3.2 Imbricational structures, welded and silicified facies maps.....	166
7.2.3.3 Magnetic fabric.....	168
7.2.3.4 Kırka caldera system.....	174
8 CONCLUSIONS.....	178
REFERENCES.....	180
APPENDIXES.....	203
ACKNOWLEDGEMENTS.....	232

1 – Introduction and background

Ignimbrites are pumiceous and ash-rich deposits originated from pyroclastic density currents (PDCs), consisting in inhomogeneous mixtures of volcanic particles and gas that flow over the topography according to their density. Because of their instantaneous deposition at geological time-scale and generally widespread distribution over extended areas, ignimbrites have been object of many paleomagnetic studies (Black et al. 1996; Urrutia-Fucugauchi et al. 2000; Urrutia-Fucugauchi and Ferrusquía-Villafranca 2001) and represent good marker beds for stratigraphic correlations (Hildreth and Mahood, 1985; Self et al., 1991; Lipman et al., 1996; Lindsay et al., 2001; Le Pennec et al., 2005). Moreover, research of the source area represents not only a merely volcanologic goal, but has also relevant economic implications, since ignimbrite eruption forming-calderas are often associated to ore deposits, mineralization and geothermal activity (Lipman and Sawyer, 1985; Lipman, 1992; Goff and Gardner, 1994; Bibby et al., 1995).

Extrapolation and interpretation of accurate and reliable data from ignimbrites to resolve the aforementioned goals may often represent difficult issues. Stratigraphic correlations are the complex result of the combination of field observations with other investigation techniques such as magnetic, geochemical, radiometric and biostratigraphic. The exploitation of such techniques requires the preservation of essential conditions in ignimbrite deposits. Field observations are based on the outcrop-scale evidence of textural and mineralogic features of the deposits, and the analysis of three dimensional sedimentary structures to infer flow directions; magnetic investigation requires deposits *in situ* which have not suffered enhanced alteration processes affecting the primary magnetic mineralogy; geochemical and radiometric analyses require the absence of strong alteration processes which can modify the bulk geochemical composition of the rock. However, such optimal conditions are not always achieved. Ignimbrite deposits are not homogeneous bodies; they predominantly comprise a poorly sorted mixture of pumice and lithic lapilli supported in a matrix of vitric shards and crystal fragments, and significant alteration processes such as divitrification and hydrothermal alteration may occur during the ignimbrite history. The ignimbrite architecture is considered to be the result of the conditions and processes affecting the flow-boundary zone of a PDC through the time (Branney and Kokelaar, 2002); clasts and magnetic fabrics, from which flow direction is inferred, are therefore not only the result of emplacement processes related to PDC rheology and paleo-topography, but they may also reflect spatial inhomogeneities within the PDC conferred by anomalous clasts concentration which may influence the flow at small-scale. Moreover, alteration processes may lead to the origin of secondary magnetic minerals and the growth of uneven magnetic mineralogy throughout the deposit that can bias the primary magnetic signal, affecting both paleomagnetic and magnetic fabric data. Alteration processes can bias radiometric data as well, if the geochemical system relative to the analyzed mineralogic phase is not strictly closed. Because of these issues, ignimbrite investigation

techniques should be devised in order to take into account all the possible variations occurring in the deposit, to obtain reliable data.

The present research proposes a combination of field, paleomagnetic and rock-magnetic techniques to the investigation of ignimbrite deposits, taking into account eventual magnetic variations occurring throughout the deposits. The first goal consists in understanding how and why variations of the magnetic properties occur throughout a same ignimbrite unit. To achieve this point, a detailed stratigraphic magnetic study was carried out on a single flow ignimbrite unit by sampling the deposit at different stratigraphic levels. Various magnetic analyzes were performed in order to investigate the variation of paleomagnetic directions, magnetic fabric and magnetic mineralogy; finally, such variations were related to physical, chemical or emplacement processes which have been acting in specific levels of the ignimbrite. The second goal aims to the improvement of magnetic fabric data, whose quality is essential to infer reliable flow directions and constrain the source area. This was realized by conceiving and testing a method based on the selection of magnetic fabric data on the ground of the specimens density, considered to be a proxy of lithic and pumice clasts concentration within the ignimbrite matrix which could contribute to the origin of micro-flows non representative of the main flow related to the source. The third goal consists in the localization of the source of large silicic ignimbrites by combining volcanologic and magnetic techniques, by exporting the magnetic investigation techniques discussed above. Moreover, U-Pb radiometric dating were performed on zircon crystals. Such technique represents a robust method for ignimbrite dating and correlation, since zircon crystals are resistant to geochemical alteration and constitute a closed system to the environment.

In the specific, the research carried out in this project has been addressed to investigate the pyroclastic deposits exposed within two large ignimbrite complexes in Anatolia (Turkey) with a dual objective:

1. Perform a stratigraphic study of the variation of the magnetic properties throughout a same ignimbrite unit in the Cappadocia region, whose volcanic stratigraphy is well constrained, in order to identify the factors at the origin of vertical magnetic variation;
2. reconstruct the volcanic stratigraphy and research of the source area of the pyroclastic deposits exposed in a region located in western Anatolia, where no similar studies were still been performed.

The two study areas are respectively located in the Cappadocia region (central Anatolia) and in the region comprised among the cities of Afyon, Kütahya and Eskişehir, more easily referable as “Afyon-Eskişehir” region (western Anatolia). The two large ignimbrite successions cropping out in these areas have been object of different attentions and number of studies through the time. The Cappadocian ignimbrite succession has been deeply investigated under many aspects as concern

stratigraphy, age, source locations and paleomagnetism (Pasquaré, 1968; Schumacher and Mues-Schumacher 1986; Le Pennec et al., 1994; Le Pennec et al., 1998 Temel et al., 1998; Le Pennec, 2000; Piper et al., 2002; Paquette and Le Pennec, 2012; Aydar et al. 2012; etc). On the contrary, few studies were performed on the Afyon-Eskişehir ignimbrite succession, which consisted mainly in geochemical and to a lesser extent in volcanologic and paleomagnetic investigations, concentrated over limited study areas (Keller and Villari, 1972; Yalçın, 1990; Aydar et al., 1998; Gürsoy et al., 2003). No stratigraphic works, including distinction and dating of the pyroclastic units, neither information about source area location exist on these pyroclastic deposits, which are exposed over an area larger than 14,000 km² and reach considerable thickness.

The Kızılıkaya ignimbrite unit, belonging to the Cappadocia region, was chosen as case study to perform a stratigraphic investigation of the variation of the magnetic properties through the deposit. The purpose in developing this objective arises because ignimbrites have been widely used in previous paleomagnetic works, but little attention has been spent in evaluating the consistency and reliability of the paleomagnetic data when results are obtained on a single volcanic unit, especially if characterized by uneven magnetic mineralogy. The present work investigates these issues on the Kızılıkaya ignimbrite through the combination of many techniques of rock-magnetism, bringing evidence of significant magnetic heterogeneities in magnetic mineralogy, susceptibility, natural remanent magnetization and coercivity, and recommending revised sampling strategies for these type of volcanic rocks.

The purpose of the work performed on the Afyon-Eskişehir ignimbrite succession has been mainly directed to the reconstruction of the stratigraphy and the research of the source, by volcanologic and magnetic techniques. Moreover, the ignimbrite succession has been dated using latest geochronologic techniques, including the exploitation of the U-Pb technique on zircon crystals and Ar/Ar technique on plagioclase crystals. Finally, ignimbrite area extension and volume were estimated to achieve the VEI index, thus calculating the magnitude of the eruption. The new insights on these topics reveal the occurrence of large ignimbrite eruptions from the upper Miocene to the lower Miocene, bringing out relevant information on a still unstudied large silicic complex of Anatolia, and conferring new data on the present-day knowledge about the volcanism of the Mediterranean region.

Summarizing, the objectives developed in the present research have been the followings:

1. Stratigraphic investigation of the variation of the magnetic properties within the Kızılıkaya ignimbrite, in order to relate vertical changes in the paleomagnetic directions, magnetic mineralogy and magnetic fabric to specific causes;

2. development of an effective sampling strategy to investigate thick ignimbrite units, in order to obtain reliable magnetic data to be used also for other types of interpretation, such as geodynamic or tectonic reconstructions;
3. development of a technique to enhance the AMS data, in order to improve the magnetic fabric and obtain reliable flow directions to better constrain the source area;
4. stratigraphic reconstruction and facies analysis of the Afyon-Eskişehir succession, by distinguishing and dating the various ignimbrite units;
5. research of the source of the Afyon-Eskişehir ignimbrite succession, by the comparison and combination of volcanologic and magnetic data;
6. calculation of the magnitude of the Afyon-Eskişehir ignimbrites forming-eruptions by volumetric data extrapolated from the isopach maps.

1.1 - Ignimbrite volcanism: from eruptions to calderas

1.1.1 - Classification of explosive eruptions and eruptive processes

Magma ascending in a volcanic conduct undergoes saturation processes which cause an enrichment of water and other volatiles in the fuse. Each decrease in pressure at near saturation-conditions causes water exsolution, vesiculation and then fragmentation of the magma.

During Plinian eruptions a column of ash, pumices and gas may develop for several kilometers above the vent. This process is enhanced by high fragmentation of magma associated with expansion in and outside the conduct, of a mixture having the features of a pseudo-gas. Magma is fragmented into fine particles which are ejected from the conduct together with gas, and an eruptive Plinian column is developed. The accumulation on the ground of the fragmented materials as unconsolidated deposits is known as tephra.

Volcanic eruptions are commonly classified into different types on the basis of the evaluation of several physical parameters which relate to the violence of the volcanic event. Volume determination of tephra deposits is crucial for the assessment of the dynamics and hazards of explosive volcanoes; this is because tephra deposits retain a large amount of information related to the dynamics and physical parameters of the associated volcanic eruptions. Several methods have been proposed during the past years, based on the analysis of tephra distribution (Walker, 1973; Pyle, 1989). Walker (1980) introduced the parameter of aspect ratio, which is related to the violence of the eruption, estimating the velocity of the pyroclastic flow on the basis of the ratio between the average thickness of the deposit and the radius of the circle having the same area of the deposit. Semi-quantitative and quantitative models were respectively proposed by Newall and Self (1982) with the VEI (Volcanic Explosivity Index) and Carey and Sigurdsson (1989), who gave

indications about magnitude and intensity of an eruption on the basis of the evaluation of physical parameters such as magma discharge rate and volume. However, eruption magnitude and intensity are not necessarily related (Carey and Sigurdsson, 1989; Pyle, 2000). Because of this, calculation of magnitude (Pyle, 2000), which takes into account the erupted mass or the DRE volume, is a preferred measure of eruption size. However, calculation of erupted volume is often complicated by various factors, e.g. non universal relationship between deposit thickness and distance from the vent, and poor preservation to significant parts of tephra deposits, particularly at proximal and distal areas. Because of this, new attempts of tephra estimations have been proposed in order to better quantify the real volume of the deposits. Recent methods involve the best fitting of deposit thinning data using exponential segments and power-law curve on a semilog plot (Fierstein and Nathenson, 1992; Houghton, 2005), and integration of the Weibull function, which assumes that thickness scales with square root of the isopach area (Bonadonna and Costa, 2012).

1.1.2 - Pyroclastic deposits and Pyroclastic Density Currents (PDCs): generalities

Pyroclastic density currents (PDCs; Valentine and Fisher, 2000) are inhomogeneous mixtures of gas and volcanic solid particles which flow over the ground under the influence of gravity (e.g. Burgissier and Bergantz, 2002). The origin of these catastrophic events is often associated to explosive magmatic eruptions which can derive from several processes: collapse of a sustained eruptive column produced by fragmentation of magma and rock in a volcanic conduit, laterally inclined blasts, or hot avalanches coming from the disruption of lava domes (Hoblitt, 1986; Anilkumar et al., 1993; Ui et al., 1999; Cole et al., 2002). Fragmented material is violently ejected from the vent as pyroclasts of various dimensions (ash, lapilli, bombs, blocks), which come to the ground forming the tephra.

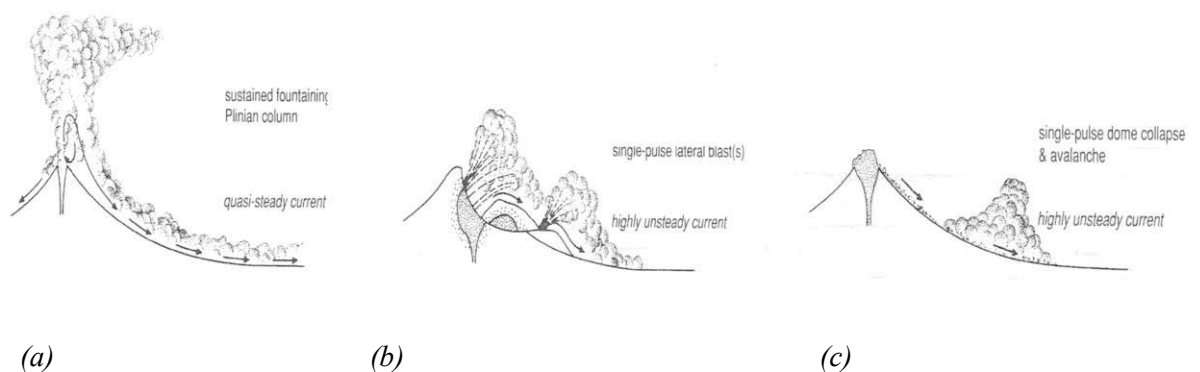


Figure 1.1 – Origins of pyroclastic density currents. (a) Sustained current derived from prolonged pyroclastic fountaining. (b) Current with a single (or multiple) surge derived from lateral blasts. (c) Single-surge current derived from a collapsing lava dome or flow front (modified from Branney and Kokelaar, 2002).

The main types of eruption that can originate a PDC are the following (fig. 1.1):

1. Pyroclastic fountaining (fig. 1.1 a). Many PDCs form directly from the gas-thrust jets in explosive eruptions. The material ejected from the eruption heats the surrounding air becoming buoyant, so it follows fountain-like trajectories to the ground (Sparks et al. 1997). In such eruptions, a buoyant, sub-Plinian or Plinian column of ash and fine juvenile products may develop above the pyroclastic fountain, originating pumice fall deposits associated to ignimbrites (e.g. eruption of Mount Vesuvius, 79 AD). Plinian fallout layers underlying ignimbrites record that initial convective eruption columns formed before the pyroclastic fountaining. Many ignimbrites may be emplaced during phreato-magmatic pyroclastic fountaining. In such events, ignimbrites may be particularly rich in fine ash because of the high fragmentation degree developed from the interaction between magma and water, and may contain some blocky phreatomagmatic shards and accretionary lapilli;
2. lateral blast (fig. 1.1 b). Part of a volcano can explode or collapse, originating pyroclastic density currents deriving from inclined or laterally directed explosive decompression jets (e.g. Mount St Helens; Hoblitt 1986). In such types of events large volume ignimbrites are not generally produced;
3. collapsing lava domes (fig. 1.1 c). Collapsing of lava domes or lava-flow fronts produce pyroclastic density currents which emplace as rock avalanches. Rapid segregation of relatively fine pyroclasts from underlying high-concentration debris fall and granular flow tends to develop overriding low-concentration dispersions. The process involves clast fragmentation with accompanying admixture and expansion of air, as in Merapi (Bardintzeff 1984) and Montserrat (Cole et al. 1998, 2002). Most pyroclastic density currents produced during these events generate small-volume block-and-ash flow deposits (Cole et al. 2002).

Two end-member models of PDCs have been developed on the basis of the concentration of the flow, which originates different lithofacies architecture in PDCs deposits (Walker, 1983; Cas and Wright, 1987): (1) Pyroclastic surges, deriving from dilute currents in which solid particles are carried in turbulent suspensions by fluid-dominated processes, and (2) Pyroclastic flows, deriving from currents in which solid particles are transported by mechanisms due to the high concentration of the current, e.g. solid-dominated processes, which is dominated by laminar regime. More recently, unified models that consider the different typologies within a continuum spectrum spanning from very dilute to very concentrated flows have been proposed (Branney and Kokelaar, 2002; Burgisser and Bergantz, 2002; Sulpizio and Dellino, 2008).

PDC deposits are grouped into three categories according to their lithofacies architecture (fig. 1.2):

1. Pyroclastic surge deposits, originated by dilute currents where the amounts of solid particles is lower compared to that of fluids. The main transport mechanisms of clasts is by saltation, intermittent suspension and traction dominated-processes (Middleton and Southard, 1984), which commonly produce well sorted and stratified deposits;
2. ignimbrite deposits, commonly generated by highly concentrated mixtures and mainly composed by ash and/or ash and pumices. They generally comprise poorly sorted mixture of pumice and lithic lapilli supported in a ashy matrix containing juvenile fragments of glassy shards and crystals. Deposits generally occur as massive bodies lacking any evidence of stratification, due to the domination of particle-particle interactions processes and inhibition of traction dominated processes during the transport;
3. block-and-ash flow deposits, originated by *nuée ardentes*. They contain a larger amount of dense, non-vesiculated blocky lava fragments within a fine-grained matrix of non-pumiceous ash with respect to ignimbrites. Deposits are not sorted, denser and generally of smaller volume than ignimbrites, and are normally associated with lava domes (Francis et al., 1974; Davies et al., 1978; Fuji and Nakada, 1999).

Materials produced during explosive eruptions accumulate on the ground forming pyroclastic deposits, which are divided into fall or PDC deposits according to the medium through which pyroclasts are carried by (fig. 1.2).

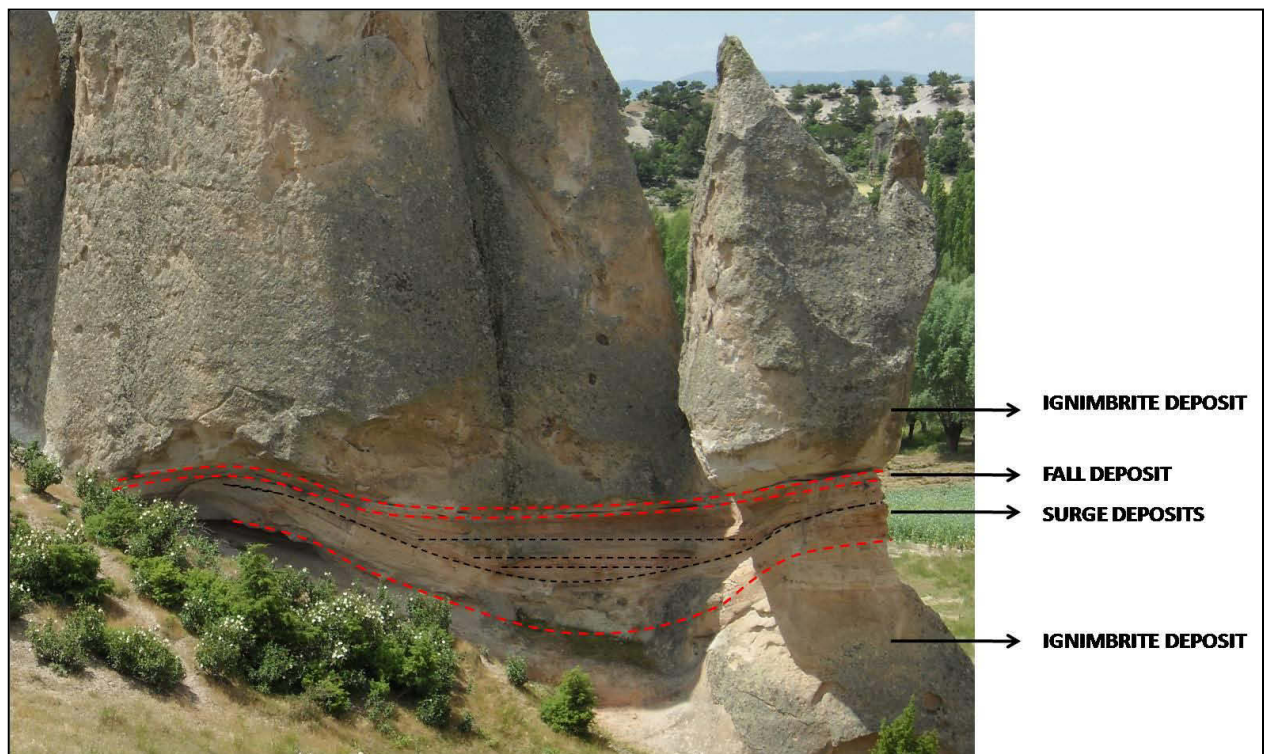


Figure 1.2 – Section of the ignimbrite deposits outcropping in the area of Afyon-Eskişehir (locality of Bayramaliler). Ignimbrite deposits are characterized by a massive structure, surge deposits are

stratified and display an erosional basal surface; fall deposit mantle the underlying topography with a constant thickness.

1.1.3 - Pyroclastic fall deposits

Pyroclastic fall deposits accumulate on the ground from sustained eruptive columns or directly thrown from the vent as ballistic clasts (fig. 1.3). Highly vesiculated pumices are commonly originated during phreato-plinian and plinian eruptions. During such eruptions magma reaches high levels of fragmentation and, besides generation of pumices, it is produced a large amount of fine ash, which can be transported by winds in eruptive columns for considerably long distances from the vent; it has been estimated that at least 20% of Plinian deposits lie outside the isopach of 1 cm (Fierstein and Natherson, 1992). Part of the fine material is also transported by co-ignimbrite clouds accompanying the main flow which form co-ignimbrite ash deposits. Particles having the same hydraulic equivalence fall at the same distance, particles with decreasing hydraulic equivalence progressively fall at greater distances from the column axis. This process, associated to the dispersal effects of wind(s), determines a distribution of such deposits which generally form ellipsoidal shaped isopach curves departing from the vent (fig. 1.4). Carey and Sparks (1986) analyzed the clasts distribution of an eruptive column, taking in account the dimensions of the coarsest grains. Curves joining the same pumice and lithic clasts dimensions (isopleths) have a circular shape in the case of absence of wind, conversely they are elongated in the presence of wind.



Figure 1.3 – Sequence of pumice-fall layers in the area of Afyon-Eskişehir (locality of Sancar).

Pyroclastic fall deposits mantle pre-existing topography with a constant thickness, and pumice and lithic clasts preserve sharp edges. Deposits are well sorted, can be massive or stratified depending on the number of eruption phases and can display a normal or reverse grading. Type of grading generally reflects variations of the height of the eruptive column, changes in wind direction and/or velocity, and variation of the eruptive energy. Reverse grading, associated to enrichment of lithic clasts, is thought to reflect increases of the eruption energy (Cas and Wright, 1987) or increases of magmatic emission rate due to the progressive widening of the eruptive

conduct (Wilson et al., 1980; Druitt and Sparks, 1984).

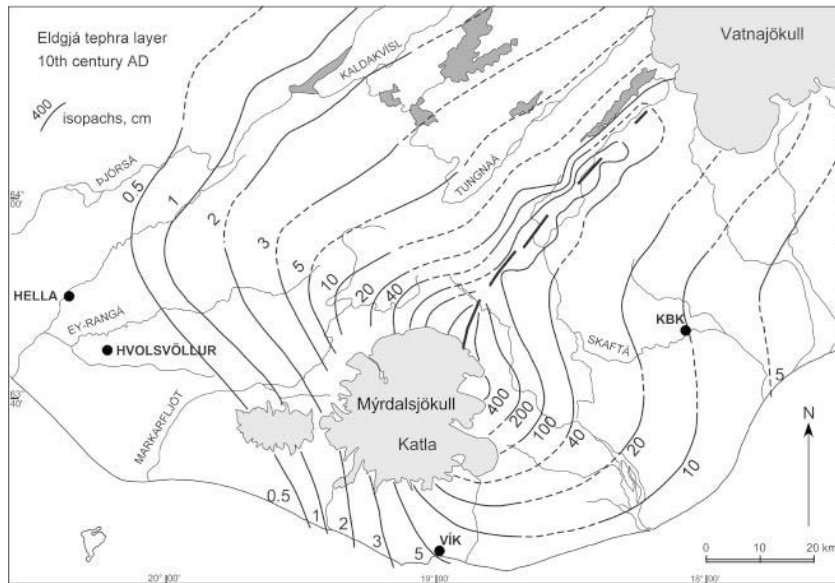


Figure 1.4 – Isopach map of the 1625 Katla tephra layer, Iceland (from Larsen, 2010).

1.1.4 – PDCs deposits

1.1.4.1 Depositional processes in PDCs

The flow of a multi-dispersed and multiphase density current can be divided into two counterparts: an underflow and a phoenix plume (e.g. Baer et al., 1997; Branney and Kokelaar, 2002). The underflow is directly in contact with the ground, and comprises a basal part dominated by particle-particle interaction overlain by a less dense, turbulent part dominated by traction processes (ash-cloud surge; Cas and Wright, 1997). The portion comprised between the lowermost part of the current and the uppermost part of the deposit is also known as flow-boundary zone (Branney and Kokelaar, 2002). In this portion of the current, particle-particle interaction dominates the transport mechanism and promotes deposition. The phoenix plume, also known as co-ignimbrite plume, is less dense than atmosphere and lofts convectively above the underflow.

Historically, two main depositional models have been proposed for PDCs: (1) *en masse* freezing (Sparks, 1976; Wright and Walker, 1981, Carey, 1991) and (2) progressive aggradation (Fisher, 1966; Branney and Kokelaar, 1992; Branney and Kokelaar, 2002). According to Sparks et al. (1973) and Sparks (1976), most pyroclastic flows are characterized by a laminar or a semi rigid (plug flow type) rheological behavior, and they deposit *en masse*. Wilson (1980) supports the idea that a turbulent or fluidized regime occur just in voluminous flows originated from the collapse of a Plinian column, in a very short time during the passage from sustained column to pyroclastic flow in the external parts of the moving current. According to Fisher (1966, 1983 and 1995) and

Branney and Kokelaar (1992, 2002), the current is comparable to a density stratified-flow with a high concentration basal portion characterized by laminar flow, and a low concentration upper portion which is moving in a turbulent way; deposition occurs according to progressive aggradation, i.e. layer-by-layer, from the base of the flow. Valentine and Fisher (1986), basing their studies on theoretical models, demonstrated that a pyroclastic flow comparable to a Bingham's fluid and with a certain velocity, is characterized by a boundary layer where the flow is turbulent because of the presence of vortices and the surface roughness. Above the boundary layer, the flow is laminar. During the propagation of a flow, transition from one type of flow regime to another is possible from transformations in the properties of the current, such as concentration, thickness and flow velocity. Debates about the two models have been several in the past. Progressive aggradation model has been found to be less consistent with small volume PDCs, but on the other hand, several geological evidences support the idea that extensive ignimbrite sheets form by progressive aggradation. This model indeed can explain vertical variations in abundance, size and type of lithic clasts (Bryan et al., 1998), and vertical variations in chemical composition which are often detected in ignimbrites (Wright and Walker 1977, 1981; Branney and Kokelaar, 1992), interpreting chemical zonings as the result of a continuous variability in flow conditions which reflect the variations of the magma composition through the evolution of the eruption. More recently, Sulpizio et al. (2007) proposed a model for small-scale PDCs that joins together *en masse* and aggradation approaches, through stepwise aggradation of discrete pulses. The model assumes that most PDC deposits are originated from stratified flows; the basal portion of the current can move down-slope as a succession of high-concentration pulses that run very close to each other, stopping *en masse*; this allows consideration of a single-pulse as a flow-boundary zone for its overall thickness. This model would be supported by several field evidences, comprising lithofacies analysis and sedimentological interpretation.

1.1.4.2 Fluidization and elutriation

Simultaneous occurrence of clasts of heterogeneous grain size in ignimbrite deposits, even at great distances from the vent, indicates that turbulence alone cannot represent the main sustenance mechanism of clasts in the current. Conversely, it is more likely the occurrence of a dense current where the gaseous phase may give origin to a particular process which is able to carry simultaneously both fine and coarser grain size clasts, so that the entire system behaves as a fluid (fluidization). This concept, adapted to PDCs, indicates the condition for that the gaseous phase exerts a drag force on the individual particles which is equal to their weight, by passing through the solid phase (Sheridan and Updike, 1975). Fluidization process can explain the great mobility of PDCs, since it erases the yield strength enabling the flow to move for every value of shear stress. PDCs, however, can only be partly fluidized, because in a system composed by grains with a high

grain size variability, all the clasts cannot contemporarily supported by fluidization. Part of the fine particles, such as ash, is commonly elutriated and lost as dust from the pyroclastic current. When a flow is very rich in gas or interacts with water, it can disperse from the 35% (Sparks and Walker, 1977) to over half of the erupted products (Walker, 1981a) as elutriated particles. The remaining particles in the current can be fluidized or not, depending on their density.

Ignimbrite deposits are generated by PDCs rich in pumice clasts and ash which are partly expanded and fluidized (Sparks et al., 1973). The term ignimbrite was used for the first time by Marshall (1935) and after by various authors. Sparks et al. (1973) use the term ignimbrite for welded and unwelded pumice rich-flow deposits; Fisher and Schmincke (1984) propose the term to be used for every type of deposit originated from a pyroclastic flow. According to Branney and Kokelaar (2002), ignimbrite lithofacies have not to imply genetic or stratigraphic meanings related to the transport mechanism, but just to refer to the processes and conditions occurring in the flow boundary zone related to depositional mechanism.

1.1.4.3 Architecture of ignimbrite deposits

The time-space association of different lithofacies represents the lithofacies architecture. Different lithofacies record the physical conditions at the flow-boundary zone at the time of deposition.

First investigations on lithofacies architecture of ignimbrite deposits were performed by Sparks et al. (1973) and Sparks (1976), who describe a typical ignimbrite dividing it into three main layers: (1) Layer 1, mainly composed by crystals and lithic clasts, interpreted as a ground surge deposit preceding or contemporary to the pyroclastic flow; (2) Layer 2, forming the main deposit and divided in a structureless, fine grained layer 2a and a generally graded, matrix supported layer 2b containing lithic and pumice clasts; and (3) Layer 3, a very fine grained layer composed by the elutriated particles (the equivalent of the co-ignimbritic ash fall deposit of Sparks and Walker, 1977).

Fisher (1979), basing his studies on the investigation of the Bandelier Tuff (New Mexico), divides the products of pyroclastic flows into four layers (a, b, c, d). The classification scheme resembles that of Sparks (1976), but it gives a major emphasis to the processes and mechanisms originating the various portions of the deposits, and adds a new layer (layer d) formed from all the fine material dispersed in the air falling on the flow deposit.

Wilson and Walker (1982), studying the Taupo ignimbrite (New Zealand), recognize two layers: a basal layer and a upper layer, corresponding to layers 1 and 2 of Sparks et al. (1973). In the basal

layer they recognized a basal jetted deposit formed by only pumice clasts followed by a ground layer containing lithic clasts and crystals.

Walker (1983) applies the concept of aspect ratio to ignimbrite deposits, which gives indication about the flow mobility. Deposits characterized by a high aspect ratio derive from low velocity currents which are more affected by paleo-topography; deposits with a low aspect ratio derive from high velocity currents whose emplacement results to be less affected by paleo-topography.

Branney and Kokelaar (1992, 2002) interpret massive ignimbrites and stratified sequences as the result of progressive aggradation from a single density stratified flow. They consider that ignimbrite lithofacies reflect the depositional mechanism of a current, in particular of the basal flow boundary zone.

Sulpizio et al. (2007) interpret ignimbrite lithofacies as the product of stepwise aggradation of discrete pulses halting *en masse*. Particularly, they explained the lithofacies architecture of repetitive succession of massive lithofacies with inverse grading of lithic blocks and fine ash, and the passage from diffusely stratified lithofacies to massive lithofacies in the same eruptive unit.

1.1.4.4 Structure and texture of ignimbrite deposits

PDCs tend to be channelized into valleys and outflank higher topographic reliefs. Therefore, deposits result thicker and generally massive in the depressions (valley ponded deposits) and thinner (or absent) and mostly stratified on topographic heights (ignimbrite veneer deposits) (fig. 1.5), generally displaying a decreasing thickness with the distance from the source, even if the topographic control is the main factor controlling thickness variations. During the flow, pyroclastic current can erode the substrate, thus deposits may display erosional surfaces at their base.

Ignimbrites generally preserve specific textures and structures. Lithic and particularly pumice clasts are rounded; intensity of roundness depends on the abrasion processes occurring during the transport in the current.

Deposits may develop grain fabric, displayed from the anisotropic orientation of the elongated (linear fabric) or planar (planar fabric) pumice or lithic clasts. Imbrication occurs when clasts are inclined with respect to the sedimentary surface (fig. 1.6 d). In ignimbrites, directional fabric is used to infer the flow direction from the clasts dipping upstream. Kamata and Mimura (1983) assert that directional fabrics record only the last increase of a laminar flow. According to Branney and Kokelaar (1992, 2002), fabric displayed in ignimbrites is originated by unsteady currents with a fluid escape-dominated flow boundary zone. Clasts, however, record only the last increase of shear, therefore fabric may not be representative of the overall behavior of the current. Intensity of the

fabric depends on the shear intensity at the flow boundary zone, residence time of the clasts within the shearing zone and clasts shape and size. Fabric is generally better developed at the base of the deposit, where the shear strain developed between the flowing current and the rigid substrate is greater than in other portions of the current. The progressive aggradation may modify eventual topographic irregularities, therefore flow direction may vary during the time and can originate vertical variations in the direction of the fabric.

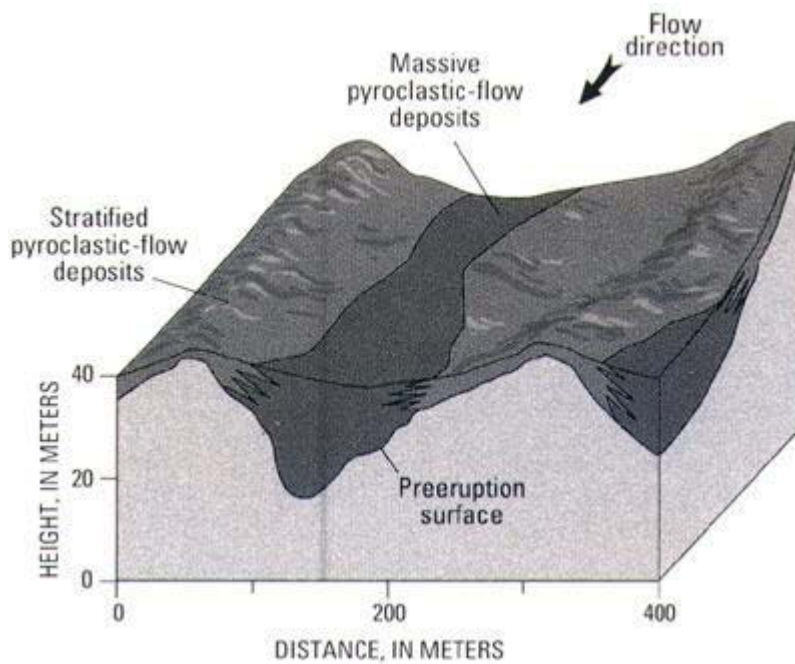


Figure 1.5 – Paleotopographic effect on the emplacement a pyroclastic current. Deposits thicken into depressions (valley ponded deposits) and thin on topographic heights (ignimbrite veneer deposits) (after Scott et al., 1996).

Vertical and lateral grading can be related to various factors: density contrast between clasts and matrix, size of clasts incorporated during the flow and competence and velocity of the current. Because of the opposite contrasting behavior between clasts and matrix densities, it is commonly detected a normal grading of lithic and inverse grading of pumice clasts (fig. 1.6 e). According to Branney and Kokelaar (2002), vertical grading records deposition changing with time. Changes in deposition may be widespread (e.g. generated by changes at the source) or localized (e.g. due to migration of local thalwegs). In the case of a waning current, the current competence decreases through time and the typical gradation pattern is normal for lithic and inverse for pumice clasts; in the case of a waxing current the situation is opposite.

Sorting degree is generally low for ignimbrite deposits, higher for surge deposits. Vertical sorting is controlled by clasts and pyroclastic current densities (during transport processes), and the time required for an effective selective filtering (during emplacement processes). According to Branney and Kokelaar (2002), poor sorting in ignimbrites can be explained by several factors: explosive fragmentation, which produce unequal grain sized-clasts; attrition processes during the transport, with production of fine ash; particle agglomeration; particle interlocking in the current; multiple transport mechanisms and rapidity of emplacement which prevents sorting.

Ignimbrite deposits may be welded or unwelded. Welding varies from incipient through intense to coalescence (Branney and Kokelaar, 1992), and it consists in the cohesion of the fuse glassy material in the emplaced deposit, which can occur during or after the deposition. Commonly, welding processes start at temperatures of about 530 °C and promotes the development of *fiamme* (fig. 1.6 g). According to Smith (1960), and Ragan and Sheridan (1972), development of welding depends on magma composition, amount and composition of the volatiles, clasts temperature, lithostatic load, cooling rate of the deposit, and crystallization velocity of the vapor phase in the deposit. Thickness of the deposit, however, seems to be not always influent for the developing of welding, since many welded deposits are relatively thin (Walker, 1983). According to Branney and Kokelaar (1992, 2002), in a density stratified-pyroclastic current where clasts temperature is high enough, clasts can agglutinate if they are concentrated in the boundary layer and the flow becomes no more granular. Since deposition occurs through aggrading processes from an agglutinated basal flow boundary zone, the deposit will result welded because of continuous aggradation processes from the sedimentary surface. Eutaxitic or reomorphic structures respectively refer to welded deposits unaffected or affected by post depositional hot-state ductile shear deformations (Schmincke and Swanson, 1967; Wolff and Wright, 1981).

Post emplacement alteration processes may affect the deposit, and mainly consist in crystallization and devitrification processes. Crystallization process is due to the escaping of gases through the current which precipitate silica and alkali phases in the pores of the upper and less compacted portion of the deposit. Devitrification process is another type of secondary crystallization which lead to the devitrification of glassy material in the middle-upper part of ignimbrite deposits, and the production of small re-crystallized grains of quartz and feldspar (Cas and Wright, 1987).

Because of their density, pyroclastic currents can host considerable amounts of gas; during emplacement gases escape from the deposit forming characteristic degassing structures (pipes), characterized by high concentration of coarse and dense clasts without fine matrix removed during elutriation processes by the escaping gases (fig. 1.6 f). Pipe structures are commonly about 50 cm long and few centimeters large, even if in proximal deposits they can be up to 2 m (Cas and Wright, 1987). Development of degassing structures is often favored from the presence of external gas sources, such as interaction between the pyroclastic current and surface water or vegetation.

Depositional structures are common in pyroclastic flow deposits. They can be pre-depositional (their formation is affected by the paleo-topography), sin-depositional (e.g. cross and oblique bedding, chute and pools structures, formation of massive and planar stratified-layers, load cast) or post-depositional (e.g. impact structures) (fig. 1.6 a, b, c). In turbidity currents, formation of traction structures such as dunes or antidunes is controlled by the Froude number. In lower-flow-regime conditions deposition originates ripple and dune structures, in upper-flow-regime conditions it favorite the growth of antidune structures. However, turbidity currents are mixtures of mud and

water, while pyroclastic currents consist in solid materials carried by a medium less denser than water (Allen, 1982; Cas and Wright, 1987), so cross stratification inclination within dune structures in surge deposits is often much lesser than the angle of repose, suggesting that the formation of dunes from surge currents does not occur in lower-flow-regime conditions (Fisher and Waters, 1970; Water and Fisher, 1971). According to Branney and Kokelaar (2002), massive and stratified lithofacies originate from different processes and conditions in the flow boundary zone. Massive lithofacies are originated by fluid-escape dominated flow boundary zones, where turbulence is suppressed because of high concentration of clasts; stratified lithofacies are produced by traction dominated flow boundary zones, where traction is induced by turbulence.



Figure 1.6 – Sedimentary and textural structures of pyroclastic flow deposits. (a) Antidune cross-bedding (at the base) and chute and pools structures (at the top of the deposit); (b) Oblique lamination; and (c) Load cast; preserved in the surge deposits in the Afyon ignimbrites near the locality of Kale. (d) Pumice clasts imbrication in the Afyon ignimbrites near to the village of Döğer; (e) Lithic clasts normal grading and pumice clasts reverse grading in the Afyon ignimbrite at the locality of Karakaya; (f) Degassing structure (pipe) in the Afyon ignimbrites at the locality of Karaağaç; (g) Welded ignimbrite displaying fiamme structures in the non devitrified portion of the Kızılkaya ignimbrite, Cappadocia, near the locality of Cemilköy. The red arrow indicates the inferred flow direction.

1.1.5 - Origin and formation of calderas

Calderas are depressions related to volcanic environments originated from the collapse of the magma chamber and wall rocks caused by the abrupt drop of pressure as a consequence of eruption of high volumes of magma. They may develop in all volcanic environments and are commonly the sites of geothermal activity, e.g. in Taupo Volcanic Zone, New Zealand (Bibby et al., 1995) and mineralization, e.g. in Arizona (Lipman and Sawyer, 1985, Lipman, 1992); New Mexico (Goff and Gardner, 1994); Nevada (Mills et al., 1988) and Fiji (Eaton and Setterfield, 1993). On Earth, calderas range in size from less than 1 km in diameter up to 40 × 75 km (La Garita Caldera, Lipman, 2000a), and are formed mainly during ignimbrite eruptions involving between 1 and > 5000 km³ of ejecta. Larger eruptions are generally less frequent than smaller ones (once every 100 years for 1 to 10 km³ eruptions; once every 100,000 years for > 1000 km³ eruptions; Fisher et al., 1997).

1.1.5.1 Classification of calderas

Calderas can develop in all geodynamic environments. Basaltic calderas are characteristic of oceanic intraplate hot spot locations (e.g. Hawaii; Walker, 1988), but can occur also at some divergent plate boundaries in a mid-ocean ridge context (e.g. Island; Gudmundsson, 1995). Andesitic-dacitic calderas are generally associated with convergent plate boundaries (e.g. Tofua, Tonga Islands; Baker et al., 1971) and continental margin arcs (e.g. Crater Lake, Oregon; Bacon, 1983). Peralkaline calderas are associated with areas of high extension (e.g. Ethiopia; Acocella et al., 2002), but also occur in areas of localized extension in convergent margins (e.g. Mayor Islands, New Zealand; Houghton et al., 1992) or intra-plate oceanic islands (e.g. Canary Islands; Marti and Gudmundsson, 2000). Rhyolitic calderas occur mostly in continental or continental-margin areas, either associated with a convergent plate boundary (e.g. Taupo Volcanic Zone, New Zealand; Wilson et al., 1995) or with rifting in continental crust (e.g. Rio Grande Rift, south central USA, Elston, 1984), but also with continental hotspots (e.g. Yellowstone, Wyoming, USA; Hildreth et al., 1984) and submarine arc-back-arc systems (e.g. Kermadec arc; Wright et al., 2003).

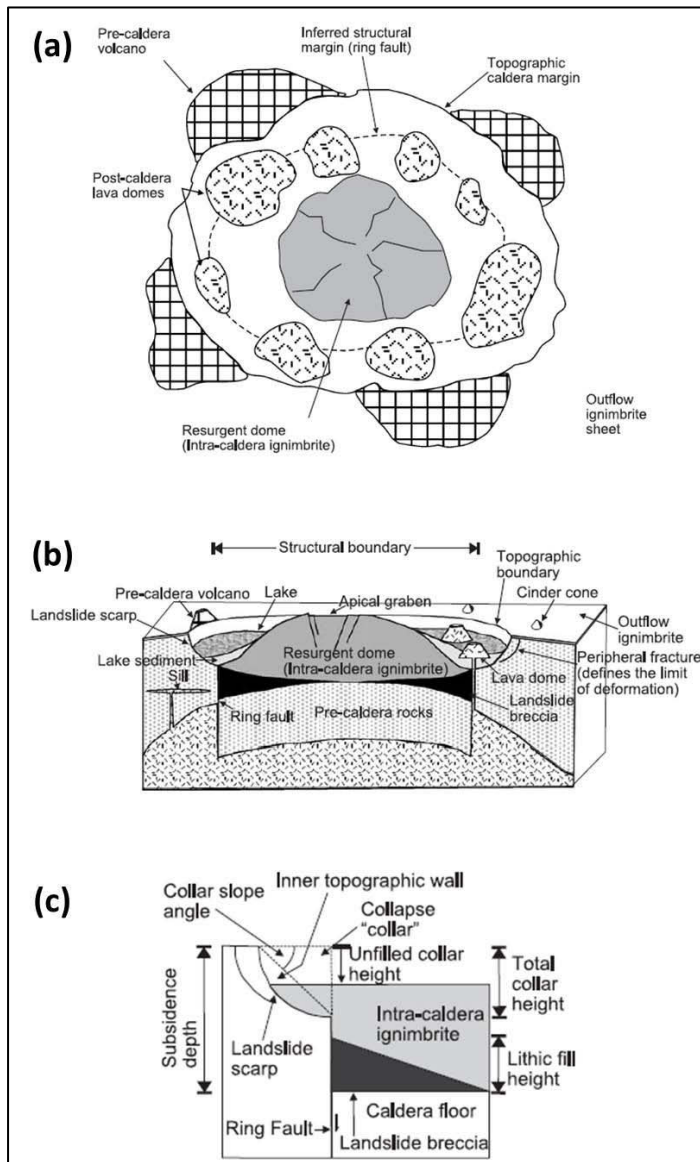


Figure 1.7 – (a) Plan view of a typical caldera structure, with pre-collapse and post-collapse volcanics, and resurgent dome; (b) Section scheme of topographic and structural elements of a caldera; (c) Terminology of a classic piston collapse structure after Lipman (1997) (from Cole et al., 2005).

After the work of Williams (1941), which described calderas as circular shaped negative volcanic structures related to the collapse of a magma chamber which is partly emptied, and made a broad classification of such a volcanic depressions in collapse, explosion and erosion calderas, many other authors redefined the concept and classifications of ‘calderas’ (Smith and Bailey, 1968; Williams and McBirney, 1979; Walker, 1984; Lipman, 1995, 2000b).

On the basis of the structure and erosional degree, calderas (in *sensu lato*) can be divided into four categories: (1) Caldera (in *sensu stricto*), if it is the result of collapse or subsidence into the top of a magma chamber after the eruptive activity; (2) Caldera complex, originated from the overlapping calderas of different ages; (3) Cauldron, an eroded caldera in which most of the eruptives produced during caldera collapse have been removed by erosion, and older

volcanic or sedimentary units below the caldera floor are exposed; and (4) Ring structure, if erosional processes have been so intense to expose the magma chamber beneath an inferred caldera structure. Lipman (1984, 1997, 2000b) identified some topographic and structural elements to characterize a caldera (fig. 1.7 b, c): a collapse collar, inner topographic wall, caldera floor, ring faults, landslide breccias and intracaldern ignimbrite. The structural boundary comprises the part of the caldera which has collapsed along the ring faults and topographic boundary joins the high points surrounding the caldera rim.

1.1.5.2 Caldera development

Lipman (1984, 2000b) recognized four main stages in the development of a caldera on the basis of observations on rhyolitic calderas of North America (fig. 1.7 a): (1) Pre-collapse volcanism, consisting in a surface volcanism which produces lava domes and small explosive eruptions, often accompanied by tumescence due to the magma accumulation and migration to shallow crustal levels; (2) Caldera subsidence, consisting in the collapse associated with eruption of large-scale magma withdrawal. During this stage it is frequent the changing style of eruption, from a central vent phase to a ring vent phase coincident with caldera collapse (e.g. Kaingaroa Ignimbrite; Beresford and Cole, 2000); (3) Post-collapse magmatism and resurgence: volcanism after the caldera collapse can be randomly scattered within the caldera or localized along the ring faults or regional structural trends. Renewed rise of magma, or intrusion of sill complexes, may uplift the central portion of the caldera either by doming or block uplift, often leading to further lava extrusions. During this stage, the central part of the caldera is uplifted as a structural dome caldera, and a caldera lake may develop in the depression, depositing sediments in the ‘moat’ surrounding the resurgent dome; and (4) Hydrothermal activity and mineralization.

Rhyolitic calderas are associated with the largest volume pyroclastic deposits erupted and are usually wide collapse depression with a diameter greater than 10 km and a subsidence of the caldera floor commonly greater than 1 km. Smith (1979) proposed that thermal energy needed to the formation of a caldera is proportional to the quadrate of its radius, therefore to its surface. The dimension of the caldera floor is related to the size of the drainage occurred in the magmatic chamber and the discharged volume of magma. As a consequence of this, the larger the erupted volumes, the larger the surface of the magma chamber. Generally, rhyolitic calderas develop in areas that have been experienced extensive volcanic activity over a long period before the caldera-forming episode (Conejos Formation prior to formation of the Platoro Caldera Complex, Colorado; Dungan et al., 1989; basaltic-to-trachytic lavas, Nemrut Ignimbrite and scoria prior to the Nemrut Caldera, eastern Turkey; Karaoğlu et al., 2005), but have not been developed a single stratovolcano. Caldera collapse is accompanied by the emplacement of huge volumes silicic ignimbrites (dacitic to high-silica rhyolite; e.g. Valles caldera, New Mexico; Smith et al., 1961; Smith and Bailey, 1968; Heiken et al., 1990).

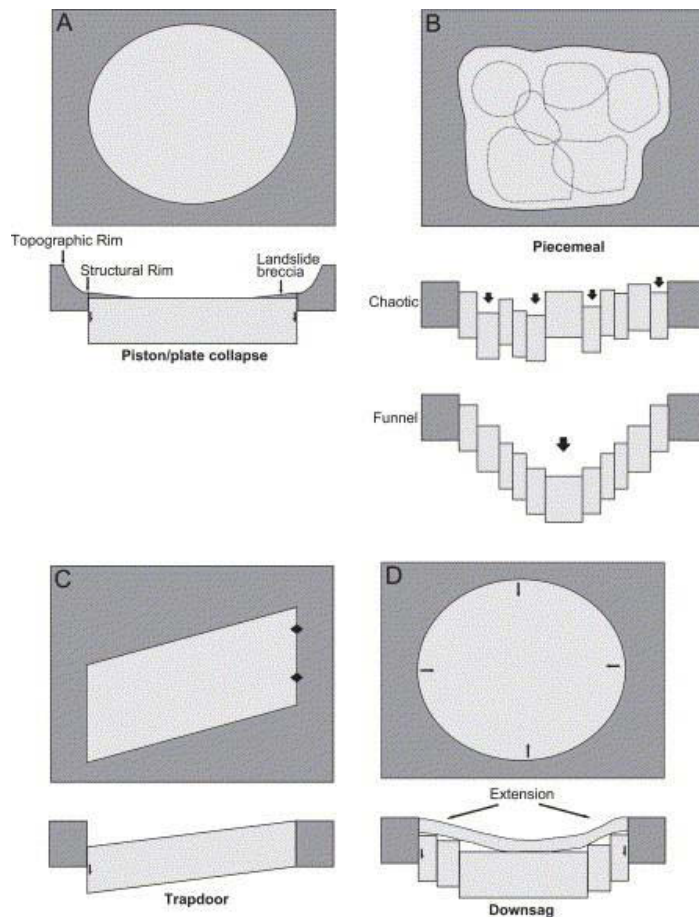


Figure 1.8 – Four end member mechanism of caldera collapse: (a) Piston/plate; (b) Piecemeal; (c) Trapdoor; and (d) Downsag (from Cole et al., 2005).

Numerous processes of caldera collapse have been suggested in the literature. Lipman (1995) suggested calderas could be categorized according to four end-member collapse styles (fig. 1.8): (1) Plate/piston collapse, involving the subsidence of a coherent block of rock into an evacuating chamber along a ring fault (e.g. Crater Lake; Bacon, 1983); (2) Piecemeal, referring to a caldera with numerous floor blocks and/or collapse centres (e.g. Glencoe Caldera; Moore and Kokelaar, 1997); (3) Trapdoor, occurring where formation of a ring fault is incomplete, so collapse is hinged on one side and is deepest towards the other side (e.g. Valles Caldera; Heiken et al., 1986); and (4) Downsag, which occur where ring

faults either do not form or do not penetrate the ground surface (e.g. Bolsena Caldera), instead some or all of the rocks overlying the magma chamber deform by bending without fracture (Walker, 1984; Milner et al., 2002).

One of the most debated questions over the last decades is the understanding of caldera development and its deep structural conformation. Collapse or subsidence is essential to form a caldera and analogue models help to investigate these issues. Studies on some eroded calderas (e.g. Grizzly Peak; Fridrich et al., 1991) have led to consider caldera collapse as occurring on steeply inward-dipping faults (Gudmundsson, 1998). Analogue models suggest that collapse principally occurs on steeply outward-dipping reverse faults accompanied by an outer set of inward-dipping normal faults and intervening tilted block (fig. 1.9; Acocella et al., 2000, 2001; Roche et al., 2000). Roche et al. (2000) suggest from their experiments that the geometry of the collapse depends on the depth, size and shape of the magma chamber. Shallow magma chambers with large diameters lead to coherent single-block collapse structures while deep chambers with small diameters lead to a series of multiple nested blocks. Analogue models also indicate that faults generated by pre-collapse tumescence may be reactivated during subsidence with opposite kinematics (Marti et al., 1994; Acocella et al., 2000). During post-collapse resurgence, faults created (or re-used) during

collapse may be reactivated in the opposite sense as part of the caldera is pushed upwards (e.g. Ischia; Acocella and Funicello, 1999), or new faults may be created and are usually exposed in the resurgent dome. Intracaldera deposits are uplifted and post-caldera sediments can provide a record of the resurgence process (Smith and Bailey, 1968). Acocella et al. (2001) find that the geometry of the resurgence is also dependent on chamber roof aspect ratio: for low aspect ratios they noted that resurgent dome produces an apical graben in its axial part, while higher aspect ratios develop a resurgent block with uniformly dipping layers.

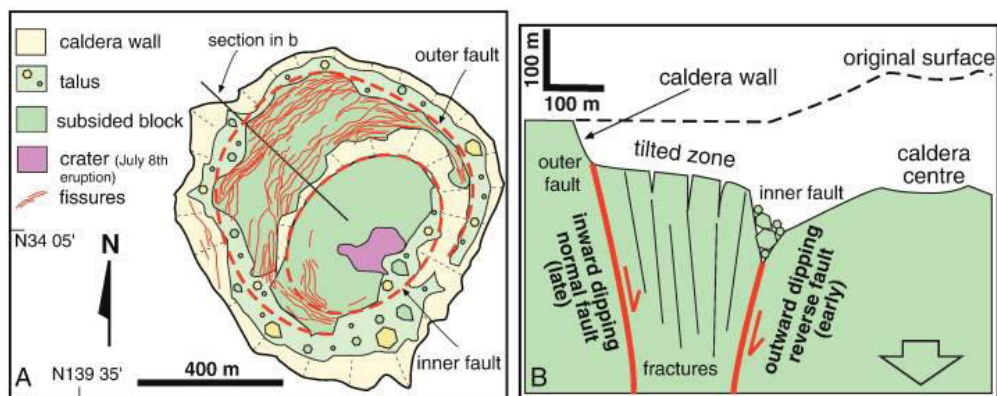


Figure 1.9 – Collapse caldera along ring faults. Characteristics of the Miyakejima caldera, Izu Bonin arc, Japan. (a) Geometry of caldera with inner and outer ring faults. (b) Section of caldera with reverse inner ring fault, normal outer ring faults and tilted block in between (from Mueller et al., 2009).

1.2 - Vent location: field indicators and fabric development in ignimbrites

1.2.1 - Origin of grain fabric in ignimbrites and implications for flow directions

The development of a fabric in ignimbrite deposits is strictly related to the shear stress gradients occurring within the flow. More specifically, fabric is the result of the shear stress exerted between two portions of materials with different rheology and velocities, i.e. a current flowing on a hard substrate, or between different portions of a density stratified current.

There are two main hypothesis on pyroclastic flow movements (fig. 1.10):

1. The expanded flow hypothesis; here the pyroclastic flows are dominantly turbulent, gas-particle, low-density flows (Fisher, 1966; Valentine, 1987; Branney and Kokelaar 1992, 2002; Sulpizio et al., 2008). According to this models, a basal high-concentration laminar flow segregates from the current, decoupling from an upper low-concentration turbulent flow (fig. 1.10 a). In this way, the denser basal flow is more affected by the topography

and may be blocked moving downhill when the flow encounters a topographic barrier (fig. 1.12 e), while the overlying turbulent portion moves downhill as a sediment gravity flow. The moving flow will be thus characterized by a depositional system (the dense flow) and a overlying transport system which continues to move. In such a situation, fabric always records downhill flow directions either away and back towards the vent, if it occurs on the lee or on stoss side of the topographic barrier respectively;

2. the dense flow hypothesis; the pyroclastic flows are primarily non-turbulent, high-density, fluidized flows (Miller and Smith, 1977; Sparks, 1976; Sparks et al., 1978; Carey, 1991). This model states that pyroclastic flows surmount topographic barriers because of their momentum (Miller and Smith, 1977; Sparks et al., 1978). However, because the flow is predominantly dense, separation of depositional and transport systems does not occur and the flow deposits freeze en-masse. In this case, fabric always records flow directions directed away from the source (fig. 1.10 b).

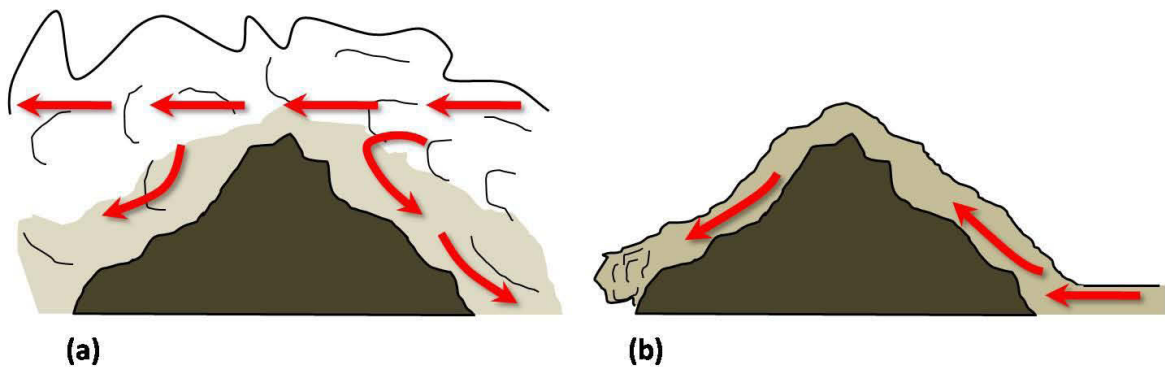


Figure 1.10 – Pyroclastic flows emplacement model: types of moving pyroclastic flows according to the: (a) expanded flow hypothesis, and (b) dense flow hypothesis (modified after Baer et al., 1997).

As discussed in paragraph 1.1.4.1, there are two possible depositional mechanism end-members postulated for pyroclastic flow: *en masse* freezing (Miller and Smith, 1977; Sparks, 1976; Sparks et al., 1978; Carey, 1991) and progressive aggradation (Wilson 1985; Branney and Kokelaar, 1992, 2002), which are joined together by the stepwise aggradation of discrete pulse model of Sulpizio et al. (2007). The two end-members models differ for what concerns the stage during which shearing occurs. In the *en masse* deposition the fabric is the result of a pervasive syn-depositional shearing. The shear gradient recorded by the fabric is thus representative of the flow transport or the final increments of movement. If flow deposits incrementally during transport, the ignimbrite aggrades progressively at the flow base, and neither its thickness nor internal structure are simply related to that of the parent flow. According to this interpretation, the vertical fabric throughout the deposit records the integrated history of shear gradients and flow directions immediately above the accreting bed, i.e. during deposition. On the contrary, it provides poor information on conditions in the flow itself. According to the model of Sulpizio et al. (2007), deposition occurs stepwise through

trains of pulses which halt en masse. Each pulse is considered as a flow-boundary zone for its entire thickness, and it is characterized by specific values of density and velocity. The contrasting effects of shear stress and particle concentration control the distribution of turbulence within each pulse, and the difference in shear stress among each pulse contributes to the origin of the fabric.

The commonest and more consistent fabric in ignimbrite deposits is preserved in its basal portion where shear stress are stronger (Cagnoli and Tarling, 1997; Hughes and Druitt, 1998). In the simulations of Campbell et al. (1995), which used a discrete particle computer simulation of landslides composed of up to 1,000,000 two-dimensional discs, velocity gradients are greatest at the base of the flow and decrease upward. In such a flow the strongest particle fabrics would be best preserved in portions near the base of the flow, where shearing is greatest, and weaker fabrics would characterize upper levels in the deposit.

1.2.2 - Field evidence for constraining the eruptive vent

Investigation of the source area, and more specifically constraining the vent location, is one of the more arduous goals of research studies on ignimbrites. Several techniques have been developed to get paleocurrent indicators in attempts to obtain flow directions and locate the source vent of pyroclastic deposits. They comprise the facies distribution or measurable petrofabric structures such as orientation of glass shards, crystals, pumice and lithic fragments, fluidal textures (Elston and Smith, 1970; Rhodes and Smith, 1972; Suzuki and Ui, 1982; Potter and Oberthal, 1987; Ui et al., 1989; Buesch, 1992; Seaman and Williams, 1992). Imbrication of pumice and lithic clasts indicate the flow direction and the sense of the motion (Kamata and Mimura, 1983; Suzuki and Ui, 1988). Finally, grain fabrics in ignimbrite provide not only information on vent location, but also on the mechanism of transport and deposition of pyroclastic flows (Schmincke and Swanson, 1967; Hughes and Druitt, 1998; Capaccioni et al., 2001).

Self et al. (1986) investigated the lithofacies and the distribution of the pre-Bandelier ignimbrites cropping out in the Jemez Mountains volcanic field (New Mexico) to localize the vents. They interpreted lithic-rich beds in the ignimbrite exposures as evidence of proximity to the caldera (fig. 1.12 c). Many researchers proposed that various lithic rich-zones occurring within outflow ignimbrite sheets are indicators of proximity to the source (Wright and Walker, 1977, 1981; Wright et al., 1979; Druitt and Sparks, 1982) and are commonly found at the edge of caldera systems. Coarseness of lithic blocks in proximal breccias and thickness of individual breccias were also evaluated, since their values generally increase toward the source. Self et al. (1986) also studied the dispersion of the Plinian pumice fall deposits of the lower Bandelier eruption: for Plinian deposits, both the isopach and the isopleth maps are useful indicators of source vents (Walker, 1980, 1981b; fig. 1.4). In particular, the average maximum lithic size map gives a more restricted dispersal and

more symmetrical distribution around the source. In the same ignimbrite, Potter (1983) recorded directions of aligned elongate pumice clasts in the base of the deposits, indicating the pyroclastic flow directions.

An effective tool to infer flow directions and locate the vent consists in the study of the grain fabric of the rock, given by the preferential orientation of elongated or slate clasts in the deposit (fig. 1.12 c-f). In a laminar flow, elongated clasts are aligned parallel to the direction of current and their orientation gives the flow direction; slate clasts are dipping upstream, therefore their imbrication gives the sense of the motion. Hughes and Druitt (1998), studying the vertical fabric of the ignimbrite deposits of the Upper Laacher See Tephra at several sections, distinguished two types of fabrics: (1) A fabric originated from inclined long lithic clasts, whose shape is defined from the a/b ratios greater than 2.5 (a the longest axis, b intermediate one); and (2) A fabric originated by slate clasts, defined from a/b ratios less than 2.5. They pointed out that in the first case, lineation is always parallel to the flow direction and it is vertically constant through the section; in the second case the a - b planes dip upstream irrespective of axial ratio, but the a axes yield girdle fabrics. On the basis of these observations and of the absence of transverse to flow direction fabrics, they assumed that deposits were emplaced by laminar flow. The occurrence of imbricated fabrics whose inferred flow direction is parallel to that of the pyroclastic flow, is consistent with emplacement as a shearing, high-concentration dispersion. This type of fabric has been previously reported for ignimbrites (Elston and Smith, 1970; Ui et al., 1989; Suzuki and Ui, 1982; Potter and Oberthal, 1987) and is attributed to non-turbulent transport; its formation is believed to occur when particles undergo to shear in high-concentration dispersion or glide into place without rolling (Rees, 1983; Postma et al., 1988).

1.2.3 - The magnetic fabric: an effective tool to resolve the problem of source location

Determination of flow directions in ignimbrites is often uneasy. Deposits displaying good sedimentary indicators such as cross stratification and clasts imbrications are not ubiquitously distributed. Occurrence of massive deposits, exposures of two-dimensional sections at high angle or perpendicular with respect to the flow, do not show any evidence of sedimentary structures or, if present, they cannot be used to infer reliable flow directions.

Many massive, structureless deposits, however, can show a developed magnetic fabric, since it is originated by the preferred orientation of microscopic magnetic grains and minerals in the rock, such as magnetite; so, as the grain fabric, it also represents the product of shear conditions during deposition. Because of these issues, analysis of the magnetic fabric can represent a very helpful and effective tool to resolve the problem of vent location, allowing to infer flow directions even in deposits that do not display any macroscopic evidence of sedimentary structures.

Anisotropy of magnetic susceptibility (AMS) is related to the iso-orientation of the magnetic phases within a rock, both paramagnetic and ferromagnetic. It is graphically described by a tri-axial ellipsoid, whose axes correspond to the principal susceptibilities ($K_1 > K_2 > K_3$). As the AMS of a rock sample is the sum of the AMS of its individual crystals, the ellipsoid can be related directly to the net shape anisotropy of the magnetic grains, therefore its magnetic petrofabric (Hrouda, 1982; Tarling and Hrouda, 1993).

Many studies on pyroclastic rocks have shown that the AMS can be used as a reliable indicator of flow direction and to constrain the source (Ellwood, 1982; Knight et al., 1986; MacDonald and Palmer, 1990; Le Pennec, 2000; Alva-Valdivia et al., 2005; Caballero-Miranda et al., 2009; Petronis and Geissman, 2009; Dedzo et al., 2011). This assumption relies on the fact that AMS is due to the preferential alignment of inequant Ti-magnetite grains, which are characterized by shape anisotropy, and the alignment is due to the flow of the volcanic material moving over the paleo-topographic surface. In magnetic-bearing rocks, however, both shape fabric and distribution anisotropy of magnetite grains have been advocated to play a major role in the resulting rock AMS (Hargraves et al., 1991; Stephenson, 1994; Canon-Tapia, 1996; Gaillot et al., 2006). Distribution anisotropy arises from magnetic interaction between neighboring grains and depends on the non-uniform spatial distribution of magnetite grains, commonly single domain (SD) grains, whose aggregation or alignment may produce particular configurations of fabric different from the grain shape resulted-fabric (Grégoire et al., 1998). Grégoire et al. (1995) experimentally verified that magnetic interaction between two magnetite grains occur when the centre-to-centre distance between the grains is less than the mean grain size. Magnetostatic interactions among adjacent grains may either reduce or enhance the magnitude of the whole-rock anisotropy depending on the distribution anisotropy of the magnetite grains. Canon-Tapia (1996), calculating the magnetic interactions occurring in multi-dimensional arrays of anisotropic magnetic particles, demonstrated that the resulting magnetic fabric may be modified in orientation and intensity when the intergrain distance is generally less than one grain size.

For magnetic fabrics defined by magnetic phases characterized by shape anisotropy, i.e. multi-domain (MD) magnetite grains whose magnetization is dominated by uniaxial anisotropy controlled by shape, relations between the K_1 directions of the AMS with the mean long-axis directions of elongated crystals and lithic clasts displaying imbrication in the deposit have been demonstrated by several workers (Hrouda, 1982; Knight et al., 1986). Some authors have interpreted the AMS fabric in ignimbrites as due to a preferred orientation of elongate ferromagnetic grains that moved within the flow, i.e. the K_1 direction is commonly parallel to the flow direction and K_3 is perpendicular to the foliation plane (Ellwood, 1982; Hrouda, 1982; Knight et al., 1986; MacDonald and Palmer, 1990; Jackson and Tauxe, 1991; Tarling and Hrouda, 1993), but flow-perpendicular K_1 directions have also been reported (Hrouda, 1982; Tarling and Hrouda,

1993; Cagnoli and Tarling, 1997). This difference, which is fundamental to any interpretation of the magnetic fabric, could be caused by emplacement transport mechanism of the grains in the current. Under laminar flow conditions magnetite grains are transported parallel to the flow, whereas under turbulent flow conditions magnetite grains are transported by rolling, i.e. with their maximum susceptibility perpendicular to the flow (fig. 1.11) (Granar, 1958; Tarling and Hrouda, 1993).

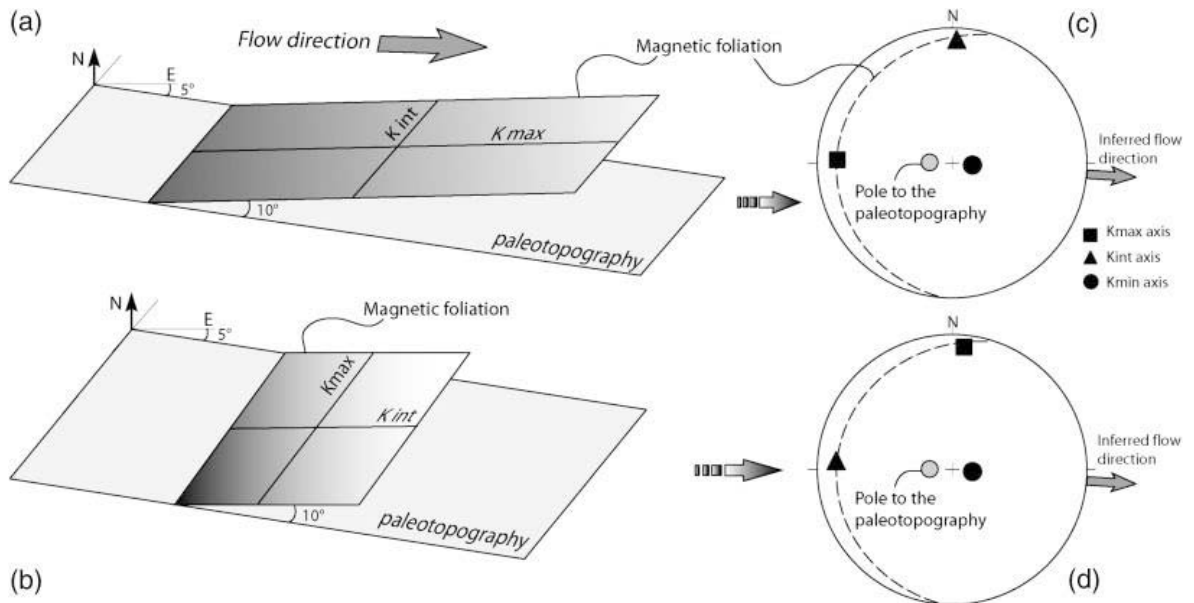


Figure 1.11 – Schematic representation of the imbrication of magnetic foliation in two ideal cases: (a) Magnetic foliation imbricated with K_1 axis oriented parallel and (b) perpendicular to the flow direction, and the related (c) and (d) stereoplots of AMS axes. The first case can represent the situation of a MD grain transported in a laminar flow, the second case can refer to a MD grain transported in a turbulent flow by rolling (from LaBerge et al., 2009).

The main critical points in the analysis of the AMS are understanding which type of magnetic phase mineral (MD or SD magnetite) originates the magnetic fabric, and its primary or secondary origin. MD magnetite grains have their maximum susceptibility parallel to the long axes of the grains, while uniaxial SD magnetite grains have it perpendicular to the long axes (Potter and Stephenson, 1988; Tarling and Hrouda, 1993). The presence of MD magnetite originates a normal fabric, where K_3 axes are close to the vertical and K_1 axes lie along the plunge direction of the magnetic foliation plane; SD magnetite originates a reverse fabric, which is characterized by the switch between K_1 and K_3 axes. SD magnetite can be detected by comparing the AMS with the AIRM (anisotropy of the isothermal remanent magnetization) ellipsoid, which is not affected by the domain state of the ferromagnetic grains because the maximum axes of the AIRM are always aligned with the long axes of magnetic grains (Potter and Stephenson, 1988; Tarling and Hrouda, 1993).

There are two situations for which the magnetic fabric corresponds to the grain fabric:

1. In the case of primary magnetic fabric, i.e. originated during the deposition of the ignimbrite. Baer et al. (1997) hypothesize that a primary AMS fabric originates from strain imparted upon the glass during eruption (fig. 1.12 a): the glass is strained in the conduit, orienting any magnetic phenocrysts imbedded in the glass. The same strain stretches the vesicles, so the magnetic phenocrysts are aligned parallel to the stretched vesicles (fig. 1.12 b). When the fragmentation takes place, conspicuous amount of non-equant ash particles is generated. During deposition under laminar flow regime, non-equant grains are oriented preferentially with the long axis parallel to the flow direction according to their shape anisotropy (i.e. K_1 parallel to it for MD magnetite grains); alignment of free magnetite grains is also possible. If clasts imbrication is also developed, the plunge direction of the clasts foliation plane is tipped slightly back upstream, parallel to the AMS K_1 direction, and the AMS K_3 direction gives the sense of the flow, since it is the pole of the magnetic foliation plane;
2. in the case of secondary magnetic fabric, which may be generated by secondary deposition of vapor-phase minerals within pore spaces as the ignimbrite cools (Seaman et al., 1991; Ort, 1993). It could be generated an AMS fabric (possibly generated by distribution anisotropy or shape anisotropy) that mimics the clasts fabric, thus without modifying the primary petrofabric.

Ort et al. (1993) and Baer et al. (1997) have shown that AMS can also be used to investigate flow processes in pyroclastic currents analyzing flow directions where pyroclastic currents interacted with topography. Ort et al. (1999) suggested that the degree of clustering and the orientation of K_1 axes may indicate flow processes during emplacement. In their study they found stronger K_1 lineation parallel to flow farther from the vent, possibly due to laminar flow, and weak K_1 lineation perpendicular to flow nearer to the vent, maybe originated by turbulent flow during emplacement. Afterwards, many other studies developed techniques based on AMS fabric to interpret flow processes (Le Pennec et al., 1998; Le Pennec, 2000; Ort et al., 2003; Porreca et al., 2003; Gurioli et al., 2005).

Caballero-Miranda et al. (2009), investigating the Cantera ignimbrite, found that a strong prolate fabric, given by strong developed magnetic lineation, characterizes the proximal facies of ignimbrite near to the borders of the caldera. Prolate shapes of the magnetic fabric in these sites can possibly be due to the influence of the caldera rim which should have acted as a barrier and produced additional shear during the flow processes. They propose that oblate magnetic fabric, found in the intermediate and distal facies of the ignimbrite deposits, is the result of low shear component during the flow process, tending probably to assume a more fluid behavior. On the other side, prolate shapes may suggest a more important shear component during the flow; probably a more viscous flow or a flow partially stopped by a physical barrier.

Cagnoli and Tarling (1997) related different orientations of the principal axes of the AMS to different depositional mechanisms. They found laminar flow deposits for AMS fabrics where the K_1 , K_2 and K_3 axes were aligned, and turbulent ones which showed an alignment of the K_3 axes and a girdle type distribution of K_1 and K_2 .

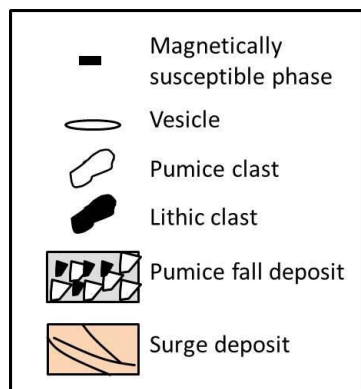
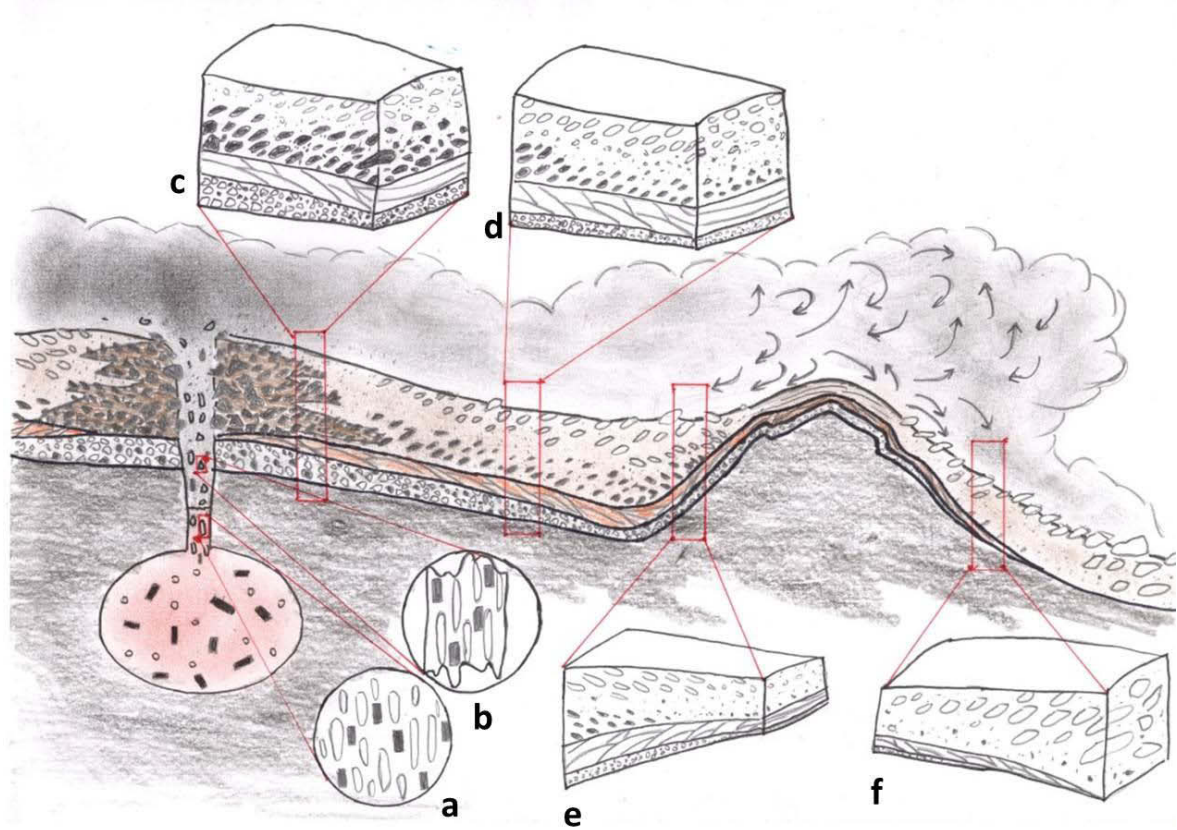


Figure 1.12 – Schematic representation of pyroclastic deposits from proximal to distal facies (not in scale) and evidence for correlation between magnetic fabric and particle fabric. (a) During eruption, the magma is strained as it passes through the conduit, this stretches the vesicles and aligns the magnetic fabric in the same direction; (b) Above the fragmentation surface, non-equant clasts are generated with their long-axis parallel to the magnetic lineation; these clasts may then be oriented during flow; (c) Proximal facies of ignimbrite deposits. Note how, from proximal facies to distal facies, average thickness of pumice fall and ignimbrite deposits decrease, as well the pumice and lithic clasts contained in the pumice fall deposit, while pumice clasts in the flow deposit display a reverse lateral grading. Both cross lamination preserved in the surge deposit, both clast imbrication in the ignimbrite give indications about the flow direction; (d) Intermediate ignimbrite facies; (e) Ignimbrite deposit preserved in the stoss side of a topographic barrier; (f) Distal ignimbrite facies.

1.3 The ignimbrite volcanism of Anatolia: features, challenges and outlook

1.3.1 Geotectonic outline

Tectonic configuration of present day Anatolia (fig. 1.13) is the result of complex geodynamic processes which have been involved the Afro-Arabian and Eurasian plates since Jurassic times, leading to their convergence, collision, subduction and development of distributed deformation. Geodynamic evolution of the Afro-Arabian and Eurasian margins can be divided in two phases (Şengör and Yılmaz, 1981; Görür et al., 1984; Şengör et al., 1985): (1) A palaeotectonic phase, characterized by the consumption of the Tethyan Ocean which originally separated the Gondwana and Eurasian super-continent. This process occurred in two stages of deformations which involved the closure of the Palaeo-Tethys Ocean culminated in the collision of the Cimmerian continent (Şengör and Yılmaz, 1981) with Eurasia and resulted in origination of the Pontide Orogen in northern Turkey (Yılmaz et al., 1997) by Jurassic times (Channell et al., 1996); and the closure of a new formed-ocean, the Neo-Tethys. Closure of Neo-Tethys was preceded by the northward drifting of two microcontinents (Sakarya and Kırşehir) and their amalgamation along the Izmir-Ankara-Erzincan Suture Zone (IAESZ) in Late Cretaceous and Early Tertiary times. Progressive closure of Neo-Tethys Ocean emplaced several terranes from the northern margin of Gondwana to the developing Eurasian margin, producing an accreted zone. These multi-phase continent-continent collisions, lasted until Paleogene and reactivated between Middle Miocene and Lower Pliocene, originated the main Anatolian orogenic belts (i.e. Anatolides and Taurus) and generated a large-scale subduction-related volcanism (Şengör and Yılmaz, 1981). (2) The neotectonic phase refers to the compressional post-collisional regime which has been characterized by the northward motion of Afro-Arabia and the resulting impingement of the Arabian plate on the Eurasian one. This new tectonic configuration produced intracontinental deformational processes, crustal thickening and uplift of eastern Anatolia and Cyprus up to 2 km (Şengör and Kidd, 1979) and the formation of the Anatolian plateau between 12-14 Ma ago (Dewey et al., 1973). During this period a great number of compressional structures developed, such as thrusts and E-W reverse faults, associated to tectonic deformation and folds (Kelling et al., 1987; Karig and Kozlu, 1990; Gürsoy et al., 1992). A late feature was the concentration of much subsequent deformation on two major intracontinental transform shear zones comprising the right-lateral North Anatolian Fault Zone (NAFZ) and the left-lateral East Anatolian Fault Zone (EAFZ).

The area between the two faults comprises most of the weak accreted crustal collage emplaced by closure of Neo-Tethys which is subjected to distributed deformation expressed in terms of westward extrusion of the Anatolian collage (Oral et al., 1995; Reilinger et al., 1997; Barka and Reilinger, 1997) and blocks rotations (Platzman et al., 1998; Tatar et al., 2002; Piper et al., 2006, 2010). The causes for the westward tectonic escape of the Anatolian plate forming-blocks are essentially three: (1) Continuing indentation of Arabia into the Anatolides; (2) Back-arc spreading

behind the S-SW retreating Hellenic Trench, responsible for the extensional regime existent in the Aegean region and western Anatolia (McKenzie, 1978); and (3) Orogenic collapse, which also contributed to the Neotectonic regime in western Anatolia by producing spreading and stretching of a thickened crust (Dewey et al., 1986; Seyitoglu and Scott, 1996; Elitok and Dolmaz, 2008). Many studies revealed evidence for rotation of the Anatolia collage, by different techniques such as GPS ground surveying, geomorphic indicators and paleomagnetic investigations. At long term time scales ($>10^5$ - 10^6 years) paleomagnetic studies are normally required to quantify deformation. The principle on which they are based is the comparison of the time-averaged ancient directions of magnetization with the reference directions of the same age predicted from the paleomagnetic records of the adjoining major continental plates that acted as rigid orogenic forelands, in this case Eurasia, Africa and Arabia. Two contrasting models for Anatolian neotectonic deformation exist:

1. Anatolia is an integral plate delimited by the NAFZ and the EAFZ in the northern, eastern and southern Anatolia and by the western Anatolia extensional province which has been undergoing uniform (Kissel et al., 2002) or episodic (Platzman et al., 1998) anticlockwise rotation around an Euler pole in northern Egypt;
2. Anatolia is a weak crustal collage segmented into fault blocks undergoing differential movement with respect to each other (Tatar et al., 2002; Piper et al., 2006, 2010).

The latter scenario is preferred on the basis of paleomagnetic results: rotation, which is strongly counterclockwise in eastern Anatolia, where compressional regime occurs, passes through zero in central Anatolia to clockwise in western Anatolia, where extensional regime occurs.

1.3.2 Anatolian volcanism

One of the most common feature in convergent plate margins is the presence of an intensive calc-alkaline volcanism, associated with the main collisional events. Volcanism in Anatolia developed during Neogene and Quaternary times represents one of the notable examples of arc volcanism related to continental collision. Other major examples of continental collision related-arc volcanism occur in the Himalaya belt (collision between Eurasian Plate and Indian Plate) and the Southern Alps belt in New Zealand (collision between Australian Plate and Pacific Plate); this type of volcanism is often accompanied by the occurrence of caldera-forming eruptions and emplacement of large volumes of pyroclastic deposits. Anatolian volcanism has been investigated in several works (Pasquarè, 1968, 1971; Keller and Villari, 1972; Innocenti et al., 1975, 1982; Pearce et al., 1990; Altunkaynak and Dilek, 2006) and it is considered a consequence of convergence phenomena and subduction processes occurring between Afro-Arabian and Eurasian plates. Volcanic activity has been concentrated within four volcanic provinces: the Galatean Volcanic

Province (GVP), the Eastern Anatolian Volcanic Province (EAVP), the Central Anatolian Volcanic Province (CAVP) and the Western Anatolian Volcanic Province (WAVP) (fig. 1.13).

The two study areas investigated in the present research are located in the Cappadocia and Afyon-Eskişehir regions, respectively belonging to the CAVP and to Western Anatolia.

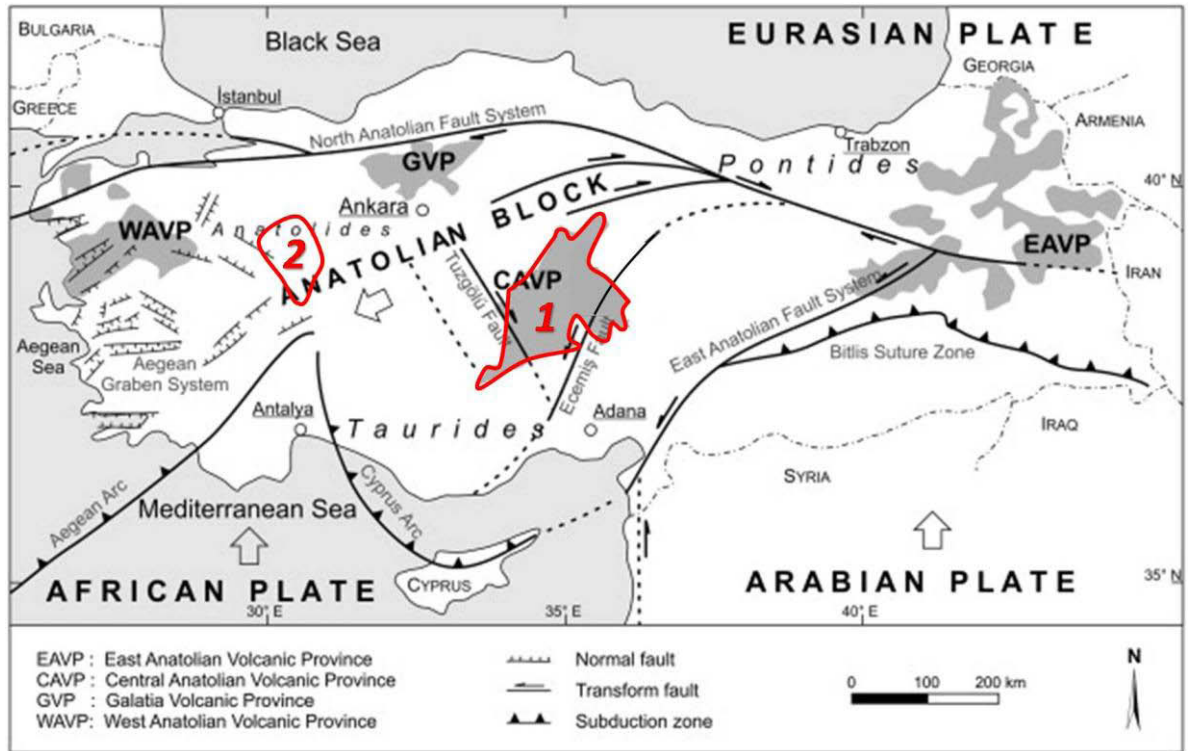


Figure 1.13 – Simplified tectonic map of Turkey showing the distribution of major neotectonic structures and Anatolian volcanic provinces and the study areas of Cappadocia region (1) and Afyon-Eskişehir region (2) (modified after Lepetit et al., 2009).

1.3.2.1 Cappadocia region

Cappadocia is a region located in central Anatolia where a widespread volcanism occurred from Neogene to Quaternary times. It belongs to the CAVP, which extends along a 100 km wide – 300 km long ENE-WSW trending belt set on several pre-existing tectonic basins filled by a thick succession of pyroclastic rock intercalated with calc-alkaline to alkaline volcanics. The CAVP developed within a complicated system of tectonic depressions during Middle-Upper Miocene (Toprak et al., 1994) on a foredeep basin, underlain and surrounded by metamorphic massifs (Niğde Massif to the south and Kırşehir Massif to the north), overthrust by Mesozoic ophiolites (intruded by granitoids) and the alpine Taurus Range (calcareous Tauride Mountains of Silurian to Paleogene age) in the southeast. The widespread calc-alkaline volcanism, ascribed to plate collision and subduction processes of a remaining oceanic wedge of African plate beneath Eurasian one

(Innocenti et al., 1975), began in the Middle Miocene and continued up to historical times passing to alkaline affinity.

Volcanism can be divided into three main periods of activity (Beekman, 1966; Pasquarè, 1968; Pasquarè et al., 1988): (1) Basaltic-andesitic effusive activity between 13.5 and 8.5 Ma (Innocenti et al., 1975); (2) Emplacement of a thick rhyolitic-riodacitic ignimbrite sequence between 11 and 2.8 Ma (Innocenti et al., 1975); and (3) Development of andesitic-basaltic stratovolcanoes (Erciyes Dağ and Hasan Dağ) and a great number of prevalently acid monogenetic centers since Pliocene times.

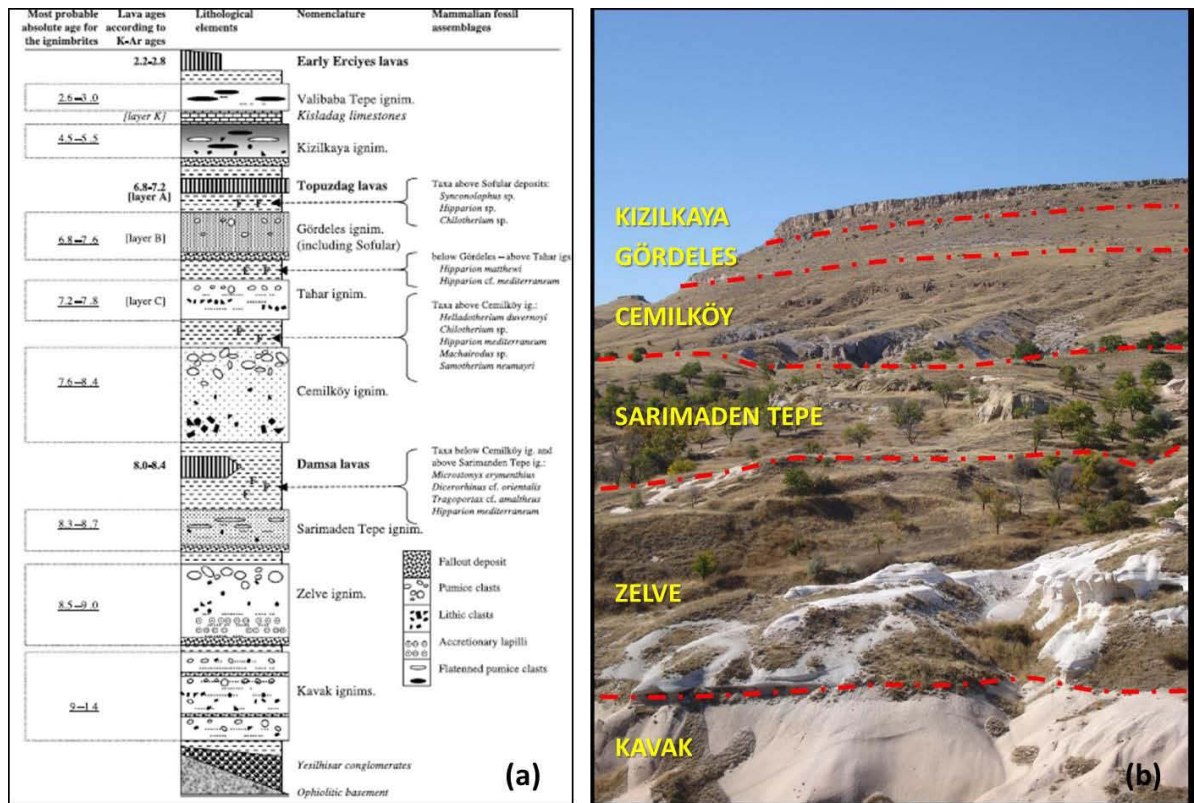


Figure 1.14 – Cappadocia ignimbrite succession: (a) Schematic stratigraphic column of the ignimbrite succession as proposed by Le Pennec et al. (2005); (b) Ignimbrite succession and flow units exposed in the locality of Ayvacık.

The ignimbrite succession (fig. 1.14) comprises a sequence of ignimbrite flow units and tephra fall deposits, intercalated with lacustrine and fluvial sediments, lahar and lava flows, for an average accumulated thickness estimated to amount more than 400 m (Pasquarè, 1968) except in caldera depressions (Froger et al., 1998) and in tectonic basins (Dirik, 2001), an estimated total tephra extension of about 20,000 km² and an estimated volume greater than 1000 km³ (Le Pennec, et al., 1994). Pasquarè (1968) combined the volcanoclastic, epiclastic and basaltic flow units members in the Ürgüp Formation, which constitutes the upper portion of the continental Neogene sequence of Cappadocia. According to Le Pennec et al. (1994), the ignimbrite succession is composed by seven main (Kavak, Zelve, Sarımaden Tepe, Cemilköy, Gördeles, Kızilkaya and Valibaba Tepe) and two

minor (Tahar and Sofular) ignimbrite flow units, both for volume and areal extension (fig. 1.14 a, b). The lower part of the volcanosedimentary succession is exposed in the north (Ürgüp Basin), while the upper members are prevalently exposed in the middle and south (Nevşehir Plateau), because of the conformation of paleogeography and the Pliocene uplift of the plateau. On the basis of stratigraphy of ignimbrite succession, the Nevşehir Plateau can be divided into three areas (Le Pennec et al., 1994): an eastern sector characterized by thicker and complete exposures, and a western and northern sector with thinner and incomplete exposures of the ignimbrite sequence.

Despite Cappadocian ignimbrite succession has been deeply investigated through several decades (see ref.), many complications still exist:

1. Ignimbrite stratigraphy has been revised by many authors (Schischwani, 1974; Innocenti et al., 1975; Pasquarè et al., 1988; Toprak et al., 1994; Le Pennec et al., 1994, 2005; Mues-Schumacher and Schumacher, 1996; Lepetit et al., 2007, Viereck-Goette et al., 2010; Aydar et al., 2012). Nevertheless, stratigraphic relations within the CAVP still remained controversial and complicated because of: great number of individual eruptions, difficulty to distinguish and correlate among flow units in the field because of similar phenocrysts content and textural features, presence of several tephra fall deposits unassociated with ignimbrite units, and source location of some local and minor pyroclastic deposits, possibly deriving from dome collapse of monogenetic structures;
2. age of ignimbrite succession has been dated through bio-stratigraphic (Chaput, 1936; Şenyürek, 1954; Ozansoy, 1962; Pasquarè, 1968; Sickenberg et al., 1975; Gaziry, 1976 and Şen et al., 1998), K-Ar (Innocenti et al., 1975; Besang et al., 1977; Temel, 1992; Mues-Schumacher and Schumacher, 1996), Ar-Ar (Aydar et al., 2012) and U-Pb isotopic techniques (Aydar et al., 2012; Paquette and Le Pennec, 2012). K-Ar dating on biotite and whole-rocks revealed to be unreliable and inconsistent with the biostratigraphic ages because of chemical alteration and weathering processes affecting the deposits as revealed by high values of LOI (loss on ignition) (Temel et al., 1998), and because of unconstrained parent-daughter isotopic disturbance (Le Pennec et al., 1994; Le Pennec et al., 2005; Mues-Schumacher and Schumacher, 1996; Pasquarè, 1968; Viereck-Götte et al., 2010). On the other side, it has been noted that Ar-Ar technique is inappropriate to date and correlate Cappadocian ignimbrites, since its resolution is too high to resolve the brief eruption age differences (Aydar et al., 2012). This problem has recently overcome by U-Pb dating, which employs zircon crystals contained in the pumices as a robust chronometer and indicator mineral that is unaffected by alteration (Aydar et al., 2012; Paquette and Le Pennec, 2012);
3. source locations of the ignimbrite units (fig. 1.15) are still debated. They were deduced from several methods, such as the study in systematic variations in their sedimentological

and physical characteristics (e.g. grain size, thickness, density and AMS) and gravity measurements. Based on regular variations in thickness and grain size, Pasquaré et al. (1988) proposed a single source for the Kavak, Cemilköy and Kızılıkaya ignimbrite of Beekman (1966), in the 15-km-wide basin called Çiftlik Caldera in the northern part of the Melendiz Dağ volcanic complex, and assumed most members to come from that source. After, four source locations were identified: (1) The older, northern caldera formed by the Çardak depression for the oldest units (Kavak and Zelve units), as postulated from sedimentological studies of Le Pennec et al. (1994) and gravimetric data of Froger et al. (1998); (2) The southern caldera located within the Derinkuyu depression for the Sarımaden Tepe, Cemilköy, Gördeles and Kızılıkaya units, as proposed from Le Pennec et al. (1994, 1998); Froger et al. (1998) and Le Pennec (2000); (3) A proposed vent near the Hodul Dağ for the Tahar Member of Le Pennec et al. (1994); and (4) The source area for the Incesu Member of Schischwani (1974) in the Kayseri region beneath the Erciyes-Koç Dağ volcanic complex (Pasquaré et al., 1988; Le Pennec et al., 1994; Kürkcüoğlu et al., 1998; Şen et al., 2003; Mues-Schumacher et al., 2004).

A debated matter is the vent location of the Kızılıkaya, as discussed later;

4. paleomagnetic analyses carried on the Cappadocian ignimbrite succession revealed a generalized anticlockwise rotation, with an estimated average rotation rate of $1.3^{\circ}/\text{Ma}$; following Piper et al. (2002) rotation accelerates by an order of magnitude on a regional scale during the latter part of the neotectonic history. As for the magnetic fabric, paleomagnetic directions too may suffer vertical variations through the ignimbrite deposits, as reported by McIntosh (1991), Palmer et al. (1996) and Paquereau-Lebti et al. (2008). To overcome this problem, a stratigraphic paleomagnetic sampling is needed.

The Kızılıkaya ignimbrite, the youngest and most widespread ignimbrite of the Neogene sequence of the Cappadocian Province, was extensively studied by Le Pennec et al. (1994, 1998) and Le Pennec (2000) using the AMS technique to infer the vent position, since the surficial expressions of the caldera structures are missing. AMS data as well as isopach and isopleth maps of the underlying fall layer and petrofabric measurements suggested a source area in the neighbourhood of the Göllü Dağ Quaternary rhyolitic complex, to the southwest of the town of Derinkuyu, on the Nevşehir plateau. The Kızılıkaya ignimbrite was emplaced on a peneplain and is now well exposed over a wide area. These features make it easier to trace back the flow directions, provided the primary nature of the magnetic fabric can be ascertained. Le Pennec et al. (1998) pointed out that the measured AMS was not only the result of the preferred orientation, during flow, of free inequant grains of magmatic origin, but also of the occurrence of small magnetite inclusions within biotite and apatite phenocrysts. The orientation of these small grains depends on both the orientation of the phenocrysts by the flow and the mutual spatial relations between their shape and the crystallographic axes of biotite and apatite. Moreover, the occurrence of different ferromagnetic

minerals resulting from chemical processes during the cooling of the ignimbrite deposits makes the problem more complex than the simple model of orientation by the flow. The vent location of the Kızılkaya ignimbrite is matter of debate. In the time, Pasquarè et al. (1988) proposed the Çiflik depression, south of the Nevşehir plateau. Froger et al. (1998) delineated a vast negative gravity anomaly in the Derinkuyu basin, that they interpreted as a sign of collapse structures. This source was also proposed by Le Pennec et al. (1998). They individuated a zone to the southwest of the town of Derinkuyu, about 20 km north-east of the Çiflik depression, on the grounds of the thickness of the basal fallout deposit, the maximum pumice size, flow direction mesoscopic indicators and AMS data. Schumacher and Mues-Schumaker (1996b), instead, placed the source in the Misli Plain, NE of Nigde, about 30 km East of the Çiflik depression, on the base of pumice-fall deposit isopach, ignimbrite welding degree and grain-size distribution. Lastly, Le Pennec (2000) localized the source in an area between the town of Derinkuyu and the Göllü Dağ rhyolitic massif in the proximity of the village of Kayırlı, where a resurgent dome structure was also been detected, on the basis of AMS and field directional data. Le Pennec (2000) also remarks that, in the case of the Kızılkaya ignimbrite, it is not safe to assume welding variation of the ignimbrite deposit and thickness variation of the underlying plinian fall deposit as proxies for source location, because welding degree is not directly related to the distance from the vent but rather to the thickness of the overlying flow deposit, while plinian fall deposit can be eroded from the emplacing pyroclastic flow.

AMS data may give significant indication about the vent location, but they also should to be treated with caution because in some cases vertical variations of the magnetic fabric through ignimbrite deposits occur (Palmer et al., 1996; Baer et al., 1997; Paquereau-Lebti et al., 2008), therefore a stratigraphic investigation of the AMS should be more appropriate.

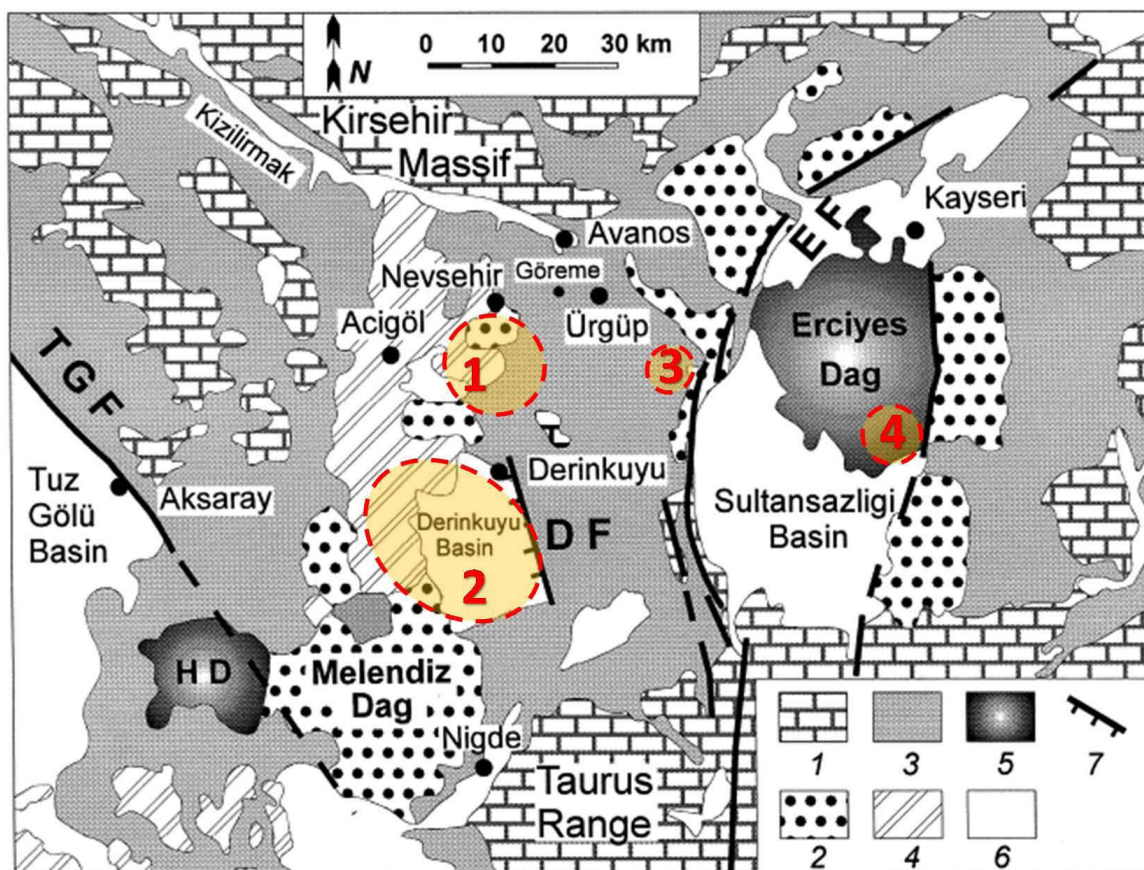


Figure 1.15 – Geological sketch map of the CAVP (modified from Pasquaré et al., 1988; Le Pennec et al., 1994; Temel et al., 1998). The numbers in the legend refer to: (1) Basement rocks; (2) Major Miocene-Pliocene volcanic monogenetic complexes and stratovolcanoes; (3) Ignimbrites and contemporaneous continental sediments; (4) Mainly monogenetic Quaternary volcanism; (5) Large Quaternary volcanoes; (6) Quaternary alluvium; (7) Major Neogene-Quaternary faults. The red numbers in the shaded areas refer to source areas location: (1) Çardak depression; (2) Derinkuyu depression; (3) Hodul Dağ; and (4) Erciyes-Koç Dağ volcanic complex.

1.3.2.2 Afyon-Eskişehir region

In Western Anatolia the most important magmatism is known as Kırka-Afyon-Isparta Volcanism (KAIV), which is concentrated along the Kırka-Afyon-Isparta Structural Trend (KAIST), a N-S oblique-slip shear zone representing the limit between the Hellenic Arc and the Cyprus Arc, and interpreted as a lithospheric tear fault on the underriding African plate (Savaşçın and Oyman, 1998; Dilek and Altunkaynak, 2010; Govers and Wortel, 2005); in such tectonic settings lithosphere faulting propagates in a direction opposite to the subduction direction, such as the volcanism which become younger from the north to the south (Govers and Wortel, 2005 (fig. 1.16). The oldest products of the Afyon volcanism are Early-Middle Miocene (21-15 My old from K/Ar radiometric ages; Besang et al., 1977; Yalçın, 1990; Savaşçın and Oyman, 1998) and consist of a lower Miocene, high K-rhyolitic ignimbrite sequence ($\text{SiO}_2 \approx 73\text{-}75\%$, containing phenocrysts of quartz, sanidine, plagioclase and minor biotite and zircon; Keller and Villari, 1972; Aydar et al., 1998)

likely produced by an anatectic magma originated by the fusion of sialic crustal rocks, as revealed by the occurrence of allanite and garnet and the K/Rb vs K trend (Keller and Villari, 1972; Aydar et al., 1998). The ignimbrite sequence is intercalated and capped by subordinate lava flows and breccias marked by a calc-alkaline geochemical signature (middle to upper Miocene in age; Sunder, 1982; Keller, 1983; Yalçın, 1990), overlapped in time and persisted successively by a K-alkaline effusive activity related to the KAIST due to extensional tectonics (Keller and Villari, 1972; Francalanci et al., 1990; Savaşçın et al., 1997; Francalanci et al., 2000; Dilek and Altunkaynak, 2010).

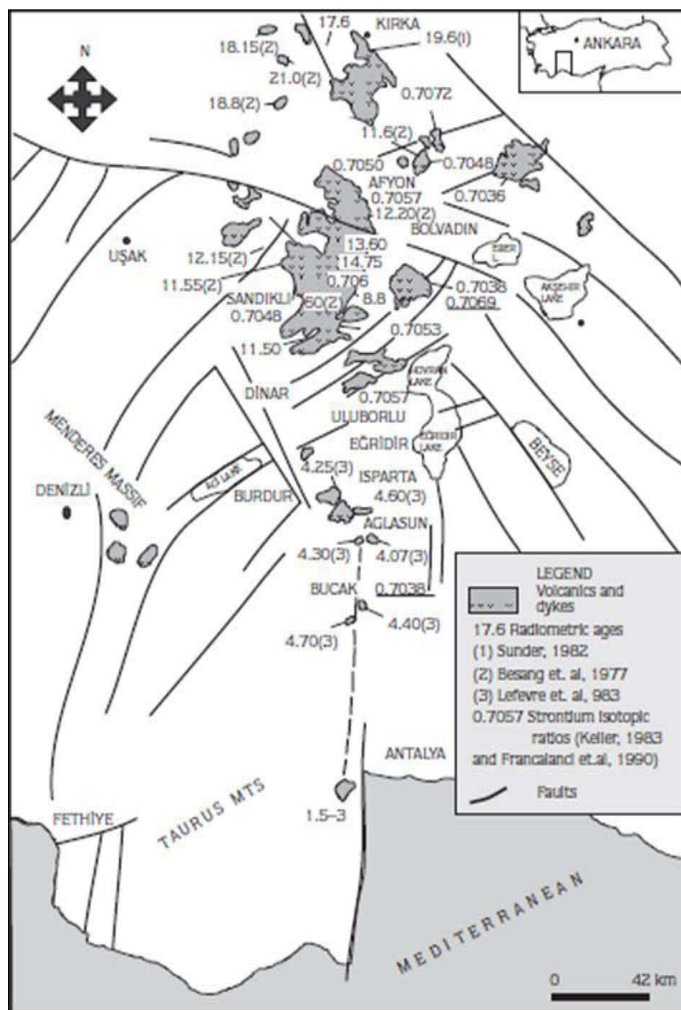


Figure 1.16 – Distribution of alkaline rocks of KAIIV with related fault systems. Radiometric age data are determined on the volcanic rocks. Volcanism becomes younger from the north (Kırka region) to the south (Isparta region); (from Savaşçın and Oyman, 1998).

The main part of the volcanic area comprised between the cities of Afyon and Kırka is underlain by low grade metamorphic rocks attributed to the Paleozoic (Parejas, 1943), mainly Paleozoic schist and marbles. Only in the south, the carbonatic series of the Taurian Mesozoic form the substratum of the volcanic formations. Terrestrial and lacustrine Neogene sediments are altered with the volcanic rocks (Keller and Villari, 1972; Yalçın, 1990).

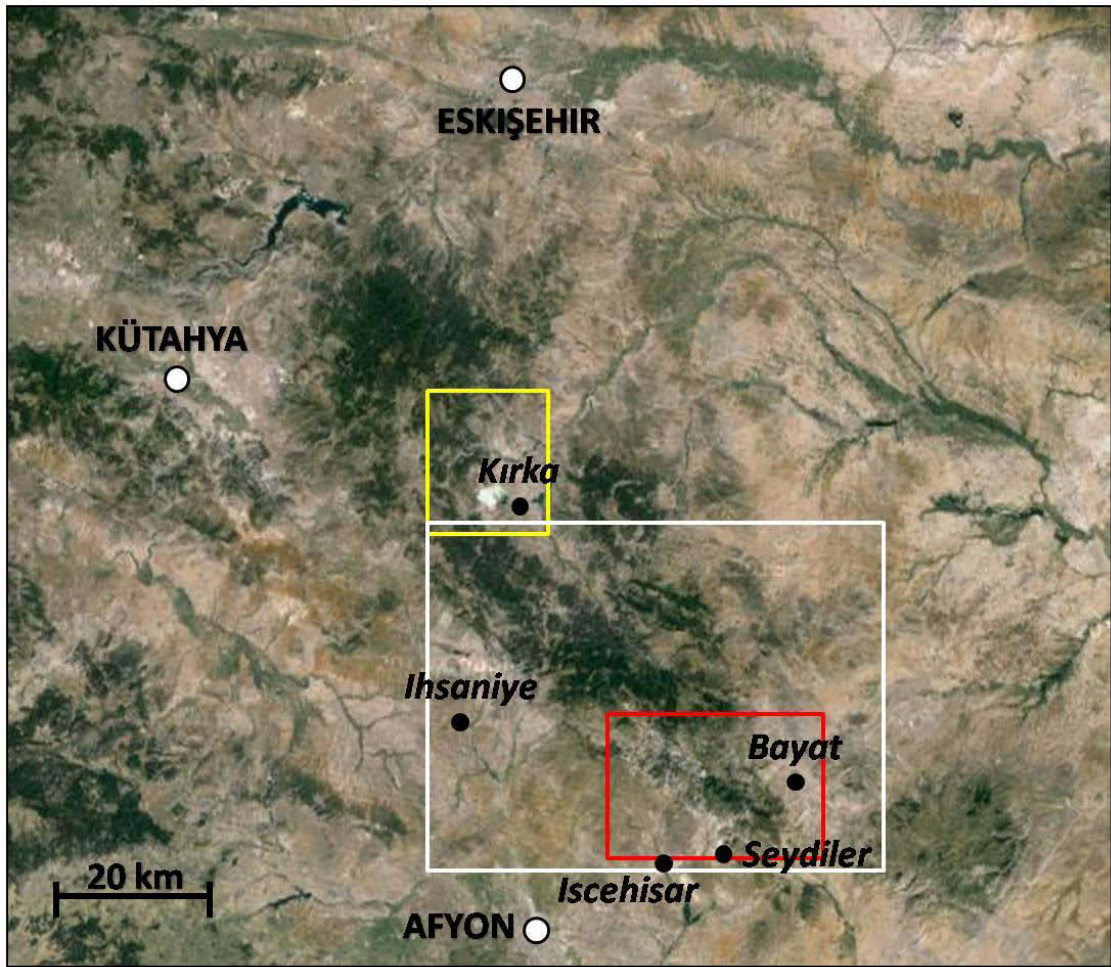


Figure 1.17 – Map of the region of Afyon-Eskişehir and representation of the investigated areas by: (1) Keller and Villari (1972): white rectangle; (2) Yalçın (1990): yellow rectangle; and (3) Aydar et al. (1998): red rectangle (from Google Earth).

The first work performed on the Afyon ignimbrites was the one of Keller and Villari (1972) in the North of the Afyon plain between the villages of Iscehisar, Bayat, Kırka and Ihsaniye (fig. 1.17). They found that rhyolitic pumice tuffs and compact rhyolites formed a large ignimbrite plateau, consisting of a basal main flow unit of about 200 m and 2-3 following minor flow units, laterally intercalated with Neogene lacustrine sediments. They estimated a maximum thickness of the ignimbrites of 300 m and an areal extension of about 2000 km².

Yalçın (1990) performed a stratigraphic and tectonic study of the Kırka Neogene volcano-sedimentary lacustrine basin (fig. 1.17). He recognized an older “İdrisyayla Formation” consisting of vulcanites (andesites and rhyolites) ranging in age from 19.6 to 15.4 Ma (Sunder, 1982; Yalçın, 1990), overlaid by the “Karaören Formation” formed by tuffs with an age of ~17.5 Ma (Yalçın, 1990), which is followed by lacustrine limestone, dolomitic limestone and marl (“Sarıkaya Formation”), basaltic lavas of Türkmen Dağ mountain (9.3 Ma; Yalçın, 1990) and resedimented tuffs (“Fetiye Formation”). Ignimbrite deposits, belonging to the Karaören Formation, were distinguished between continental and lacustrine tuffs, which are respectively distributed mainly

toward SW and toward SE with respect to Kırka. Yalçın (1990) asserted that pyroclastic deposit were produced from a Plinian eruption.

Aydar et al. (1998) investigated the ignimbrite deposits exposed in a ~50 km NW-SE X 30 km NE-SW wide-area near the village of Seydiler (fig. 1.17). They individuated a resurgent caldera (Koroğlu cladera) situated 40 km north-east of the city of Afyon, which is the result of the eruption of the Seydiler ignimbrites, distinguished into two sequences (Lower and Upper Seydiler) and separated by reworked tuff. The northern and northwestern parts of the caldera represent two stages of ring fracturing, each stage with the generation of a corresponding ignimbrite sequence. They recognized four stages in the volcanological evolution of the caldera: (1) Updoming (evidenced by chloritoid isograde related to regional metamorphism which is found at different heights within and outside the caldera; Erkan et al., 1996); (2) Ignimbrite eruption and caldera collapse; (3) Resurgent doming (identified by deformation and silicification processes of the ignimbrites); and (4) Post-caldera lava extrusions (with two generations of alkaline lava: an older one related to caldera ring fractures and a younger one generated independently from caldera system). On the basis of their observations, ignimbrites have been transported up to 50 km away from the source area, and a total unit thickness of 400 m at proximal locations has been measured. At distances greater than 50 km ignimbrites are no longer identified in the field, instead a transition to secondary volcanoclastic lacustrine deposit is detected. Both Lower both Upper Seydiler ignimbrites are composed by two texturally identical main flow units, respectively formed by several minor ignimbrite flows. Welded facies were identified just inside the caldera and on top of the unit forming the caldera rims. They estimated a ignimbrite areal extension of 1100 km² and a volume of 77 km³; the caldera is supposed to have a diameter of 13 x 18 km (on the basis of SPOT images), to contain a resurgent dome in its center and the collapse estimation is of 700 m.

More recently, GURSOY et al. (2003) performed a paleomagnetic study on the ignimbrite deposits and lava in the area between Afyon and Eskişehir, in order to estimate neotectonic deformation and quantify the tectonic rotation.

Many questions and unstudied issues have be left in this area:

1. Real extension and volume of the pyroclastic products and their lateral correlation. Neither real areal extension nor volumes of the ignimbrite succession is exactly known. The only works on the ignimbrites cropping out in the Afyon region have been performed over relatively restricted areas (Keller and Villari, 1972; Yalçın, 1990; Aydar et al., 1998) without any attempts to correlate the various ignimbrite deposits. Moreover it has been investigated just the area between Afyon and Kırka, but there are no studies in the northern part of the region between Kırka and Eskişehir and toward Kütahya, where the ignimbrite succession is considerably thick;

2. classification of the eruption event. Yalçın (1998) asserted that ignimbrite deposits in the Kırka basin were originated from a Plinian eruption, even if no calculations on ignimbrite volumes neither isopach and isopleth maps of the deposits were performed in supporting this hypothesis;
3. stratigraphy of the ignimbrite sequence. Ignimbrite deposits have been mainly studied about their petrographic and chemical composition (Keller and Villari, 1972), age (Sunder, 1982; Yalçın, 1990) and they have been broadly subdivided into flow units recognizable in the field (Keller and Villari, 1972; Aydar et al., 1998), but little attention has been given in the study of the stratigraphy and facies analysis, which is of primary importance in order to perform stratigraphic correlations and volcanological reconstruction;
4. localization of the source areas. Aydar et al. (1998) proposed as source area for the Seydiler ignimbrite the Koroğlu caldera, on the basis of few sedimentological (pumice clasts dimension) and textural (welding degree) features of the flow deposit. However, these data are insufficient to constrain a source area, because isopleths map of the maximum pumice flow may be influenced by the paleotopography, therefore giving misleading indications about the vent; moreover, it has been pointed out that for some ignimbrites, welding degree is not only related to the distance from the vent, but also to the thickness of the deposit (i.e. Kızılkaya ignimbrite case; Le Pennec, 2000), which is also affected by paleotopography (e.g. valley pond and ignimbrite veneer deposits). Isopleth maps of pumice and lithic clasts of the ignimbrite flow may be useful if combined also with isopleths and isopach maps related to the pumice fall deposit, since its distribution and variation is not affected by paleotopography, but only from the hydraulic equivalence of the transported clasts and the wind direction. Their interpretation would require a revision and an integration with other data. No studies about localization of source area(s) of ignimbrite deposits investigated by Keller and Villari (1972) and Yalçın (1990) exist. A detailed study of the flow directions (inferred from sedimentological and/or from the AMS analysis) relative to the various flow units seems essential to constrain the source area(s);
5. identification of the Koroğlu caldera. Aydar et al. (1998) recognized a caldera structure on the basis of SPOT image and structural evidence, estimating a caldera collapse of about 700 m. However, the interpreted structural map lacks of geographic references, and it is not explained how they quantified the caldera collapse;
6. age of the ignimbrite sequence. Ignimbrites and lavas have been dated by using K-Ar method (Sunder, 1982; Yalçın, 1990). There are two main problems related to this issue. The first inaccuracy arises because ignimbrite stratigraphy is unknown, so it is also unknown the ignimbrite unit to which dating refers to. The second problem is analytical: it has been pointed out that K-Ar technique is not always accurate because it is very sensitive to alteration processes and weathering (e.g. Cappadocian ignimbrite case). Alteration

processes may have affected the ignimbrite deposits, since some of them were emplaced in a lake (Yalçın, 1990). In such a case, U-Pb dating technique is much more effective in giving reliable ages;

7. quantification of tectonic rotations. Gürsoy et al. (2003) measured the paleomagnetic directions of many lava and ignimbrite deposits in the region of Afyon and Eskişehir, obtaining average declination and inclination values which, compared with the reference paleomagnetic directions, would quantify the tectonic motion. However, if stratigraphy of the ignimbrite sequence is unknown, paleomagnetic sampling is performed randomly in ignimbrite units which may have different ages and have recorded different directions of the geomagnetic field. In such a case, the obtained average paleomagnetic direction value would not be reliable nor usable to speculate about geodynamic reconstructions.

2 – Field and laboratory methods

The dual objective of the present thesis, consisting in a primarily stratigraphic rock-magnetic study of the Kızılkaya ignimbrite and a combined stratigraphic-sedimentologic and rock-magnetic study of the Afyon-Eskişehir ignimbrite succession, implied the use of different techniques.

For the Kızılkaya ignimbrite it was performed a detailed paleomagnetic sampling, by sub-dividing each section into several sites at different stratigraphic heights. Laboratory method consisted in paleomagnetic analysis (NRM), magnetic fabric (AMS, AIRM and AARM) and magnetic mineralogy investigations (IRM, thermal demagnetization of the IRM and S-ratio).

The work performed on the Afyon-Eskişehir ignimbrites firstly consisted in a volcanologic investigation that concentrated on facies analysis, description and comparison of cross-sections through the performance of stratigraphic measurements, detection of field directional structures and production of isopach and isopleth maps of the pyroclastic deposits; moreover, geochronologic techniques (U-Pb and ^{40}Ar - ^{39}Ar) were used to date the ignimbrite units. Stratigraphic paleomagnetic sampling preceded the rock-magnetic study, that concentrated on magnetic fabric (AMS and AIRM techniques) and magnetic mineralogy investigation (IRM and demagnetization of the IRM techniques).

2.1 - Field investigation

2.1.1 - Stratigraphic measurements

Stratigraphic measurements were performed at 76 sections in the area of Afyon-Eskişehir and consisted in thickness and clasts grain size measurements of the fall and ignimbrite deposits. Grain size and thickness data were used to produce the cross sections representing the type sections and lateral facies variations of the ignimbrite units described in paragraph 3.1.

Once have been distinguished the ignimbrite eruption and unit which the pyroclastic deposit belongs to, for every section were firstly determined the geographic coordinates and altitude a.s.l. through the use of a GPS. Thickness and grain size measurements were performed by using a 3-m-long graduated measuring-tape with a precision of 0.1 cm.

Thickness was vertically measured from the base to the top of the deposits. Grain size measurements were performed to get the MP (maximum pumice) and ML (maximum lithic) dimension, whose values are obtained by the average of the 5 largest pumice and lithic clasts. In order to avoid possible underestimations or overestimations in the evaluation of the real clasts dimensions, grain size was measured following this procedure:

1. Largest lithic and pumice clasts were identified and then extracted, when possible, from the same stratigraphic layer of the deposits (an average of 5-15 clasts were selected for each section). Clasts extraction permits a 3-dimensional estimation of the clasts size, resulting in a reliable evaluation of the effective dimension and a major accuracy of the measure, especially if the clast is elongated;
2. both the maximum, a , and the intermediate, b , clasts elongation axes were measured. Where clasts extraction has not been possible, because of welded or indurated deposits, only the a axes were measured while the clast was still *in situ*, and the corresponding b axes were calculated by considering a linear relationship between a and b axes values for each unit, as pointed out by the well fit of data points on the regression lines, indicated by the high R^2 parameter (example of Incik 1c unit in fig. 2.1);
3. each clasts dimension were obtained by averaging the values of their a and b axes;
4. MP and ML values were finally obtained by the average of the 5 largest clasts.

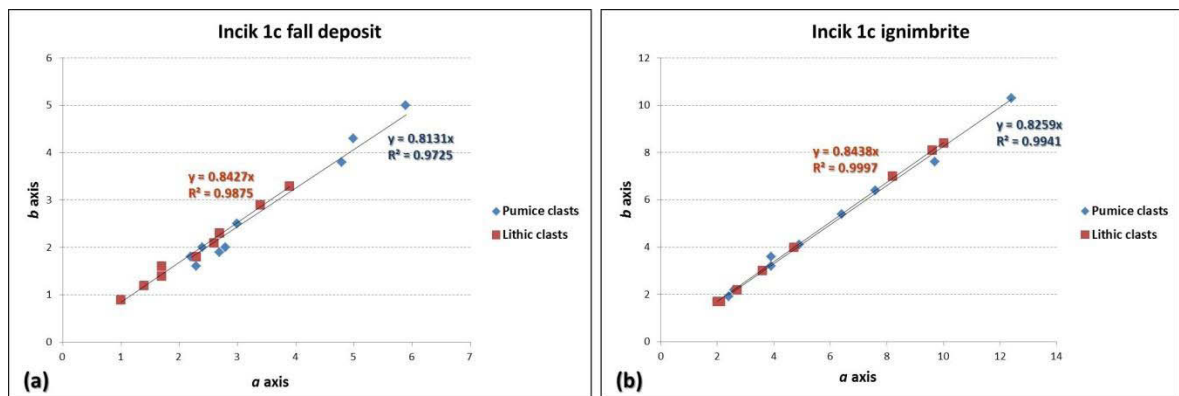


Figure 2.1 – Example of linear relationship between a and b axes of pumice and lithic clasts contained in the Incik 1c unit: a) Fall deposit; b) ignimbrite deposit. Each point represents a measured stratigraphic section. Symbols: y = slope of the regression line; R^2 = coefficient of determination.

Each section was accurately described in the field taking into account, besides its thickness and clasts grain size, also its structure and textural characteristic. In particular, stratigraphic analyses concentrated on the number, geometry and relations among the various forming layers, gradation, features of the juvenile clasts (phenocrysts content, vesiculation degree, shape) and facies analysis based on sedimentary structures preserved in the deposit. These observations led to the production of cross-sections which were used to reconstruct the volcanic stratigraphy.

2.1.2 - Field directional structures

Field directional structures were detected both in ignimbrite and surge deposits. They were oriented with a geologic compass and used to produce imbrication maps, reported in paragraph 7.2.3.2, in order to infer flow directions and localize the source area. Sedimentary indicators are in fact complex 3-dimensional structures, and the accuracy of the orientation data strongly depended on

the presence of suitable exposing surfaces where the real trend of the structure could be reconstructed. Figure 2.2. shows the types of sedimentary structures detected in the field, which are represented by: cross lamination, antidune cross-bedding, load cast, chute and pools and clasts imbrication (both pumice and lithic).

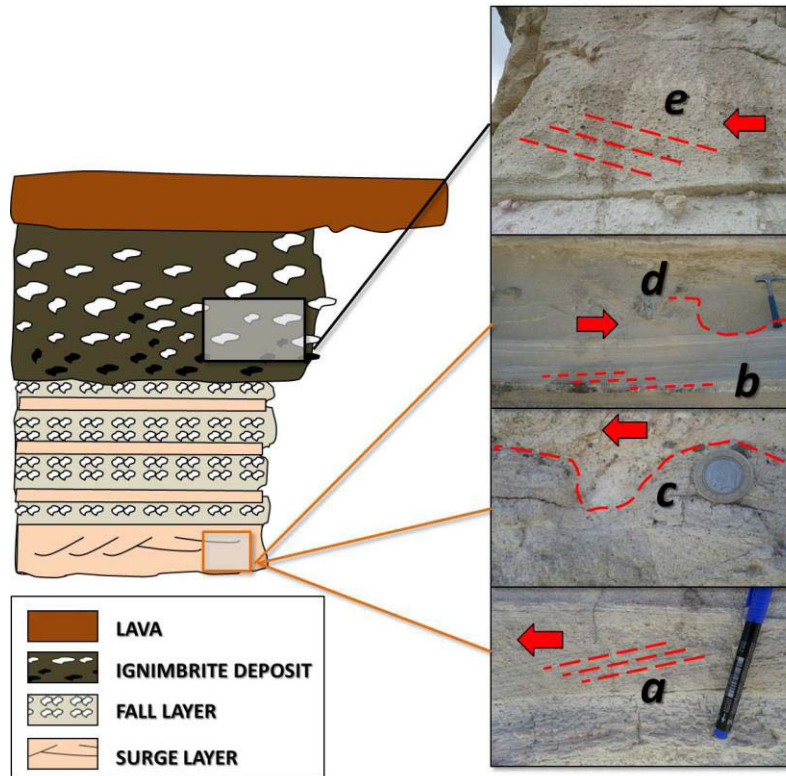


Figure 2.2 – Sedimentary structures detected in the surge deposits: a) cross laminations (Kale); b) antidune cross-bedding (Kale); c) load cast (Yeşilyayla); d) chute and pools (Kale); and in the ignimbrite deposits: e) clasts imbrication (Göçeri). Arrows indicate the inferred flow direction.

2.1.3 - Isopach and isopleth maps

For each pyroclastic unit, isopach and isopleth maps of the fall and flow deposits were performed reporting on a DEM map (Digital Elevation Model) thickness, MP and ML data obtained as described in paragraph 2.1.1. Maps are reported in paragraph 3.2 and used in paragraph 7.2.3.1 to get indications about the paleo-topography and infer the source area. Isopach and isopleth maps of the fall deposits result to be suitable to infer the source area, since tephra dispersion is not affected by the paleo-topography but just by the dominant wind directions. On the contrary, isopach and isopleth maps of flow deposits give important indications about the conformation of paleo-topography, highlighting the presence of paleo-valleys and topographic barriers.

2.1.4 - Volume estimation and calculation of the eruption magnitude

Area extension and volume estimations are calculated using the program Global Mapper (version 15.0.5), taking into account the present-day and the inferred pre-erosional exposition areas of the

pyroclastic deposits, respectively determined by field study and analyses of the isopach and isopleth maps of the deposits. Data are reported in paragraph 7.2.2.

Procedure used for volume determination consisted in the estimation of the minimum and pre-erosional area extensions, respectively by taking into account the enveloped area of the cropping out deposits and extrapolating the enclosed area of the non-eroded deposits through analyses of isopach and isopleth maps and on the basis of considerations about paleo-topography, which is discussed in the paragraph 7.2.1. The corresponding minimum and pre-erosional volumes were obtained by sub-dividing the enclosed areas into several sub-areas characterized by a specific average thickness value inferred by the isopach map, then multiplying each sub-area for the relative average thickness value and summing the sub-volumes.

The magnitude of the eruption was defined conferring a VEI index (Newhall and Self, 1982) on the basis of the bulk volume of the deposits, and calculating the magnitude M (Pyle, 2000) according to the equation:

$$M = \log_{10}[\text{erupted mass}(\text{kg})] - 7 \quad (1)$$

Finally, the DRE volume was calculated according to the equation:

$$DRE(\text{km}^3) = [\text{tephra volume}(\text{km}^3) \cdot \text{tephra density}(\text{kg}/\text{m}^3)] / \text{magma density}(\text{kg}/\text{m}^3) \quad (2)$$

2.2 - Paleomagnetic sampling and laboratory methods

2.2.1 - Paleomagnetic sampling

Paleomagnetic sampling was performed according to a stratigraphic criterion (fig. 2.3), i.e. coring the ignimbrite at different stratigraphic heights, when possible, in order to evaluate possible variations of the magnetic properties through the deposit. Maps of the sampled localities for the Kızılkaya and Afyon-Eskişehir ignimbrites are shown in chapter 4.

For the Kızılkaya ignimbrite, stratigraphic sampling represented an essential point in order to resolve the intended goals. At each section, deposit was sampled along subvertical profiles with limited lateral offset, using an electric-powered drill (2 to 9 sites along a single profile), within the devitrified portion of the deposit. If sampling was performed over large horizontal distances and/or over different rock exposure surfaces, sites were further sub-divided into blocks lying at the same stratigraphic heights. Distances between the sites were measured using a 3-m-long graduated measuring-tape. The coring sites are typically 2 – 3 m in length-width, with an inter-site distance in the range of 1 – 15 m. At each site, 5 to 17 cores were collected, which were oriented using both magnetic and, when possible, solar compasses, and applying a correction of +5° to each core to

account for a measured magnetic declination of 5°E, consistent with IGRF2010 reference field (online calculator at <http://www.ngdc.noaa.gov>). The cores were cut to standard cylindrical specimens ($\Phi = 25 \text{ mm}$, $h = 23 \text{ mm}$).

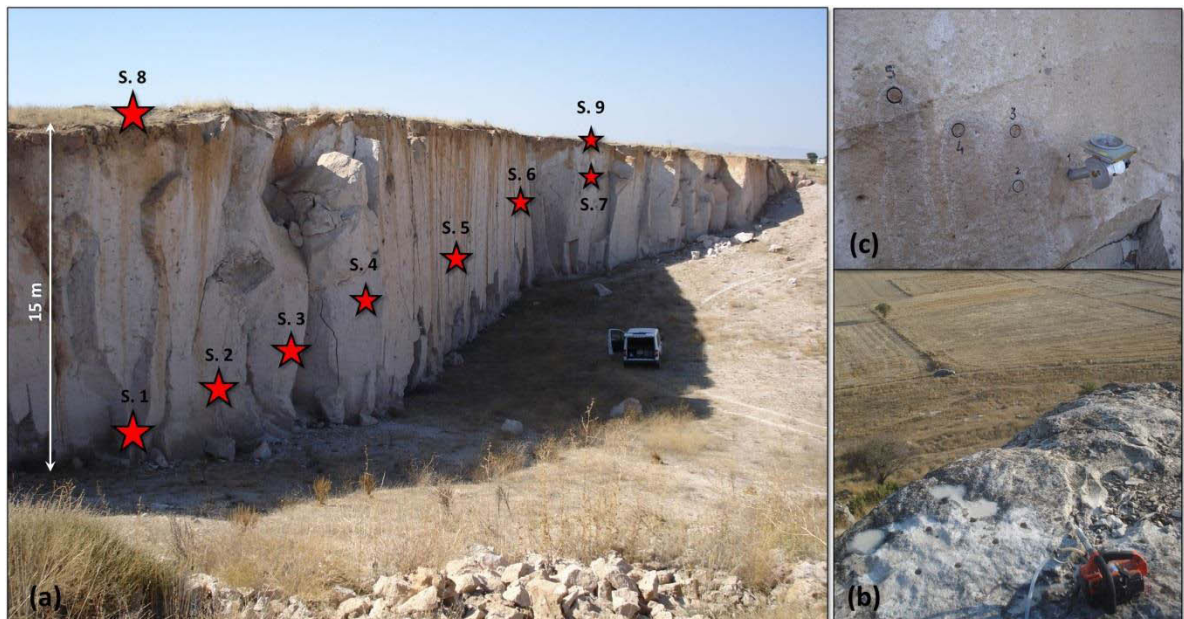


Figure 2.3 – Paleomagnetic sampling procedure: a) each section was divided into several sites (s.1 – s.9) at different stratigraphic heights, then b) sampled using an electric-powered drill; c) samples were finally oriented in situ and extracted.

For the Afyon-Eskişehir ignimbrites, for which the main goal consisted in locating the source, it has been chosen a distributed paleomagnetic sampling strategy which resulted in more sampled localities, rather than a detailed stratigraphic sampling. Each locality has been sampled from 1 to 3 sites along subvertical profiles. Subdivision into sites was done taking into account several criteria including: (1) exposures of complete ignimbrite sections from the base to the top, in order to check the possible vertical variability of the magnetic mineralogy and magnetic fabric; (2) occurrence of well-preserved sedimentary structures in the ignimbrite and surge deposits to be compared with flow directions inferred from magnetic fabric; (3) suitability of the rock to be cored. Sampling details (i.e. number of cores extracted for each site and orientation procedures) are the same as for the Kızılkaya ignimbrite.

2.2.2 - Rock-magnetic methods

Sample preparations and magnetic measurements were performed at Alpine Laboratory of Paleomagnetism (ALP, Peveragno, Italy). The cores were cut to standard cylindrical segments (25 mm in diameter and 23 mm in length). Before magnetic analyses, the mass of each specimen was

measured with an electronic balance, then the density was obtained by dividing the mass by the specimen volume (10 cm^3), with an accuracy of 10^{-2} g/cm^3 .

2.2.2.1 - Magnetic mineralogy

In order to understand the geological meaning of the natural remanent magnetization (NRM) and to attest which magnetic phases contribute to the origin of the magnetic fabric, identification of the magnetic minerals which carry the magnetization in a rock constitutes the essential starting point. The investigation methods exploited in the present work to identify the magnetic mineral assemblage, are based on the analysis of the variation on the magnetic properties (i.e. magnetic susceptibility, coercivity of remanence and IRM saturation values) when a specimen undergoes changes in temperature and/or applied magnetic field.

Isothermal remanent magnetization (IRM) acquisition was tested both for the Kızılkaya and Afyon-Eskişehir ignimbrites (chapter 4). It was performed applying a stepwise increasing external magnetic field through a AGICO PUM-1 pulse magnetizer and measuring the remanent magnetization (J_r) at the end of each step with an AGICO JR-6 spinner magnetometer. When specimen reached the saturation magnetization (J_s), a back-field measurement was performed in order to get the coercivity of remanence B_{cr} . Identification of ferromagnetic phase assemblage was made on the basis of the evaluation of saturation isothermal magnetization (SIRM) and B_{cr} values, following the method proposed by Kruiver et al. (2001). This method evaluates statistically the number of magnetic components and then discriminates the different magnetic phases on the basis of different mineral coercivity. The principle relies on the cumulative log Gaussian analysis, and it is based on the curve fitting of the IRM acquisition curve versus logarithm of the applied field with: (1) The acquisition curve on a linear scale (LAP); (2) The acquisition curve expressed as gradient (GAP); and (3) The acquisition curve on a probability scale (SAP). Low-coercivity phases, such as Ti-magnetite, saturate at low fields (0.1 – 0.3 T) and show low values of the coercivity of remanence B_{cr} , generally $< 50 \text{ mT}$. High-coercivity phases, such as hematite, are not saturated by fields $< 1.5 \text{ T}$ and show high values of B_{cr} , mainly $> 100 \text{ mT}$.

Thermal demagnetization of the IRM components, tested both for the Kızılkaya and Afyon-Eskişehir ignimbrites (chapter 4), was performed according the 3D IRM unblocking technique of Lowrie (1990), by imparting a IRM along three orthogonal directions in three different fields (0.1 T, 0.5 T and 1.5 T) through an AGICO PUM-1 pulse magnetizer. The first IRM, applied along X_1 , should target low coercivity minerals such as Ti-magnetite. The second field, applied along X_2 , should be sufficient to saturate altered magnetite, but not to realign high coercivity phases such as goethite or hematite, which are saturated by field largest than 1.5 T. The composite magnetization can be characterized by determining the blocking temperature spectra for each component. This is done by heating stepwise the specimen in zero field to successively larger temperatures with a

Schonstedt thermal demagnetizer, cooling, and then measuring the remaining magnetization. The magnitude of the three Cartesian components of the remaining remanence, get with a AGICO JR-6 spinner magnetometer, is then plotted versus demagnetizing temperature.

The S-ratio was calculated only for the specimens belonging to the Kızılkaya ignimbrite (chapter 4), in order to better discriminate the magnetic mineralogy. This parameter is the ratio of the IRM acquired in a back-field of a certain magnitude, for this work at 0.1 T and 0.3 T, to the saturation IRM ($S_{0.1\text{ T}} = -\text{IRM}_{0.1\text{ T}} / \text{SIRM}_{1\text{ T}}$; $S_{0.3\text{ T}} = -\text{IRM}_{0.3\text{ T}} / \text{SIRM}_{1\text{ T}}$) (Thompson and Oldfield, 1986). Therefore, the S-ratio represents the difference between the saturation IRM remaining after application of a back-field of a certain magnitude and the fraction of SIRM “harder” than that field.

2.2.2.2 - Natural Remanent Magnetization (NRM)

Most volcanic rocks contain ferro- and ferri-magnetic minerals that record past geomagnetic field in both direction and intensity. Rocks record their NRM through various processes, which have been acting at the moment of their formation (primary magnetization) or during subsequent times (secondary magnetization). Therefore, NRM can be composed by more than a single component, each one representing a different geological and chronological meaning. Aim of the paleomagnetic analysis is recognize and separate the primary magnetization, usually identified with the characteristic remanent magnetization (ChRM), from secondary one(s), thus understating their origin.

Paleomagnetic analyses were performed on the Kızılkaya ignimbrite, and data are reported in chapter 6. In order to isolate the ChRM, two demagnetizing techniques were used:

1. Thermal demagnetization. When heated to a certain unblocking temperature, below the Curie one, grains with relaxation times this short will be in equilibrium with the field, and their magnetization will be null. At least 3-4 pilot specimens for each site were thermally demagnetized at 10-15 steps up to a temperature of 580-600 °C;
2. AF demagnetization. Also in this case, at least 3-4 pilot specimens for each site were AF demagnetized at 8 steps up to a peak-field of 80 mT, by a 2G AF demagnetizer. The results suggested demagnetizing the remaining specimens at 4-5 steps, between 10 and 80 mT.

Data were plotted on Zijderveld diagrams (Zijderveld, 1967), and the ChRM directions were extrapolated. Their site mean values were computed using Fisher’s (1953) statistics or following Engebretson and Beck (1978) technique, respectively if the arrangement of the ChRM directions showed a circular or elongated distribution on stereoplots.

2.2.2.3 - Magnetic fabric

Magnetic anisotropy of a rock depends on both the contribution of all the intrinsic susceptibilities of the magnetic mineral phases (para- and ferromagnetic), both by their spatial disposition within the rock. The main application of magnetic susceptibility measures consists in the study of the magnetic fabric, which is defined by the preferential orientation of the magnetic minerals constituting the rock. Anisotropy of magnetic susceptibility (AMS) measurement has the advantage to be a high resolution, fast (less than 5 minutes for specimen) and low expensive technique. Moreover, they involve rock volumes where hundreds or thousands of grains are measured, so that AMS is a powerful structural tool for determining lineations (K_1) and foliation poles (K_3) of mineral fabrics in ferromagnetic rocks.

The relationship between a small applied magnetic field vector, H , and the induced magnetization vector, J , is the magnetic susceptibility, K , expressed according to the equation:

$$J = K \cdot H \quad (3)$$

Magnetic susceptibility is described by a symmetrical second order tensor, whose diagonal terms (K_{11} , K_{22} and K_{33}) are the eigenvalues, and represent the principal susceptibilities. They are generally indicated as K_1 , K_2 and K_3 : their directions correspond to the axes of a tri-axial ellipsoid (fig. 2.4), whose lengths are proportional to the corresponding eigenvalues. Values of K_1 , K_2 and K_3 can be combined mathematically into different equations, to define some parameters describing the shape of the ellipsoid:

$$P = K_1/K_3 \quad (4)$$

$$L = K_1/K_2 \quad (5)$$

$$F = K_2/K_3 \quad (6)$$

$$T = 2 \ln (K_2/K_3) / \ln (K_1/K_3) - 1 \quad (7)$$

The degree of anisotropy P , whose value is usually low for ignimbrites, is a measure of the iso-orientation of ferromagnetic minerals. L and F describe the shape of the ellipsoid: the first prevails for prolate ellipsoids ($K_1 > K_2 = K_3$), the second for oblate ellipsoid ($K_1 = K_2 > K_3$). Shape parameter T equally describes the shape of the ellipsoid: prolate for $-1 \leq T < 0$, oblate for $0 < T \leq 1$.

Magnetic susceptibility was measured both for the Kızılkaya and Afyon-Eskişehir ignimbrites (chapter 5). Measurements were performed with a AGICO KLY-3 kappabridge, orientating the specimen in 15 different positions in order to reconstruct the susceptibility tensor and get the principal susceptibility directions.

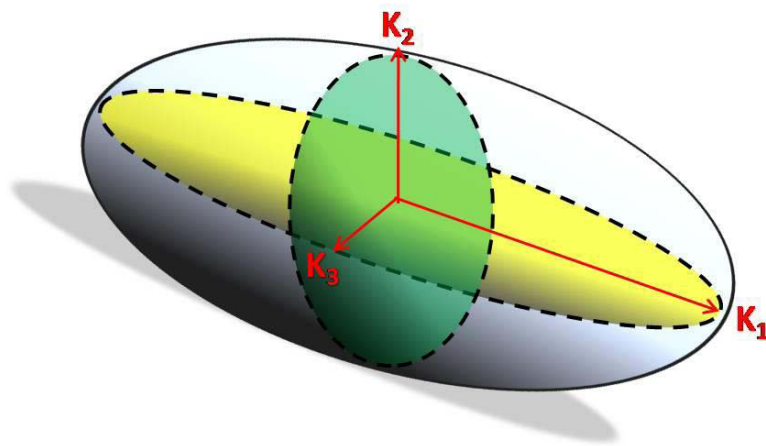


Figure 2.4 – Triaxial ellipsoid of AMS with the principal axes of susceptibility: K_1 = maximum susceptibility axis); K_2 = intermediate susceptibility axis) and K_3 = minimum susceptibility axis).

For ignimbrite rocks, in the case of laminar flow regime, normal fabric is that characterized by an upstream gently dipping magnetic foliation plane (usually $< 30^\circ$) and a lamination aligned along the its plunge direction (field 1 in fig. 2.5; Knight et al., 1986; Hillhouse and Wells 1991; Seaman et al., 1991; Ort 1993; Le Pennec et al., 1998; LaBerge et al., 2009). This type of fabric is referred to be conferred by multi-domain (MD) magnetite grains, which are characterized by shape anisotropy, even if distribution anisotropy cannot be ruled out if grains are unevenly distributed and close enough to interact magnetostatically. Flow direction is considered to be parallel both to the direction of the magnetic foliation pole (K_3) both to the lamination (K_1). In some cases a reverse fabric may occur (field 4 in fig. 2.5), characterized by an exchange between K_1 and K_3 axes. This situation may be ascribed to the occurrence of single-domain (SD) magnetite (Rochette et al., 1999; Palmer and McDonald 2002), whose principal susceptibility axes disposition is opposite with respect to the crystallographic one. Cases of intermediate fabrics (fields 2 and 3 in fig. 2.5) have also been reported (Wiedenmann, et al., 1986; Rochette et al., 1992; Rochette et al., 1999). Its origin is imputed to the presence of silicate phases such as orthopyroxenes and riebeckite, or to the contemporary occurrence of two ferromagnetic minerals which share the susceptibility, resulting in a two-components AMS (Rochette et al., 1999).

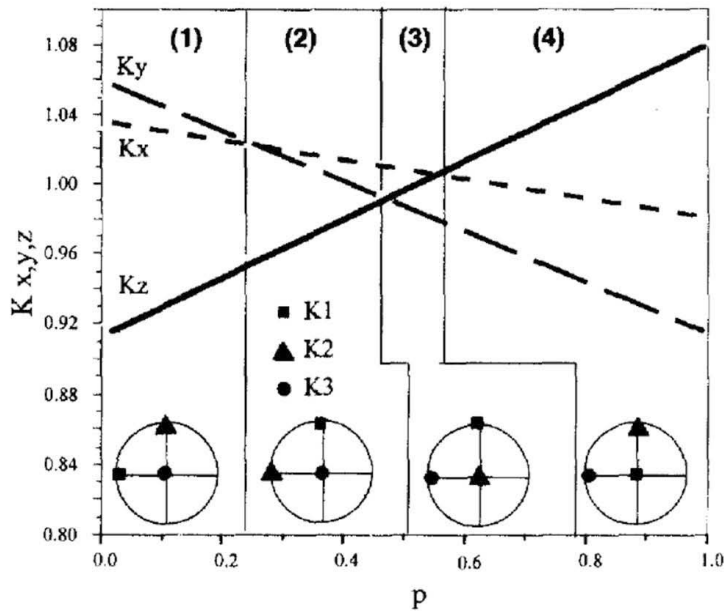


Figure 2.5 – Mixing model of normal and inverse AMS fabric, showing the normalized value of principal susceptibility axes along x, y (structural lineation) and z (pole of structural foliation) as a function of the proportion p of the inverse component (from Rochette et al., 1999).

Eventual occurrence of distribution anisotropy was checked both for the Kızılkaya and Afyon-Eskişehir ignimbrites by performing the Crossover diagrams (Cisowski, 1981), which are reported in chapter 4. These plots represent the acquisition and demagnetization of isothermal remanent magnetization (IRM), and demonstrate the presence of SD (or MD) interacting grains. Indeed, interaction fields between SD (or MD) grains shift the coercivity spectrum to lower values for AF demagnetization and to higher values for IRM acquisition. The intersection point projected on the abscissa approximates the remanent coercive force H_{CR} . Wohlfarth (1958) showed that the R ratio ($R = IRM(H_{CR})/IRM_{max}$) is equal or greater than 0.5 for non-interacting magnetic SD (or MD) grains and is lower than 0.5 for interacting grains. The acquisition curve has been obtained by measuring with the JR6 spinner magnetometer an IRM induced with the AGICO PUM-1 pulse magnetizer from 0 to 500-800 mT along the z -axis of the specimen. The demagnetization curve has been obtained by stepwise AF treatment with peak values in the same range than the acquisition curve.

In order to investigate the orientation of the ferromagnetic minerals, which are the only remanence carriers, measurements of anisotropy of remanence magnetization (both anisotropy of isothermal remanent magnetization, AIRM, and anisotropy of anhysteretic remanent magnetization, AARM) were performed; data are reported in chapter 5. Anisotropy of magnetic remanence is sensitive only to the ferromagnetic fraction irrespectively to the minerals grain size (i.e. SD or MD magnetite crystals).

Measurements procedure for the AIRM was as follows: first, each specimen was tumbling demagnetized using a Molspin AF demagnetizer at 60 or 80 mT peak-field, and then given an isothermal remanent magnetization (IRM) with a steady field of 20 mT, by an AGICO PUM-1 pulse magnet. After measurement with a JR-6 spinner magnetometer, the sequence was repeated

for a total of twelve different positions in order to calculate the anisotropy tensor. The Jelinek (1977) statistics was used to get the anisotropy parameters at each site, and thus the magnetic fabric.

Anisotropy of anhysteretic remanent magnetization (AARM) was measured for one locality of the Kızılıkaya ignimbrite according to the following procedure: the specimens were first tumbling demagnetized in a peak AF of 100 mT, which was enough to erase the initial NRM carried by Ti-magnetite. Then the ARM was given by a bias direct field of 0.1 mT applied during static AF demagnetization. As before, the procedure was repeated in twelve different positions. Three runs were done: one was intended to study the ARM of the low-coercivity fraction of the ferromagnetic grains, with the bias field applied in the window 40-0 mT; one to study the high-coercive fraction, with the bias field in the window 100-40 mT, and one to study the whole of the grains, in the window 100-0 mT.

2.2.3 - Geochronologic datings

U-Pb sample preparations and analyses were performed on the zircon crystals contained in the ignimbrite deposits at Laboratoire Magmas et Volcans under the supervision of Jean-Louis Paquette (LMV, Clermont-Ferrand, France). ^{40}Ar - ^{39}Ar dating was performed on plagioclase crystals contained in lava; samples were prepared and analyzed at Laboratoire des Sciences du Climat by Hervé Guillou (LSCE, CEA, Gif-Sur-Yvette, France).

Zircon represents a robust chronometer and indicator mineral to date rocks, since it reliably dates crystallization in a magma and is unaffected by post-magmatic heating or alteration, constituting a closed system to the surrounding environment. However, zircons sometimes display significant pre-eruptive residence or recycling, and because of their occurrence in silicic magmas, they strictly provide the maximum age of the eruption. $^{40}\text{Ar}/^{39}\text{Ar}$ dating can yield reliable eruption ages, but the K-Ar decay system can be more disturbed than zircon (e.g. by excess ^{40}Ar , or K mobility; Cerling et al., 1985; Hora et al., 2001), therefore it is essential that rocks have not been suffered substantial alteration over the geological time.

U-Pb dating was performed on zircon crystals contained both in pumice clasts and in whole rock sampled from the Afyon-Eskişehir ignimbrite succession. Samples were collected in the field manually or using a rock hammer and cataloged, for a total of 10 samples. Mineral separation to extract zircons from the samples consisted in crushing, sieving, a Wilfley table, a magnetic separator and heavy liquids. Before crushing, hand samples were preliminary broken into smaller pieces; pumice clasts were directly crushed in the machine. For each sample, crushing and successive sieving were made at three steps of increasing degrees of grinding, in order to obtain a

very fine granulometry comparable to dimensions of zircon crystals. After that, crushed samples were reversed on a Wifley table and collected the heaviest mineral fraction, which was put in an oven to dry. Magnetic separation was performed manually using a magnet; zircon crystals were therefore recognized using an optical microscope, crystals were picked-up and collected to be subsequently analyzed by laser ablation-inductively coupled plasma-mass spectrometry (LA-ICP-MS). Analyses involved the mineral ablation at spot diameters of 26 μm and 44 μm ; the ablated material was carried into helium and then mixed with nitrogen and argon before injection into the plasma source. Calculated ratios were exported and concordia ages and diagrams were generated using the Isoplot/Ex v. 2.49 software package of Ludwig (2001). Zircon analyses were projected on $^{207}\text{Pb}/^{206}\text{Pb}$ vs. $^{238}\text{U}/^{206}\text{Pb}$ plots (Tera and Wasserburg, 1972; Claoué-Long et al., 1995; Jackson et al., 2004), from where the zircon age has been determined.

3 – Afyon-Eskişehir ignimbrites: Field data

3.1 Stratigraphy

The region located between the cities of Afyon, to the south, Eskişehir, to the north, and Kütahya to the west, exposes a thick pyroclastic succession, whose deposits have been investigated over a $\approx 14,300 \text{ km}^2$ area in order to reconstruct the volcanic stratigraphy by the identification and correlation of ignimbrite units, estimate the areal extension and volume of the deposits, constrain the eruptive source by the analysis of sedimentary characteristics of the flow and fall deposits (clasts size, thickness and sedimentary structures) and the analysis of the magnetic fabric (AMS and AIRM).

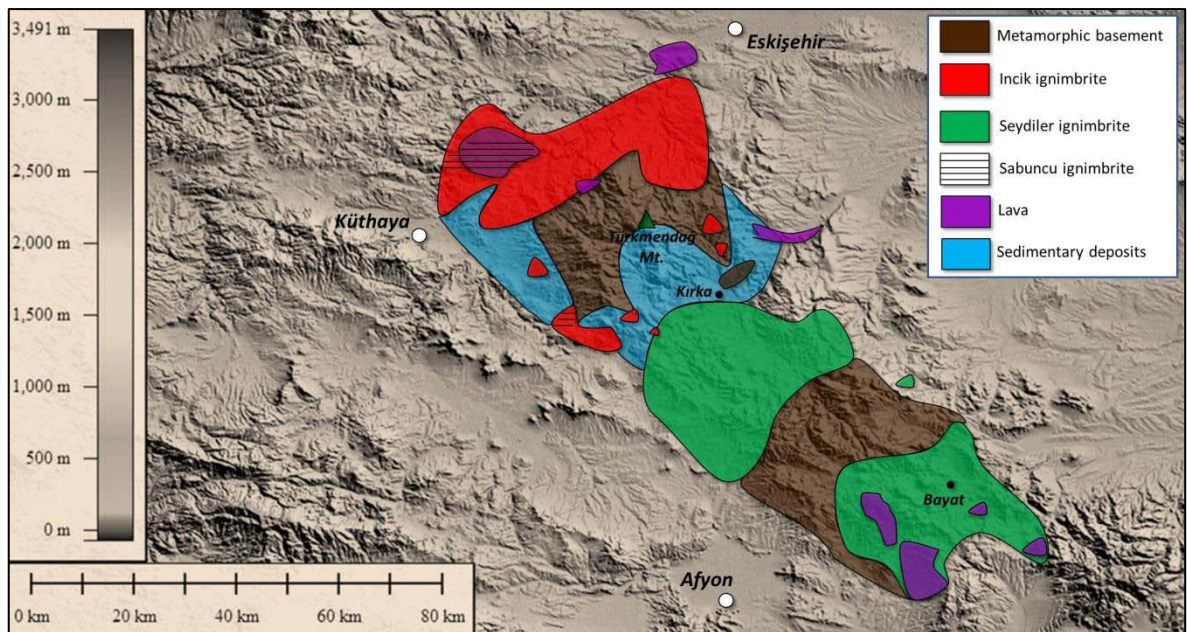


Figure 3.1 – Schematic areal distribution map of the pyroclastic deposits cropping out in the area between Afyon and Eskişehir.

Pyroclastic deposits cropping out in the region of Afyon-Eskişehir constitute a thick succession composed by a series of ignimbrite units and relative fall layers interbedded with surge and volcanoclastic deposits and overlain by limestone deposits and lava. Stratigraphic analysis performed in the present research revealed the presence of three distinct ignimbrite units groups, with different age, mineralogical composition and related to different sources (fig. 3.2): the Incik ($18.866 \pm 0.071 \text{ Ma}$; U-Pb dating) and Sabuncu ($9.43 \pm 0.09 \text{ Ma}$; U-Pb dating) ignimbrites are exposed in the northern area of the study region between the cities of Eskişehir, Kütahya and Kirka, and are related to a caldera source between Kirka city and the Türkmenadağ basaltic complex; the Seydiler ignimbrite (older than 14.8 Ma ; Ar-Ar dating) is exposed in the southern area between the cities of Afyon, Bayat and Kirka, and is related to a source in the proximity of Bayat (fig. 3.1). Ignimbrites are constituted by several flow units, some of them characterized by multiple eruption

stages. Incik ignimbrite (fig. 3.3 a) is formed by a lower Incik 1 unit, composed by 3 sub-units separated by fall and/or surge layers: Incik 1a, Incik 1b and Incik 1c, and an upper Incik 2 unit. It is widespread distributed over the northern part of the study region, where it constitutes the thickest ignimbrite. The Sabuncu ignimbrite comprises two main flow units, Sabuncu 1 and Sabuncu 2, exposed in the western part of the northern area toward the city of Kütahya, where the lava sheets locally cap the ignimbrite succession. Seydiler ignimbrite (fig. 3.3 b) is made up of two main units, Seydiler 1 and Seydiler 2, comprising multiple small and local sub-units. A sequence of surge and pumice fall layers is interbedded between Seydiler 1 and Seydiler 2 units.

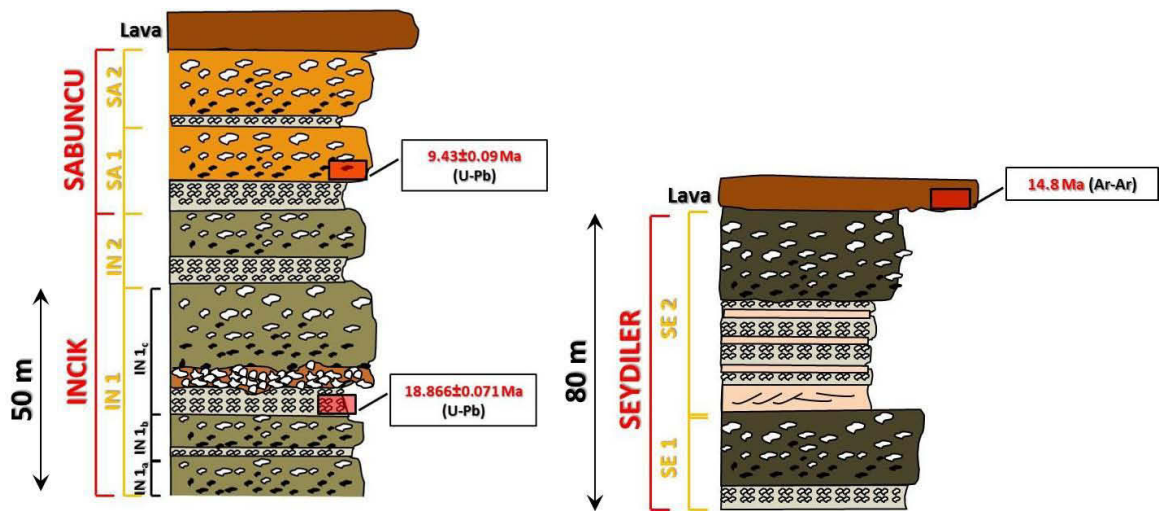


Figure 3.2 – Generalized stratigraphic sections of the Incik, Sabuncu and Seydiler ignimbrites. Representation is not in scale; thicknesses are indicative. Graphic symbols: as in table 3.1.

The contact between Incik and Sabuncu ignimbrites is observed at few localities in the area of Kütahya, the one between Incik and Seydiler ignimbrites is only observed in the proximity of the village of Ovacık, between Kütahya and Kırka, where the Incik 2 unit is separated from Seydiler 1 ignimbrite by limestone deposits.

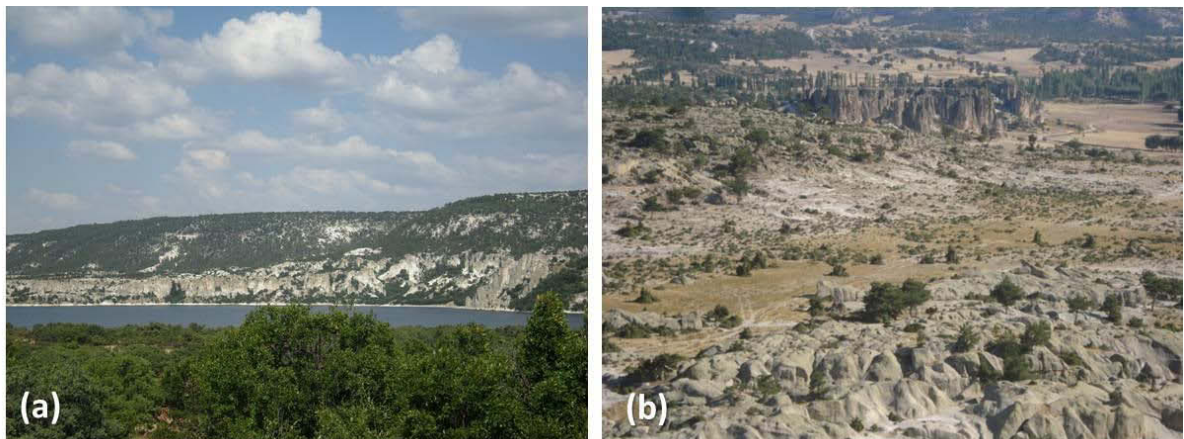


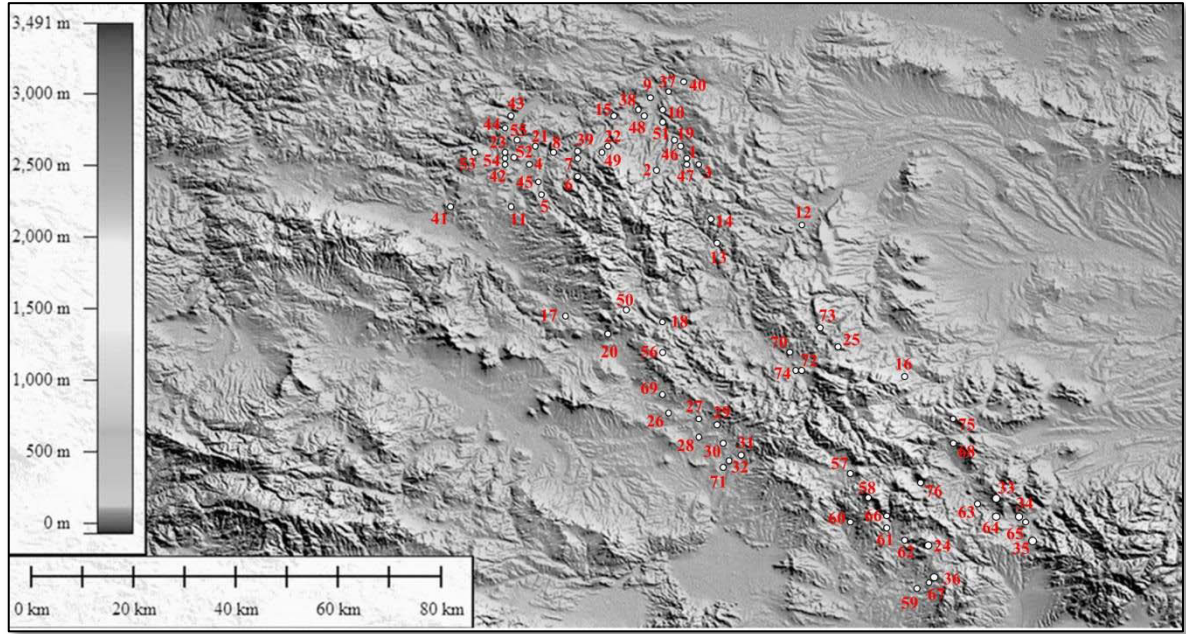
Figure 3.3 – Aspect of the Incik ignimbrite exposed in the area between Kütahya and Eskişehir along the Porsuk river (a) and Seydiler ignimbrite near the village of Bayramaliler (b).

The base of the ignimbrite succession is visible at few localities. In the area of Afyon, the base of the Seydiler ignimbrite is observed at the village of Kale and near the village of Kayı, where the metamorphic basement crops out. The base of the Incik ignimbrite is exposed near the village of Üçsaray, at the margin of the caldera, where the contact between Incik 1 ignimbrite and the magmatic chamber rock crops out. Welding has not been observed in the Incik and Sabuncu ignimbrites; varies from incipient to moderate in Seydiler 2 ignimbrite, particularly in proximal facies and in the Frig Valley close to Yazılıkaya. A slightly inclined regional tilt characterized by a SW plunge is observed at many places.

Stratigraphic measurements were performed at 76 locations (fig. 3.4) and consisted in the evaluation of clasts size and thickness of the deposits, which led to the realization of stratigraphic correlations and isopach and isopleth maps of the pyroclastic flow and fall units.

Ignimbrites were distinguished according to several criteria based on macroscopical features of the juvenile clasts (phenocrysts type and content, shape, color and pumice vesiculation degree) and structure of the flow deposit (detailed description of each ignimbrite unit is given in next paragraphs), specifically:

- a. features of the pumices contained in the flow deposit. The Incik ignimbrite is characterized by the variation from aphyric (Incik 1a, Incik 1b and lower portion of Incik 1c) to porphyric pumices (upper portion of Incik 1c and Incik 2), with a phenocrysts content of biotite and minor quartz. The Sabuncu ignimbrite contains porphyric pumices with phenocrysts of biotite, quartz and minor K-feldspar. Pumice phenocrysts content of Seydiler ignimbrite is represented by K-feldspar, quartz and minor biotite; peculiar is the occurrence of perlitic obsidian within the pumices;
- b. structure and texture of the pumice fall deposit. The Incik 1c ignimbrite is associated to a fall deposit made up by three main normally graded aphyric pumice fall layers; massive pumice fall layers underlain Incik 1b sub-unit. The fall deposit associated to Incik 2 unit displays massive porphyric pumice fall layers. Sabuncu 1 fall deposit is made up by three main porphyric and vesiculated pumice fall layers with massive basal and uppermost layers and a reverse graded intermediate layer. Peculiar is the texture of the Sabuncu 2 fall deposit, formed by several layers of highly porphyric bluish juvenile clasts with intermediate structure between pumice and scoriae with a “blocky” shape. Seydiler 2 fall deposit comprises three main slightly porphyric pumice fall layers interbedded with two surge deposit and a basal ash fall layer;



1	<i>Aşağı Ilica</i>	20	<i>Haymana</i>	39	<i>Incik</i>	58	<i>Olukpınar</i>
2	<i>Aklarmaç Çiftliği</i>	21	<i>Fındık</i>	40	<i>Aşağı Çağlan</i>	59	<i>Akkoyunlu</i>
3	<i>Ayvacak</i>	22	<i>Seklice</i>	41	<i>Çalca</i>	60	<i>Karaağaç</i>
4	<i>Doğuluşah</i>	23	<i>Seydiköy North</i>	42	<i>Seydiköy South</i>	61	<i>Karakaya</i>
5	<i>Inli</i>	24	<i>Sağırılı</i>	43	<i>Sofça</i>	62	<i>Seydiler</i>
6	<i>Kayserkale</i>	25	<i>Kayı</i>	44	<i>Karacaören</i>	63	<i>Derbent West</i>
7	<i>Incik</i>	26	<i>Döğer South</i>	45	<i>Sökmen</i>	64	<i>Derbent East</i>
8	<i>Incik-Fındık</i>	27	<i>Bayramaliler</i>	46	<i>Akçakaya</i>	65	<i>Derbent-Kurudere</i>
9	<i>Gökçekısıık</i>	28	<i>Beyköy</i>	47	<i>Yukarı Ilica</i>	66	<i>Keserler</i>
10	<i>Uluçayır</i>	29	<i>Demirli (Eskişehir)</i>	48	<i>Yenisofça</i>	67	<i>Kale South</i>
11	<i>Soğut</i>	30	<i>Kayhan-Demirli</i>	49	<i>Demirli (Afyon)</i>	68	<i>Bayat North</i>
12	<i>Sancar</i>	31	<i>Ayazini</i>	50	<i>Damlalıkaraağaç</i>	69	<i>Döğer North</i>
13	<i>Göknebi</i>	32	<i>Yeşilyayla</i>	51	<i>Akçakaya West</i>	70	<i>Kumbet</i>
14	<i>Üçsaray</i>	33	<i>Derbent</i>	52	<i>Sabuncu West</i>	71	<i>Kayhan</i>
15	<i>Akkaya</i>	34	<i>Kemerkaya</i>	53	<i>Ahmetoğlu</i>	72	<i>Yapıldak</i>
16	<i>Han</i>	35	<i>Avdan</i>	54	<i>Seydiköy</i>	73	<i>Çukurca</i>
17	<i>Göçeri</i>	36	<i>Kale North</i>	55	<i>Sabuncu</i>	74	<i>Yapıldak West</i>
18	<i>Ovacık</i>	37	<i>Karaalan</i>	56	<i>Inlice Mahallesi</i>	75	<i>Bayat-Eskigözü</i>
19	<i>Aşağı Kalabak</i>	38	<i>Yorükkırka</i>	57	<i>Alanyurt</i>	76	<i>Bayat</i>

Figure 3.4 – Map and list of the measured stratigraphic sections.

- c. structure of the flow deposit and lithic clasts content. The Incik 1c ignimbrite often display a widespread distributed fine-depleted zone at its base, which has been considered as a

good quality marker bed, and a lithic rich concentration zone occurs above it. Many reddish banded rhyolite clasts, besides millimetric up to pluri-centimetric dark perlitic obsidian clasts occur in this ignimbrite. Sabuncu ignimbrite does not contain reddish banded rhyolite clasts and perlitic obsidian content in the matrix is very low with a millimetric grain size. Lithic content of Seydiler ignimbrite mainly consists in metamorphic (schist and quartzite) and andesite lithologies.

3.1.1 The Incik ignimbrite

The Incik ignimbrite comprises three main pyroclastic units which include ignimbrite flows and their relative pumice-fall deposits.

Identification and distinction of the different Incik units and sub-units were made on the basis of:

- a. features of the pumices contained in the flow deposit. Lower sub-units (Incik 1a, Incik 1b and the lower portion of Incik 1c) contain aphyric pumices; phenocrysts content gradually increases through Incik 1c up to 20% (biotite and minor quartz phenocrysts). Incik 2 unit contains only porphyric pumices with the same phenocrysts type and content of the upper portion of Incik 1c. Vesiculation tends to increase from lower to upper units;
- b. structure and texture of the pumice fall deposits. The Incik 1b ignimbrite is underlain by two massive and relatively coarse aphyric pumice fall layers, which are locally split into several layers associated to intraplanar flow deposits related to local partial collapses of the ignimbrite cloud. Incik 1c ignimbrite is preceded by a sequence of pumice fall and ash layers composed by three coarser normal graded layers containing low vesiculated aphyric pumice clasts with fibrous and “blocky” shapes. The upper portion of Incik 1c fall deposit is generally characterized by a more pervasive presence of ash fall layers interstratified with thinner and finer grained pumice fall layers. The fall deposit associated to Incik 2 ignimbrite is characterized by a sequence of pumice-fall and ash layers containing porphyric and generally quite vesiculated pumice clasts. Pumice fall layers are massive, with a tendency of max grain size decrease toward the top;
- c. structure of the flow deposit and lithic clasts content. The presence of a widespread distributed fine-depleted zone at the base of Incik 1c unit, followed by a lithic-rich concentration zone in the basal part and diffuse stratified pumice layers (dsLT) in the upper part of the main ignimbrite deposit, permits to distinguish this unit from the other ones. The presence of centimetric black and greenish perlitic obsidian clasts is ubiquitous in Incik ignimbrite, with an increasing content in Incik 1c and Incik 2 units.

3.1.1.1 Type section

Two type sections were chosen for the Incik ignimbrite, since no localities expose a complete section of Incik 1 and Incik 2 units. At a few places (e.g. Haymana and Göçeri) the contact between Incik 1c and Incik 2 crops out, but these sections lack the exposure of the lowermost sub-units, and both ignimbrites both fall deposits are not fully preserved and don't exhibit the typical facies. The selected type section for Incik 1 is exposed near the village of Incik (fig. 3.5 a), the type section of Incik 2 is exposed between the villages of Aklarmaç Çiftliği and Aşağı Kalabak (fig. 3.5 b). These sections exhibit a complete sequence of the Incik units and are considered to represent well the typical facies of the deposits.


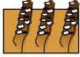









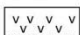
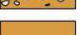





	Pumice clast		Pipes
	Lithic clast		Lava
	Pumice fall deposit		Epiclastic deposits
	Ash fall deposits		Lacustrine deposits
	Surge deposit		Limestone deposits
	Ignimbrite deposit		Silicified facies
	Fine-depleted zone		Welded facies
	Inferred flow direction		
<p>GRADATION (white=pumices; black=lithics)</p>  Normal  Reverse  Ungraded		<p>WELDING</p> <p>uw = Unwelded w = Welded</p>	
<p>LITHOLOGY</p> <p>mlt = Massive lapilli-tuff pml = Massive pumice lapilli //bT = Parallel-bedded tuff dslT = Diffuse-stratified lapilli-tuff lenslBr = Lens of lithic-rich breccia fpoormLT = Fines-poor massive lapilli-tuff</p>			

Table 3.1 – Legend of the stratigraphic sections represented in the following paragraphs. Lithologic terms and abbreviations are those proposed by Branney and Kokelaar (2002).

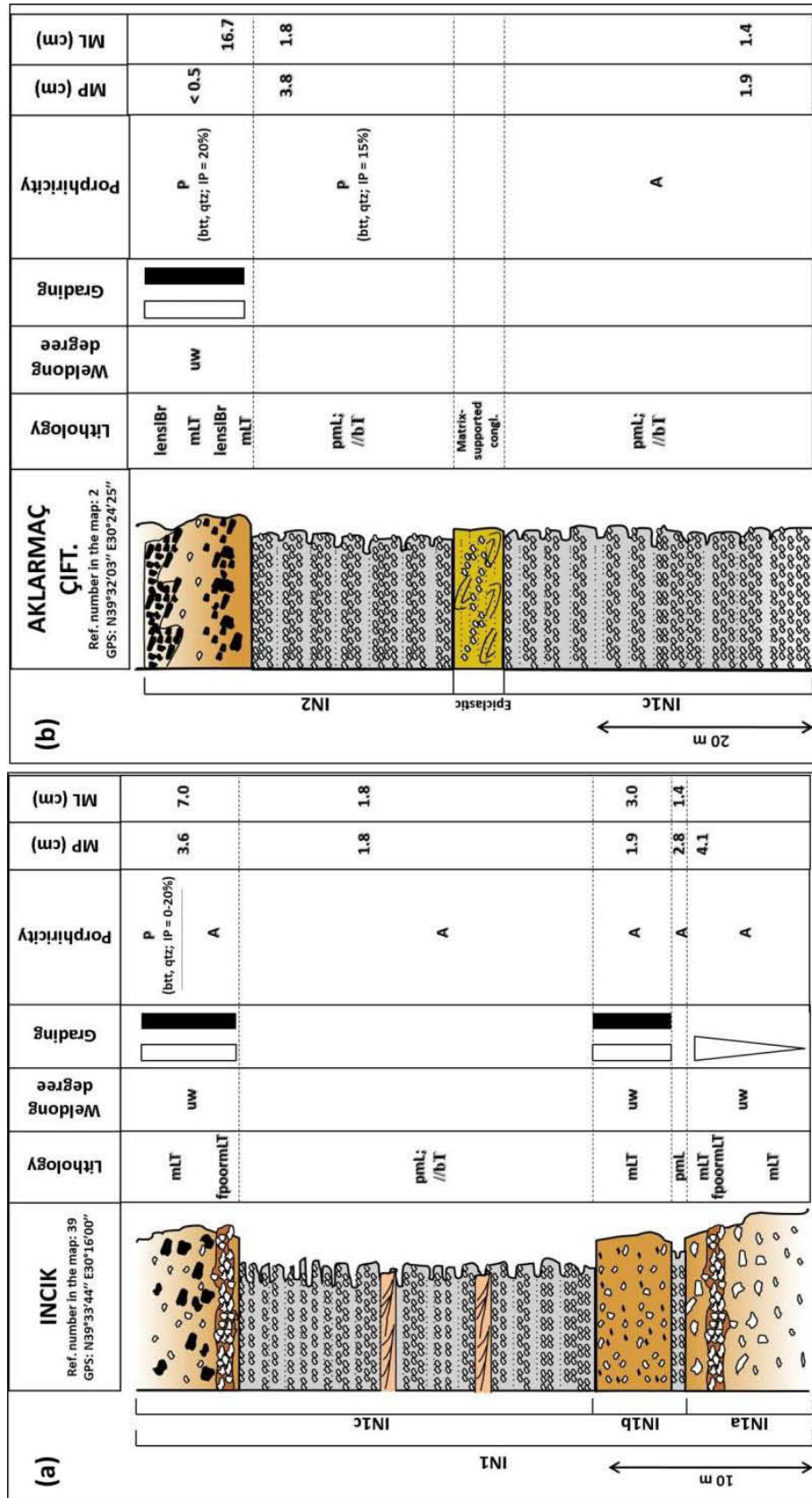


Figure 3.5 – (a) Type section of Incik 1 unit at Incik; (b) Type section of Incik 2 unit at Aklarmaç Çiftliği. Abbreviations: A = aphyric pumices; P = porphyric pumices; MP = maximum pumice; ML = maximum lithic.

INCIK SECTION

The Incik section (fig. 3.5 a; 3.6 a) exposes the flow and fall deposits of Incik 1 unit, from the lower Incik 1a to the upper Incik 1c sub-unit; the very base of Incik 1 unit doesn't crop out.

1. Incik 1a sub-unit

- Main flow deposit. It is exposed the upper pumiceous portion of the ignimbrite deposit, which contains low vesiculated, white to grey colored, “blocky” shaped, aphyric pumice clasts displaying reverse grading. Accessory lithic clasts are absent. In the upper part of the deposit is present a ≈ 20 cm thick fine-poor zone occur, formed by a high concentration of centimetric sub-rounded pumice clasts and millimetric black perlitic obsidian (fig. 3.6 b);

2. Incik 1b sub-unit

- Fall deposit. Three massive, reverse graded, aphyric pumice fall layers interbedded with three ash fall layers, for an overall thickness of 70 cm (fig. 3.6 e);
- Main flow deposit. Massive ignimbrite deposit ≈ 3 meters thick, containing low-medium vesiculated, white, “blocky” shaped, aphyric pumice clasts;

3. Incik 1c sub-unit

- Fall deposit (fig. 3.6 c). Sequence of pumice fall layers intercalated with ash fall and surge layers for an overall thickness of 17 m. The deposit contains three coarser grained, normal graded pumice fall layers in the lower, central and upper portion. Pumice fall layers tend to thin in the upper part of the deposit, where the occurrence of ash fall layers is more pervasive. Pumice clasts are white colored, aphyric with low-middle vesiculation degree and generally have a “blocky” shape. Occurrence of two centimetric levels of ash containing accretionary lapilli in the central and lower portion of the deposit;
- Main flow deposit. It is exposed the lower and intermediate portion of the ignimbrite, characterized by a lower lithic rich zone above a basal fine-poor zone (fig. 3.6 d). Lithic clasts are mainly represented by centimetric banded rhyolites displaying a normal grading, and millimetric-up to centimeter black perlithic obsidian, whose content increases toward the top. White, fibrous pumice clasts are aphyric in the lower portion; phenocrysts content gradually increases and become porphyric in the central portion (PI=10%; biotite and minor quartz). Vesiculation degree increases vertically through the deposit.

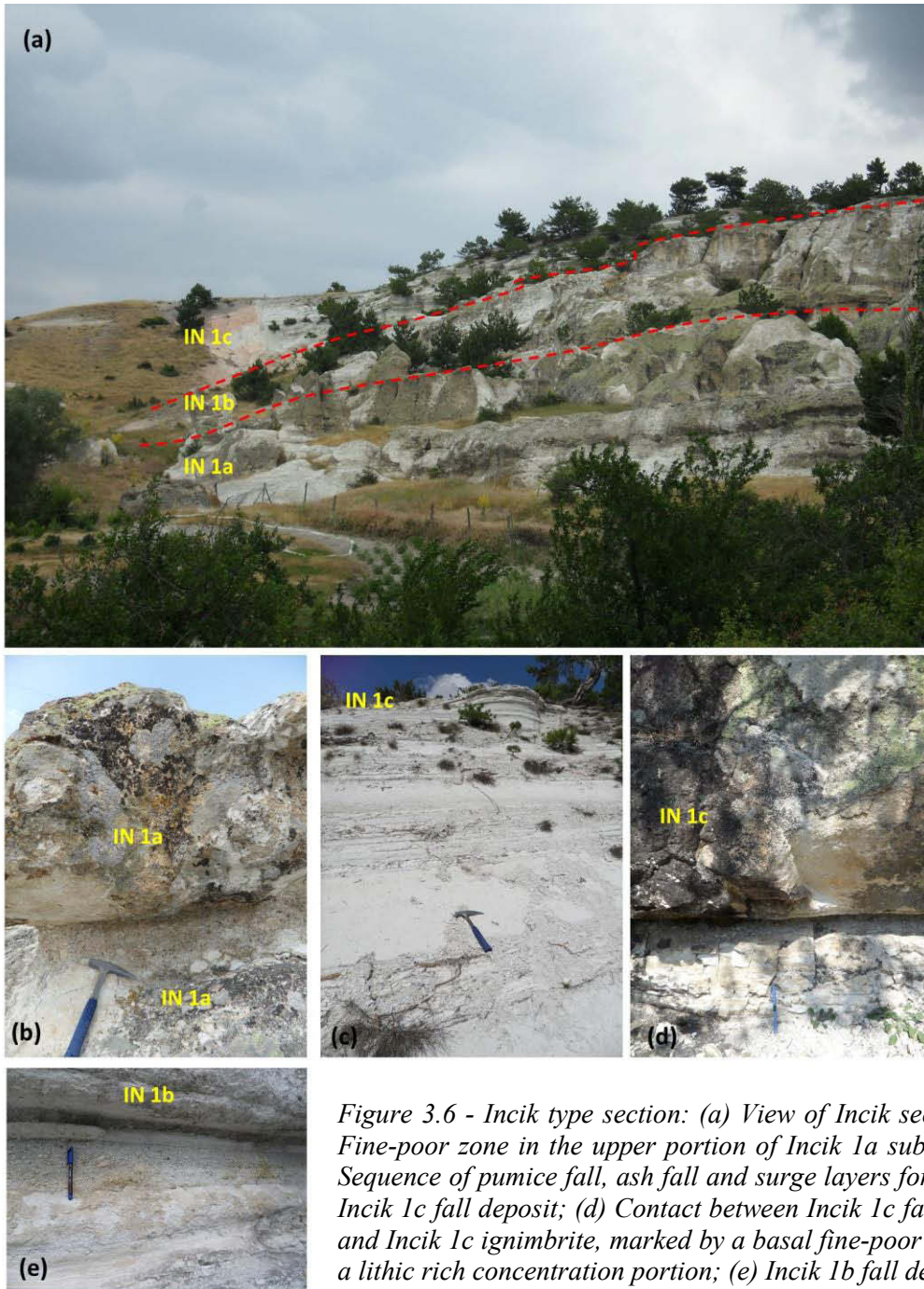


Figure 3.6 - Incik type section: (a) View of Incik section; (b) Fine-poor zone in the upper portion of Incik 1a sub-unit; (c) Sequence of pumice fall, ash fall and surge layers forming the Incik 1c fall deposit; (d) Contact between Incik 1c fall deposit and Incik 1c ignimbrite, marked by a basal fine-poor zone and a lithic rich concentration portion; (e) Incik 1b fall deposit.

AKLARMAÇ ÇİFTLİĞİ SECTION

The Aklarmaç Çiftliği section (fig. 3.5 b; 3.7 a) exposes the fall deposit of Incik 1c unit and the fall and flow deposits of Incik 2 unit.

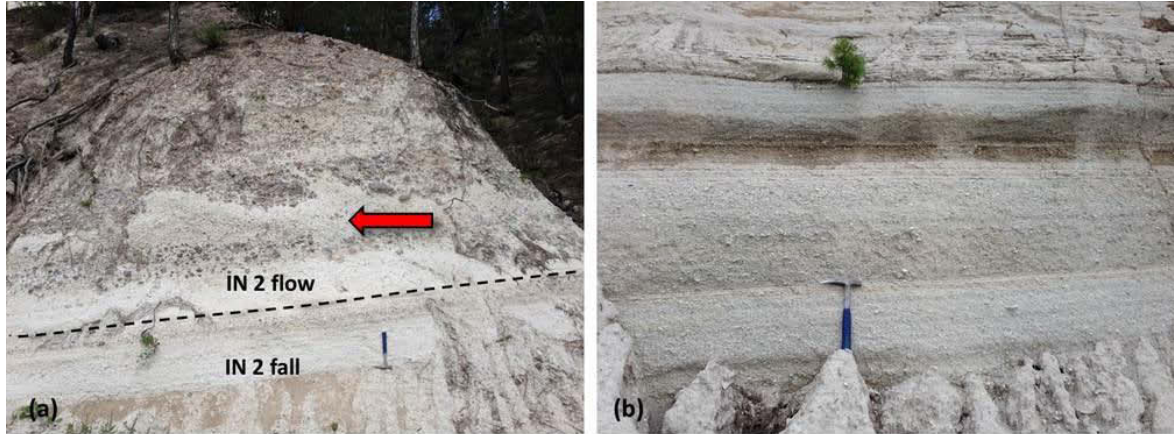


Figure 3.7 – Aklarmaç Çiftliği type section: (a) Incik 2 fall and flow deposit; (b) Pumice fall layer forming the Incik 2 fall deposit. Arrow indicates the inferred flow direction.

1. Incik 1c sub-unit

- Fall deposit. Sequence of pumice fall layers intercalated with ash fall layers for an overall thickness greater than 30 m (the base is not exposed). Pumice fall layers tend to thin in the upper part of the deposit, where the occurrence of ash fall layers is more pervasive. Pumice clasts are greenish, aphyric with low vesiculation degree and have a “blocky” shape;

2. Incik 2 unit

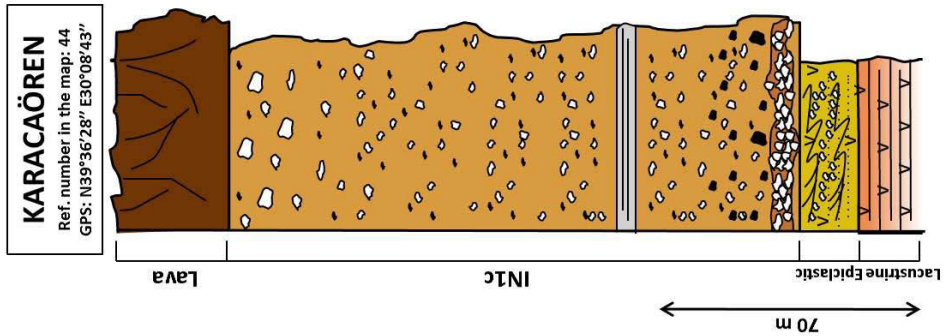
- Fall deposit. Incik 2 fall deposit is separated from the underlying Incik 1c fall deposit by ≈ 5 m of fluvial sediments. The fall deposit is about ≈ 20 m thick and it is composed by a sequence of pumice fall layers intercalated with ash fall layers. Pumice clasts are greenish, porphyric (PI=15%; phenocrysts of biotite and minor quartz) and moderately vesiculated (fig. 3.7 b);
- Main flow deposit (fig. 3.7 a). The Incik 2 ignimbrite is formed by a lower and an upper lithic-rich portion interbedded by relatively fine grained ignimbrite deposit. The upper lithic rich portion forms asymmetric lithic pockets structures (vergence direction: N188; fig. 3.7 a) and displays imbricated lithic clasts (plane dip direction/inclination: 120/38). Pumice clasts are greenish, moderately vesiculated and porphyric (PI=15%; phenocrysts of biotite and minor quartz).

3.1.1.2 Lateral facies variations

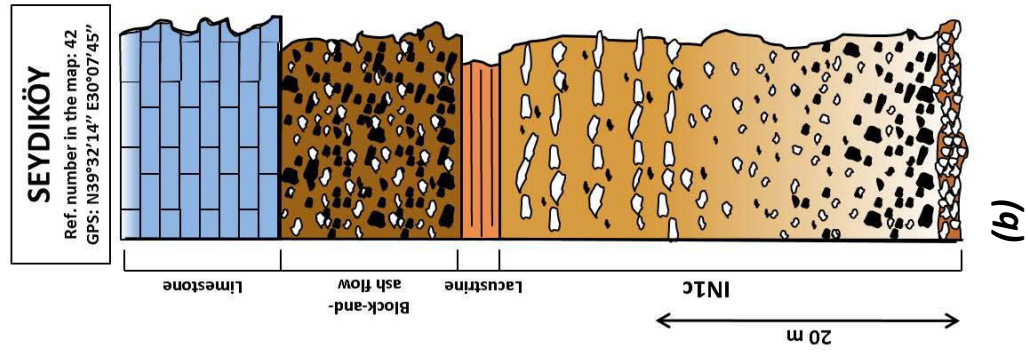
The Incik ignimbrite deposits are well preserved and laterally sub-continuous in the area north-east from Kütahya, where presence of lava sheets and limestones preserve the ignimbrite from erosion. Further to the east, specifically south from Eskişehir, the deposits are more eroded, discontinuous, and generally overlain by reworked detritic deposits. Incik 1 unit is widespread distributed over the whole investigated area, Incik 2 unit is less extended and mainly exposed in restricted areas in the proximity of northern margin (Aklarmaç Çiftliği, fig. 6.4 b) and southern margin of the caldera (Göçeri, Haymana, Ovacık and Damlalıkaraağaç).

The very base of Incik ignimbrite is visible only at Üçsaray (fig. 3.8 g; fig. 3.10 a-1), where the contact between the intrusive rock and the ignimbrite crops out. Contact with the metamorphic basement, where ignimbrite and schists are juxtaposed, crops out at several places (e.g. south of Akçakaya, Seklice, Demirli, north of Incik and Akkaya).

Thick sequences of fall deposits related to Incik 1c and Incik 2 units are exposed in the southern edge of Incik ignimbrite outcropping area. The thickest Incik 1c fall deposit was measured at Kayserkale (fig. 3.9 a-c), where 32 meters of tephra fall layers overlain the Incik 1a ignimbrite, which is 40 meters thick. Here, the fall deposit is formed by 25 m of intercalated pumice and ash fall layers (MP=2.1 cm, ML=1.8 cm; fig. 3.9 c) overlain by 7 meters of stratified ash fall deposit. The Incik 1c ignimbrite overlains the fall sequence (fig. 3.9 b). Thick Incik 1c fall deposits have also been measured at Aklarmaç Çiftliği (>30 m), Ayvacık (20 m; MP=1.6 cm, ML=0.9 cm; fig. 3.8 f), Incik (17 m; fig. 3.5 a), Han (>10 m; MP=2.4 cm, ML=0.3 cm) and Sancar (>9.21 m; MP=5.0 cm, ML=3.3 cm; fig. 6.7 c). At several places Incik 1c fall is overlain by 5 to 7 m of volcanoclastic deposits which separate it from Incik 2 fall. This is observable at Aklarmaç Çiftliği and Aşağı Ilica, where Incik 2 fall deposit reaches the maximum thickness (respectively 20 and 10 m). At Aşağı Ilica, 4.9-m-thick Incik 1c fall layers (pumice clasts are greenish, aphyric and show a “blocky” shape) are intercalated with intraplinian flow deposit and overlain by ash levels containing accretionary lapilli and a lahar deposit (fig. 3.8 e; fig. 3.9 d).



IN1c- Lithology and structure: $mLT_{(ol, ip)}$ deposit with a thick basal fine-depleted zone (thickness=3 m). Occurrence of a lower lithic-rich portion. Pinkish matrix contains a lot of perlitic obsidian whose amount increases toward the top. Pumice mineralogy and texture: white pumices; phenocrysts content increase from the lower portion (aphyric) to the upper portion (biotite and quartz phenocrysts; IP=10%). Rounded pumice clasts in the main deposit, angular clasts in the fine-depleted zone. Clasts dimension: MP=8.4 cm; ML=4.5 cm



IN1c – Lithology and structure: $mLT_{(ol, ip)}$ deposit with a basal fine-depleted zone. The deposit is formed by a lower lithic-rich portion and an upper portion characterized by diffuse stratified pumice layers (dslT). Pinkish matrix contains great amounts of perlitic obsidian. Pumice mineralogy and texture: phenocrysts content increase from the lower portion (aphyric) to the upper portion (biotite phenocrysts; IP=5-10%). Pumice clasts in the lower portion often contain obsidian bands. Clasts dimension: MP=12.4 cm; ML=7.3 cm

HAYMANA
 Ref. number in the map: 20
 GPS: N39°14'36" E30°19'21"

IN2

- FLOW DEPOSIT - Lithology and structure: $mLT_{(pl)}$ indurated deposit; pinkish matrix. Pumice mineralogy and texture: white and grey porphyric pumice clasts (phenocrysts of quartz and K-feldspar; IP=20%), isotropic shape, middle-high vesiculation degree and rounded. Clasts dimension: MP=7.3 cm; ML=4.9 cm

• FALL DEPOSIT – Pumice fall layers interbedded with ash fall layers toward the top. Normal graded, porphyric pumice clasts. MP=0.9 cm; ML=0.7 cm

IN1c - Lithology and structure: $mLT_{(pl)}$ deposit, interbedded by a surge and pisolitic ash fall layer. Pumice mineralogy and texture: white porphyric pumice clasts (phenocrysts of quartz and K-feldspar; IP=5% in the lower portion, increasing up to 15% in the upper portion), medium-high vesiculation degree and rounded. Pumice clasts are both elongated with a fibrous structure and isotropic. Clasts dimension: MP=4.2 cm; ML=4.0 cm

(c)

INLI
 Ref. number in the map: 5
 GPS: N39°29'12" E30°12'12"

IN1c₂ - Lithology and structure: $mLT_{(pl)}$ deposit with a basal fine-depleted zone showing an erosional surface contact with the underlying ash fall deposit. Occurrence of a lower lithic-rich portion. Great amounts of perlitic obsidian in the matrix. Pumice mineralogy and texture: pumices are white and aphyric. Clasts dimension: MP=7.6 cm; ML=6.6 cm

IN1c₁

- FLOW DEPOSIT - Lithology and structure: mLT deposit. Pumice mineralogy and texture: white aphyric pumices.
- FALL DEPOSIT – Pumice fall layers interbedded with ash fall layers and cross stratified surge deposits. Two coarser grained layers are found at the base and at the top of the deposit; aphyric pumice clasts. MP=1.4 cm; ML=1.0 cm

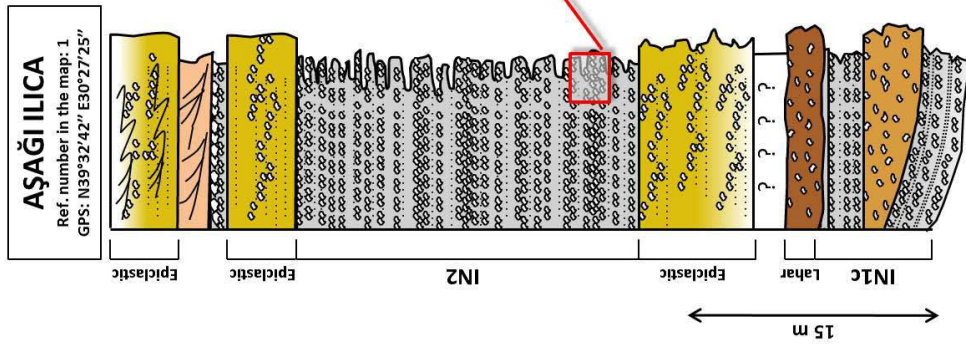
IN1b

- FLOW DEPOSIT - Lithology and structure: mLT deposit with a basal fine-depleted zone. Pumice mineralogy and texture: white aphyric pumices. Clasts dimension: MP=4.0; ML=4.8
- FALL DEPOSIT – Two main massive pumice fall layers interbedded with ash fall layers. Aphyric pumice clasts

IN1a – Lithology and structure: mLT deposit pervasively silicified; presence of pipe structures; pinkish matrix. Pumice mineralogy and texture: aphyric, fibrous and often silicified pumices. Clasts dimension: MP=7.8; ML=1.4

(d)

99



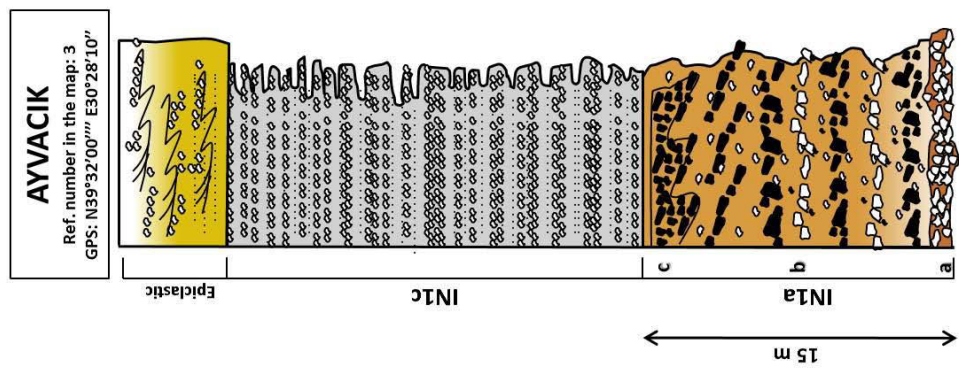
Pumice fall layer formed by a lower fine grained lithic poor portion and an upper coarse grained lithic rich portion. High vesiculated pumice clasts containing few phenocrysts of quartz and minor biotite. MP=4.6 cm; ML=3.0 cm

IN2 - Sequence of pumice fall layers intercalated with ash fall layers. White, porphyric (quartz and biotite phenocrysts), normal graded and low vesiculated pumice clasts. Presence of levels formed by perlitic obsidian fragments. MP=1.4 cm; ML=1.4 cm

Age: 18.89±0.16 Ma (U-Pb; pumices)

IN1c - Sequence of pumice fall layers intercalated with ash fall layers and intraplinian flow deposit. Greenish, aphyric, non vesiculated and "dense" structure-type pumice clasts. Fall layers contain a great amount of crystals. Deposit doesn't display gradation. MP=2.0 cm; ML=1.2 cm

(e)



IN1c - Sequence of pumice fall layers intercalated with ash fall layers. Ash fall layers increase and thicken toward the top. Two coarser grained layers are found near the base and toward the top of the deposit. Greenish, aphyric and "dense" structure-type pumice clasts. MP=1.6 cm; ML=0.9 cm

IN1a - Lithology and structure: (a) basal fine-depleted zone, overlain by (b) mLT deposit characterized by 30-40 cm thick pumice- and lithic-rich layers with lithic clasts imbrication in the middle-upper portion, and (c) lithic pockets structures in the upper portion. Presence of perlitic obsidian in the matrix. Pumice mineralogy and texture: white, aphyric, low vesiculated and fibrous pumice clasts. Clasts dimension: MP=5.6 cm; ML=12.1 cm

(f)

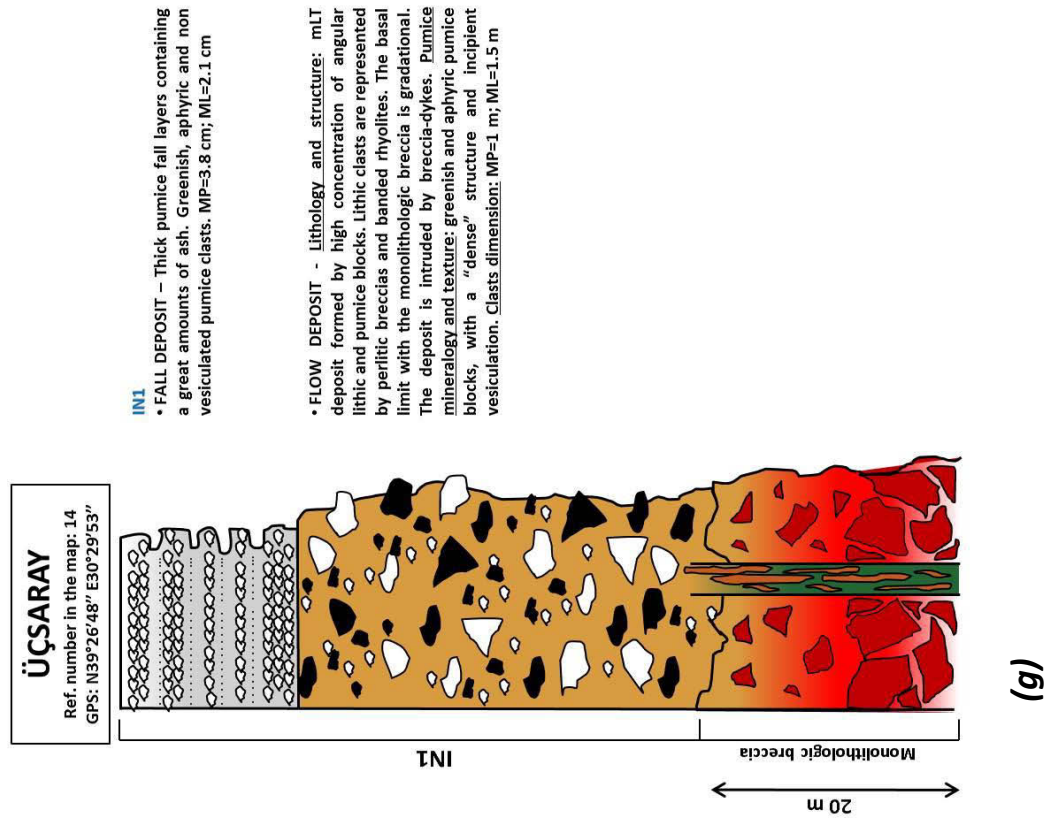


Figure 3.8 – Lateral facies variation of the Incik ignimbrite: (a) Karacaören section; (b) Seydiköy section; (c) Haymana section; (d) Inli section; (e) Aşağı Ilica section; (f) Ayvacık section; (g) Üçşaray section. Symbols: as in table 3.1.

Above, volcanoclastic deposits separate Incik 1c unit from the tephra fall deposit of Incik 2, formed by a sequence of white, porphyric and strongly vesiculated pumice fall layers interbedded with perlitic obsidian rich levels toward the top. At Ayvacık volcanoclastic deposits overlain the Incik 1c fall deposit which contains the same type of pumice clasts of Aşağı Ilica, but the fall layer of Incik 2 doesn't crop out. The lowermost sub-units fall deposits are mainly exposed in the south-western part of the investigated area. Incik 1b fall deposits are exposed at Söğüt, Sökmen, Inli (fig. 3.8 d) and in the area between Incik and Fındık. Incik 1a fall deposit does not crop out.

The Incik ignimbrite thickness is maximum along the Porsuk valley (170 m at Karacaören; >65 m at Sofça), where only the Incik 1c ignimbrite occurs; thickness is also considerable (>77 m; fig. 3.8 c) at Haymana where both Incik 1c and Incik 2 ignimbrites occur, Fındık (64 m; fig. 3.17), Aşağı Kalabak (>45 m) and Kayserkale (>40 m). The ignimbrite is nowhere welded, even at proximal facies.

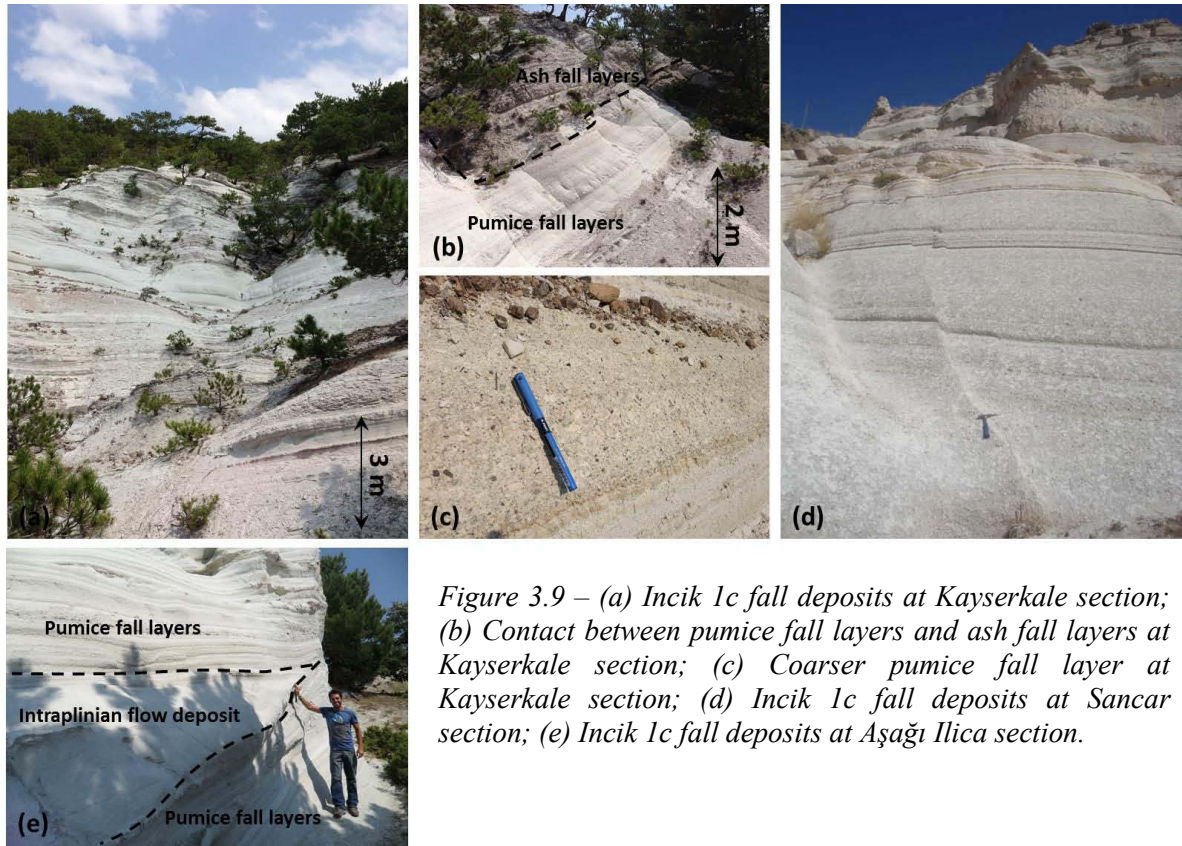


Figure 3.9 – (a) Incik 1c fall deposits at Kayserkale section; (b) Contact between pumice fall layers and ash fall layers at Kayserkale section; (c) Coarser pumice fall layer at Kayserkale section; (d) Incik 1c fall deposits at Sancar section; (e) Incik 1c fall deposits at Aşağı Ilica section.

Proximal facies ignimbrite exposures are found at Üçsaray and Göknebi. At Üçsaray, the section shows the contact between Incik 1 ignimbrite and a brecciated monolithologic cumulate, containing crystals of plagioclase, biotite, amphibole, pyroxene within a glassy matrix (fig. 3.10 a). The ignimbrite matrix at this level infiltrates the fractures of the breccia (fig. 3.10 a, h) and vertically gradually passes to ordinary ignimbrite deposits, characterized by chaotic breccia of angular shaped pumice and lithic blocks (MP \approx 1 m, ML \approx 1.5 m; fig. 3.10 i, l). Pumice blocks are greenish, aphyric, dense and foliated (fig. 3.10 j). Juvenile clasts contained in the deposit show different textures reflecting all the transition of increasing vesiculation degree from the very dense and incipiently inflated green perlitic obsidian to poorly vesiculated and slightly more inflated pumice clasts. Lithic blocks are essentially represented by green perlitic obsidian and reddish banded rhyolite clasts (fig. 3.10 f, g). The ignimbrite deposit is faulted (fig. 3.10 i), intruded by syn-depositional irregular trending dacitic and rhyolitic breccia-dykes (fig. 3.10 c, e) and by post-depositional rhyolite dome extrusions (fig. 3.10 b, k). In the upper portion of the deposit a sequence of pumice fall layers intercalated with many ash fall layers occurs (fig. 3.10 d); pumice clasts are greenish, aphyric, dense and with a “blocky” shape (MP=3.8 cm; ML=2.1 cm).

At Göknebi, 5 meters of pumice and ash fall layers (MP=2.5 cm; ML=1.6 cm) precede the 4-m-thick Incik 1 ignimbrite which contains aphyric, dense and angular pumice clasts (MP=40 cm) such as at Üçsaray, followed by lacustrine limestone deposits.

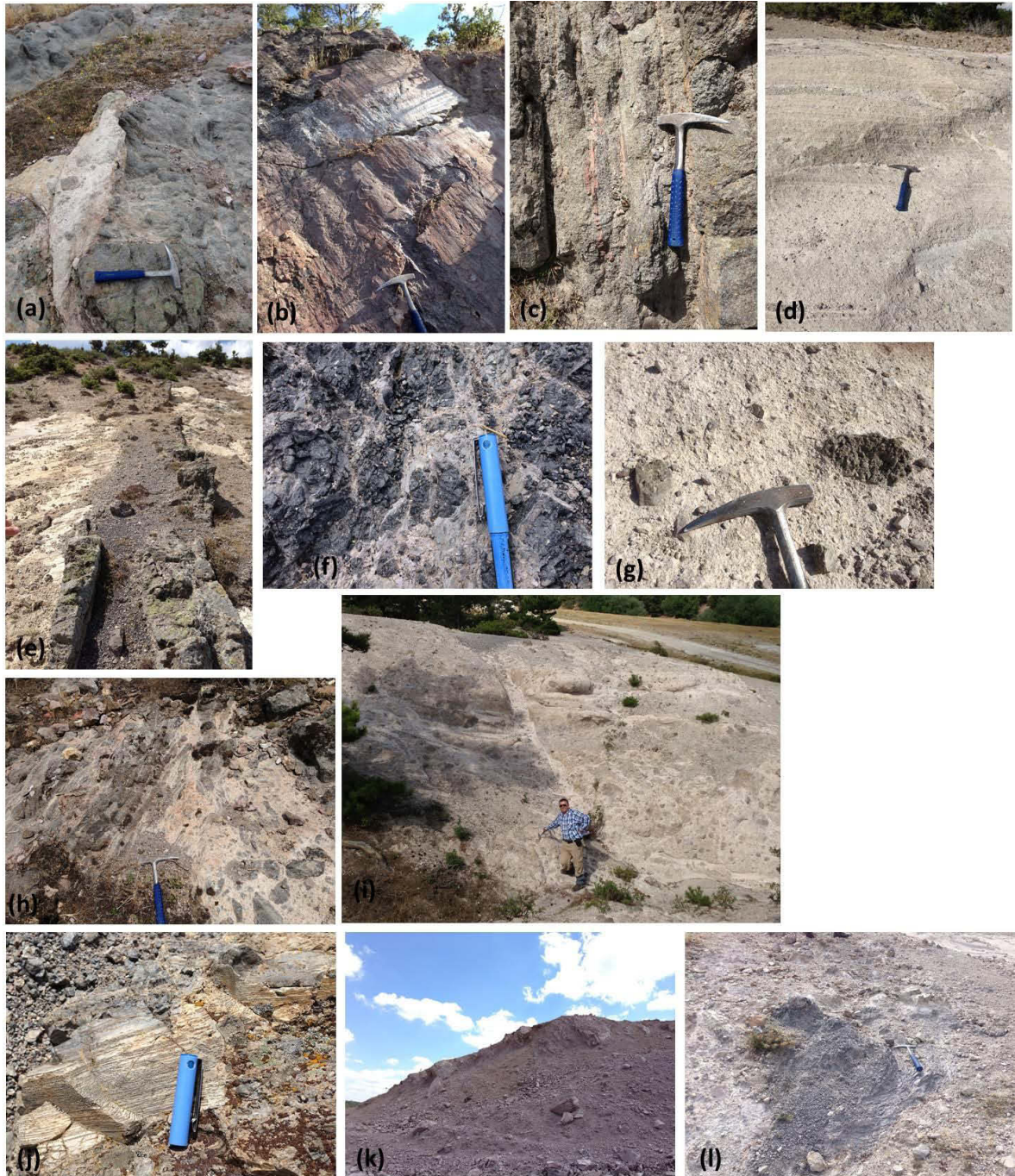


Figure 3.10 – Aspect of the proximal facies of the Incik ignimbrite at Üçsaray. (a) Monolithologic cumulate forming magma chamber rock; (b) Faulted post-depositional rhyolite dome intrusion; (c) Dacitic and rhyolitic breccia-dike; (d) Pumice and ash fall layers overlaying the ignimbrite deposit; (e) Breccia-dyke intruding ignimbrite deposit; (f) and (g) Green perlitic obsidian clasts within the ignimbrite deposit; (h) Ignimbrite infiltration in the cumulate breccia; (i) Faulted ignimbrite deposit; (j) Aphyric, foliated and angular pumice clast; (k) Rhyolitic dome; (l) Metric perlitic obsidian block within the ignimbrite deposit.

Outflow sheet facies are mainly represented by the occurrence of Incik 1c unit, which crops out as the only Incik ignimbrite unit along the Porsuk valley and within the northern edge of the ignimbrite outcropping area (i.e. in the area comprised between Aşağı Çağlan, Akçakaya and Akkaya), elsewhere is underlain by the lower 1b and 1a sub-units (in the area between Incik,

Fındık, Inli and Söğüt), it is directly in contact with Incik 1a sub-unit at Kayserkale and Ayyacık, or it is followed by Incik 2 unit.



Figure 3.11 – (a) Re-crystallized pumice clasts as flint nodules in Incik 1a ignimbrite at Inli; (b) Pipe structure in Incik 1a ignimbrite at Inli; (c) Lithic clasts imbrication in Incik 1a ignimbrite at Kayserkale (arrow represents the inferred flow direction); (d) Incik 1b fall deposit and ignimbrite at Inli; (e) Fluvial sandstone displaying convolute laminae at Karacaören; (f) Contact between fluvial sandstone and lacustrine silt at Karacaören; (g) Aspect of perlitic obsidian clasts found out in Incik 1c ignimbrite at Karacaören; (h) Banded perlitic obsidian contained within pumice clasts in Incik 1c ignimbrite at Karacaören; (i) Surge layer of the Incik 1c₁ ignimbrite unit at Inli; (j) Erosional surface between the basal Incik 1c₂ ignimbrite fine-poor zone and the underlying ash fall layers at Inli.

The Incik 1a sub-unit at Sökmen and Inli (fig. 3.8 d) comprises a 14-m-thick, pinkish ignimbrite deposit containing silicified pumice clasts (some of them completely re-crystallized as flint nodules; fig. 3.11 a). Few non-silicified pumice clasts are aphyric and with a fibrous shape; pumice and lithic maximum clast size of 4.1 and 5.8 cm. Deposit is affected by the presence of many pipe structures with a length of ≈ 30 cm (fig. 3.11 b). The upper part of Incik 1a ignimbrite is also exposed at Söğüt, where it is characterized by a white matrix containing white aphyric pumices

with a low vesiculation degree. At Kayserkale the Incik 1a ignimbrite thickness is up to 40 m. The deposit exhibits strong silicification and pumice dissolution cavities. Lithic content is very high and is mainly represented by banded rhyolite clasts, which display imbrication (dip direction/inclination of imbricated slaty clasts: 183/28; direction of aligned elongated clasts: N80; fig. 3.11 c). At Ayvacık (fig. 3.8 f) the 15-m-thick Incik 1a ignimbrite displays a basal fine-depleted zone; the main deposit is formed by pumice and lithic rich layers containing imbricated lithic clasts and lithic pockets structures in the upper portion. Lithic clasts are represented by reddish banded rhyolites.

The Incik 1b sub-unit forms thin ignimbrite deposits with a thickness comprised between 1.3 m near Fındık and 6 m at Söğüt. At Sökmen, Inli and near Fındık it is underlain by a fall deposit composed by two main fall layers intercalated with ash layers. At Inli the basal part of the 5-m-thick Incik 1b ignimbrite is characterized by the occurrence of a fine-poor zone (fig. 3.11 d), such as the Incik 1c ignimbrite but distinguishable from it because of its stratigraphic position and the absence of a lithic rich zone above it. Pumice clasts are white and crystal-poor.

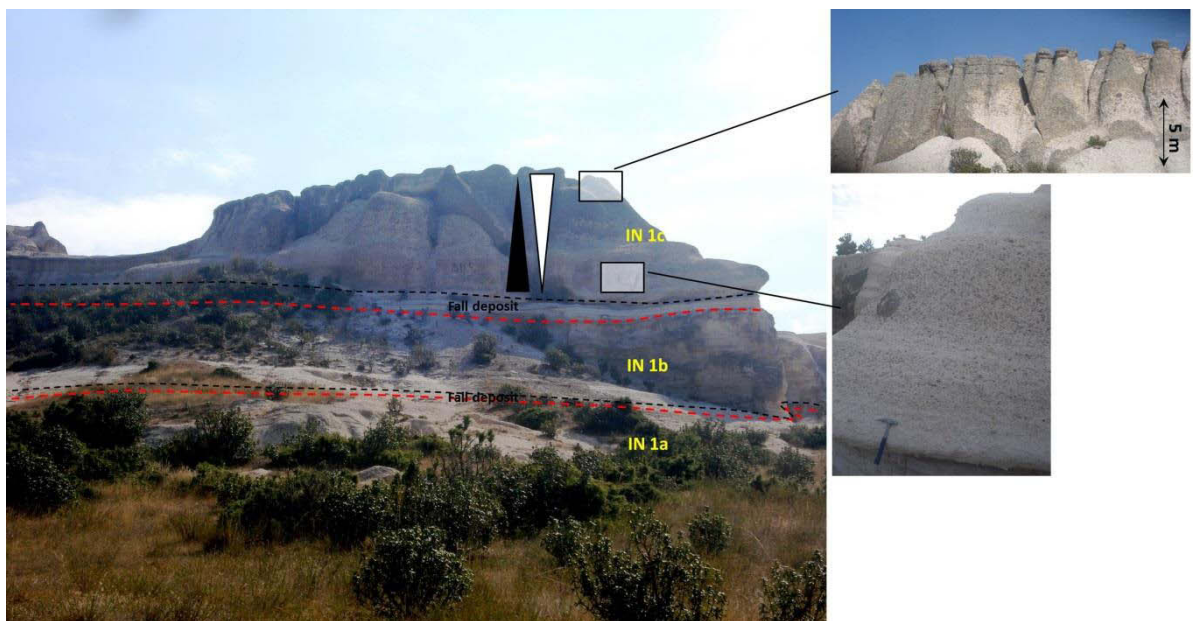


Figure 3.12 – Aspect of Incik 1 unit from the lower Incik 1a to the upper Incik 1c sub-unit at Söğüt. The Incik 1c ignimbrite is characterized by a lower lithic rich portion and an upper pumiceous portion.

The Incik 1c sub-unit presents significant thickness variations. Thickness is maximum along the Porsuk valley (170 m), a SW-NE trend depression, which is ≈ 35 km far from the source and tends to thin out of the valley even at localities near to the source. At Karacaören (fig. 3.8 a) the Incik 1c ignimbrite is preceded by 15 m of volcanoclastic deposits represented by silicified coarse grained fluvial sandstone containing rounded reworked aphyric pumice clasts displaying convolute and oblique laminae (fig. 3.11 e), underlain by 15 m of stratified silicified lacustrine siltstones (fig. 3.11 f). The overlying Incik 1c ignimbrite displays a 3-m-thick fine-depleted zone containing pumice clasts up to 13 cm. The ignimbrite deposit is characterized by a pinkish matrix containing dispersed

dark perlitic obsidian clasts (fig. 3.11 g). White, aphyric pumice clasts in the lower portion gradually increase their phenocrysts content to become porphyric in the central and upper portion of the deposit. The ignimbrite deposit is capped by a 25-m-thick lava sheet. Lacustrine deposits underlying the base of Incik 1c ignimbrite occur also at Fındık and Demirli.

At Demirli (fig. 3.14 b), a 30-m-thick Incik 1c silicified ignimbrite is underlain and overlain by silicified lacustrine siltstones. This latter deposit is stratigraphically overlain by volcanic surge

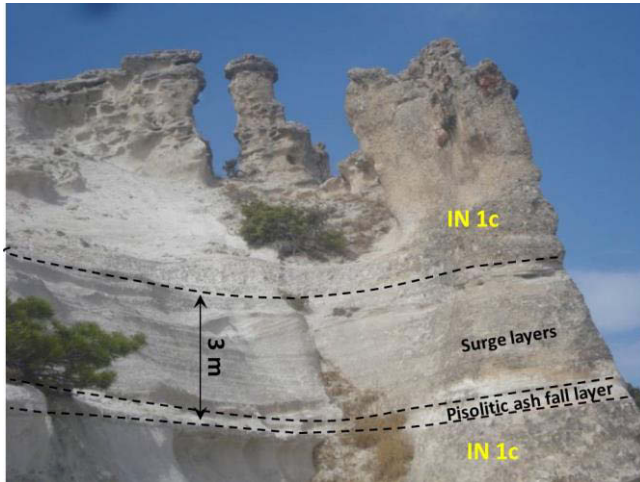


Figure 3.13 – Sequence of ash fall layer containing accretionary lapilli and surge layers interbedded within the Incik 1c ignimbrite deposit at Haymana

deposits and a 3-m-thick block-and-ash-flow deposit containing a high concentration of accessory lithic clasts without any pumices. The same stratigraphic sequence occurs at Seydiköy (fig. 3.8 b; fig. 3.14 a), where 30-m-thick Incik 1c ignimbrite deposit is overlain by 2-m-thick lacustrine silt deposits underlying 10-m-thick block-and-ash-flow

deposit, which is capped by lacustrine limestones.

More to the east, in the area among Söğüt, Inli, Seydiköy, Fındık, Incik and Akkaya, the Incik 1c ignimbrite facies is the similar to that described in the Incik type section (fig. 3.12): a fine-poor zone underlies a lithic-rich ignimbrite lower portion and an upper pumiceous portion characterized by diffuse stratified pumice layers (dsLT); many pumice clasts contain bands of perlitic obsidian (fig. 3.11 h).

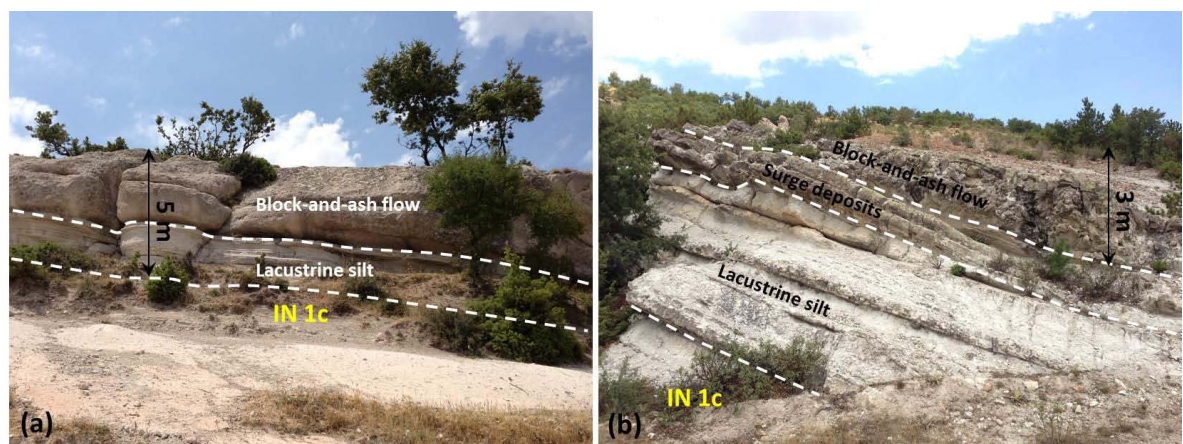


Figure 3.14 – Stratigraphic section above the Incik 1c ignimbrite at (a) Seydiköy and (b) Demirli.

At Inli the Incik 1c ignimbrite is split into two ignimbrites separated by 3-m-thick ash fall deposits (fig. 3.8 d): a lower 4-m-thick Incik 1c₁ ignimbrite, preceded by the main fall deposit sequence of

intercalated pumice fall, ash fall and surge layers (fig. 3.11 i), and an upper 28-m-thick Incik 1c₂ ignimbrite, displaying a fine-poor zone with evidence of an erosional surface (fig. 3.11 j). At Göçeri and Haymana, the Incik 1c ignimbrite is interbedded by a sequence of 3 m-thick surge layers with a basal ash fall layer containing accretionary lapilli (fig. 3.13). This surge sequence has been also found at Yukarı Ilica in the same stratigraphic position.

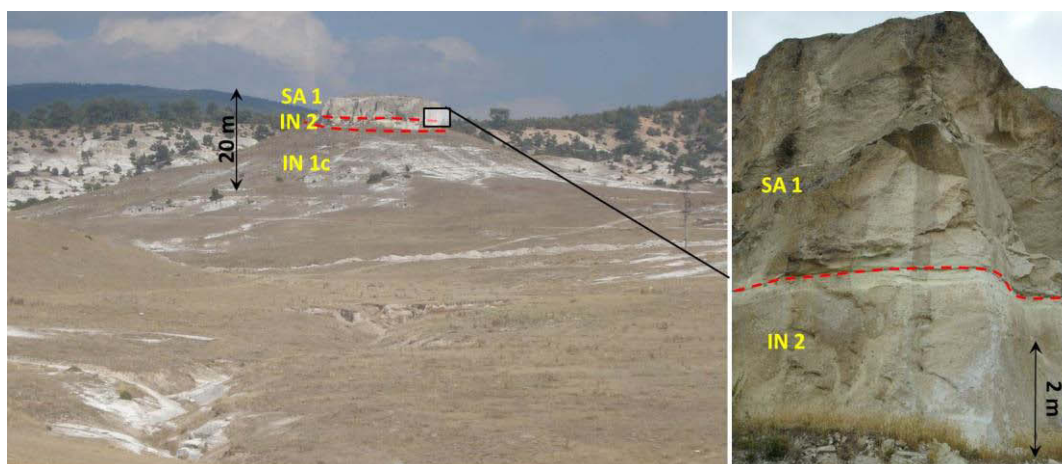


Figure 3.15 – Stratigraphic succession exposed in the section of Göçeri.

The Incik 2 unit exposed north of the caldera crops out between Aklarmaç Çiftliği and Ayvacık, i.e. about 15 km away from the northern rim of the caldera. In the area near Kütahya Incik 2 unit has not been observed; here Incik 1 unit is directly overlain by lacustrine limestones, as at Çayca, or by lavas, as at Seydiler and Karacaören. The ignimbrite exposed south of the caldera at Göçeri (fig. 3.15) is underlain by a thin graded pumice fall deposit (MP <0.3 cm) and comprises a 2.3-m-thick flow deposit containing white aphyric and greyish porphyric pumice clasts (PI≈20%; phenocrysts of biotite and minor quartz). Here, the Incik 2 unit is underlain by Incik 1c unit and is directly in contact with Sabuncu 1 unit.

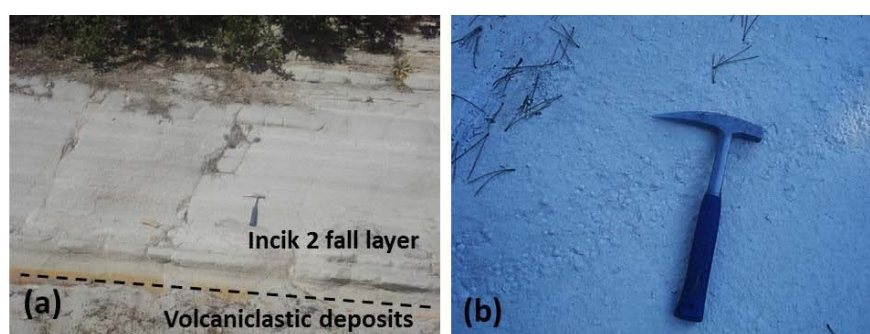


Figure 3.16 – (a) Incik 2 fall deposit and (b) co-ignimbrite ash deposit containing accretionary lapilli at Ovacık.

At Haymana Incik 2 ignimbrite thickness is up to 33 m (fig. 3.8 c), is characterized by pinkish matrix, white and grey porphyric pumice clasts and exhibits moderate induration. Induration and silicification are very strong at Damlalıkaraağaç, where the Incik 2 ignimbrite is exposed along the south-western rim of the caldera; ignimbrite strata dip toward the caldera system (dip direction/inclination: 30/70). At Ovacık the Incik 2 unit overlies volcaniclastic deposits whose base

doesn't crop out. Here, 2.5-m-thick fall deposits precede a 4-m-thick pumice rich ignimbrite deposit (fig. 3.16 a), with pumice maximum clast size of 4 cm. The ignimbrite deposit is overlain by 7 meters of ash deposit containing accretionary lapilli (fig. 3.16 b).

The Incik ignimbrite is overlain by the Sabuncu unit in a restricted area near Fındık; at Ovacik it is overlain by Seydiler unit. Elsewhere it is capped by lavas or continental deposits (fluvial sandstone and lacustrine limestone). At Gökçekısıık, the ≈3-m-thick Incik 1c ignimbrite is overlain by 12 m of reworked deposits of continental conglomerates containing silicified pumice clasts and pluridecimeteric lithic blocks of the basement in the upper portion (ophiolite and schists). A few kilometers to the south, similar reworked deposits thicken and exhibit stronger silicification. At Yenisoğça, the >20 m Incik 1c ignimbrite is overlain by 3 m of intensely silicified and indurated levels of reworked clast-supported conglomerates formed by rounded pumice clasts, which vertically grades to 30 m thick laminated fluvial sandstones containing pumice and some lithic clasts. At Uluçayır, the stratigraphy is similar. Here the Incik 1c sub-unit is entirely exposed, from the fall deposit to the Incik 1c ignimbrite upper pumiceous portion. The ignimbrite deposit is overlain by 15 m of lacustrine deposits of fine graded sandstone containing rounded pumice clasts, followed by 5 m of intensely silicified ignimbrite deposit containing many rounded pumice clasts. These lacustrine deposits overlying the Incik 1c ignimbrite are correlated with those at Seydiköy and Demirli. The occurrence of volcanoclastic deposits above the Incik 1 unit has been also detected more to the South at Ayvacık (fig. 3.8 f) and Aşağı İlica (fig. 3.8 e), where the Incik 1c fall deposit is overlain by reworked fluvial sandstones. From Çalca toward the North-East, Incik 1 unit is overlain by lacustrine limestones which reach a thickness of 13 m at Seydiköy.

3.1.2 The Sabuncu ignimbrite

The Sabuncu ignimbrite comprises two main pyroclastic units, which include ignimbrite flow and their associated pumice fall deposits.

Identification and distinction of the different Sabuncu units and were made on the basis of:

- a. features of the pumices contained in the flow deposit. Pumice clasts contained in Sabuncu 1 and Sabuncu 2 ignimbrites are mineralogically and texturally very similar. A slight increase of pumice vesiculation degree and phenocrysts content is observed from Sabuncu 1 to Sabuncu 2 unit. Sabuncu 1 ignimbrite contains moderately-highly vesiculated, porphyric pumice clasts (PI≈10-20%; phenocrysts of biotite and minor quartz and K-feldspar); Sabuncu 2 ignimbrite contains highly vesiculated, porphyric pumice clasts (PI=15-25%; phenocrysts of biotite, quartz and K-feldspar);
- b. structure and texture of the pumice fall deposits. The Sabuncu 1 and Sabuncu 2 fall deposit are structurally and texturally different. The first one is formed by three main

pumice fall layers interbedded with thinner ash fall layers, containing white, moderately-highly vesiculated porphyric pumice clasts and minor bluish, poorly vesiculated, highly porphyric clasts. Sabuncu 2 fall deposit is entirely formed by pumice fall layers containing bluish, highly porphyric, “blocky” shaped pumice clasts with a texture between pumice and scoria.

3.1.2.1 Type section

The selected type section for Sabuncu ignimbrite is exposed at Findık (fig. 3.17), where the most complete section from the base of Sabuncu 1 to the top of Sabuncu 2 unit crops out.

FINDIK SECTION

The Findık section exposes the flow and fall deposits from the lacustrine silt at the base of Incik 1c sub-unit to the capping lava above Sabuncu 2 unit.

1. Incik 1c sub-unit

- Main flow deposit. The 64-m-thick Incik 1c ignimbrite deposit occurs above a stratified lacustrine siltstone. The ignimbrite displays the usual facies characterized by a basal fine-poor zone underlying a lower lithic-rich portion and an upper pumiceous portion (fig. 3.18 a). White, fibrous pumice clasts are aphyric in the lower portion; phenocrysts content then gradually increases and is porphyric in the intermediate and upper portions (PI=20%; biotite and minor quartz). Vesiculation degree increases vertically through the deposit;

2. Sabuncu 1 unit

- Fall deposit. Occurrence of three pumice fall layers intercalated with ash fall layers, for an overall thickness of 2 m (fig. 3.18 b). The basal pumice fall layer is massive and contains white, porphyric (PI≈15%; phenocrysts of biotite), moderately-highly vesiculated pumice clasts; the overlying pumice fall layer is thicker, reversely graded, with bluish, “blocky” shaped, highly porphyric, non vesiculated pumices; the uppermost pumice fall layer is formed by two thinner levels containing bluish, fine grained pumice clasts;
- Main flow deposit. The ignimbrite deposit is 25 m thick and displays a normal grading of pumice clasts, which are white, porphyric and with a moderately-highly vesiculation degree; lithic clasts are rare and display no gradation. Absence of perlitic obsidian clasts in the ignimbrite matrix.

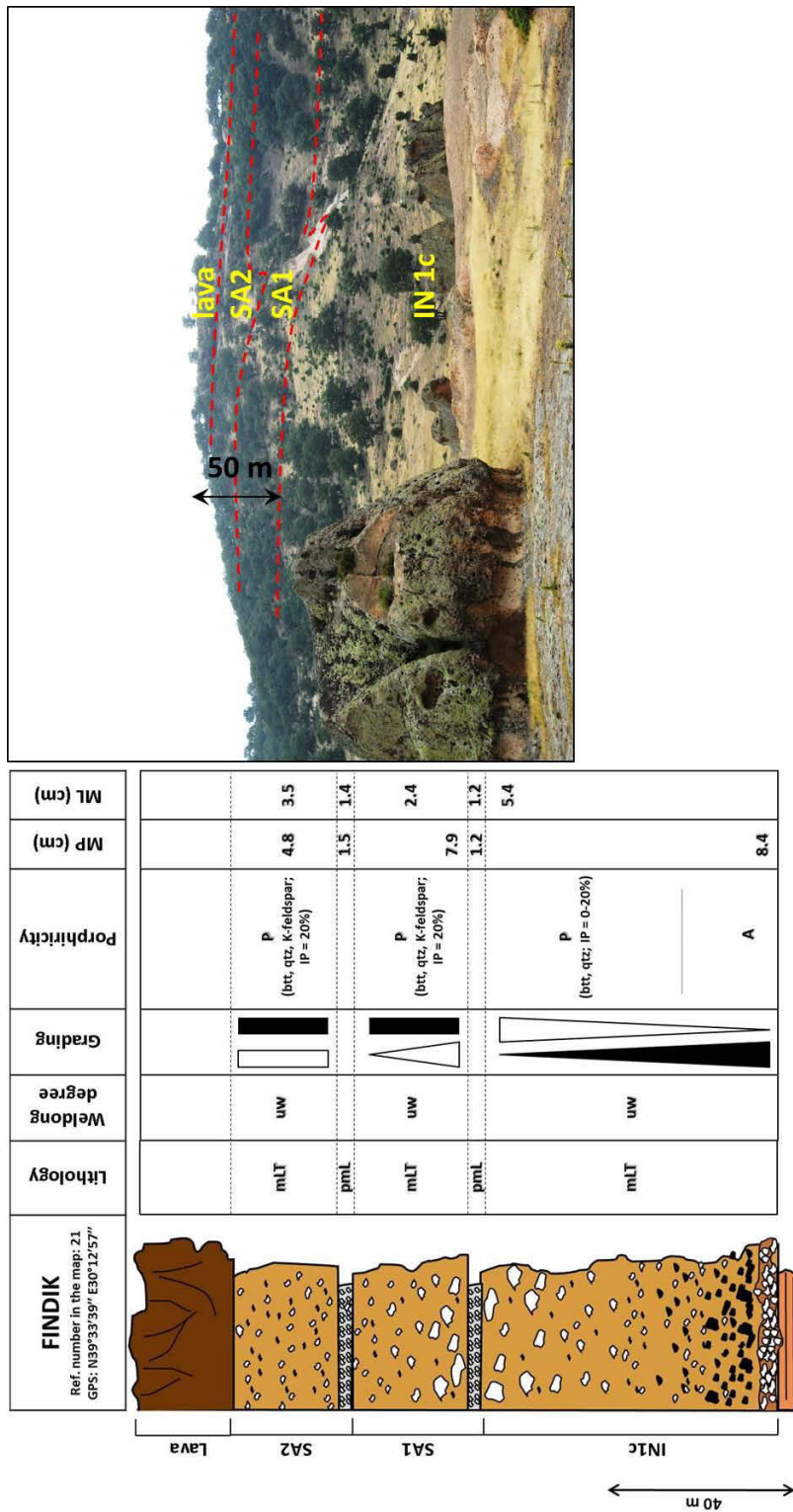


Figure 3.17 – Type section of Sabuncu ignimbrite at Findik.

3. Sabuncu 2 unit

- Fall deposit. Occurrence of several pumice fall layers containing bluish, highly porphyric, non vesiculated, “blocky” shaped pumice clasts with a texture between pumice and scoria (fig. 3.18 c). The dark tone of the pumices is due to alteration processes which is evidenced by the presence of a greenish mineral phase, possibly

chlorite, within pumice clasts. Pumice fall layers increase both thickness and clasts grain size vertically;

- Main flow deposit. The ignimbrite deposit is 22 m thick and massive. Pumice clasts are white, porphyric and highly vesiculated.

4. Lava

Basaltic lava with phenocrysts content of feldspar and pyroxene (fig. 3.18 d). Thickness: 25 m.

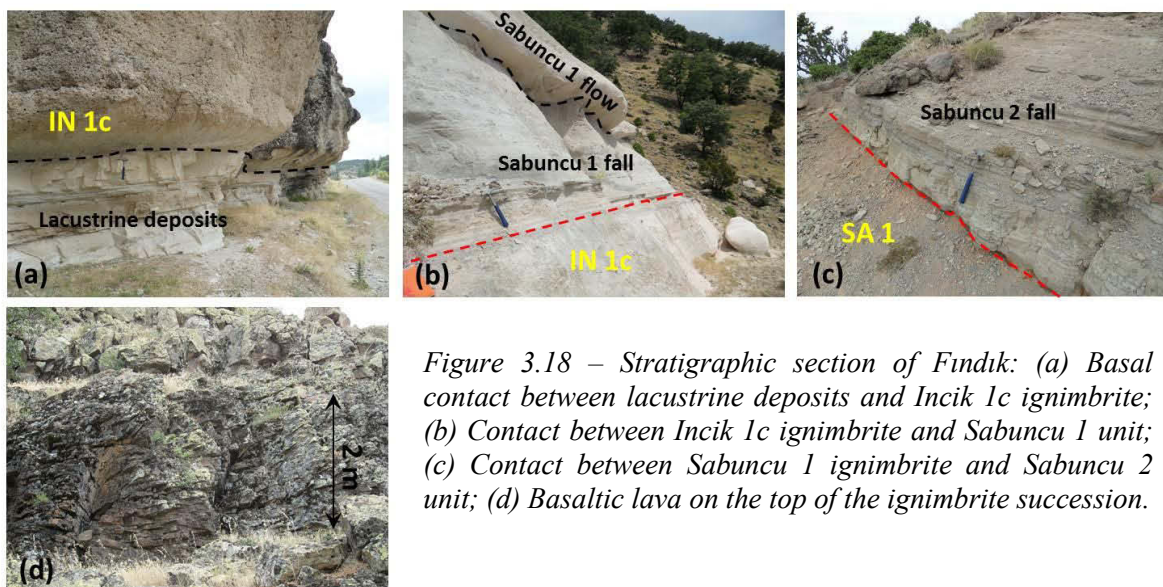


Figure 3.18 – Stratigraphic section of Fındık: (a) Basal contact between lacustrine deposits and Incik 1c ignimbrite; (b) Contact between Incik 1c ignimbrite and Sabuncu 1 unit; (c) Contact between Sabuncu 1 ignimbrite and Sabuncu 2 unit; (d) Basaltic lava on the top of the ignimbrite succession.

3.1.2.2 Lateral facies variations

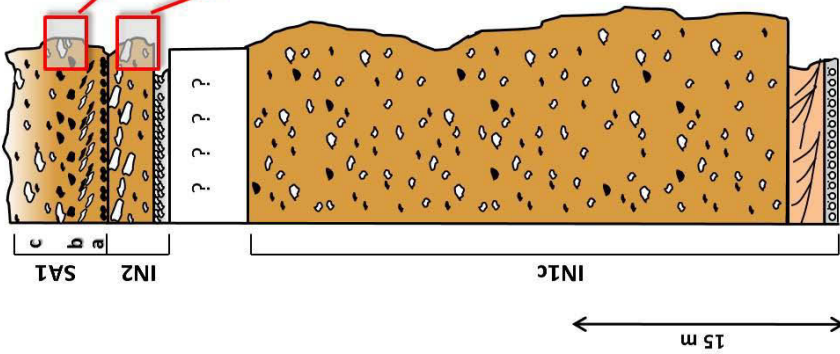
Sabuncu ignimbrite deposits are exposed over a restricted area, but are generally well preserved and laterally continuous. The presence of lava sheets in many places cap the Sabuncu unit in the area comprised between Fındık, Sabuncu, Seydiköy and Ahmetoluğu. The only Sabuncu deposit found in the southern part of the investigated area is exposed at Göçeri and it constitutes the last term of the ignimbrite succession (fig. 3.15).

The Sabuncu ignimbrite reaches maximum measured thickness in the area between Seydiköy and Fındık (>52 m at Seydiköy; 47 m at Fındık; >44 m at Sabuncu west). Thickness is also considerable at Ahmetoluğu (>35 m) and Sabuncu (>25 m), it decreases down to 5 m at Göçeri. Exposures of both Sabuncu 1 and 2 units occur where the ignimbrite succession is capped by lava sheets (i.e. at Fındık and Seydiköy), elsewhere only the Sabuncu 1 unit crops out, with the exception of Sabuncu village, where Sabuncu 2 ignimbrite is also exposed. The ignimbrite is nowhere welded and proximal facies have not been observed.

The Sabuncu 1 unit at Seydiköy comprises 13-m thick massive pink ignimbrite containing white, porphyric (PI \approx 10%; phenocrysts of biotite and minor quartz), moderately-highly vesiculated, partly silicified pumice clasts (fig. 3.19 b). At Ahmetoluğu (3.19 c) this unit displays a slight inverse grading of pumice clasts, with the same features as the Seydiköy section, but are not silicified. Ignimbrite deposit contains some millimetric perlitic obsidian clasts. At Göçeri, the 5-m-thick Sabuncu 1 ignimbrite presents a lithic and crystal rich basal layer overlain by a finer graded portion containing millimetric-to-centimeter imbricated lithic and pumice clasts, and an upper coarser grained portion displaying normal grading of lithic clasts. This succession is similar to the standard of Sparks et al. (1973).

The Sabuncu 2 ignimbrite at Seydiköy (fig. 3.20 a, e) is preceded by a dark fall deposit (fig. 3.20 a, b, c) formed by a sequence of 8 pumice fall layers between 1.5-30 cm thick for an overall thickness of 5 m, and overlain by lavas (fig. 3.20 e). Pumice fall layers are interbedded with thinner ash fall layers; the fall deposit displays a general vertical inverse grading of pumice clasts. A similar stratigraphic sequence is also exposed at Fındık. Sabuncu 2 ignimbrite at the locality of Sabuncu is made up of two flow deposits. The 15-m-thick lower flow deposit is characterized by a zone of high pumice clasts concentration (size up to 7 cm) containing phenocrysts of biotite, quartz and K-feldspar (PI=25%); the upper flow deposit contains a greater amount of accessory lithic clasts.

GÖÇERİ
 Ref. number in the map: 17
 GPS: N39°16'21" E30°16'38"



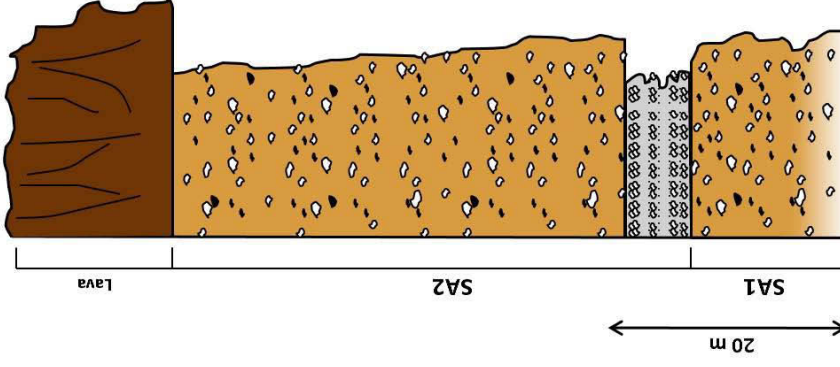
SA1 - Lithology and structure: (a) basal layer formed by high concentration of crystals and lithic clasts, overlain by (b) fine grained layer containing imbricated pumice and lithic clasts, followed by (c) mLT_(fp) portion. Pumice mineralogy and texture: white, high vesiculated, porphyric pumice clasts. Clasts dimension: MP=3 cm; ML=1.6 cm
Age: 9.78±0.18 Ma (U-Pb; pumices)

IN2
 • FLOW DEPOSIT - Lithology and structure: mLT_(fp) deposit. Pumice mineralogy and texture: two types of pumices: (1) white, mostly aphyric and (2) greyish, porphyric clasts; high vesiculation and roundness degree; imbrication in the upper part of the deposit. Clasts dimension: MP=9.2 cm; ML=2.7 cm
Age: 18.51±0.18 Ma (U-Pb; pumices)

• FALL DEPOSIT - Massive pumice fall layers containing porphyric pumice clasts. MP<0.3 cm; ML: not measurable

IN1c - Lithology and structure: mLT deposit underlain by cross stratified surge and pisolitic ash fall layer. Pumice mineralogy and texture: white, low vesiculated, "dense" structure-type, low porphyric pumice clasts (phenocrysts of quartz and biotite; IP<5%).

SEYDIKÖY
 Ref. number in the map: 54
 GPS: N39°32'46" E30°08'51"



SA2
 • FLOW DEPOSIT - Lithology and structure: mLT deposit, pinkish matrix. Presence of few and small perlitic obsidian fragments in the matrix. Pumice mineralogy and texture: presence of two types of pumices: (1) white, high vesiculated, elongated porphyric clasts (phenocrysts of quartz, biotite and K-feldspar; IP=25%), and occasional (2) white, non vesiculated, isotropic shaped, low porphyric clasts. Clasts dimension: MP=7.0 cm; ML= not measurable

• FALL DEPOSIT - Seven main pumice fall layers intercalated with ash fall layers. Juvenile clasts with intermediate texture between pumice and scoria. MP=1.5 cm

SA1 - Lithology and structure: mLT deposit. Presence of few and small perlitic obsidian fragments in the matrix. Pumice mineralogy and texture: white, partly silicified, medium-high vesiculated porphyric pumice clasts (phenocrysts of quartz and minor biotite; IP=10%). Clasts dimension: MP=7.6 cm; ML=2.8 cm

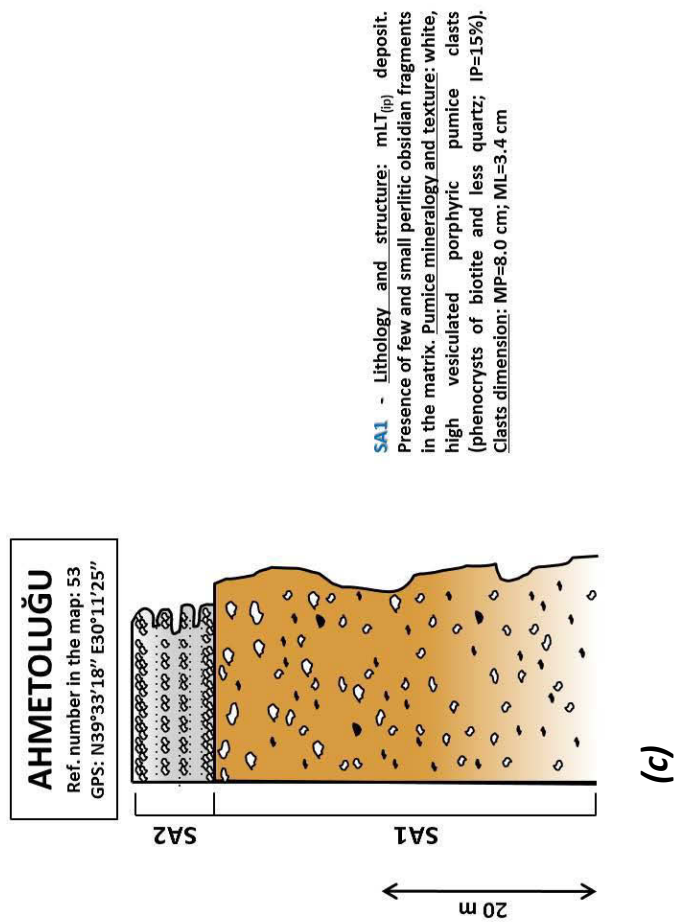


Figure 3.19 – Lateral facies variation of the Sabuncu ignimbrite: (a) Göçeri section; (b) Seydiköy section; (c) Ahmetoluğu section.

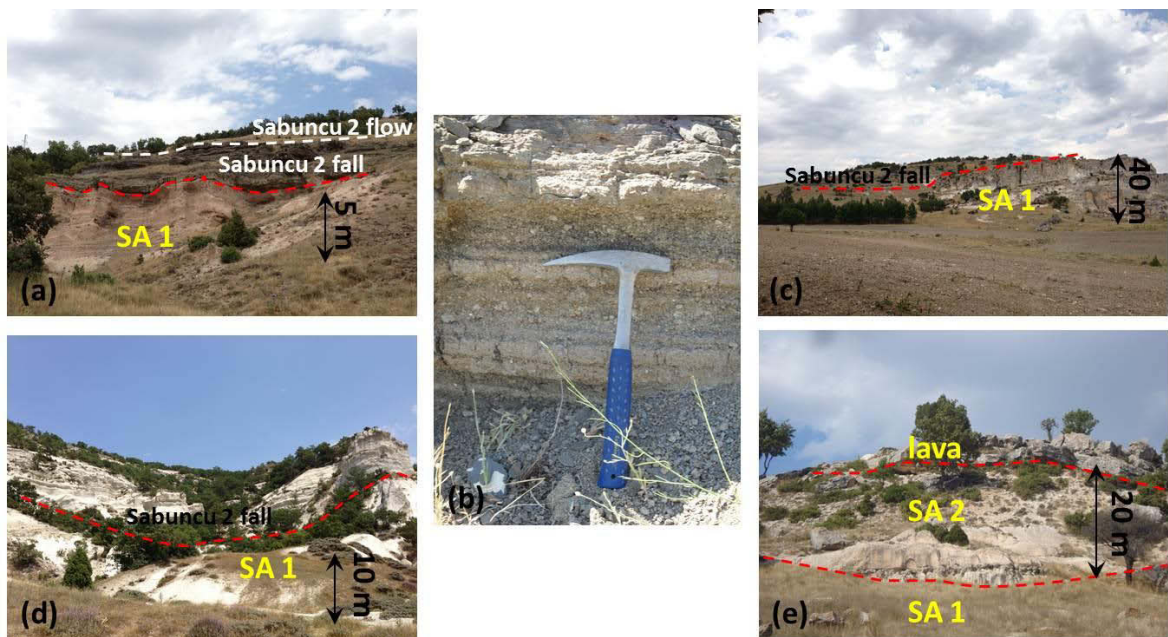


Figure 3.20 – The Sabuncu unit: (a) Contact between Sabuncu 1 and Sabuncu 2 units at Seydiköy; (b) Detail of the dark pumice fall deposit preceding the Sabuncu 2 ignimbrite at

Seydiköy; (c) Contact between Sabuncu 1 and Sabuncu 2 units between Seydiköy and Sabuncu; (d) Contact between Sabuncu 1 ignimbrite and Sabuncu 2 fall deposit at Ahmetoluğu; (e) Stratigraphic sequence from Sabuncu 1 unit to lava flow at Seydiköy.

3.1.3 The Seydiler Ignimbrite

The Seydiler ignimbrite comprises two main pyroclastic units which include ignimbrite flows and their associated pumice fall deposits.

Identification and distinction of the different Seydiler units were made on the basis of several macroscopical evidence found in the deposits, specifically concerning the structure of flow deposits and concomitant fall deposits. Pumice mineralogy (PI \approx 15-20%; phenocrysts of K-feldspar, quartz and minor biotite) and texture (both fibrous and non-fibrous, moderately vesiculated clasts) is the same both in Seydiler 1 both in Seydiler 2 unit; pumice clasts everywhere contain millimetric black perlitic obsidian grains.

Distinctive criteria were based on:

- a. structure and texture of the pumice fall deposits. The fall deposit preceding Seydiler 2 ignimbrite is considered as a reliable marker bed for ignimbrite identification and correlation, since it crops out over a wide area (approximately between Döğer and Ayazini, and from Bayat to Kurudere villages). Its typical facies consists in a sequence of three surge layers intercalated with three massive pumice-fall layers, comprising a thicker, well laminated basal surge deposit and a coarser upper pumice fall layer;
- b. structure of the flow deposit and presence of peculiar lithofacies. The Seydiler 1 ignimbrite is characterized by the intercalation of a \approx 50-cm-thick sequence of ash-fall layers in its lower portion, followed by an upper diffuse-stratified lapilli-tuff facies (dsLT; Branney and Kokelaar, 2002) displayed by concentration of coarser pumice clasts. In the area of Bayat, Seydiler 1 ignimbrite displays a lithic rich zone within its middle and upper portions containing by metamorphic clasts (schists and quartzite lithologies), which generally form breccia-lenses (lensBr; Branney and Kokelaar, 2002);
- c. regional tilt. A general gently SW tilt affects the investigated region, which is usually pointed out by bedding of the sequence of pumice and surge layers intercalated between Seydiler 1 and Seydiler 2 ignimbrites. Because of this this tilt, the Seydiler 1 unit is prevalently exposed over the south-eastern part (from Kayıhan to the east) and the Seydiler 2 unit over the north-western part of the Seydiler ignimbrite outcropping area.

3.1.3.1 Type section

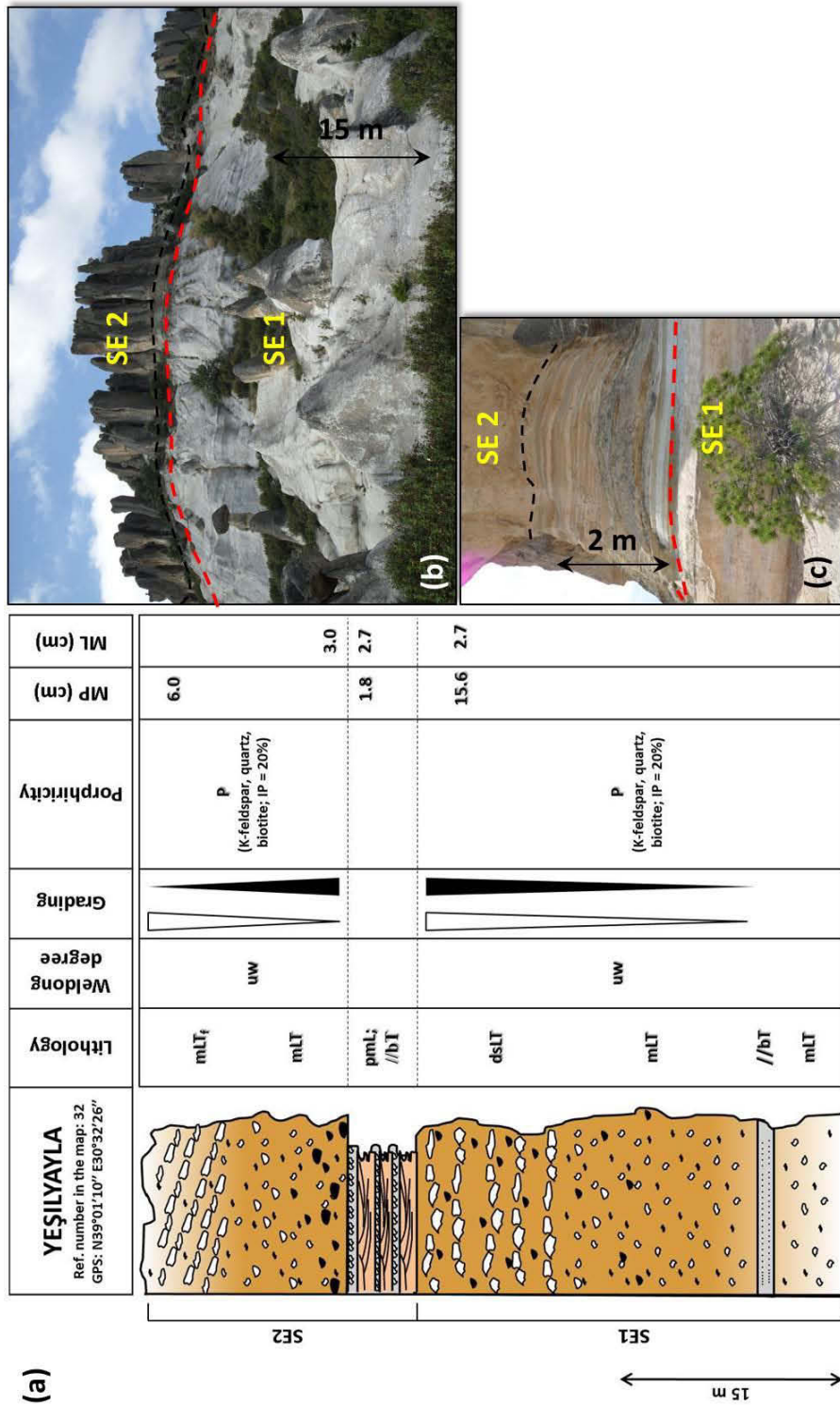


Figure 3.21 – Type section of Seydiler ignimbrite at Yeşilyayla: a) Stratigraphic section; (b) Aspect of the ignimbrite deposits; (c) Sequence of interbedded pumice-fall and surge layers between Seydiler 1 and Seydiler 2 ignimbrites.

The type section selected for the Seydiler ignimbrite is exposed in the area of Yeşilyayla. It exhibits the typical facies of Seydiler 1 ignimbrite (i.e. the parallel bedded ash-fall layers occurring in the middle portion and the coarser pumice rich layers in the upper portion), separated from the Seydiler 2 ignimbrite by a preserved pumice fall and surge layers sequence.

YEŞILYAYLA SECTION

The Yeşilyayla section (fig. 3.21; 3.24) exposes Seydiler 1 and Seydiler 2 units separated by the pumice fall and surge layers sequence. The base of Seydiler 1 unit doesn't crop out.

1. Seydiler 1 unit

- Main flow deposit. The lower and middle portions of the deposit are massive, characterized by a high amount of white matrix with respect to pumice and lithic clasts; the lower portion is interbedded with ≈ 40 -cm-thick ash fall layers. The upper portion of the deposit exhibits a diffuse-stratified lapilli-tuff facies characterized by many pumice-rich layers, displaying reverse grading of pumice clasts. Lithic content is lower, but clasts also display a reverse grading. Pumices are white, porphyric (PI \approx 20%; phenocrysts of K-feldspar, quartz and minor biotite), moderately vesiculated and contain millimetric perlitic obsidian grains;

2. Seydiler 2 unit

- Fall deposit. The sequence consists of three surge alternated with three main pumice fall layers (fig. 3.21 a, c). The 36-cm-thick basal surge, at the contact with the Seydiler 1 ignimbrite, is formed by pinkish ash layers alternated with thin layers (up to 2 cm) of coarser grains (millimetric size); the deposit is pervasively laminated and the coarser grained layers display dune bedforms. The overlying 30-cm-thick pumice-fall layer is made up of three levels, interbedded in the intermediate part by thinner ash fall layers.

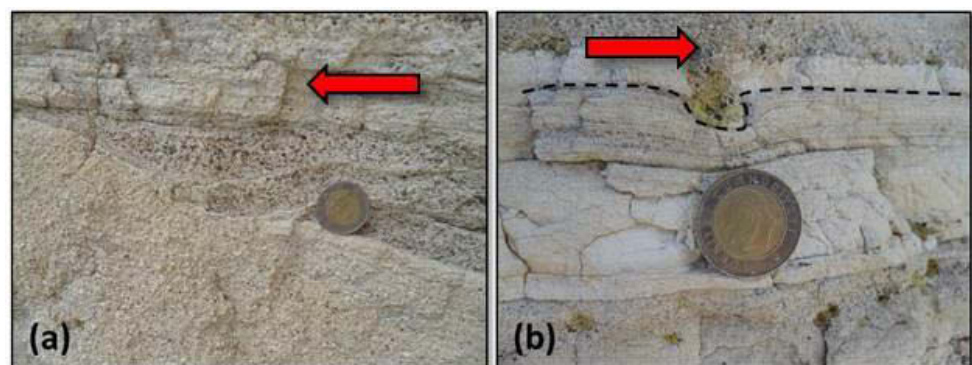


Figure 3.22 – Sedimentary structures preserved in the second surge layer at Yeşilyayla: (a) Cross-lamination; (b) Load cast. The arrow indicates the flow direction.

The lower level is reverse graded, with a coarser grained massive sub-layer. The upper levels display a reverse grading of lithic and pumice clasts, which are coarser (up to 1 cm) with respect to the lower level. The following 80-cm-thick surge is formed by a massive pinkish ash deposits containing levels of coarser pumice and lithic clasts (diameter < 1 mm), displaying cross-lamination and load cast structures (fig. 3.22 a, b). The overlying 66-cm-thick pumice-fall layer is massive, and formed by pumice and lithic clasts (diameter < 0.5 cm) and perlitic obsidian. The following 20-cm-thick surge layer is composed by two portions: a lower pinkish level and a thicker upper reddish layer. The uppermost 10-cm-thick pumice fall layer is the coarsest one of the sequence. It is made up of four levels of pumice and lithic clasts intercalated with three finer grain sized levels; it displays a normal grading of pumice and lithic clasts;

- Main flow deposit. The pinkish, 12-m-thick ignimbrite deposit displays a normal grading of lithic clasts and reverse grading of pumice clasts. Lithics are andesitic in composition and reach maximum size up to 6 cm. Pumice clasts are altered in the lower portion; the upper portion displays pumice dissolution cavities, exhibiting imbrication (dip direction/inclination: 211/9).

3.1.3.2 Lateral facies variations

The Seydiler ignimbrite deposits are well preserved and laterally sub-continuous. Because of a SW gently dipping of the strata, Seydiler 1 unit is mainly exposed in the south-eastern part of the Seydiler outcropping region, Seydiler 2 unit in the north-western part (fig. 3.24). The very base of the Seydiler ignimbrite is exposed at the village of Kale and Kayı, where Seydiler 1 unit occurs over the schists of metamorphic basement, and near the village of Ovacık, where Seydiler 1 ignimbrite is separated from the Incik ignimbrite by limestones. In the south-eastern area between the villages of Olukpınar, Kale and Derbent, lava sheets cap the ignimbrite deposits and evidence of a widespread effusive activity consisting of lava flows, lava breccias and peperite deposits occur. Elsewhere the Seydiler ignimbrite is overlain neither by volcanoclastic nor sedimentary deposits.

Maximum thicknesses are reached in the proximity of Bayat village (>250 m), between Döğür and Yapıldak (>250 m) and in the Frig valley (>150 m at Kayı), but ignimbrite is still > 30 m thick in the proximity of the north-western edges of the outcropping area at Döğür (65 m), Inlice Mahallesi (55 m) and Ovacık (35 m).

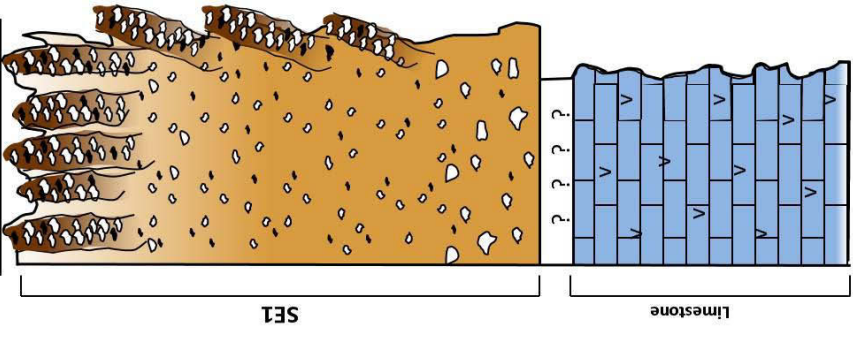
Welding degree varies from incipient to moderate and affects deposits in the Bayat area (e.g. north of Bayat, Sağırılı and Doğlal), and in the Yazılıkaya valley (Kayı section, fig. 3.23 b); silicified

facies occur over a more restricted area around Bayat, between Derbent, Karakaya, Alanyurt and Han.

Proximal outflow sheet facies occur in the area of Bayat. The ignimbrite deposits are welded and reach thickness greater than 250 m. At Olukpınar, the 74-m-thick ignimbrite deposit contains pumice clasts up to 50 cm, which increase up to 1 m at Seydiler. In this area the Seydiler 1 ignimbrite exhibits breccia-like facies, characterized by lithic-rich lens containing pluri-decimetric clasts, up to 1 m in diameter at Karakaya.

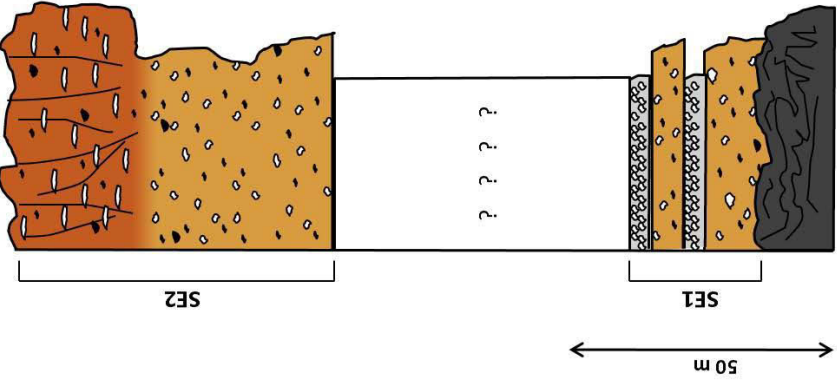
The Seydiler 1 unit is prevalently exposed in the south-eastern part of the investigated area; in the north-western area it locally crops out at the base of Seydiler 2 unit, more to the north-west in the area of Ovacık it crops out isolated. Here (fig. 3.23 a), the 35-m-thick ignimbrite lies at direct contact with a >20-m-thick dolomitic limestones without the occurrence of the associated fall deposit. The lower portion of the deposit contains a low amount of white and grey pumice clasts within a white matrix; grey clasts are fibrous and have a sub-triangular shape, white ones are more vesiculated and isotropic in shape. Lithic content is represented by millimetric perlitic obsidian grains and rare metamorphic clasts of the basement. Pumice clasts are normally graded, lithic clasts don't display any type of gradation. The upper portion of the deposit is indurated and exhibits pumice dissolution cavities. The whole ignimbrite hosts many large pipe structures (length up to 8 m and width up to 1 m; fig. 3.25 a) and matrix contains dolomitic clay chips. The base of Seydiler 1 ignimbrite is also cropping out at Kayı (fig. 3.23 b) and Kale (fig. 3.23 e), where the associated fall deposit overlays the metamorphic basement. At Kale, the 2.1-m-thick fall deposit is made up by four main pumice-fall layers directly in contact (fig. 3.23 b). The massive basal pumice-fall layer is the coarsest-grained one (MP=3.5 cm; ML=1.8 cm); it is overlain by two thinner layers and a thicker layer displaying many levels of pumice clasts intercalated with thinner ash-fall levels in the upper portion; the whole pumice-fall sequence exhibits a normal grading of pumice clasts. The pumice fall layers contain a large amount of crystals (quartz, biotite and minor K-feldspar). The overlying 7-m-thick ignimbrite deposit is massive and characterized by the occurrence of several pumice-rich layers.

OVACIK
 Ref. number in the map: 18
 GPS: N39°13'46" E30°23'37"



SE1 - Lithology and structure: $mL_{(np)}$ deposit, pervasive presence of many pipe structures (diameter up to 1 m and length of several metres). The upper part of the deposit is indurated and shows pumice dissolution cavities. Pumice mineralogy and texture: white and grey pumice clasts respectively characterized by a more vesiculated fibrous structure and a less vesiculated denser structure; porphyric. Presence of triangular and elongate shaped pumice clasts. Low lithic content (<5%). Clasts dimension: MP=6.7 cm; ML=1.2 cm

KAYI
 Ref. number in the map: 25
 GPS: N39°12'46" E30°43'55"

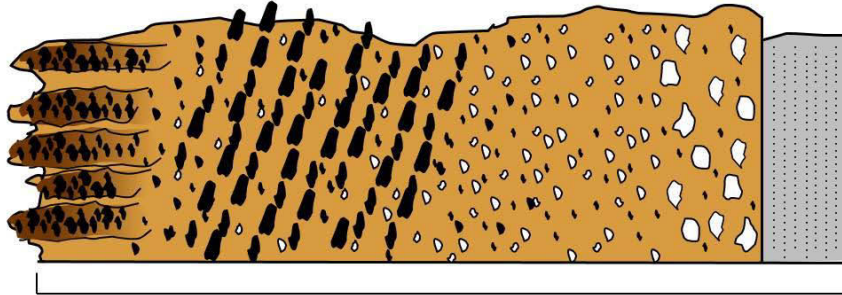


SE2 - Lithology and structure: mL deposit; non welded basal portion and incipiently welded upper portion, characterized by the occurrence of flattened pumice clasts and columnar jointing. Pumice mineralogy and texture: white porphyric pumice clasts

SE1

- FALL DEPOSIT - Massive pumice fall layer containing aphyric pumice clasts. MP=3.5 cm; ML=1.8 cm
- FLOW DEPOSIT - mL deposit
- FALL DEPOSIT - Massive pumice fall layer containing aphyric pumice clasts. MP=1.8 cm; ML=0.5 cm
- FLOW DEPOSIT - mL deposit containing lithic clasts of the basement

KARAAĞAÇ
 Ref. number in the map: 60
 GPS: N38°54'50" E30°44'51"



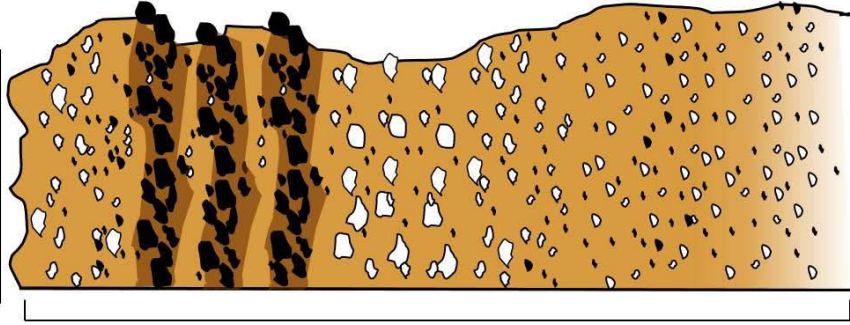
SE1

6 m

(c)

SE1 - Lithology and structure: mL_(i, np) deposit underlain by ash fall deposit; presence of many pipe structures at the top of the deposit (diameter comprised between 5-25 cm and length up to 60 cm); mL_T in the middle-upper portion, given by lithic clasts orientation. Slaty clasts (mainly scists) display imbrication, elongated clasts (scists and quartzites) display lineation. Plunge direction of the imbrication plane varies counterclockwise toward the base, from N42 to N286. Plunge direction of the lineation is more homogeneous through the section, varying between N354 and N78.
Pumice mineralogy and texture: white porphyryic pumice clasts
Clasts dimension: MP=10.9 cm; ML=27.6 cm

KARAKAYA
 Ref. number in the map: 61
 GPS: N38°53'57" E30°48'46"



SE1

30 m

(d)

SE1 - Lithology and structure: mL_(ip) in the lower-middle portion, lenslike toward the top. Lithics are metamorphic (mainly scists and less quartzites). **Pumice mineralogy and texture:** white porphyryic pumice clasts. **Clasts dimension:** MP=40 cm; ML>1 m.

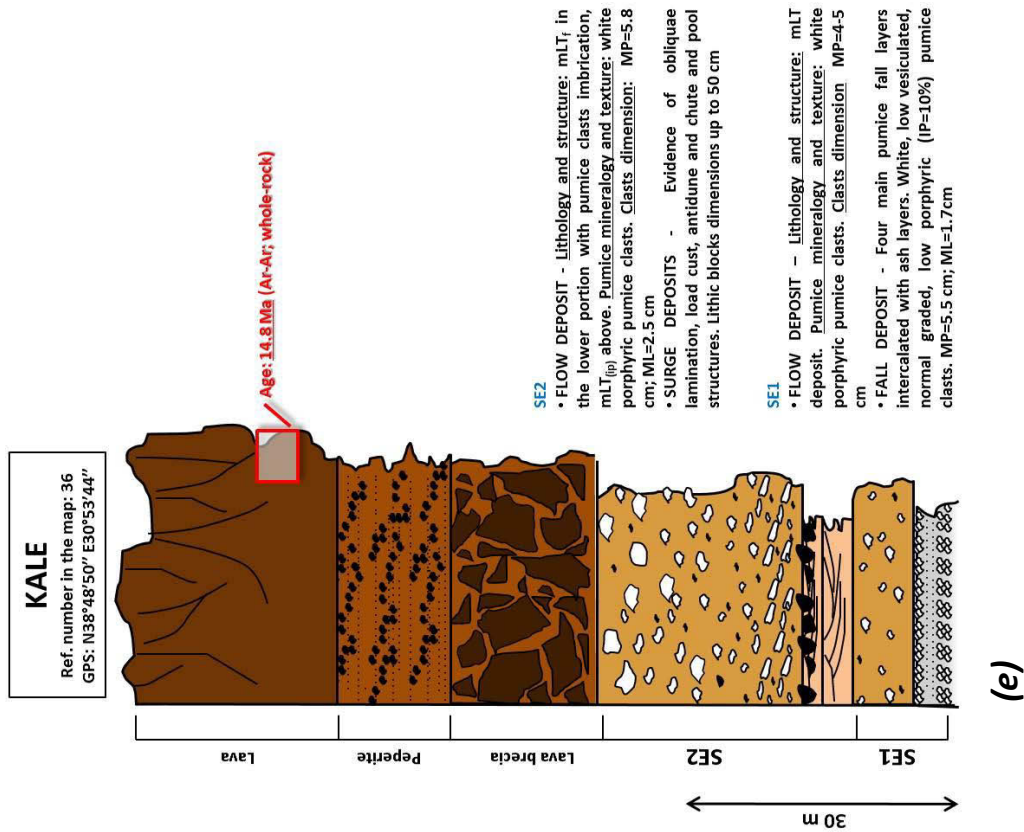


Figure 3.23 – Lateral facies variation of the Seydiler ignimbrite: (a) Ovacık section; (b) Kayı section; (c) Karaağaç section; (d) Karakaya section; (e) Kale section.

In the area comprised between Döğer and Kayihan, the Seydiler 1 unit crops out beneath the Seydiler 1 pumice-fall and surge layers sequence, exposing its upper pumiceous portion, which is characterized by the occurrence of many stratified pumice-rich layers.



Figure 3.24 – Aspect of the Seydiler ignimbrite between Kayihan and Yeşilyayla villages. Seydiler 1 and Seydiler 2 ignimbrites are separated by a sequence of pumice-fall and surge layers.

More to the south-east, specifically in the area among Olukpınar, Karaağaç and Karakaya, the ignimbrite is characterized by the occurrence of a middle-upper breccia-like portion generally forming discontinuous lenses (fig. 3.25 c). At Karaağaç (3.23 c) the breccia-like upper portion of the deposit is composed of metamorphic clasts (schists and quartzite lithologies), characterized by a strong clasts imbrication. Pumice clasts are normally graded and mostly occur in the basal portion of the ignimbrite, which is underlain by an ashy bed. The upper portion of the ignimbrite is affected by many pipe structures with a diameter between 5 to 25 cm, and a length up to 60 cm (fig. 3.25 e). At Karakaya (fig. 3.23 d), the 100-m-thick ignimbrite is formed by an upper portion displaying lithic-lenses containing lithic and pumice blocks with dimensions up to 1 m and 40 cm respectively; both lithic and pumice clasts display reverse grading. Lithic clasts lithologies are similar to those preserved at Karaağaç. This breccia-like facies laterally passes to a lithic-rich facies, such as that in the area between Bayat and Avdan. Lava sheets cap the thick Seydiler 1 ignimbrite deposits at Olukpınar, Seydiler and Sağırlı.

The Seydiler 2 unit is prevalently exposed over the north-western part of the investigated area, in the area of Kale and from Bayat to Avdan, where it is separated from the lower Seydiler 1 unit by the relative pumice-fall and surge deposit; in the Yazılıkaya valley it occurs as an isolated unit.

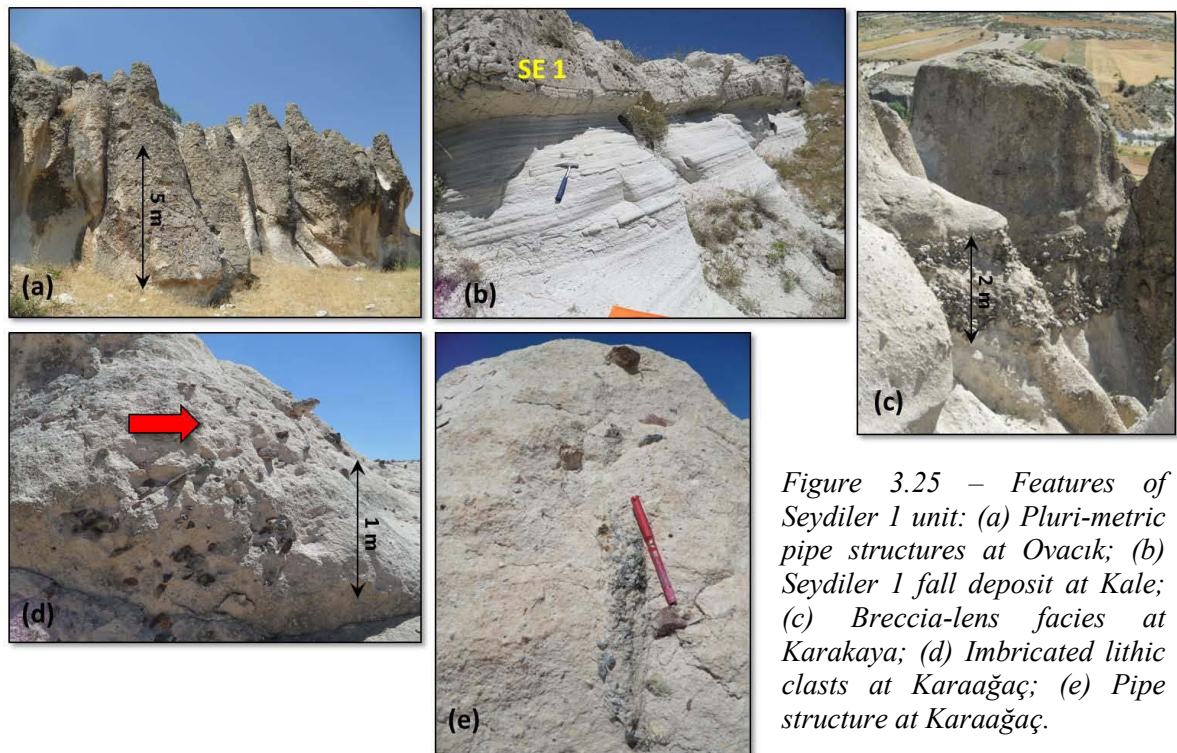
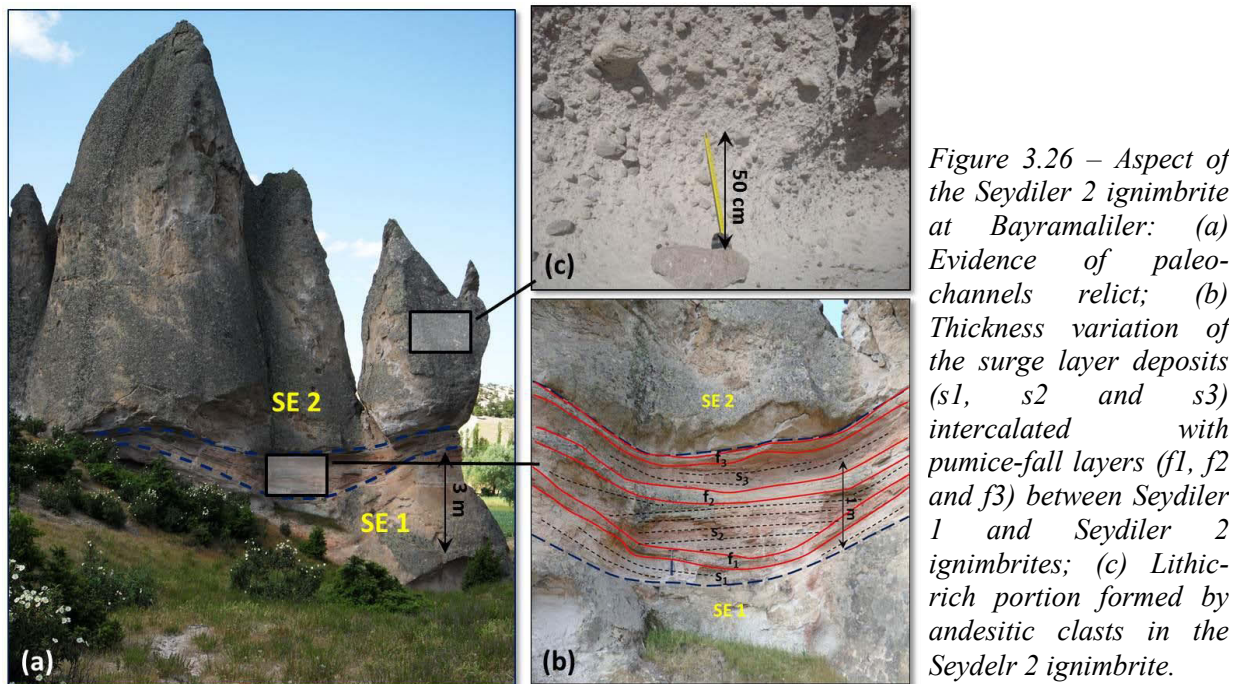


Figure 3.25 – Features of Seydiler 1 unit: (a) Pluri-metric pipe structures at Ovacık; (b) Seydiler 1 fall deposit at Kale; (c) Breccia-lens facies at Karakaya; (d) Imbricated lithic clasts at Karaağaç; (e) Pipe structure at Karaağaç.

The pumice fall and surge deposit preceding the ignimbrite in the area between Bayramaliler and Demirli shows the evidence of the interaction with the paleo-topography. Here, the presence of paleo-channels are evidenced by thickness variations and trend of surge deposits intercalated with

the pumice fall layers (fig. 3.26 a, b). At other places the surge layers thickness and trend don't display such evident lateral variations.



Ignimbrite deposits exposed in the north-western part of the area, between the villages of Döğler and Demirli, are generally massive; they are made up of a lower pumice-rich portion containing white and grey, sub-triangular and elongated clasts, and an upper lithic-rich portion containing andesitic clasts up to 10 cm in size (fig. 3.26 c). This lithic-rich facies gradually passes laterally to massive lapilli tuff deposits.

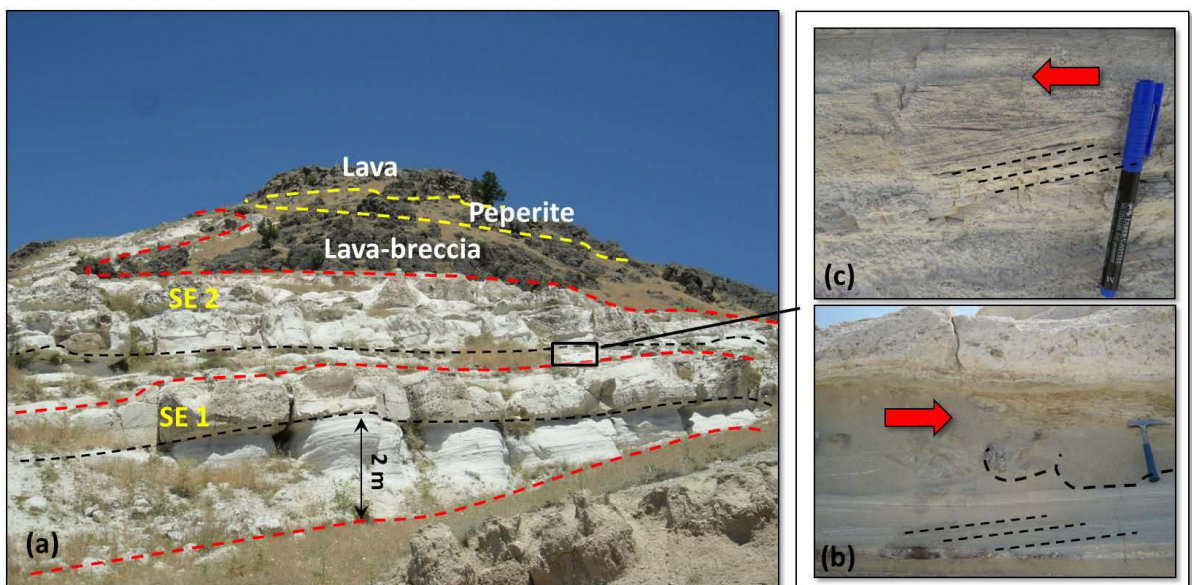


Figure 3.27 – Seydiler ignimbrite at Kale: (a) Stratigraphic section. Sedimentary structures preserved in the surge deposits at the base of Seydiler 2 ignimbrite: (b) Antidune cross-bedding (at the base), chute and pools structures (at the top); (c) Oblique lamination.

At Kale (fig. 3.23 e; 3.27 a) the ignimbrite deposit is preceded by 5-m-thick surge layers deposit, with many sedimentary structures such as load casts, antidune cross-bedding, oblique lamination and chute and pools (fig. 3.27 b, c). These features yield constrains on the paleo-flow direction. The overlying ignimbrite deposit displays a basal ground layer formed by accessory lithic clasts and crystals, overlain by the main part of the deposit, characterized by inverse grading of pumice clasts and exhibiting imbrication. Lithic clasts content is very low ($< 5\%$). The ignimbrite deposit is overlain by lava-breccia, peperite deposits and lavas, with the evidence of a relict volcanic conduct (fig. 3.27 a).

At Döğer, Kayıhan, Yeşilyayla, and Çukurca, the upper portion of the ignimbrite deposits is locally indurated and displays pumice dissolution cavities; pumice imbrication is generally clearly developed.

b. Incik 1b ignimbrite deposit

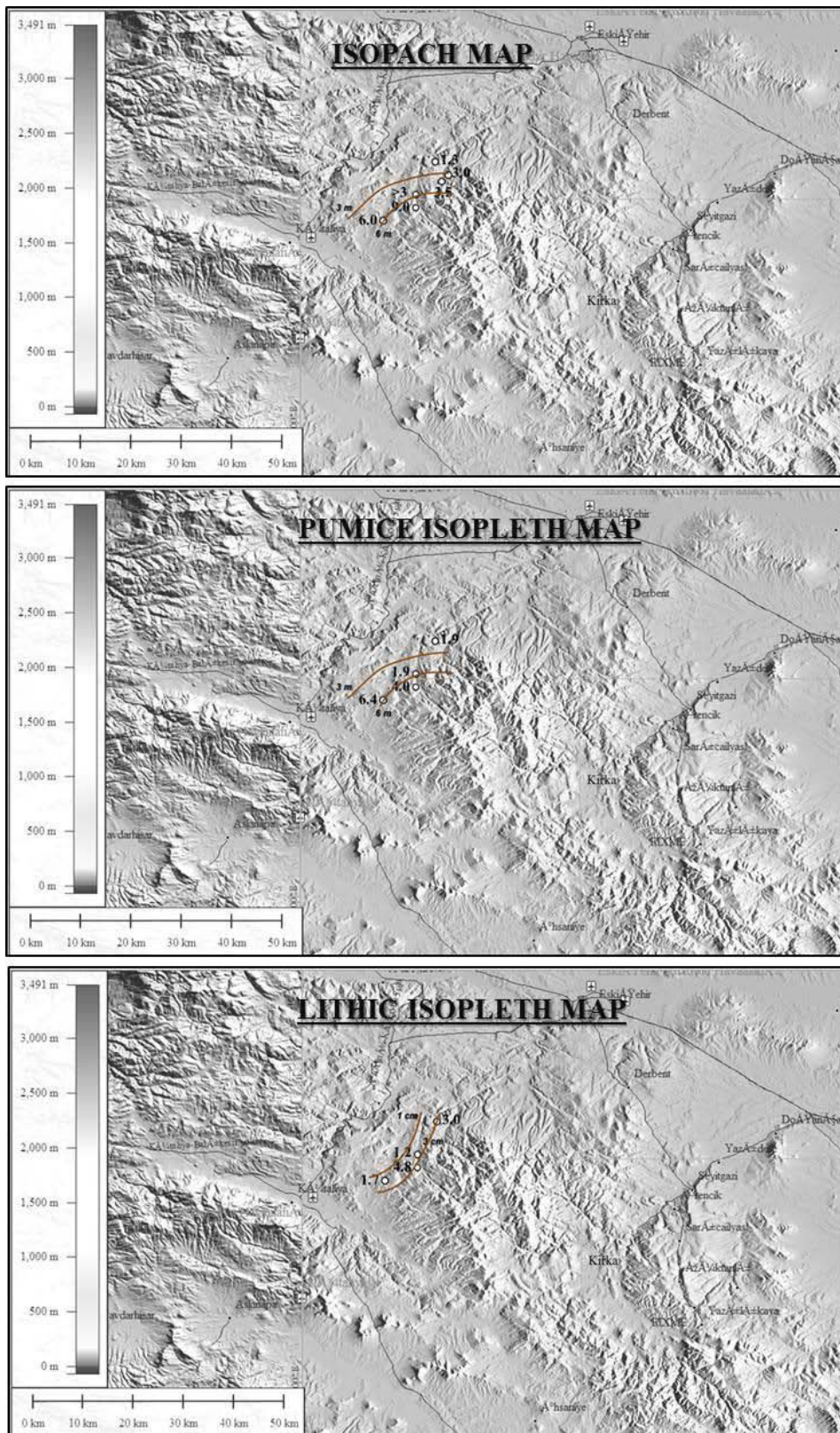


Figure 3.29 – Incik 1b sub-unit ignimbrite (thickness values are expressed in meters; clasts grain size values are expressed in centimetres).

c. Incik 1c fall deposit

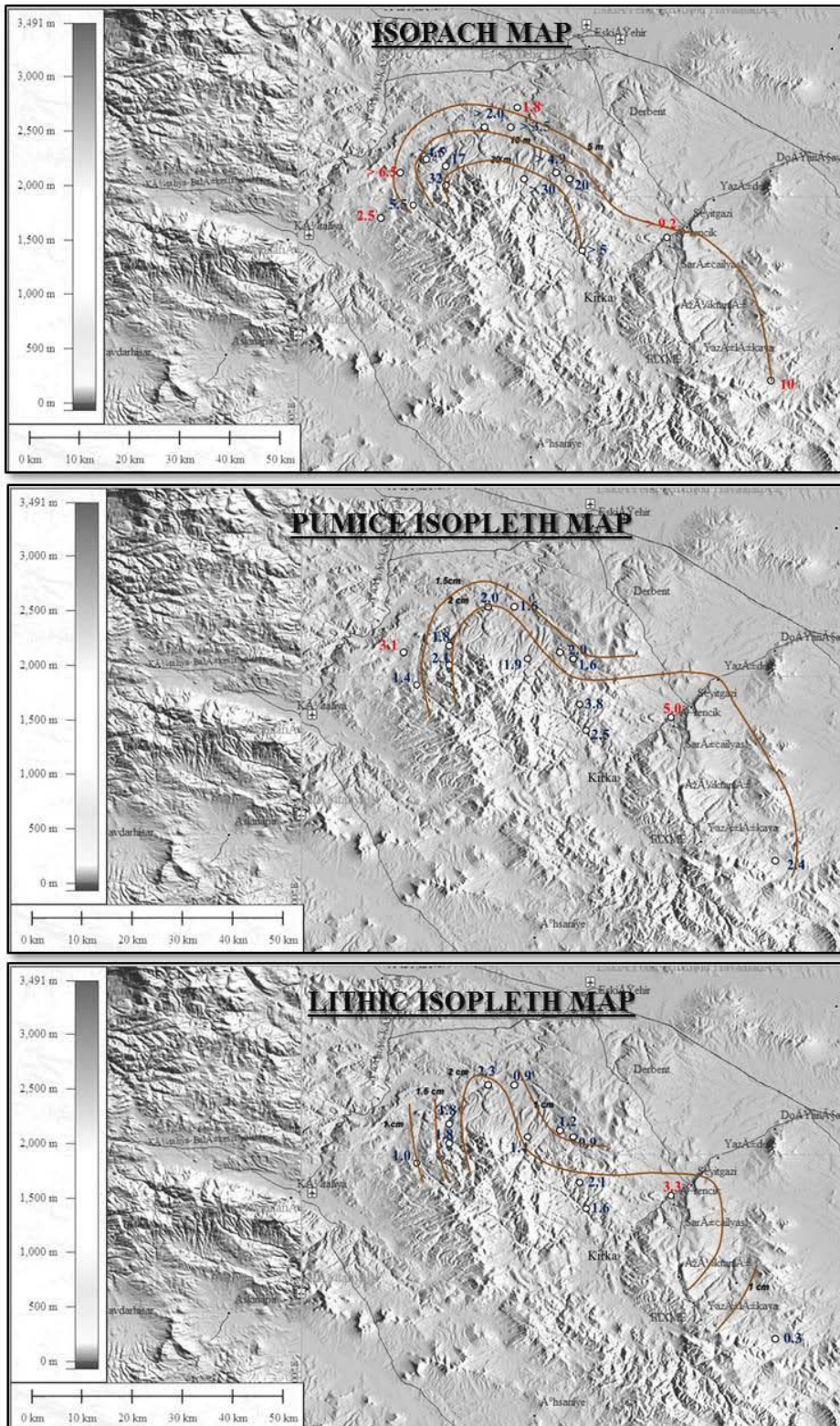


Figure 3.30 – Incik 1c sub-unit fall deposits (thickness values are expressed in meters; clasts grain size values are expressed in centimetres).

2. Incik 2 unit

a. Incik 2 fall deposit

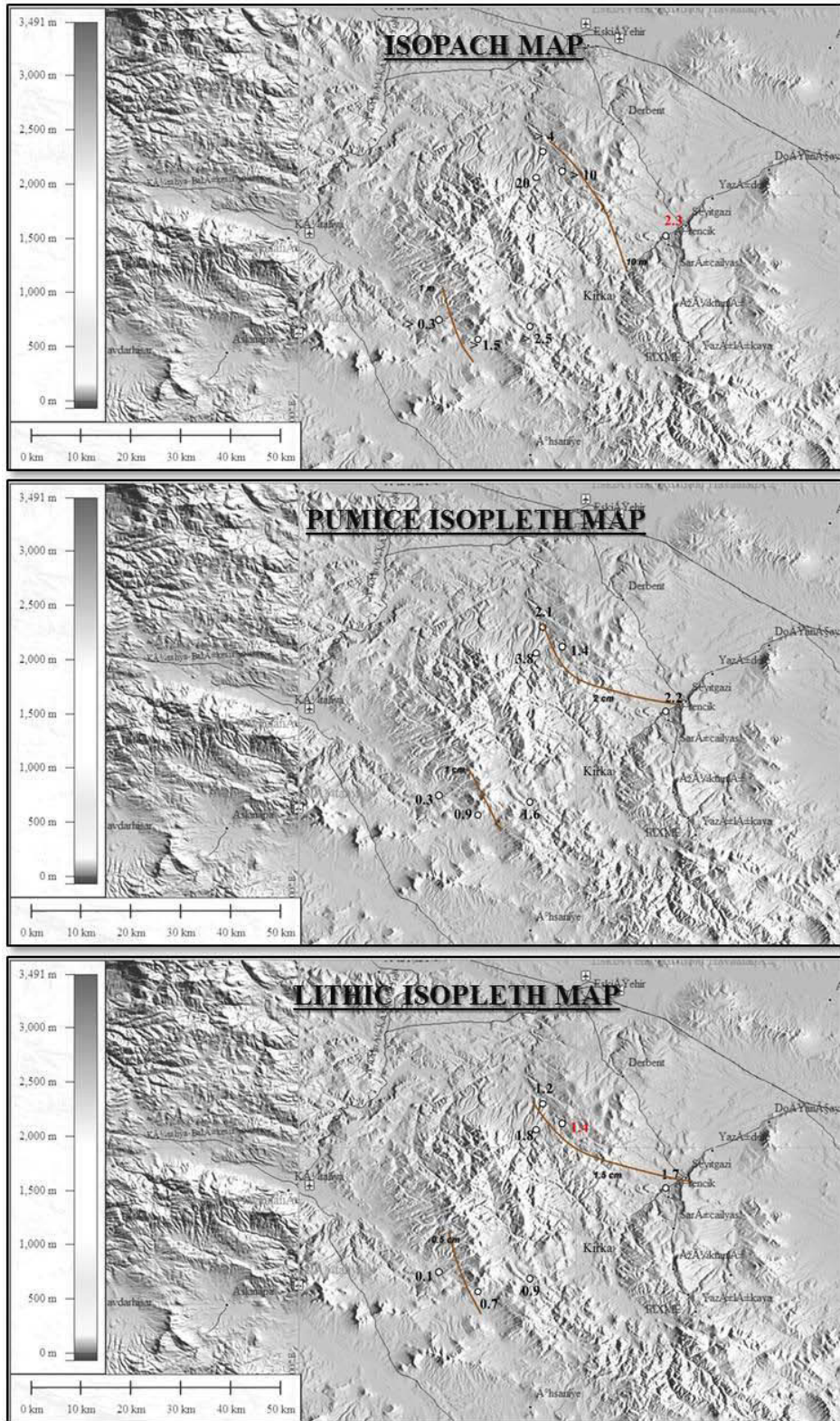


Figure 3.32 – Incik 2 unit fall deposits (thickness values are expressed in meters; clasts grain size values are expressed in centimetres).

b. Incik 2 ignimbrite deposit

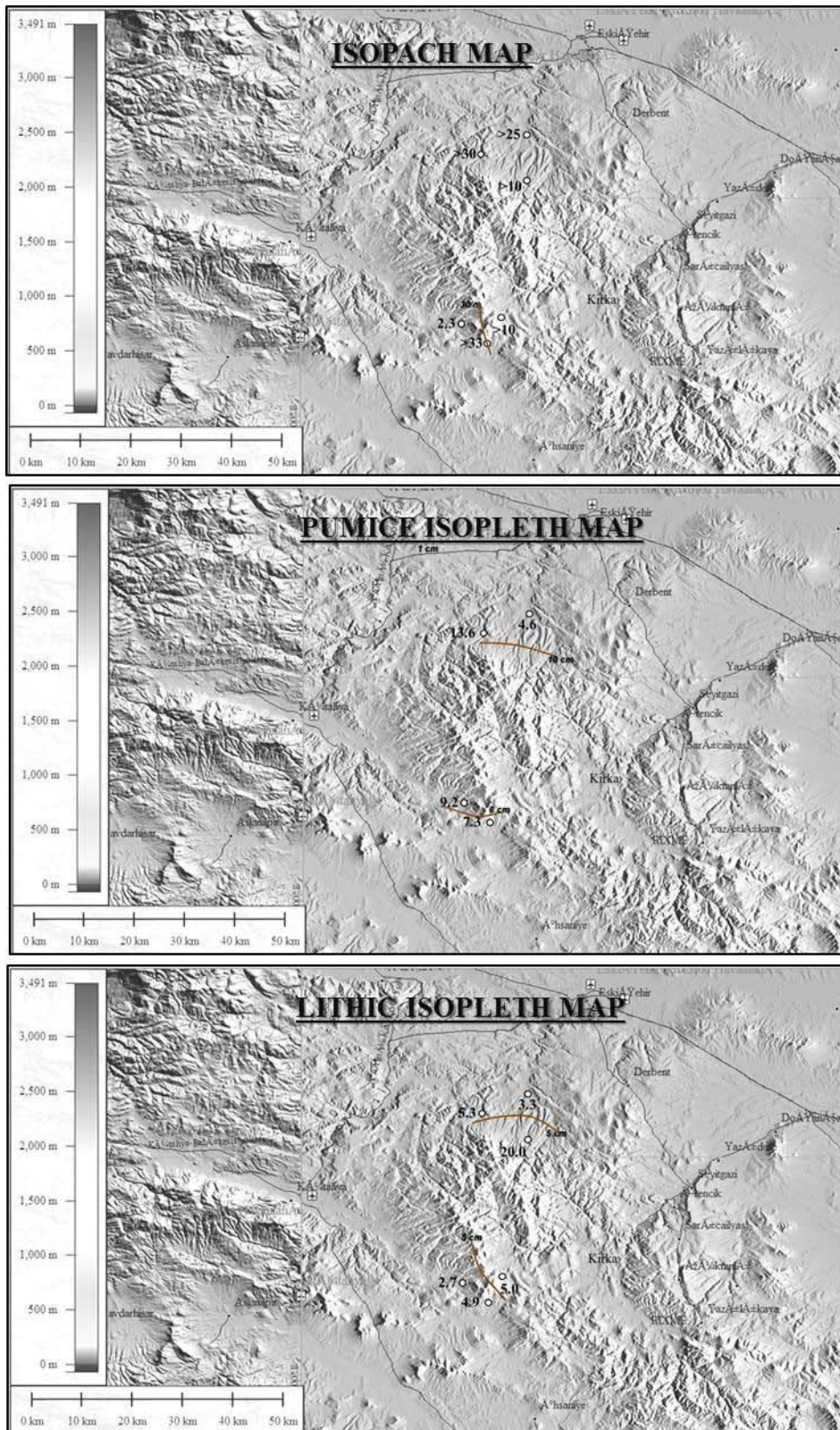


Figure 3.33 – Incik 2 unit ignimbrite (thickness values are expressed in meters; clasts grain size values are expressed in centimetres).

b. Sabuncu 1 ignimbrite deposit

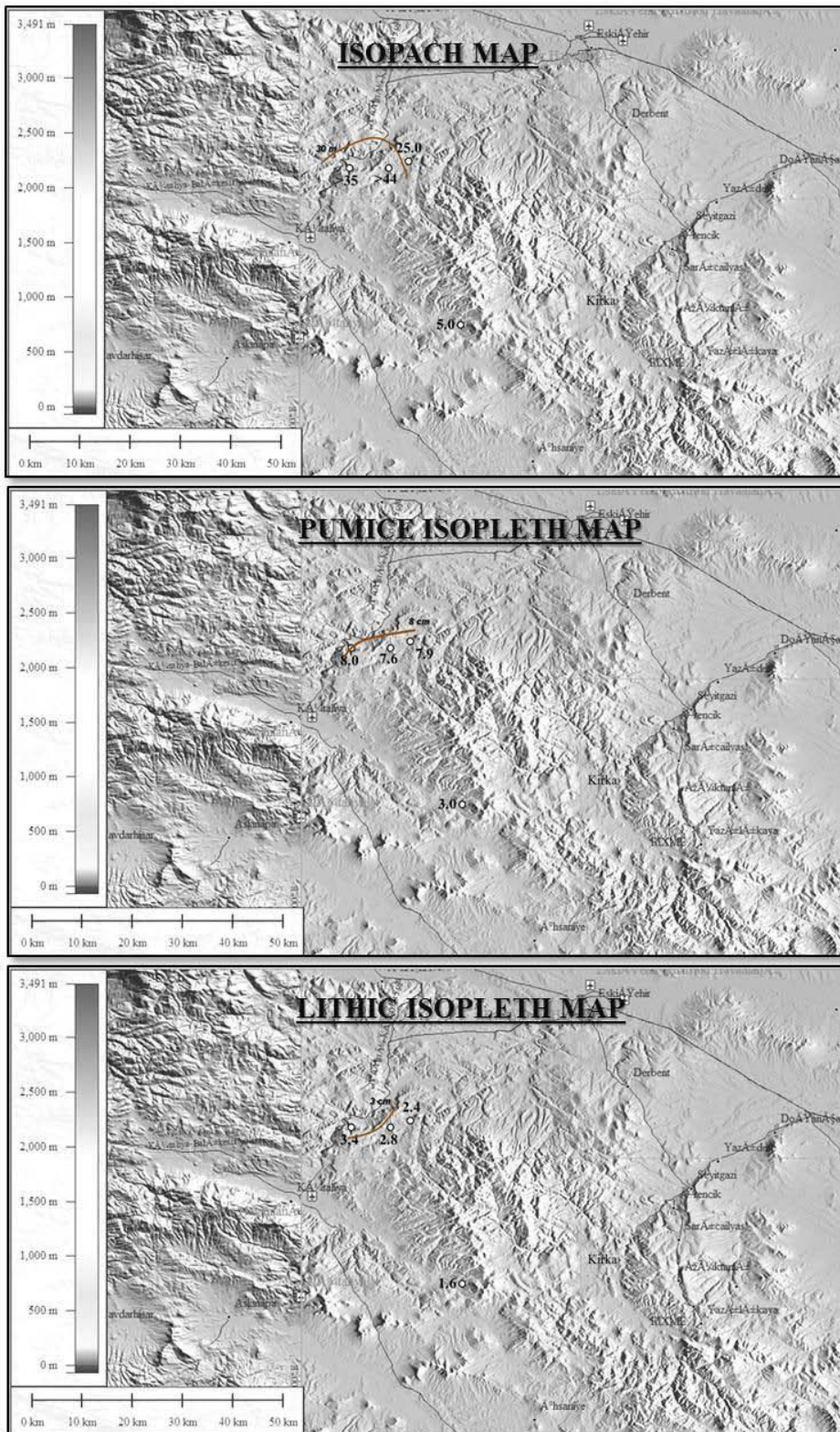


Figure 3.35 – Sabuncu 1 unit ignimbrite (thickness values are expressed in meters; clasts grain size values are expressed in centimetres).

2. Sabuncu 2 unit

a. Sabuncu 2 fall deposit

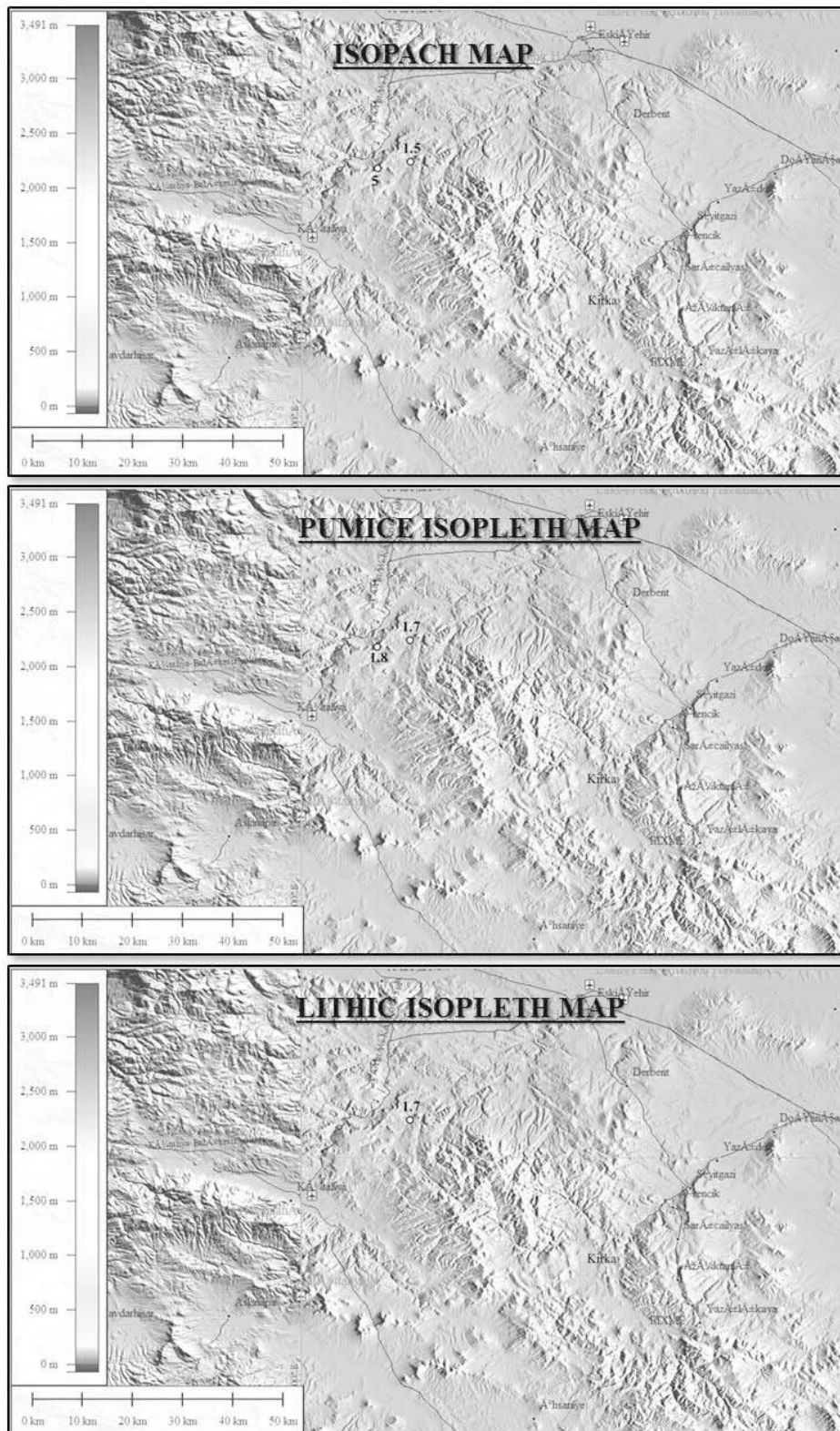


Figure 3.36– Sabuncu 2 unit fall deposits (thickness values are expressed in meters; clasts grain size values are expressed in centimetres).

b. Sabuncu 2 ignimbrite deposit

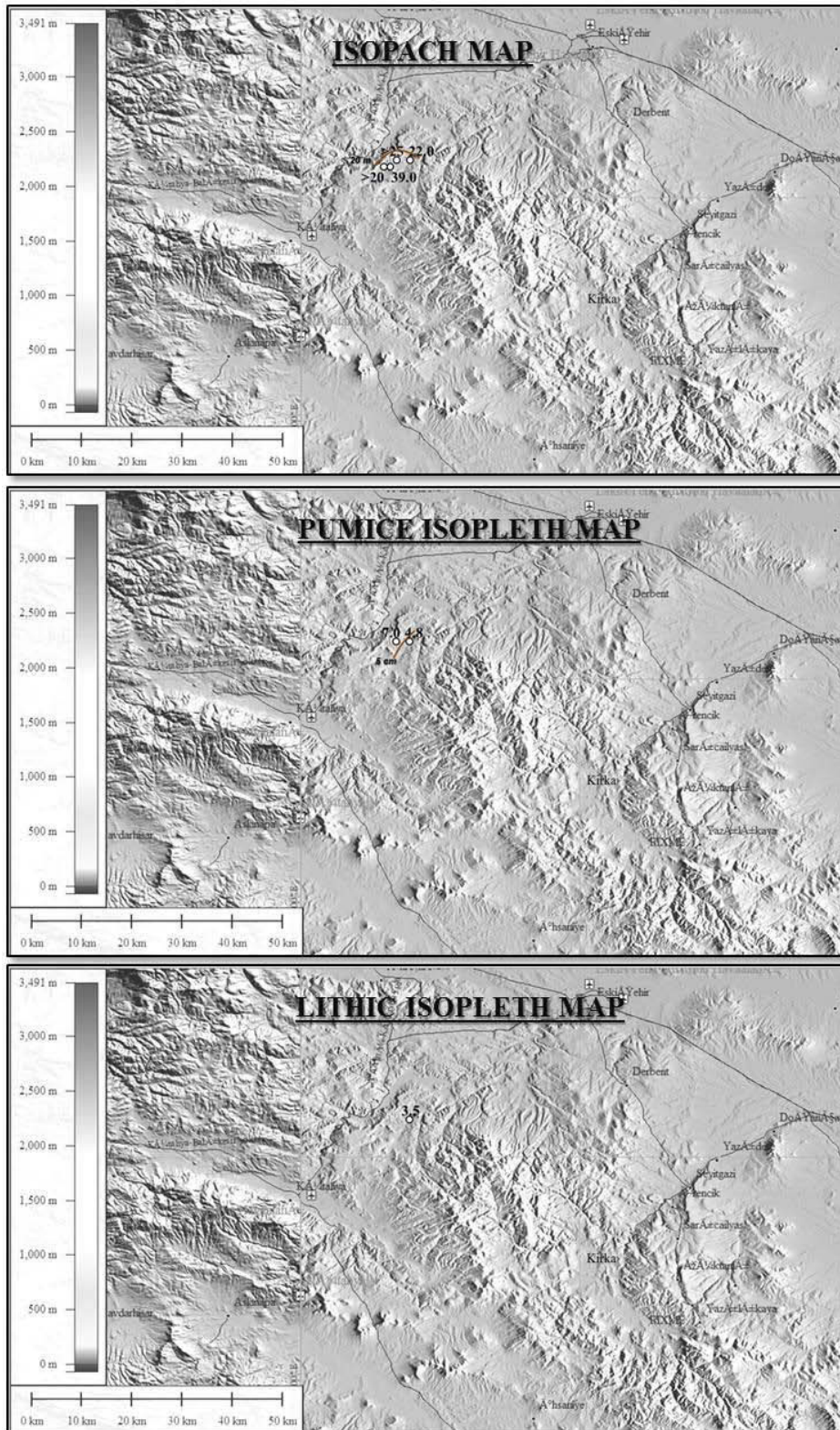


Figure 3.37 – Sabuncu 2 unit ignimbrite (thickness values are expressed in meters; clasts grain size values are expressed in centimetres).

➤ SEYDILER IGNIMBRITE

1. Seydiler 1 unit

a. Seydiler 1 ignimbrite deposit

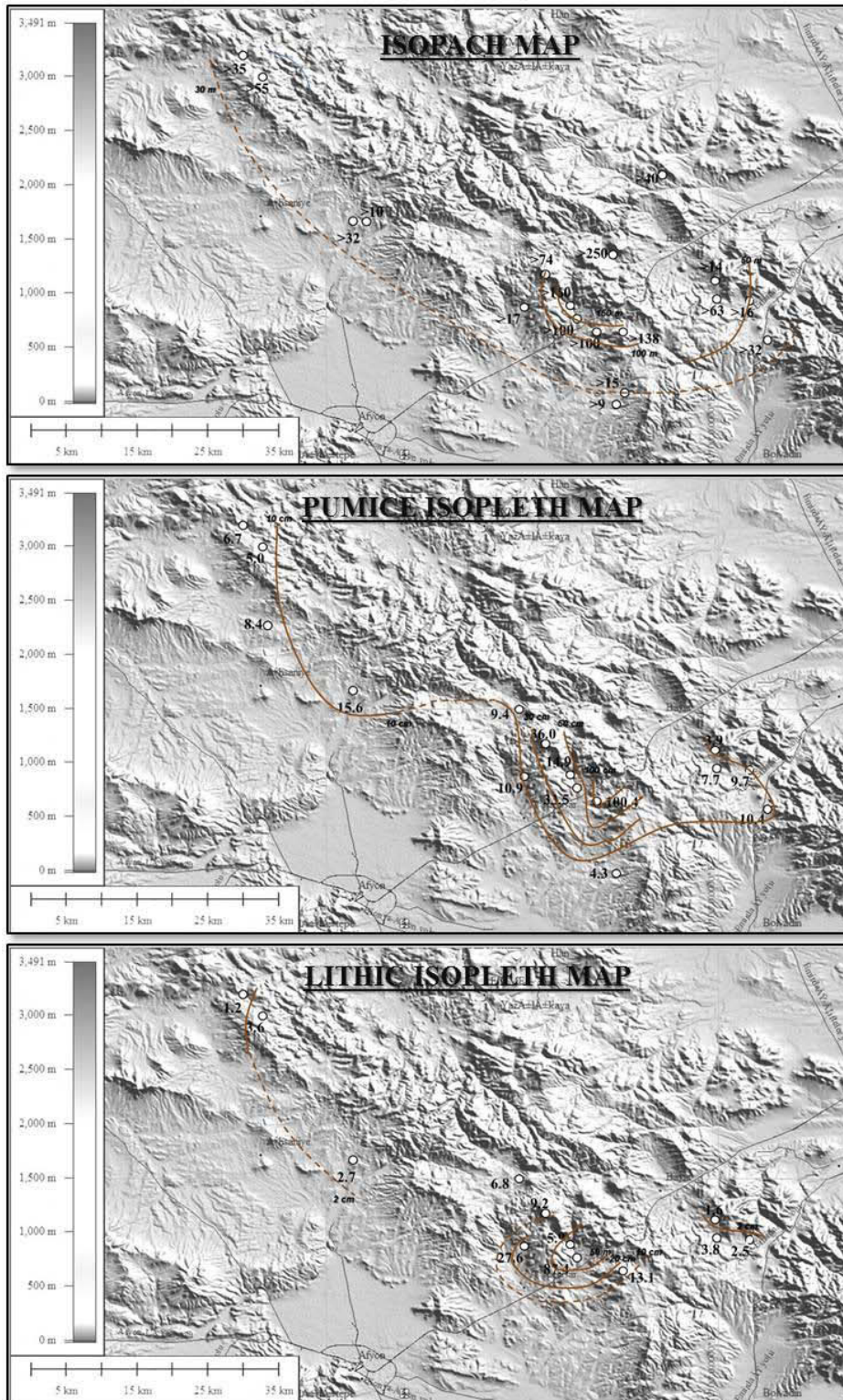


Figure 3.38– Seydiler 1 unit ignimbrite (thickness values are expressed in meters; clasts grain size values are expressed in centimetres).

1. Seydiler 2 unit

a. Seydiler 2 fall deposit

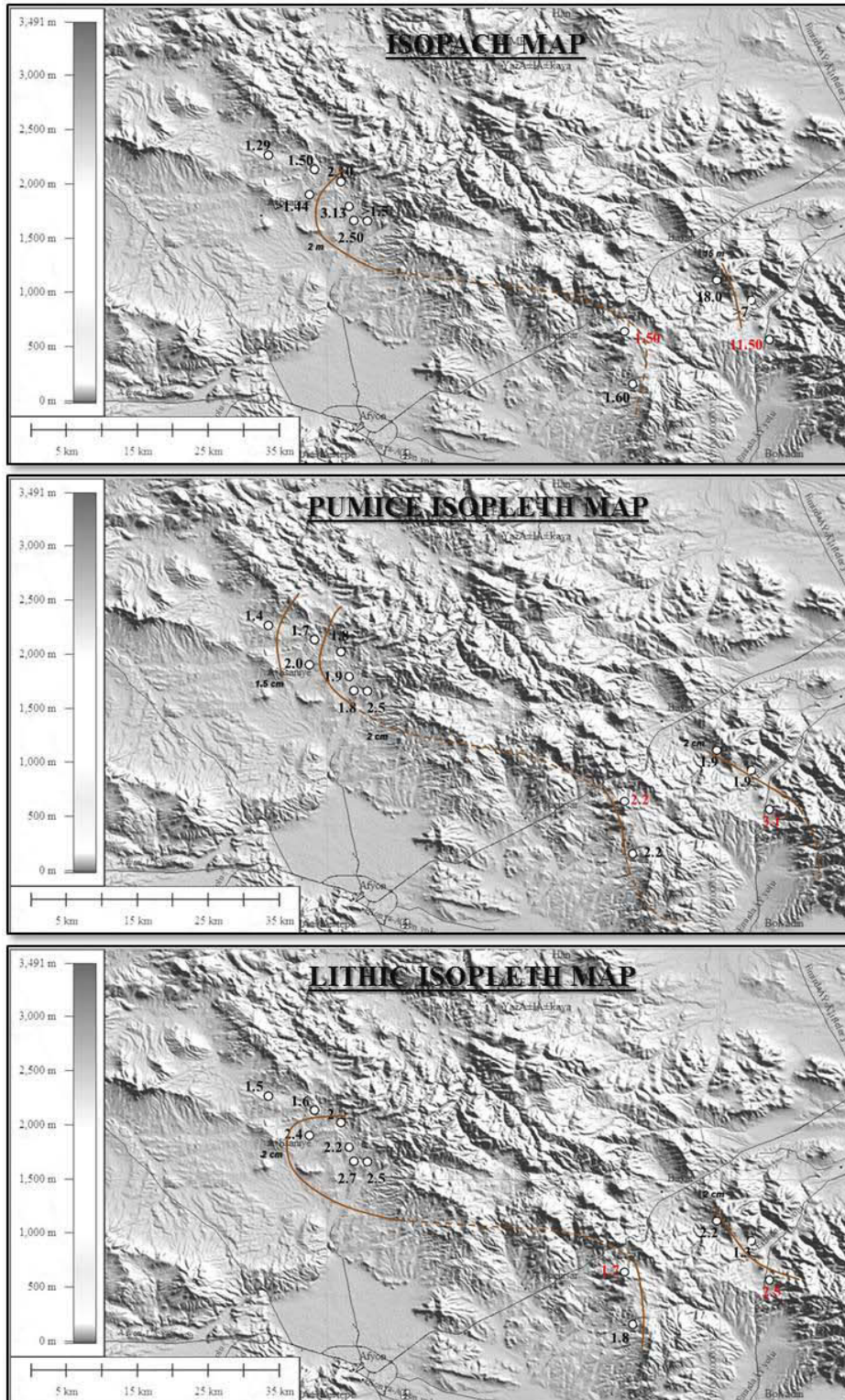


Figure 3.39– Seydiler 2 unit fall deposits (thickness values are expressed in meters; clasts grain size values are expressed in centimetres).

b. Seydiler 2 ignimbrite deposit

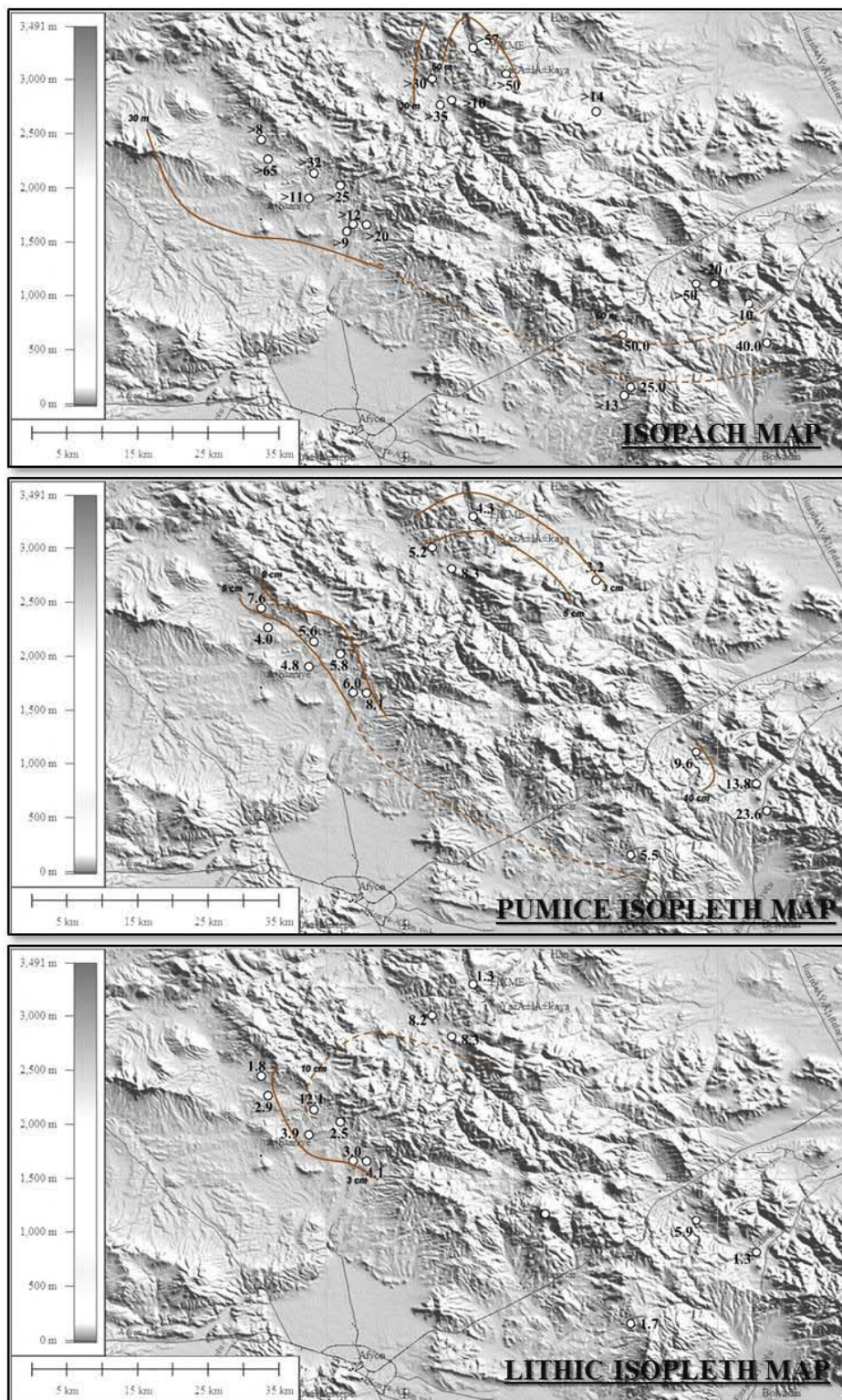


Figure 3.40 – Seydiler 2 unit ignimbrite (thickness values are expressed in meters; clasts grain size values are expressed in centimetres).

4 – Paleomagnetic sampling and Magnetic mineralogy

4.1 – Kızılıkaya ignimbrite

Paleomagnetic sampling was performed at 35 sites in 7 localities at different distance and relative position from the vent position inferred by Le Pennec et al. (1998) and Froger et al. (1998), namely: Akköy, Güzelöz, Ihlara, Soğanlı, Tilköy, Yeşilöz and Ovacık (fig. 4.1). All the sampled sections localities have a near-horizontal basal contact. The cores were cut to standard cylindrical specimens for a total of about 444 specimens.

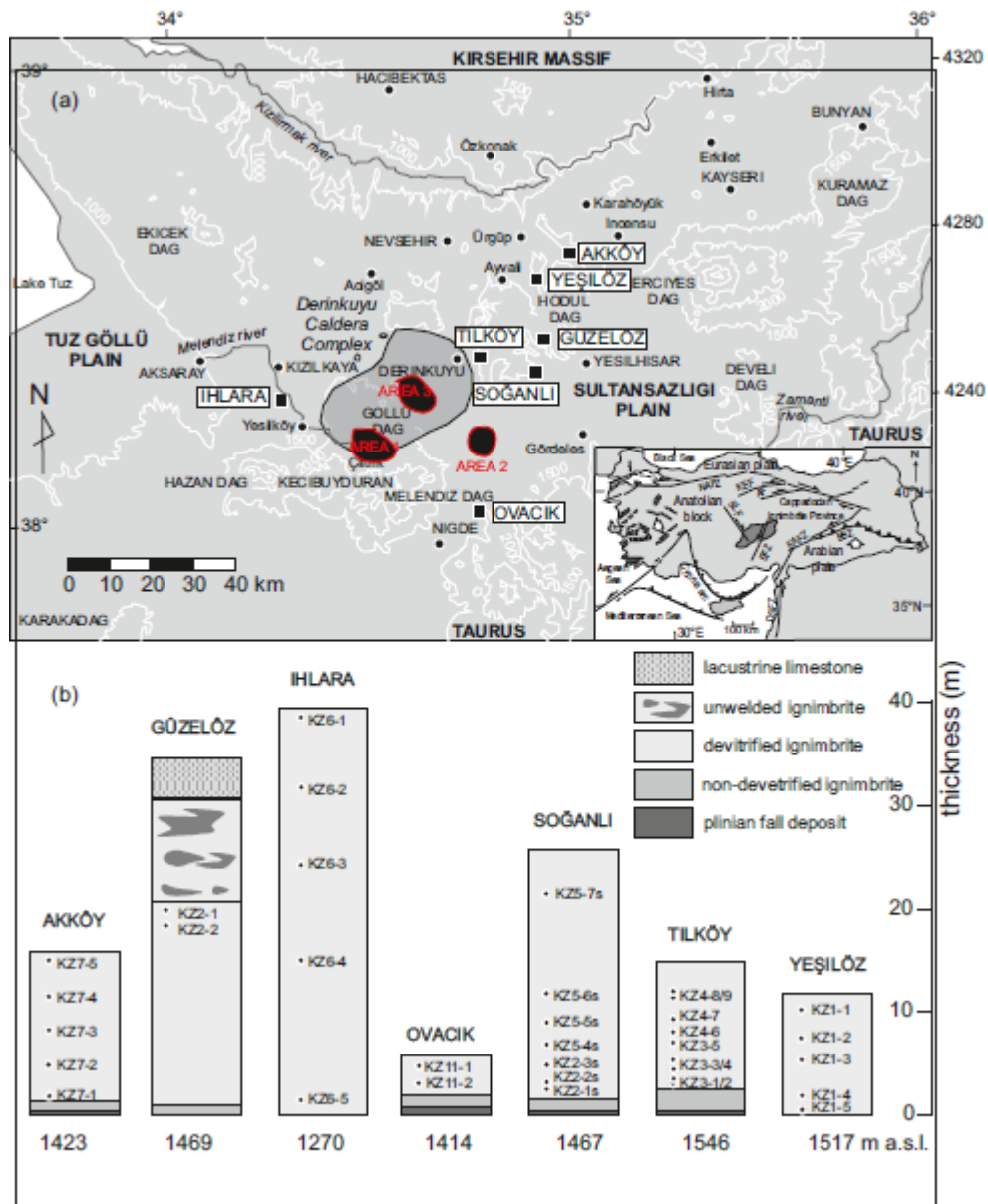


Figure 4.1 - (a) Sketch map of the Nevşehir plateau in the Central Anatolian Volcanic Province (CAVP). Contour lines = 500 m, square = sampled localities; the grey area represents the inferred source area after Le Pennec et al. (2005). Black areas represent the inferred vent position

according to: Pasquaré et al. (1988) (area 1); Schumacher and Mues-Schumacher (1996b) (area 2); and Le Pennec (2000) (area 3). Inset: tectonic sketch map of Anatolia plate. Acronyms: NAFZ/EAFZ = North/East Anatolian Fault Zone; KEF = Kırkkale-Erbba Faul; AF = Almus Fault; SLF = Salt Lake Fault; EFZ = Ecemiş Fault Zone; DSFZ = Dead Sea Fault Zone; BSZ = Bitilis Suture Zone; (b) Stratigraphy at sampling localities. Labels refer to sampling sites; figures at the bottom = elevation.

Thermal demagnetization of the IRM components shows dominant low and medium coercivity components (fig. 4.2). The maximum blocking temperature is mainly around 560-580 °C, up to 650 °C. These results point to low-Ti titanomagnetite as the main ferromagnetic mineral in the Kızılkaya ignimbrite, locally associated to a high coercivity phase, probably altered magnetite and/or hematite.

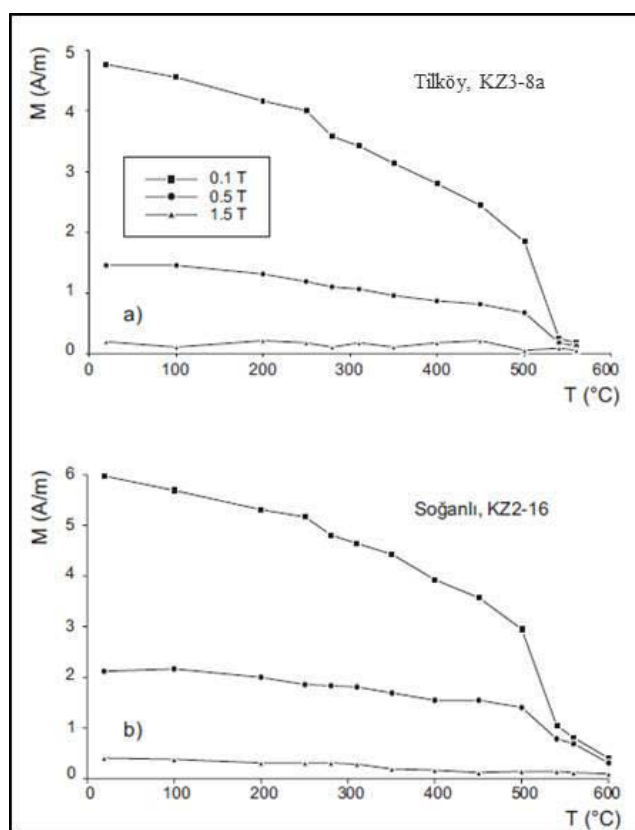


Figure 4.2 - Thermal demagnetization of the IRM components, after Lowrie (1990). In a) a specimen from Tilköy; in b) a specimen from Soğanlı.

To better resolve the occurrence of different magnetic phases at site level, it has been used the cumulative log-Gaussian analysis proposed by Kruiver et al. (2001) for the IRM acquisition data. Magnetic mineral assemblage can be distinguished in three different types (fig. 4.3 and fig. 4.5):

1. a single low-coercivity phase, which saturates at low field (0.1 – 0.3 T) and shows low values of the coercivity of remanence B_{cr} , ranging from 20 to 40 mT. It is highlighted by the presence of a single ferrimagnetic component in the Linear, Gradient and Standardized Acquisition Plot (LAP, GAP, SAP) (fig. 4.3 a). This phase is interpreted as Ti-magnetite. It is present at all localities; at Güzelöz, Tilköy, the lower part of Akköy and in the upper half part of Ihlara section it is the only component. A special case is Yeşilöz, where Ti-magnetite is associated to an iron sulfide mineral;
2. two magnetic phases (fig. 4.3 b), both with low- to medium-coercivity. One has the same characteristics described in point (1). The second saturates at higher fields (< 1 T); B_{cr} values range from 50 to 100 mT. These results suggest Ti-magnetite plus altered Ti-magnetite (i.e. Ti-magnetite which suffered maghemitization processes), as also pointed out by thermal

demagnetization of IRM (fig. 4.2 b). Soğanlı, the basal portion of the ignimbrite at Ihlara, and the upper portion at Akköy, typically show the presence of these phases.

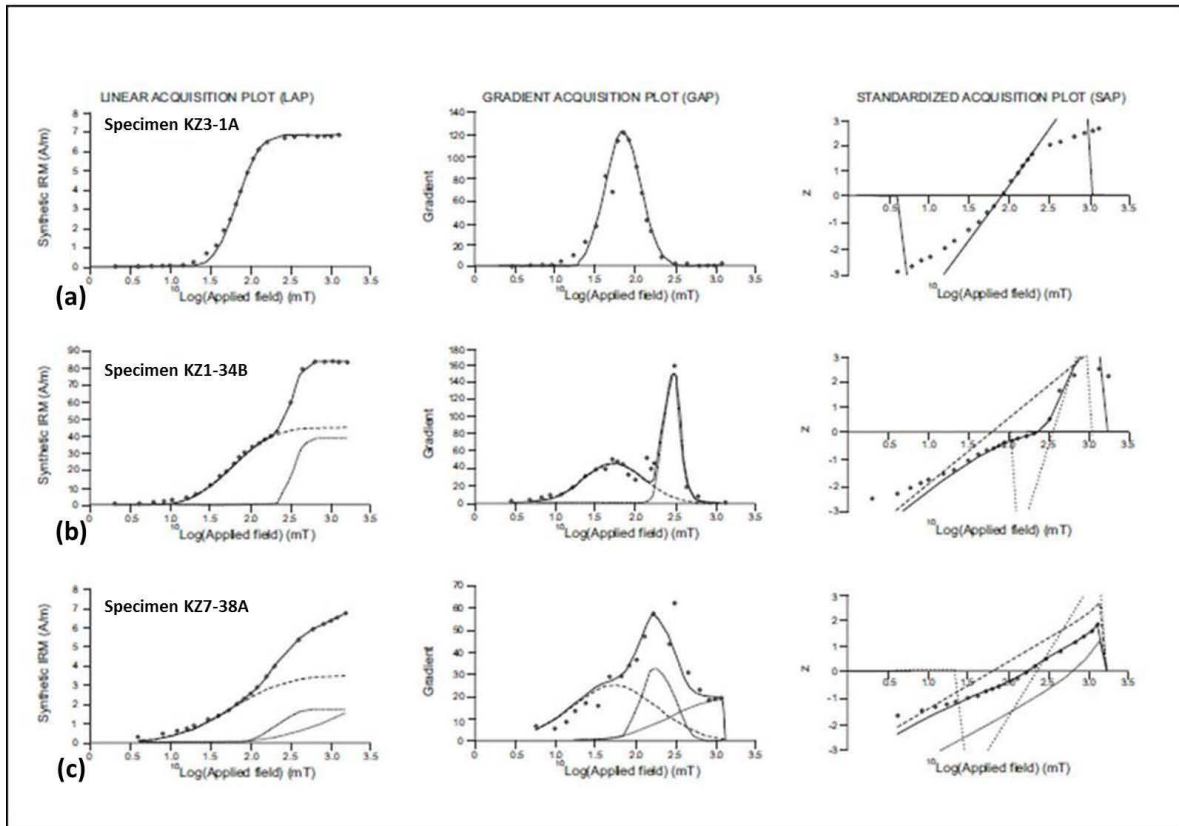


Figure 4.3 - IRM component analysis by Kruiver et al. (2001) method. Data are fitted in three different graphics: on the left, a linear acquisition plot, LAP, in the middle, a gradient acquisition plot, GAP; on the right, a standardized acquisition plot, SAP. In (a) one magnetic component (Tilköy); in (b) two magnetic components (Yeşilöz); in (c) three magnetic components (Akköy). Symbols: dot = IRM data; thick solid line = sum of the individual components; long dash line: component 1; short dash line: component 2; thin short dash line: component 3.

3. Three magnetic phases. The occurrence of a high-coercivity component, not saturated by fields < 1.5 T, whose B_{cr} values are high, mainly ranging from 100 to 200 and in one case up to 400 mT (fig. 4.4) reveals the presence of a minor amount of hematite (fig. 4.3 c). This behavior is characteristic of the upper part of Soğanlı section. Here, from the base to the top of the deposit, all magnetic parameters point out to an increasing effect of oxidation processes: at the base, we only found Ti-magnetite ($B_{cr} = 30\text{-}40$ mT, Median Destructive Field (MDF) = 30 mT), then also altered Ti-magnetite ($B_{cr} = 50\text{-}60$ mT, MDF = 40-50 mT), and in the upper part hematite is present ($B_{cr} = 100\text{-}400$ mT, MDF > 60 mT). The top of the Akköy section falls as well within this type.

Both S-ratio at 0.1 and 0.3 T are computed to assess the relative contribution of high- versus low-coercivity components. Normally computed for marine sediments, S-ratios were used by Sweetkind et al. (1993), for the Carpenter Ridge Tuff, Colorado, for the definition of different oxide groups,

resulting from hydrothermal alteration. For Kızılkaya, in the 60% of the sites, $S_{0.3T}$ is higher than 0.9; in the remaining sites the $S_{0.3T}$ drops to 0.3 and varies mainly between 0.3 and 0.5. The variation of both B_{cr} and $S_{0.3T}$ ratio as a function of the stratigraphic height is displayed in figure 5.4; the grey area indicates the typical range of variability associated with the presence of Ti-magnetite. $S_{0.1T}$ is more variable, ranging from -0.16 to 0.84, its value being also affected by the ferrimagnetic grain-size (Kruiver et al. 2001).

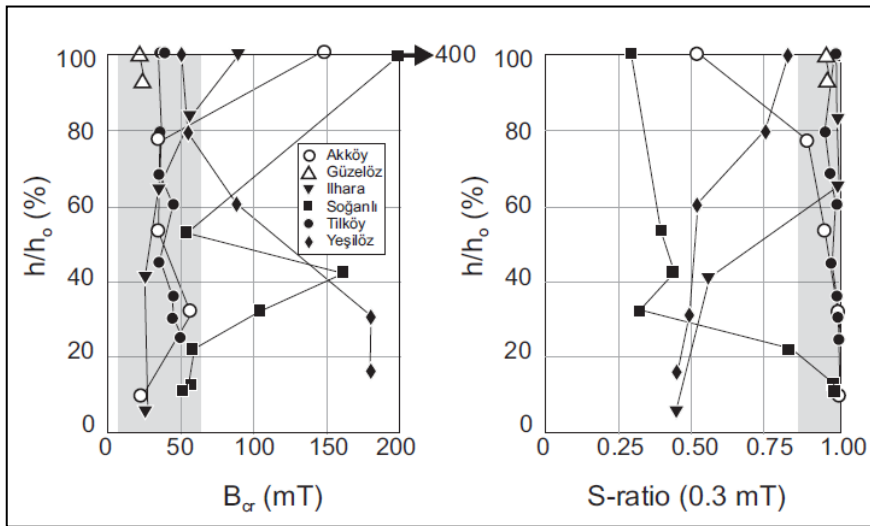


Figure 4.4 - B_{cr} and $S_{0.3T}$ variation as a function of normalized stratigraphic height. Grey area indicate the variability range for occurrence of low-coercivity ferrimagnetic component.

No correlation between oxidation and deposit stratigraphic height, is possible (fig. 4.5). Only on four out of six localities the base contact of the ignimbrite deposits crops out (fig. 4.1 b) and only at one locality, the top contact is observed and the whole height sampled.

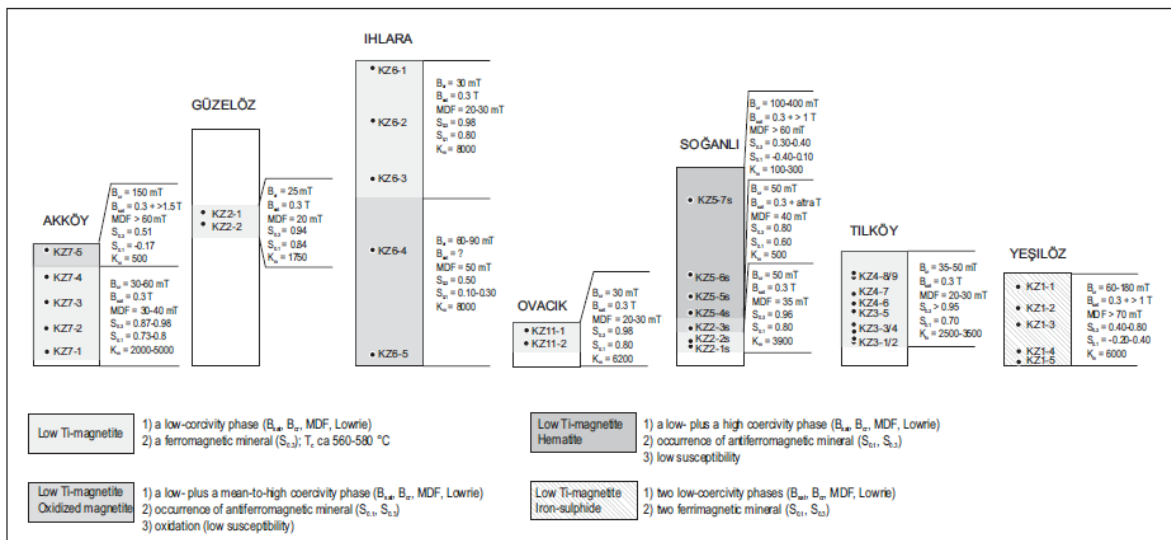


Figure 4.5 - Magnetic mineralogy assemblages at sampling localities. Main magnetic parameters are reported: B_{cr} = remanent coercive force; B_{sat} = saturation field; MDF = median destructive field during alternating field demagnetization; $S_{0.1}$, $S_{0.3}$ = S-ratios ($S_{0.1} = -IRM_{0.1T}/SIRM_{1T}$; $S_{0.3} = -IRM_{0.3T}/SIRM_{1T}$, Thompson and Oldfield 1986); k = bulk susceptibility.

On the whole, these results are consistent with those of the thin section analyses (Le Pennec et al., 1998), which showed abundant equant to elongate Fe-oxide grains, typically 50 to 400 μm in size. They suggested the presence of multidomain (MD) magnetite, but also recognized some small magnetite crystals included in biotite and apatite. Piper et al. (2002) report values from 0.07 to 0.11 for the ratio between the saturation remanent magnetization and the saturation magnetization (M_{rs}/M_s). They confirm the occurrence of dominant MD grains, plus a small fraction ($\sim 10 - 30\%$) of single-domain (SD) grains.

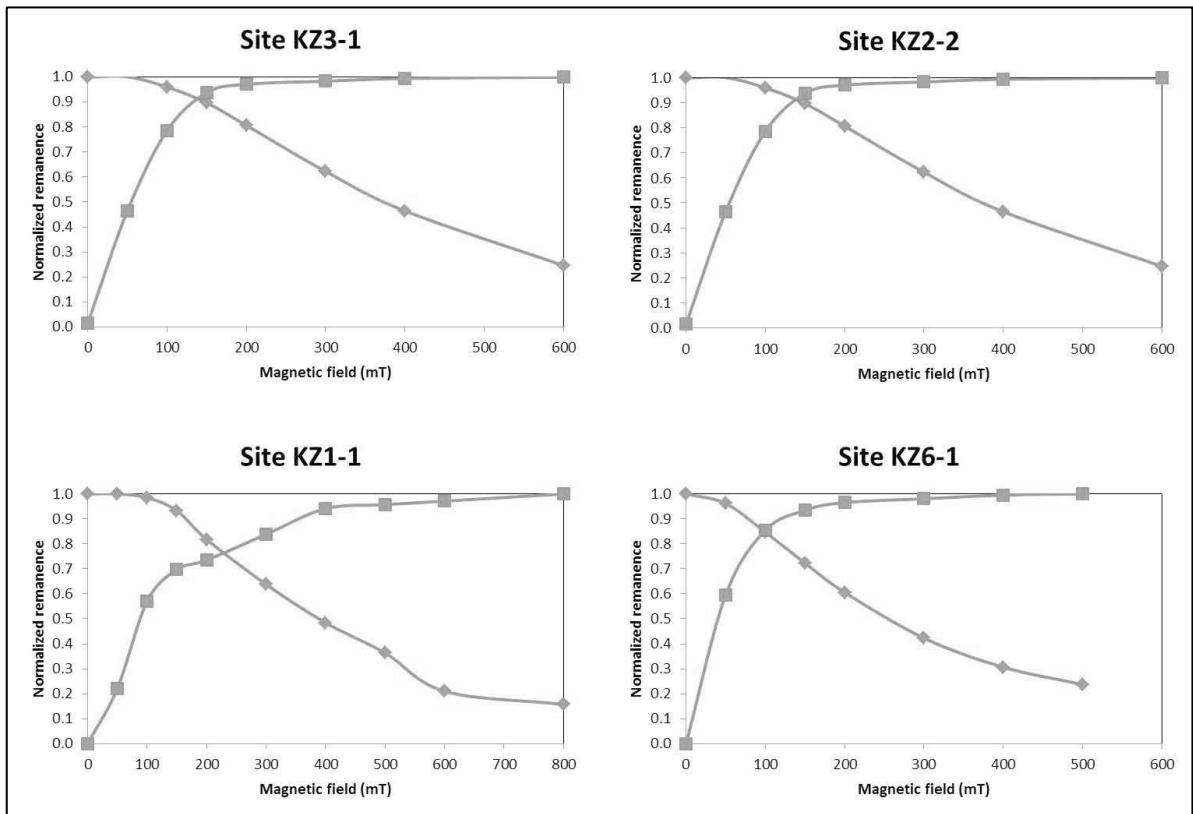


Figure 4.6 – Crossover diagrams for selected sites in the Kızılkaya ignimbrite: magnetization and demagnetization curves (normalized to the maximal magnetization) as a function of the applied AF field (mT).

In order to evaluate the presence of interaction fields among SD or MD grains, crossover diagrams (Cisowski, 1981) were performed for selected sites of the Kızılkaya ignimbrite, and results are reported in fig. 4.6. All samples present an asymmetrical acquisition curve compared to the demagnetization curve: R values range between 0.7 and 0.9. These results confirm the absence of SD and/or MD grains interacting grains.

4.2 – Afyon-Eskişehir ignimbrites

Paleomagnetic sampling was performed at 22 distributed localities (fig. 4.7), for a total of 36 sites and about 600 specimens.

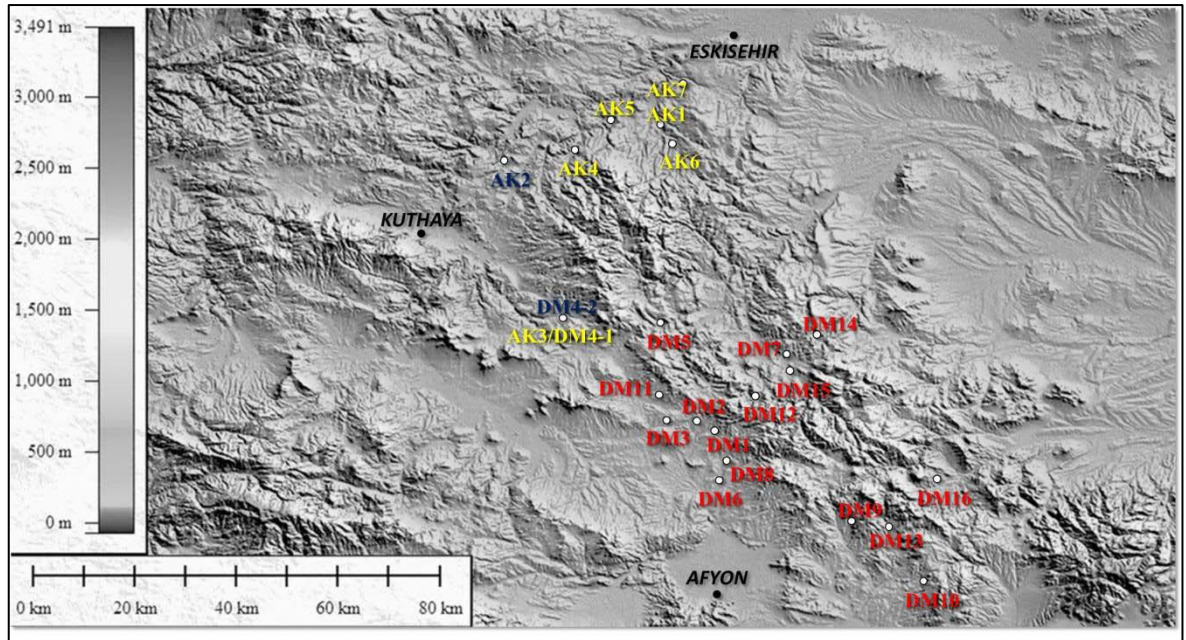


Figure 4.7 – Map of the sampled localities. In yellow: Incik ignimbrite; in blue: Sabuncu ignimbrite; in red: Seydiler ignimbrite.

The Incik ignimbrite was sampled at 6 localities and 8 sites for a total of 150 specimens; the Sabuncu ignimbrite comprises two sampled localities and sites for a total of 50 specimens; the Seydiler ignimbrite includes 15 localities and 25 sites (one site has been split into two blocks) for a total of 400 specimens. One lava site (AK2-2) was cored at the top of the Sabuncu 2 ignimbrite at Seydiköy (fig. 4.8).

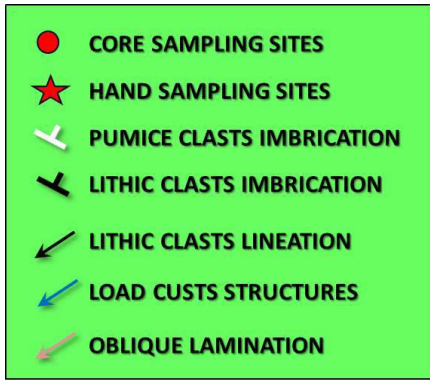
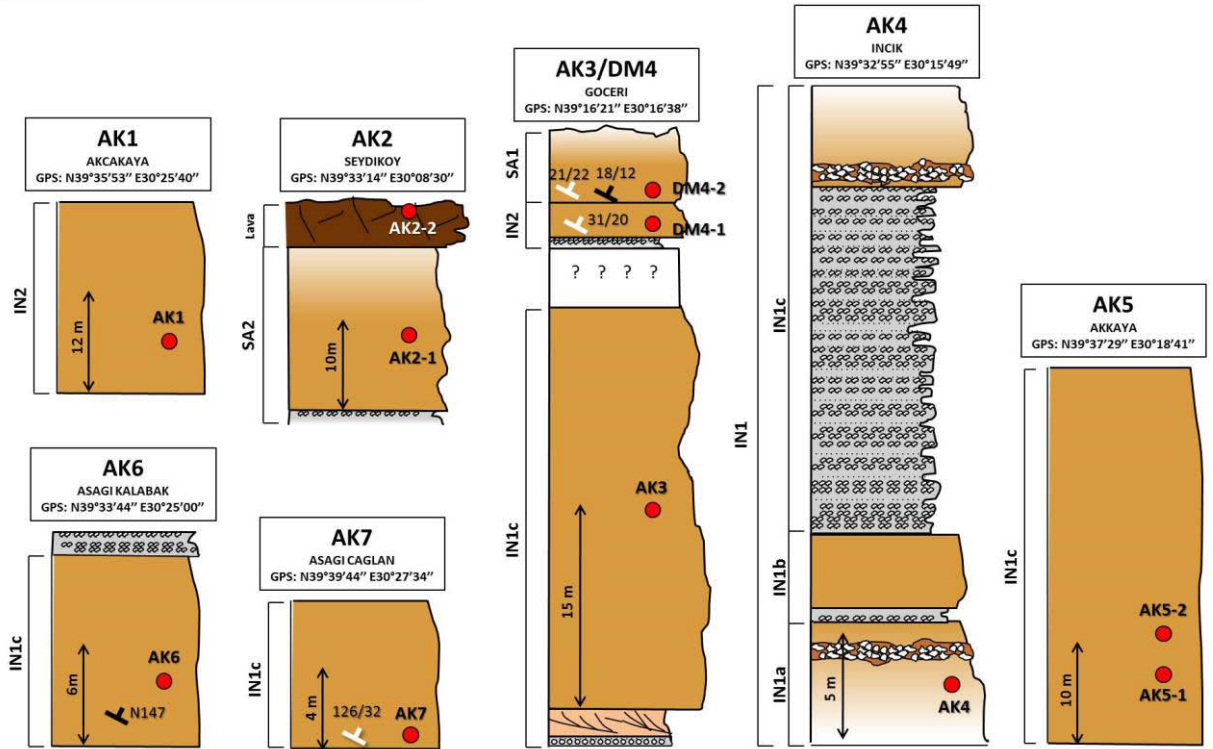
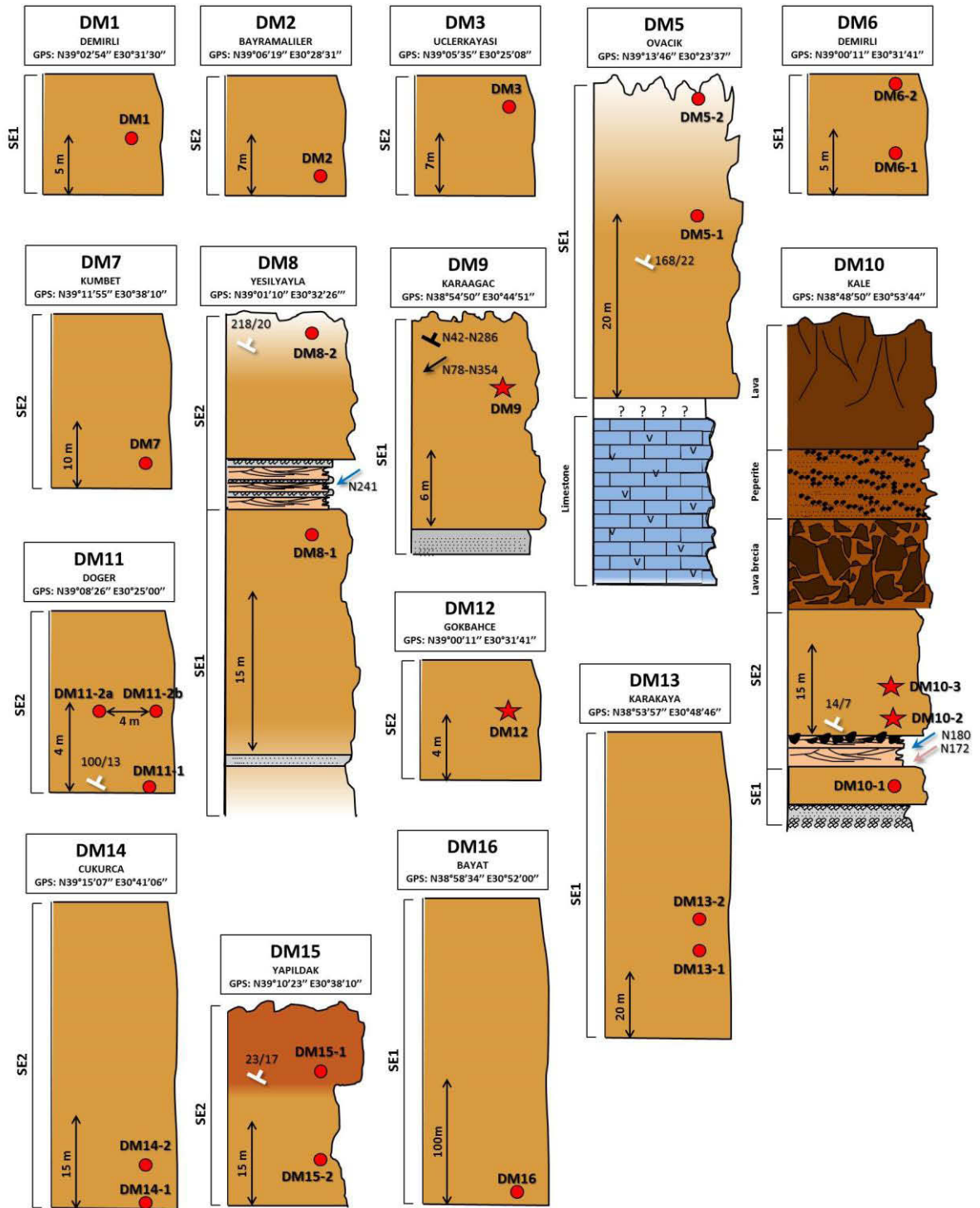


Figure 4.8 – Sampled localities and sites (continues in the following page). Graphic representations of lithofacies in the sections are the same as in the table 3.1.





IRM components analyses was performed using the method proposed by Kruiver et al. (2001), in order to attest the magnetic mineral assemblage. IRM analyses are integrated with back-field measurements and thermal demagnetization of the IRM components as well.

LOCALITY	SITE	SIRM (mT)		B_{cr} (mT)	Magnetic mineral		
		Component 1	Component 2		Ti-M	aTi-M	H
AK1		< 300		30-40			
AK2	AK2-1	< 300	< 1500	30-40		< 10%	
AK3		< 300		30			
AK4		< 300	< 1500	60		< 10%	
AK5	AK5-1	< 300		60			
	AK5-2	< 300	< 1500	40-60		< 5%	
AK6		< 300		40-60			
AK7		< 300		40-60			
DM1		< 300	< 1500	20-30		< 5%	
DM2		< 300		30-40			
DM3		< 300	< 1500	60-80		< 5%	
DM4	DM4-1	< 300		40-60			
	DM4-2	< 300		40-60			
DM5	DM5-1	< 300	< 1500	30-40		< 10%	
	DM5-2	< 300		20-30			
DM6	DM6-1	< 300		30-40			
	DM6-2	< 300		40-60			
DM7		< 300	> 1500	40-60		45%	
DM8	DM8-1	< 300		40-60			
	DM8-2	< 300		40-60			
DM9		< 300	> 1500	60-80		< 10%	
DM10	DM10-1	< 300	< 1500	80-120		< 5%	
	DM10-2	< 300		60-80			
	DM10-3	< 300	< 1500	60-80		< 5%	
DM11	DM11-1	< 300		40-60			
DM12		< 300	> 1500	80-120			< 5%
DM13	DM13-1	< 300	< 1500	60		< 5%	
	DM13-2	> 300	< 1500	60		< 5%	
DM14	DM14-1	> 300		30-40			
	DM14-2	< 300		30-40			
DM15	DM15-1	< 300		40-60			
	DM15-2	< 300	< 1500	60-80		< 5%	
DM16		< 300		30-40			

Table 4.1 – Magnetic mineral assemblages in the ignimbrites of Afyon-Eskişehir. It is also reported the fraction of secondary minerals detected in the mineral assemblage. Ti-M: Ti-magnetite; aTi-M: altered Ti-magnetite; H: hematite.

Two main types of mineral assemblages are distinguished in the ignimbrites of Afyon-Eskişehir (table 4.1; fig. 4.9):

1. Presence of a single low-coercivity phase, which saturates at low fields (< 0.3 T) and characterized by low values of the coercivity of remanence B_{cr} , typically ranging from 20 to 60 mT (fig. 4.9 a). The IRM acquisition plots of site DM10-2 point out the presence of a single ferromagnetic component saturated by fields < 0.3 T but with higher values of B_{cr} with respect other sites, between 60 and 80 mT. Thermal demagnetization of the IRM components shows dominant low coercivity component, whose maximum blocking temperature is mainly around 560 °C (fig. 4.10 a). This phase is interpreted as Ti-magnetite and it is present at all localities. At AK1, AK3, AK5-1, AK6, AK7, DM2, DM4, DM5-2, DM6, DM8, DM10-2, DM11, DM14, DM15-1 AND DM16 sites it represents the only ferromagnetic phase;

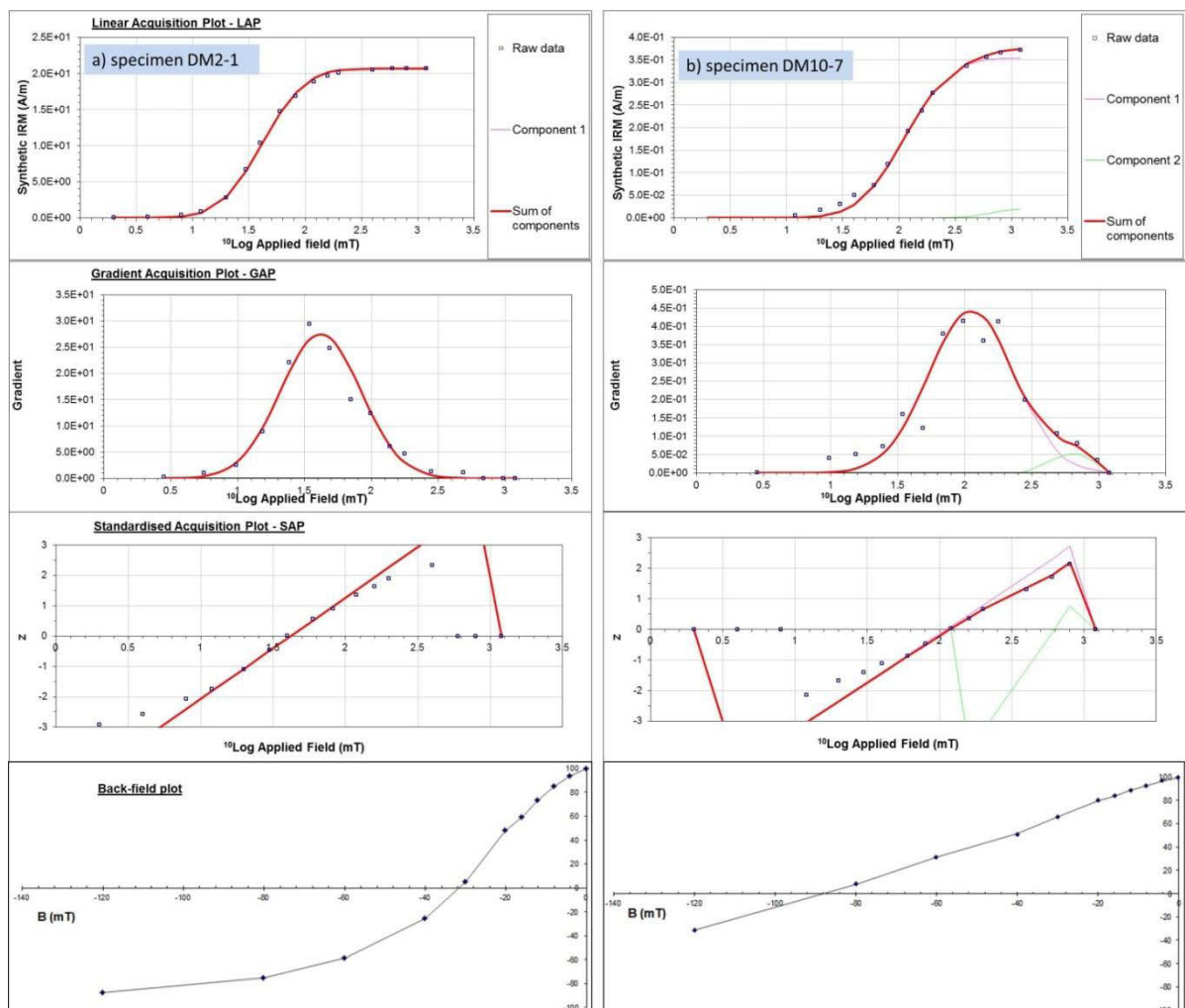


Figure 4.9 – IRM component analysis by Kruiver et al. (2001) method. In the back-field plots the intersection of the curve with the x axis corresponds to the value of B_{cr} . (a) Single magnetic component (DM2 locality); (b) two magnetic components (DM10-1 site).

2. presence of two magnetic phases, both with low- to medium-coercivity. In this case IRM acquisition plots are composed by two components saturated by two different fields values, the first one having the same characteristics described in point (1), the second one saturated by higher fields (< 1.5 T) and characterized B_{cr} values ranging from 20 to 120 mT, but generally greater than 60 mT (fig. 4.9 b). Thermal demagnetization of the IRM components shows dominant low and medium coercivity components (fig. 4.10 b), with the same maximum blocking temperature as in point (1). This second phase is interpreted as a secondary magnetic phase, identified as altered Ti-magnetite, and occurs also together with Ti-magnetite in the remaining sites generally for low fraction ($< 10\%$), with the only exception of locality DM7 which evidences a higher fraction (45%). At DM12 the occurrence of hematite as secondary magnetic phase, instead of altered Ti-magnetite, is evidenced by the needing of a higher saturating field (> 1.5 mT) associated with a high B_{cr} value comprised between 80 and 120 mT. In this locality the ignimbrite is highly indurated and fractured, and its density is the highest (fig. 5.8); then the presence of hematite may be explained by the hydrothermal alteration of the ignimbrite possibly by fluids which have been circulating through the fractures and have also indurated the deposit.

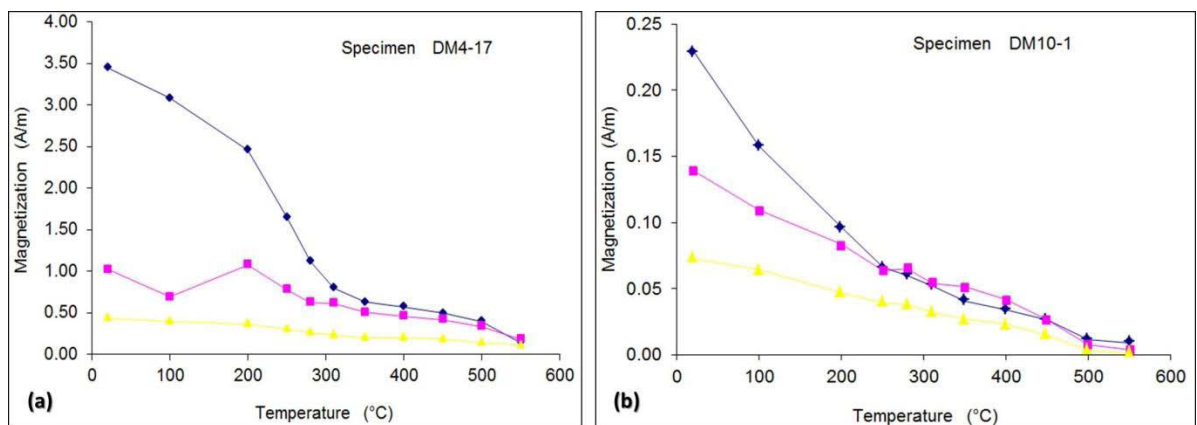


Figure 4.10 – Thermal demagnetization of the IRM components, after Lowrie (1990). (a) Specimen from DM4-1 site; (b) specimen from DM10-1 site. Symbols: diamonds: 0.1 T; squares: 0.5 T; triangles: 1.5 T.

Crossover diagrams of selected sites of the Afyon-Eskişehir ignimbrites are reported in fig. 4.11. All samples present an asymmetrical acquisition curve compared to the demagnetization curve: R values range between 0.7 and 0.9. These results confirm the absence of SD and/or MD grains interacting grains.

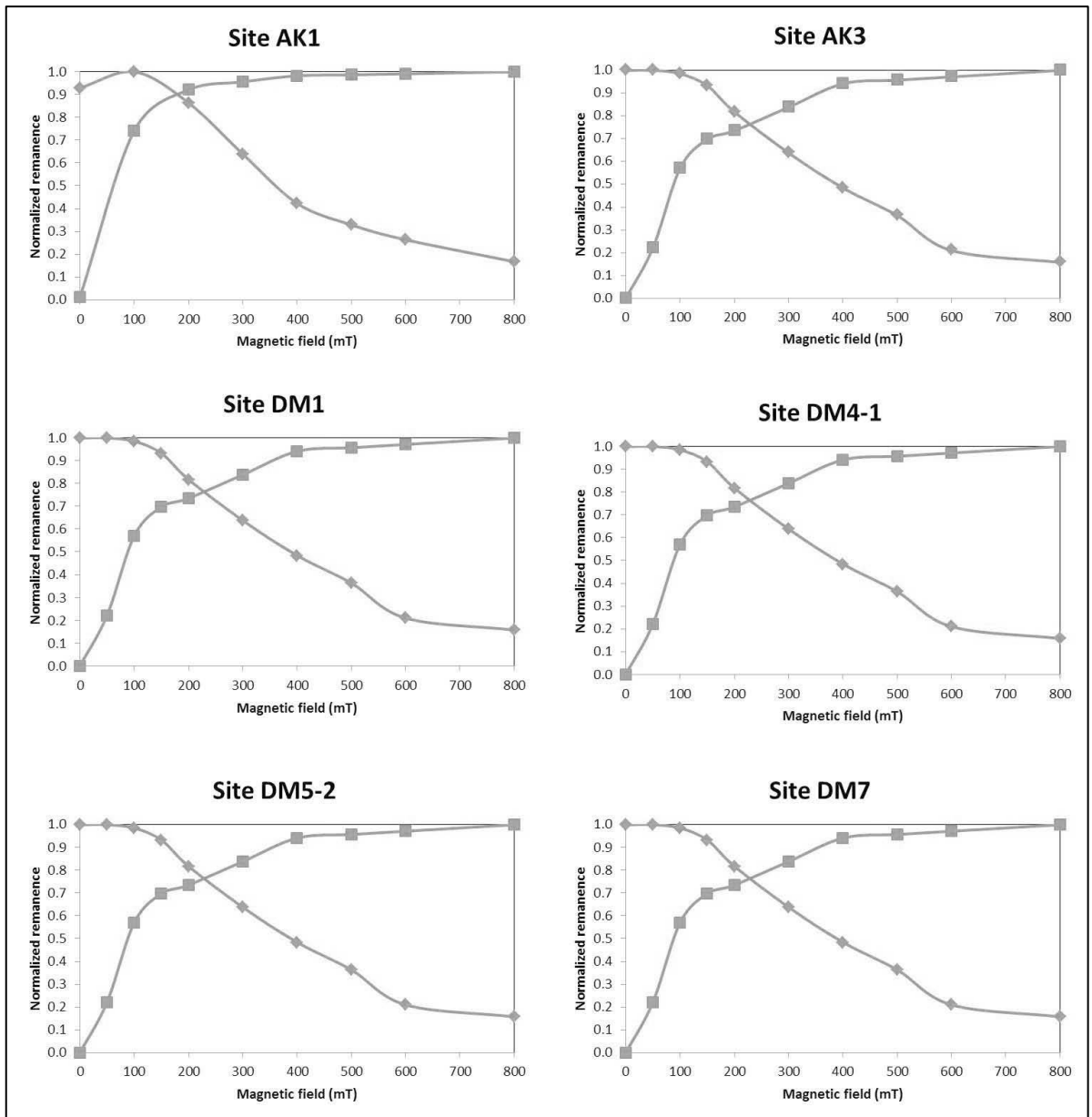


Figure 4.11 – Crossover diagrams for selected sites in the Afyon-Eskişehir ignimbrites: magnetization and demagnetization curves (normalized to the maximal magnetization) as a function of the applied AF field (mT).

5 – Magnetic fabric

5.1 – Kızılkaya ignimbrite

5.1.1 – Density and bulk susceptibility

The dispersion of the density and the bulk susceptibility of the Kızılkaya ignimbrite is significant at both the locality and site level (fig. 5.1). The mean value of the density is 1650 kg/m³, and most

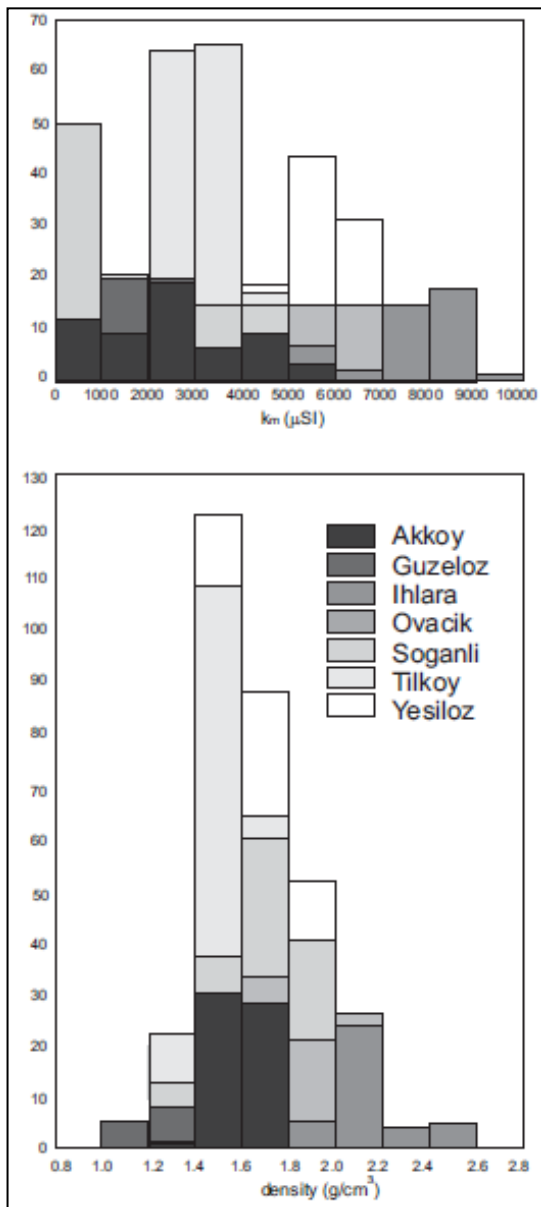


Figure 5.1 - Frequency histograms of site mean a) bulk susceptibility, b) density

specimens fall in the range 1400 to 1800 kg/m³ (fig. 5.1), with minimum and maximum values around 1100 kg/m³ and 2500 kg/m³ respectively. The bulk susceptibility varies between 100 and 10,000 μSI . The highest variability at the locality level occurs at Soğanlı, where large variation in the oxidation degree also occurs. Magnetic susceptibility and density vary with the degree of welding compaction with a positive linear trend (fig. 5.2). Le Pennec et al. (1998) distinguished two groups: one, characterized by density and susceptibility values higher than 1.5 g/cm³ and 3000 μSI , respectively, as representative of non-altered ignimbrite; the other, with lower values, is affected by hydrothermal alteration and weathering. Here, low susceptibility values are independent of density and are associated with the occurrence of haematite at Soğanlı and Akköy. This continuous trend of density vs. magnetic susceptibility suggests a possible bias in the sampling protocol of Le Pennec et al. (1998), and is resolved in the sampling strategy performed in this research, through systematic vertical coring. The variation of the density can be also related to the lithic and pumice clasts content. Both hydrothermal alteration both embedded clasts can affect the magnetic properties in general, the bulk susceptibility in particular.

Therefore the mean density was calculated at each sampling site and the specimens deviated more than $\pm 1\sigma$ were given closer examination, in order to check for any systematic difference from the mean characteristics of the site.

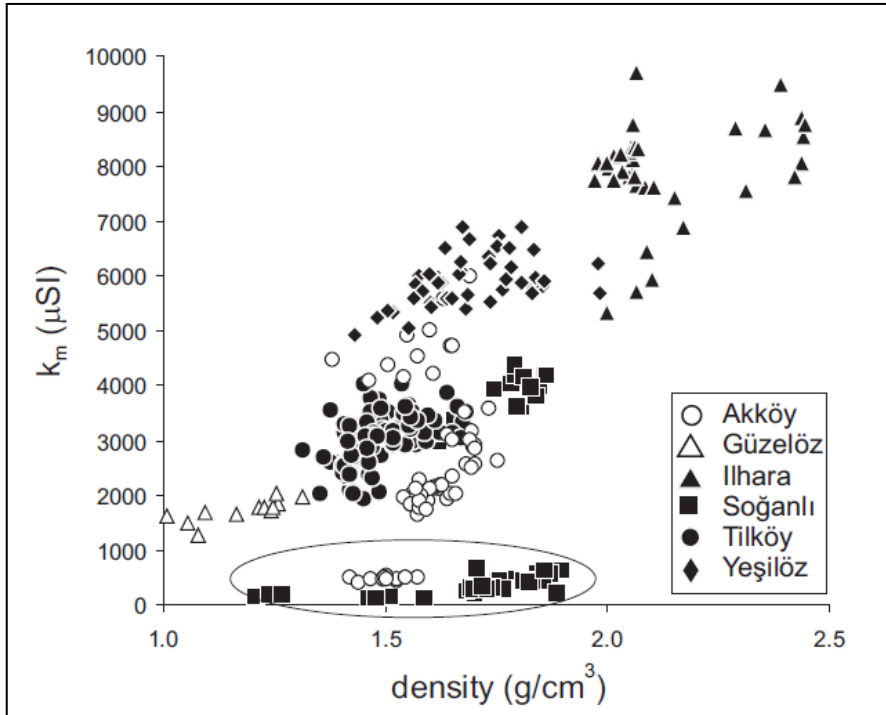


Figure 5.2 - Plot of magnetic susceptibility, K_m , versus density for each specimen.

5.1.2 – AMS and magnetic fabric

The value of the degree of anisotropy in the Kızılkaya ignimbrite is low, $P < 1.035$, as is typical for ignimbrites. It shows no systematic variations between sites (table 5.1), with the only exception at Yeşilöz ($1.040 < P < 1.049$), nor is any relation to the bulk susceptibility apparent.

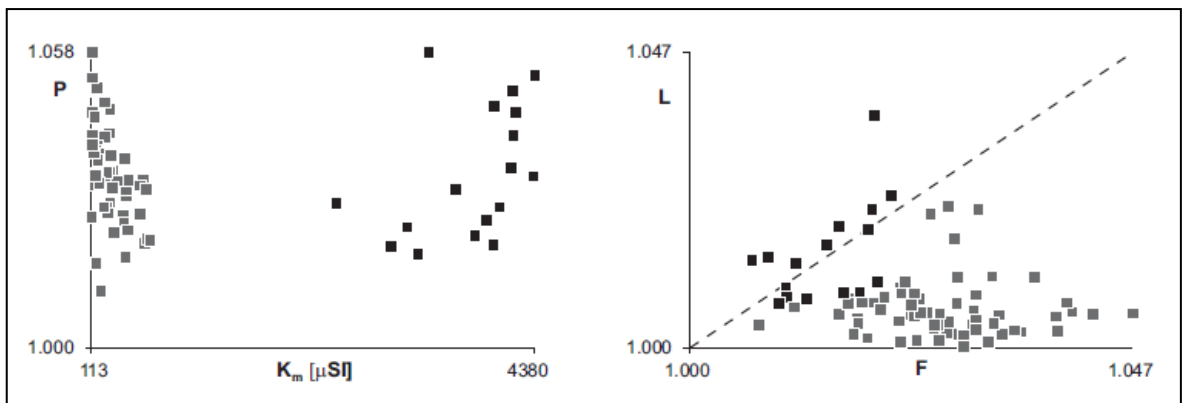


Figure 5.3 - Magnetic lineation versus magnetic foliation of the specimens at Soğanlı. Symbols: square = KZ2-1, KZ2-2; circle = KZ2-3, KZ5-4 to KZ5-7.

The fabric is mainly oblate, because the magnetic foliation prevails over the lineation ($F > L$). A special case is represented by the Soğanlı locality, where a systematic difference occurs between the base and the central and upper parts of the section (fig. 5.3), which mirrors the difference in the bulk susceptibility and the magnetic mineralogy variation. The basal levels of the deposit (KZ2-1, KZ2-2), where only Ti-magnetite occurs and bulk susceptibility is high, have a prolate fabric ($L > F$), whereas in the other levels, where oxidized phases also occur, susceptibility is low and the fabric oblate ($F > L$). Paquereau-Lebti et al. (2008) refer the P and F variations in an ignimbrite succession at Arequipa (Peru) to the type of ferromagnetic mineral. They associate high P values with the occurrence of high-coercivity Ti-hematite and a strong decrease of F to the stratigraphic levels with a high content of Ti-magnetite.

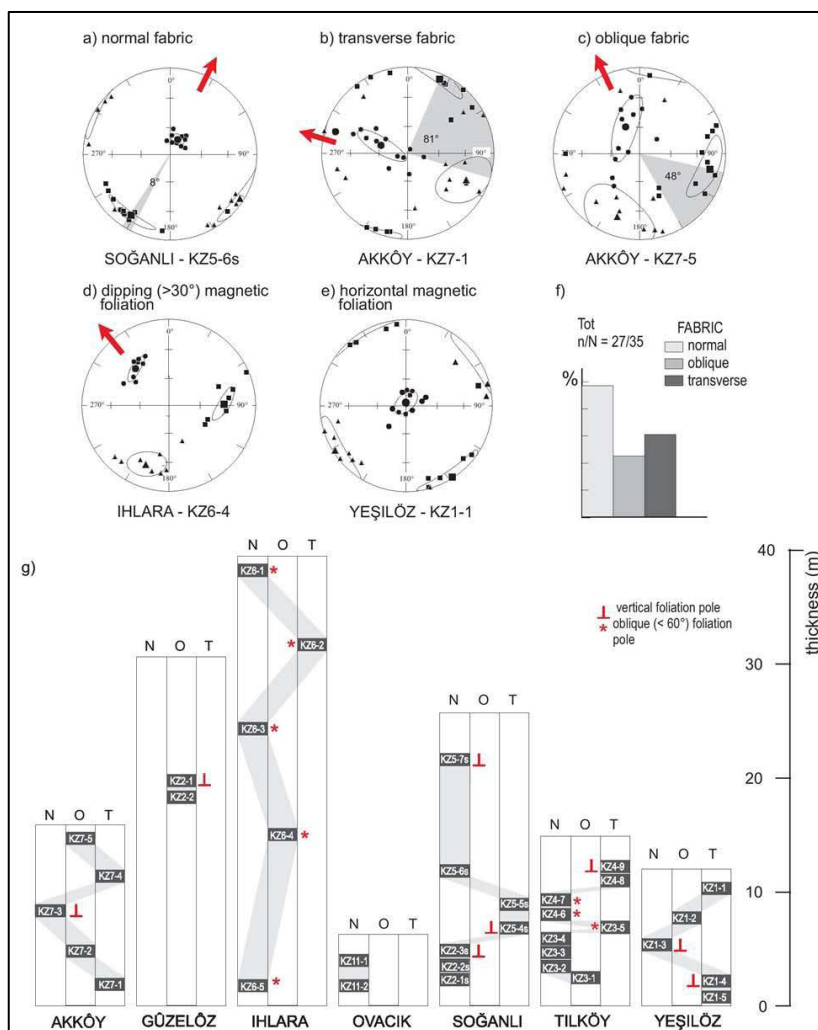


Figure 5.4 - Magnetic fabric in the Kızılkaya ignimbrite. (a) to (e) representative fabrics. Symbols: square = K_1 direction; triangle = K_2 direction; dot = K_3 direction. Larger symbols with ellipse represent the site mean value and its 95% confidence limit (Jelinek, 1977). Grey arrow shows the flow direction inferred from the imbrication of the foliation plane. The grey area highlight the angle (θ) between the magnetic lineation and the magnetic foliation plunge; (f) percent frequency of normal, oblique, transverse fabric; (g) sequence of the fabric type as a function of stratigraphic height at each section. Label: N/O/T = normal/oblique/transverse fabric.

The AMS fabric is typically well developed (fig. 5.13 a-e): the dispersion of the principal axes is small and the site mean directions, calculated using the Jelinek's statistics (1977), are well defined. The basic model for the interpretation of the fabric relies on the fact that titanomagnetite is the main ferromagnetic mineral in the Kızılkaya ignimbrite (the only one in 27 out of 35 sites) and two assumptions:

- 1) AMS is due to the preferential alignment of inequant Ti-magnetite grains, which are characterized by shape anisotropy. Distribution anisotropy is excluded from the obtained data, as pointed out by the crossover diagrams in fig. 4.6. Assuming shape anisotropy originating the magnetic fabric and the presence of mostly MD magnetic grains, as evidenced from the data, susceptibility is maximum parallel to the longest dimension of the grain, minimum parallel to the shortest;
- 2) the alignment is due to the flow of the volcanic material moving over the palaeotopographic surface.

Taking into account the dispersion of the lineation of the individual specimens within the foliation plane, which is given by the E_{1-2} angle of the 95% ellipse of confidence of K_1 (table 5.1), three types of fabric can be defined in the Kızilkaya ignimbrite on the ground of the angle θ between the direction of the magnetic lineation and that of the foliation plunge (fig. 5.4 f):

- 1) parallel ($\theta < 35^\circ$), in 18 out 35 sites. The foliation plane is gently imbricated and the lineation is close to the foliation plunge (Fig. 5a). According to the literature (Knight et al. 1986, Hillhouse and Wells 1991, Seaman et al. 1991, Ort 1993, Le Pennec et al. 1998; LaBerge et al. 2009), this fabric meets both the above assumptions and is regarded as “normal”. Both fabric elements give the flow direction: the imbrication is upflow toward the source area and the lineation is clustered in the same direction;
- 2) transverse ($\theta > 55^\circ$), in 10 sites. The lineation is orthogonal to the foliation plunge (fig. 5.4 b). This fabric may be regarded as analogous to that of sediments in rivers where the current is strong enough to make the grains and clasts to roll on the bottom bed load, with the long rotation axis orthogonal to the current direction (Ort, 1993; Ort et al., 1999). A transverse fabric is therefore often called a “rolling fabric” (Baas et al. 2007);
- 3) oblique ($35^\circ < \theta < 55^\circ$), in 7 sites. The lineation is oblique with respect to the foliation plunge (fig. 5.4 c). Baas et al. (2007) argue that oblique fabric is common in sedimentary rocks. In turbidite deposits, deviations of the grains, mean orientation from the flow direction by up to several tens of degrees may be ascribed to: (1) spatial changes in current direction, due to turbulent eddies, current meandering, flow channel, bed surface irregularities, particularly in the case of low velocity currents with insufficient momentum to maintain the direction; (2) partial reorientation of a rolling fabric to flow-aligned fabric, or vice versa; (3) changes in bed roughness; and/or (4) post-depositional modification by bioturbation, fluidisation or soft-sediment deformation. Paquereau et al. (2008) suggest that AMS probably records only the last increment of the flow movement and this too may produce oblique fabric.

The magnetic foliation is the plane that contains the maximum and intermediate dimensions of the grains and thus its attitude is expected to be close to the bedding, with any difference being related to grains imbrications. The K_3 axis, in turn, is expected to be close to vertical. At Ihlara and some

sites at Tilköy, K_3 is more than 30° from vertical (fig. 5.4 d). In other ignimbrites, this deviation has been attributed to rheomorphism (Wang et al., 2001), but evidence of rheomorphic flow has not been found in the Kızılakaya ignimbrite (Le Pennec et al., 1998).

The reverse fabric, consisting of the exchange of the maximum and minimum anisotropy axes and commonly attributed to the occurrence of SD magnetite (Rochette et al., 1999, Palmer and McDonald, 2002) or distribution anisotropy (Le Pennec et al., 1998), was not detected. Finally, the foliation plane is nearly horizontal and no plunge can be confidently defined at 8 sites (fig. 5.4 e). The magnetic lineation, even if well defined, is not enough to infer the flow direction and these cases must be interpreted cautiously.

The distribution of the fabric type within each section appears random (fig. 5.4) and no correlation with the stratigraphic position and other rock characteristics is apparent.

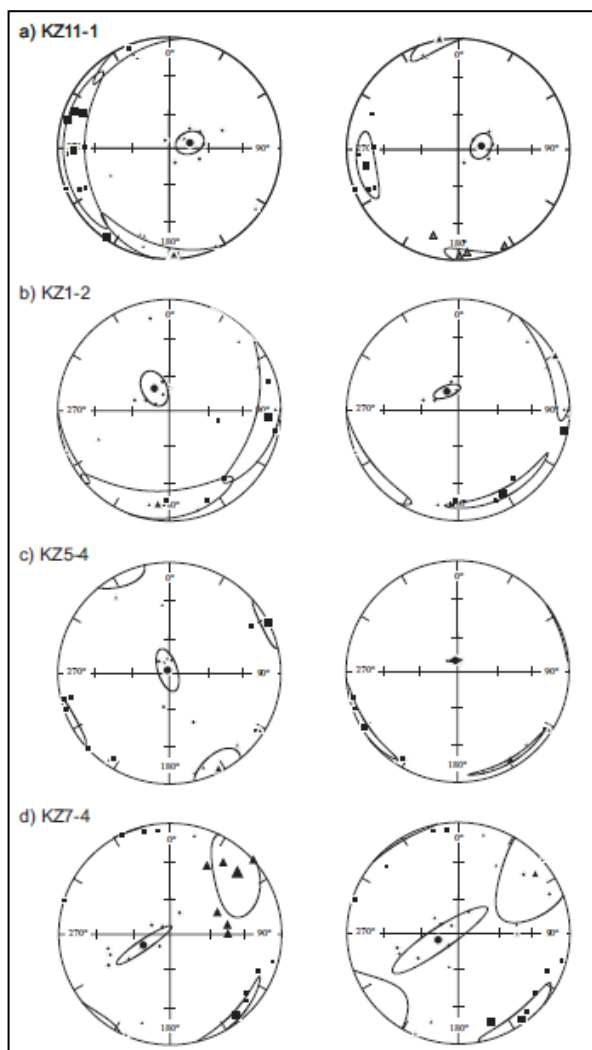


Figure 5.5 - Enhancement of magnetic fabric. Left column: AMS fabric; right column: AMS fabric after removal of specimens more deviated than $\pm 1\sigma$ from the site mean density. Symbols as in fig. 5.4.

Baer et al. (1997) checked the vertical variations of the magnetic fabric of Ito ignimbrite deposits. They found large variations in the flow directions that did not correlate with paleo-topography, a finding that they interpreted as due to turbulence during flow. The Kızılakaya ignimbrite was deposited on a peneplain with minor elevation differences and no evidence of topographical control is manifest (Schumacher and Mues-Schumacher, 1996b; Le Pennec et al., 1998).

Based upon the above assumptions, the magnetic fabric results from the preferential alignment of the free Ti-magnetite grains by the clastic flow. However, in the Kızılakaya ignimbrite, Ti-magnetite occurs as well as inclusions in other minerals and glass shards. The flow orients these particles and not the Ti-magnetite they include, whose orientation can be assumed as random. Their contribution to the measured

susceptibility can therefore be regarded as noise that increases the dispersion of the fabric elements. The same occurs for lithic clasts, which, in addition, act as micro-topography, causing local deviation in the flow path of fine particles (La Berge et al. 2009).

Le Pennec et al. (1998) calculated the site mean value of the lineation L and discarded as outliers all the specimens with a L value lower than it. This exercise resulted in a better cluster of the principal axes and improved the definition of the fabric. In the Kızılkaya ignimbrite, due to the composite magnetic mineralogy, the signal is heterogeneous: Ti-magnetite occurs as small grains precipitated within the glass shards during the initial cooling, as magmatic phenocrysts, and as crystals within lithic and pumice clasts (Le Pennec et al. 1994). A high content of clasts produces a large variation in density (lithic clasts increase the density whereas pumice clasts decrease it). The density values that differ more than $\pm 1\sigma$ from the site mean value were regarded as strongly inhomogeneous and discarded and the statistics recalculated.

The main result is that, in the sites in which Ti-magnetite is the only ferromagnetic mineral, the oblique fabric changes to normal or transverse. This fabric can therefore be interpreted as the result of compositional inhomogeneities and not of poor alignment by the flow.

On the whole, these data filters produce a small improvement in the confidence values (fig. 5.5 a; table 5.2) and, in a few cases, a change of the mean lineation direction and foliation pole (fig. 5.5 b). The number of sites with a horizontal magnetic fabric is reduced from 8 to 4 (fig. 5.5 c). In some sites, however, the number of remaining specimens for inclusion in the statistical analysis is small and the dispersion increases (fig. 5.5 d). At several sites, K_1 and K_2 directions are distributed along a girdle in the foliation plane; in these cases, both K_1 and K_2 95% confidence limits exceed 45 degree. Table 5.2 lists all new AMS parameters and directions.

5.1.3 – AIRM, AARM and magnetic fabric

All minerals contribute to the measured value of the magnetic susceptibility in a rock, according to their relative abundance and intrinsic susceptibility. AMS thus depends on the spatial orientation of both para- and ferro-magnetic minerals, whose preferential directions do not necessarily coincide. In LaBerge et al. (2009), the comparison of low-field and high-field AMS data highlighted a substantial consistency between the ferromagnetic and the paramagnetic fabrics.

The anisotropy of remanent magnetization, on the other hand, investigates the orientation of the ferromagnetic minerals, which are the only remanence carriers. An artificial remanence is thus given to the specimens, usually isothermal or anhysteretic. AIRM was acquired in a direct field of

20 mT, enough to magnetize most low-coercivity grains such as Ti-magnetite. Measurements were done on specimens with different magnetic mineralogy from 16 sites from 5 sampling localities.

The magnetic fabric is well-defined and mostly oblate. The degree of anisotropy, $1.067 < P < 1.384$, is higher than for susceptibility. The lowest values occur in the sites with abundant oxidized phases, such as KZ7-5 at Akköy. The AMS and AIRM fabrics are fully consistent at 9 out of 16 sites (fig. 5.6), aside from the mineral assemblage. Tit-magnetite is the only ferromagnetic mineral at sites KZ11-2 (Ovacık), KZ1-3, KZ1-4 and KZ1-5 (Yeşilöz), KZ2-1 (Soğanlı) KZ6-1 (Ihlara). It occurs together with an oxidized phase at KZ6-4 (Ihlara) and KZ7-5 (Akköy) and with hematite at KZ5-5 (Soğanlı). In the other 5 sites, the principal axes (K_1 - K_2 for AMS and I_1 - I_2 for AIRM) exchange their direction. This could be ascribed to a change to a strongly oblate fabric, with $K_1 \approx K_2 > K_3$, as pointed out by similar K_1 - K_2 and I_1 - I_2 values (table 5.2 and table 5.3) at these sites.

At all sites at Akköy, the inclination of the AIRM minimum principal axis I_3 is always lower than that of the AMS corresponding axis. This change, which only occurs at Akköy, is tentatively ascribed to the occurrence of a minor amount of Ti-magnetite in single-domain grains.

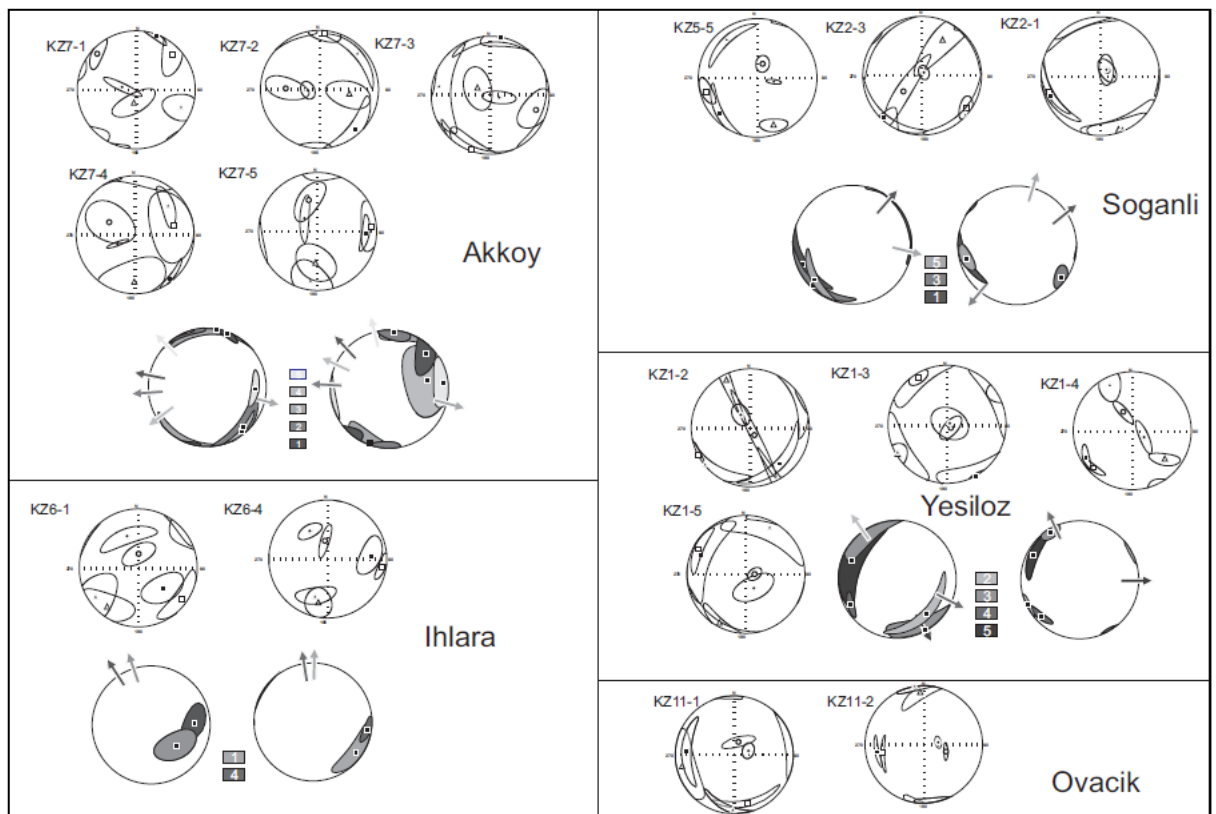


Figure 5.6 - Equal area projection of the site mean AMS (full symbols) and AIRM (open symbols) principal axes with 95% confidence limit. Symbols as in fig. 5.5.

On the whole, these results show that AIRM is mainly controlled by the low-coercivity ferrimagnetic fraction.

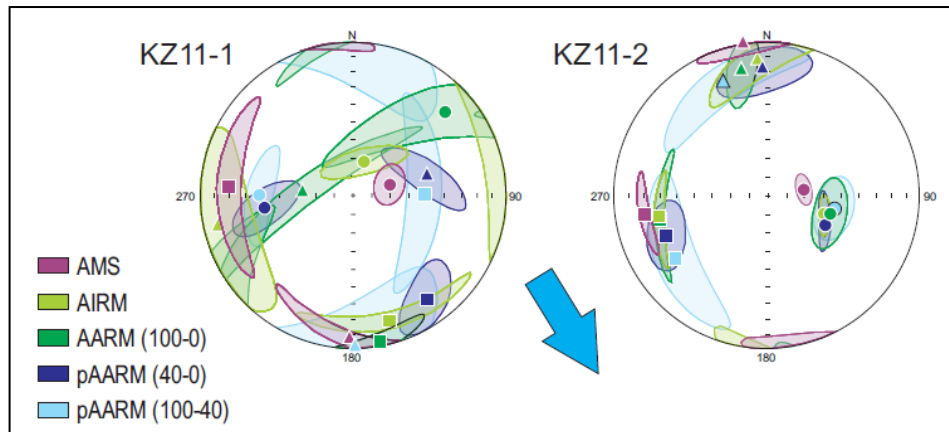


Figure 5.7- Site KZ11-2 at Ovacık: equal area projection of the site mean AMS, AIRM and AARM principal axes with 95% confidence limit (shaded ellipse). Symbols as in fig. 5.5.

Sites KZ11-1 and KZ11-2 at Ovacık were chosen for preliminary measurements of AARM because only Ti-magnetite occurs in it. The measurements were repeated three times in order to detect different ferromagnetic grains: the low-coercivity grains (bias direct field in the demagnetization range 40-0 mT), grains with higher coercivity (100-40 mT), and all grains (100-0 mT). The principal directions of the three fabrics are consistent with each other as well as with those of the AMS and AIRM fabrics (fig. 5.7). The AMS data are also related to the preferred orientation of magnetite grains, as also suggested by mean susceptibility values (table 5.1). Therefore it is possible to conclude that the magnetic fabric is controlled by multi-domain Ti-magnetite grains.

Locality	Geographic coordinates	site	n/N	k (μ SI)	Magnetic lineation, K_1				Magnetic foliation pole, K_3						
					L K_1/K_2	F K_2/K_3	P K_1/K_3	D	I	E_{1-2} (°)	E_{1-3} (°)	D	I	E_{3-2} (°)	E_{3-1} (°)
AKKOY	427119	KZ7-5	12/12	488	1,013	1,015	1,028	102	19	27,6	10,8	334	60	33,5	10,8
		KZ7-4	9/12	1980	1,016	1,010	1,026	145	6	25,6	3,9	252	69	24,8	3,8
		KZ7-3	10/12	2210	1,008	1,017	1,025	255	9	75,6	13,3	93	81	14,6	5,0
		KZ7-2	12/12	3060	1,013	1,017	1,030	147	11	34,0	10,3	273	71	10,8	8,8
		KZ7-1	12/12	4740	1,006	1,013	1,019	24	4	21,8	7,9	286	64	27,3	7,6
GUZELOZ	4249956	KZ2-1	4/5	1650	1,007	1,009	1,016	230	11	23,9	9,4	13	76	17,7	13,3
		KZ2-2	6/7	1840	1,010	1,011	1,021	215	15	29,5	9,4	97	60	12,9	6,5
ILHARA	4236157	KZ6-1	6/6	6290	1,007	1,024	1,032	130	45	31,0	17,7	342	40	31,0	9,9
		KZ6-2	4/4	8850	1,012	1,015	1,027	147	16	43,9	17,0	30	59	24,1	15,5
		KZ6-3	5/5	8210	1,005	1,022	1,027	199	16	36,4	12,1	53	71	34,3	10,6
		KZ6-4	8/11	8010	1,009	1,015	1,024	87	35	17,6	5,5	320	41	13,0	4,5
		KZ6-5	12/12	8050	1,008	1,026	1,034	260	32	46,2	8,3	39	50	13,2	7,8
OVACIK	4215587	KZ11-1	10/10	6250	1,007	1,024	1,031	269	15	49,6	9,9	74	75	10,9	8,0
		KZ11-2	13/13	6200	1,014	1,022	1,037	252	20	28,8	4,3	85	70	10,6	3,8
SOGANLI	4245526	KZ5-7s	12/12	137	1,009	1,027	1,035	250	7	32,0	11,9	44	82	24,4	11,8
		KZ5-6s	11/12	167	1,006	1,030	1,036	214	16	22,3	4,4	26	74	6,5	5,1
		KZ5-5s	17/17	298	1,004	1,027	1,032	11	5	70,7	5,0	113	66	10,7	4,6
		KZ5-4s	7/7	371	1,007	1,018	1,025	68	0	14,0	7,4	334	88	16,1	7,0
		KZ2-3s	11/12	503	1,006	1,021	1,027	232	6	45,9	6,6	45	85	11,9	6,9
		KZ2-2s	5/5	3970	1,016	1,016	1,032	283	12	9,1	6,0	84	77	10,9	3,2
		KZ2-1s	13/13	3680	1,014	1,020	1,034	258	11	32,4	10,0	46	77	16,2	9,7
TILKOY	4251150	KZ4-9	10/13	2940	1,010	1,015	1,025	84	2	31,4	15,5	180	69	22,7	15,1
		KZ4-8	7/10	3160	1,011	1,011	1,021	2	6	45,4	11,5	104	65	16,6	7,9
		KZ4-7	12/13	3230	1,006	1,011	1,017	224	26	33,8	7,0	83	58	8,8	6,1
		KZ4-6	10/12	3230	1,008	1,007	1,015	267	34	76,6	11,9	67	54	20,0	14,4
		KZ3-5	12/12	2970	1,006	1,011	1,017	190	14	34,7	10,3	78	58	15,7	4,6
		KZ3-4	13/16	3370	1,008	1,012	1,019	324	13	47,6	10,2	153	77	16,9	10,2
		KZ3-3	12/12	2490	1,007	1,009	1,016	10	22	39,1	14,0	152	64	24,9	13,6
		KZ3-2	10/12	2600	1,009	1,017	1,026	318	26	52,7	12,0	109	61	17,5	12,3
KZ3-1	10/12	2480	1,008	1,013	1,021	44	9	18,3	8,3	174	76	17,0	8,8		
YESILOZ	4267442	KZ1-1	5/6	5880	1,015	1,027	1,043	269	2	28,4	1,5	2	68	11,0	1,1
		KZ1-2	7/8	5570	1,013	1,028	1,041	101	10	66,7	7,5	330	74	8,7	4,5
		KZ1-3	11/15	6200	1,019	1,028	1,048	147	3	25,5	8,0	350	87	13,4	7,9
		KZ1-4	14/16	5760	1,019	1,021	1,040	234	5	22,3	7,3	114	80	19,3	10,1
		KZ1-5	7/11	5780	1,018	1,031	1,049	217	3	57,5	6,6	119	72	13,6	5,2

Table 5.1 - Magnetic susceptibility and AMS data of the Kızılkaya ignimbrite. At each locality the sites are listed in stratigraphical order. Symbols: Geographic coordinates (UTM geographic system); n/N = number of specimens used for calculation/number of measured specimens; k = bulk susceptibility, L, F = magnetic lineation, foliation; P = degree of anisotropy; Magnetic lineation: D, I = declination, inclination of the K_1 axis with angles of the 95% confidence ellipse (E_{1-2} , E_{1-3});

Magnetic foliation pole: D, I = declination, inclination of the K₃ axis with angles of the 95% confidence ellipse (E₃₋₁, E₃₋₂).

Locality	site	n	K _m (μ SI)	L K ₁ /K ₂	F K ₂ /K ₃	P K ₁ /K ₃	Magnetic lineation, K ₁				Magnetic foliation pole, K ₃			
							D	I	E1-2	E1-3	D	I	E3-2	E3-1
AKKOY	KZ7-5	8	489	1,013	1,018	1,031	100	20	28,7	8,5	332	59	26,3	8,4
	KZ7-4	9	488	1,015	1,010	1,025	144	5	25,4	7,5	251	74	42,9	8,1
	KZ7-3	9	2130	1,008	1,015	1,023	7	1	71,1	9,0	100	74	26,5	9,0
	KZ7-2	8	3050	1,012	1,018	1,031	156	5	35,7	9,3	265	75	9,4	9,0
	KZ7-1	9	4700	1,007	1,013	1,020	17	3	25,5	7,5	279	69	22,2	6,1
GUZELOZ	KZ2-1	3	1650	1,008	1,007	1,015	230	17	13,5	6,4	29	72	30,1	6,2
	KZ2-2	5	1810	1,010	1,012	1,022	205	13	31,1	10,3	94	58	12,9	4,4
ILHARA	KZ6-1	4	6390	1,007	1,027	1,034	106	49	17,0	5,9	324	35	24,2	1,5
	KZ6-2	2	9070	1,011	1,013	1,025	-	-	-	-	-	-	-	-
	KZ6-3	4	8380	1,006	1,021	1,027	193	20	40,3	11,1	52	65	38,6	0,9
	KZ6-4	7	8060	1,009	1,015	1,024	84	34	19,5	2,9	318	41	11,7	3,3
	KZ6-5	9	8050	1,008	1,024	1,033	244	32	32,7	11,4	36	55	20,0	11,5
OVACIK	KZ11-1	6	6200	1,006	1,027	1,033	260	17	20,1	8,4	83	73	9,7	7,3
	KZ11-2	7	6130	1,012	1,023	1,035	261	21	11,2	3,5	79	69	10,9	3,9
SOGANLI	KZ5-7s	7	128	1,010	1,030	1,040	243	7	15,2	7,0	105	81	23,5	4,9
	KZ5-6s	8	169	1,006	1,031	1,037	207	17	32,2	4,7	17	73	7,2	5,6
	KZ5-5s	13	280	1,004	1,028	1,032	219	12	59,1	5,6	102	66	10,2	4,6
	KZ5-4s	5	298	1,006	1,02	1,026	240	3	24,8	3,7	348	81	4,2	0,9
	KZ2-3s	8	505	1,004	1,021	1,025	202	2	45,7	9	36	88	13,6	6,1
	KZ2-2s	3	3980	1,019	1,019	1,039	280	12	8,1	0,8	76	77	11,6	2,7
	KZ2-1s	9	3890	1,015	1,021	1,037	257	9	18,4	7,9	76	81	9,2	7,9
TILKOY	KZ4-9	10	3020	1,010	1,016	1,025	82	0	25,7	19,4	163	67	28,3	18,4
	KZ4-8	6	3350	1,011	1,010	1,022	338	8	43,6	11,6	80	57	38,6	9,3
	KZ4-7	9	3290	1,007	1,010	1,017	231	32	32,9	4,2	84	54	17,0	4,6
	KZ4-6	10	3160	1,008	1,007	1,015	268	34	66,6	15,9	61	53	21,6	15,9
	KZ3-5	7	3060	1,006	1,012	1,018	178	11	45,1	7,8	71	55	15,5	2,7
	KZ3-4	12	3420	1,007	1,012	1,02	326	13	34,7	11,3	136	77	19,7	11,2
	KZ3-3	8	2470	1,007	1,011	1,018	342	25	32,2	14,3	142	64	23,9	14,4
	KZ3-2	8	2670	1,008	1,018	1,026	322	25	37,4	11,9	100	57	16,8	10,7
	KZ3-1	9	2520	1,008	1,013	1,021	46	8	27	12,2	169	75	23,1	12,4
YESILOZ	KZ1-1	5	5900	1,014	1,027	1,042	90	1	29,9	3,5	357	72	18,2	4,3
	KZ1-2	6	5800	1,008	1,029	1,037	151	16	35,2	3,8	330	74	10,2	4,1
	KZ1-3	8	6160	1,020	1,029	1,049	145	5	44,8	10,4	319	85	14,1	11,1
	KZ1-4	11	5790	1,022	1,021	1,043	232	3	24,0	6,3	132	74	19,3	10,3
	KZ1-5	7	5950	1,017	1,028	1,046	340	14	44,4	15,7	188	75	27,4	16,4

Table 5.2 - Magnetic susceptibility and AMS data of the Kızılkaya ignimbrite after removal of specimens more deviated than $\pm 1\sigma$ from the site mean density. Symbols: n = number of measured specimens; other symbols as in table 5.1.

Locality	site	n	K _m (μ SI)	L K ₁ /K ₂	F K ₂ /K ₃	P K ₁ /K ₃	Magnetic lineation, K ₁				Magnetic foliation pole, K ₃			
							D	I	E1-2	E1-3	D	I	E3-2	E3-1
AKKOY	KZ7-5	8	61	1,028	1,039	1,067	84	9	27,3	16,8	346	43	32,5	15,0
	KZ7-4	9	208	1,039	1,054	1,098	78	34	45,6	33,9	295	50	40,4	24,1
	KZ7-3	9	23100	1,080	1,153	1,247	11	2	24,8	14,8	102	14	23,1	11,6
	KZ7-2	8	242	1,066	1,063	1,132	5	3	18,0	13,8	273	42	34,0	13,6
	KZ7-1	9	961	1,026	1,076	1,103	47	14	36,4	12,4	314	13	18,7	9,6
ILHARA	KZ6-1	4	1050	1,041	1,062	1,106	125	12	33,3	13,6	1	70	25,3	12,6
	KZ6-4	7	1260	1,045	1,040	1,087	98	8	15,7	6,3	350	65	24,5	5,9
OVACIK	KZ11-1	6	899	1,057	1,069	1,13	164	16	40,4	5,5	18	71	24,2	6,9
	KZ11-2	7	852	1,064	1,108	1,179	259	30	32,1	2,9	107	57	11,8	3
SOGANLI	KZ5-5s	13	52,1	1,057	1,138	1,201	252	11	15,1	10,9	17	70	12,8	9,8
	KZ2-3s	8	67,1	1,035	1,134	1,176	126	9	14,9	9,4	230	56	63,0	10,0
	KZ2-1s	9	401	1,074	1,127	1,207	252	11	33,4	5,2	51	78	17,9	10,2
YESILOZ	KZ1-2	6	642	1,049	1,255	1,321	243	0	12,6	5,6	151	79	72,7	5,8
	KZ1-3	8	526	1,069	1,107	1,182	329	7	11,8	10,4	133	83	20,0	9,3
	KZ1-4	11	494	1,059	1,301	1,384	227	10	15,4	5,2	335	61	20,6	5,7
	KZ1-5	7	429	1,058	1,110	1,174	300	13	38,7	5,5	104	77	9,9	5,1

Table 5.3 - Magnetic susceptibility and AIRM data of the Kızılkaya ignimbrite performed at several sites. Data are obtained from specimens comprised between the values $\pm 1\sigma$ from the site mean density. Symbols: the same as in table 5.2

5.2 – Afyon-Eskişehir ignimbrites

5.2.1 – Density and bulk susceptibility

The plot of specimens magnetic susceptibility versus density (fig. 5.8) does not evidence any relations between these parameters, however it is possible distinguish three groups of sites characterized by different ranges of K_m and density values: (1) a main group with low susceptibility (30 μ SI < K_m < 1430 μ SI) and low density values (0.97 g/cm³ < density < 2.01 g/cm³); (2) a group characterized by high susceptibility (2100 μ SI < K_m < 5700 μ SI) and low density values (1.40 g/cm³ < density < 2.00 g/cm³), and (3) a group, represented by site DM12, displaying low susceptibility values around 250 μ SI and high density values comprised between 2.44 and 3.06 g/cm³.

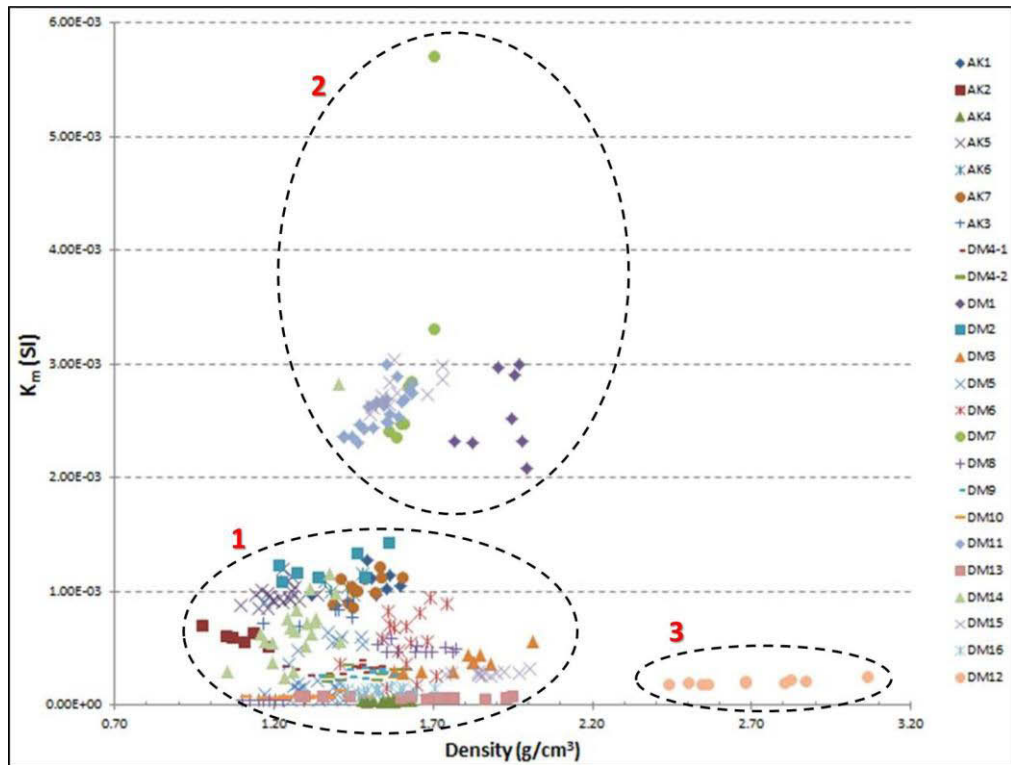


Figure 5.8 – Plot of the magnetic susceptibility versus density for each specimen. Dashed ellipses include specimens belonging to the three groups identified on the basis of K_m and density values.

5.2.2 – AMS and magnetic fabric

The AMS fabric is usually well developed in the Afyon-Eskişehir ignimbrites (fig. 5.14). The Incik ignimbrite is characterized by low values of the degree of anisotropy P , as typical for ignimbrites, comprised between 1.007 and 1.024 (appendix 1). The highest P value is reached at DM4-1 site, which is also characterized by the highest values of L (1.011) and F (1.013); the site AK4 displays the lowest values of P and is characterized also by the lowest values of L (1.005), F (1.003) and K_m (37 μ SI). All specimens fall in the group (1) of the plot K_m versus density. Incik ignimbrite mean density value is 1.39 g/cm^3 , varying between 1.21 g/cm^3 at AK5-2 site and 1.55 g/cm^3 at AK4 site. The low density of AK5-2 site is imputable to the presence of pumice dissolution cavities in the ignimbrite rock possibly due to hydrothermal alteration which led also to the formation of altered Ti-magnetite phase as evidenced by the IRM acquisition curves (table 6.3). The fabric is mainly oblate as pointed out by positive values of the shape parameter T and by foliation prevailing on lineation at 6 out of 8 sites. At AK4 locality lineation prevails on the foliation, while at AK6 locality foliation and lineation value is the same.

The Sabuncu ignimbrite is characterized by P values comprised between 1.026 and 1.028. Specimens fall in the group (1) of the plot in fig. 6.34, because of low susceptibility (260-600 μ SI)

and density values (1.09-1.48 g/cm³). Magnetic fabric is oblate with a positive value of T, and foliation prevails on lineation.

The Seydiler ignimbrite displays higher variation range of P values which is comprised between 1.005 at DM13-1 site and 1.077 at DM7 site. The DM7 site evidences also the highest values of lineation (1.021), foliation (1.052) and magnetic susceptibility (3100 μSI) among all the sites. Specimens fall in all of the three groups of the plot in fig. 5.8. Variation in magnetic susceptibility among sites is wide, up to two orders of magnitude, and so the density values, which is comprised between 1.18 g/cm³ at DM8-1 site and 2.70 g/cm³ at DM12 locality. Foliation prevails on lineation at 18 out of 25 sites, at DM8-1 and DM16 sites foliation and lineation value is the same, in the remaining sites lineation prevails on foliation. The fabric is mainly oblate as evidenced by positive values of the T parameter at most of the sites with the only exception of DM9, DM13, DM10-2 and DM8-1 where T values are slightly negative, pointing out the presence of prolate fabric.

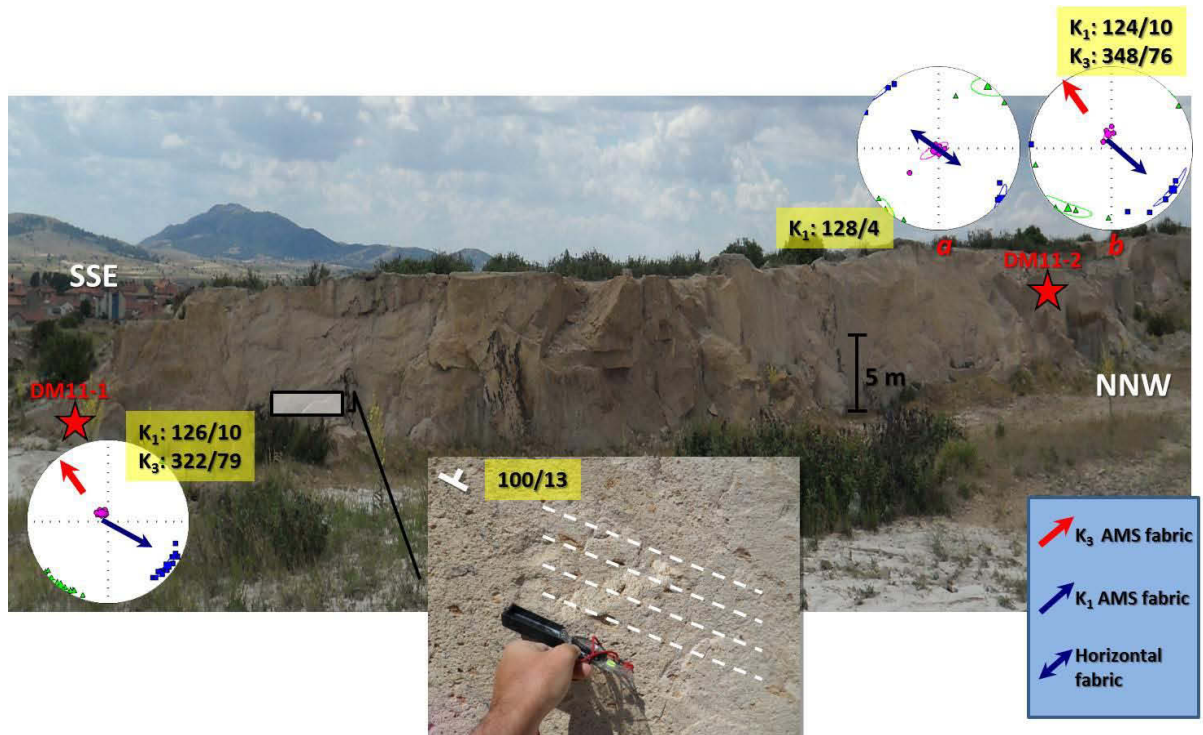


Figure 5.9 – Evidence of pumice clasts and AMS fabric consistence (site DM11, locality of Döğür). The AMS fabric, characterized by $F > L$, is consistent with pumice clasts foliation

The criterion adopted to extrapolate flow directions from the AMS stereoplots consists in evaluating and comparing F and L parameters which describe the magnetic fabric. In the case of grain fabric, a well-defined foliation is representative of high shear intensities exerted between the emplacing pyroclastic flow and the underlying substrate, or between different layers within the pyroclastic flow. According to Branney and Kokelaar (2002) the intensity of grain fabric depends, besides high shear intensity at the flow boundary zone, also on the residence time of the clasts

within the shearing zone and clasts shapes and sizes. The occurrence of high shear intensity which originates well defined grain fabrics, produces in principle well defined magnetic fabric too, if Ti-magnetite represents the main ferromagnetic carrier. In MD Ti-magnetite crystals the direction of the longest axis corresponds to that of maximum susceptibility (K_1), the shorter axis corresponds to that of minimum susceptibility (K_3). In the case of pyroclastic flow and laminar regime, the MD Ti-magnetite crystals tend to orientate their longest axis parallel to the flow, so the magnetic fabric mimics the grain fabric. The ideal condition consists in the presence of normal fabric, where the magnetic foliation plane is slightly imbricated (generally $< 30^\circ$) and the magnetic lineation (K_1) lies along its plunge direction, or at small angle with respect to it. In this case the imbrication of the pole of the magnetic foliation (K_3) gives the sense of the flow, and both K_1 both K_3 directions can be used as proxies for flow direction. To equal degrees of anisotropy P, sites characterized by foliation prevailing on lineation ($F > L$) display clustered K_3 axes and K_1 and K_2 axes dispersed along a plane; sites characterized by lineation prevailing on foliation ($L > F$) display clustered K_1 axes and more dispersed K_2 and K_3 axes. Because of this reason, in the first case the extrapolation of flow direction is made by considering the K_3 mean direction, in the second case by considering the K_1 mean direction. This assumption is confirmed at the sites where grain fabric is evident, so it is possible to compare directional field evidence with the AMS fabric (fig. 5.9 and 5.10).

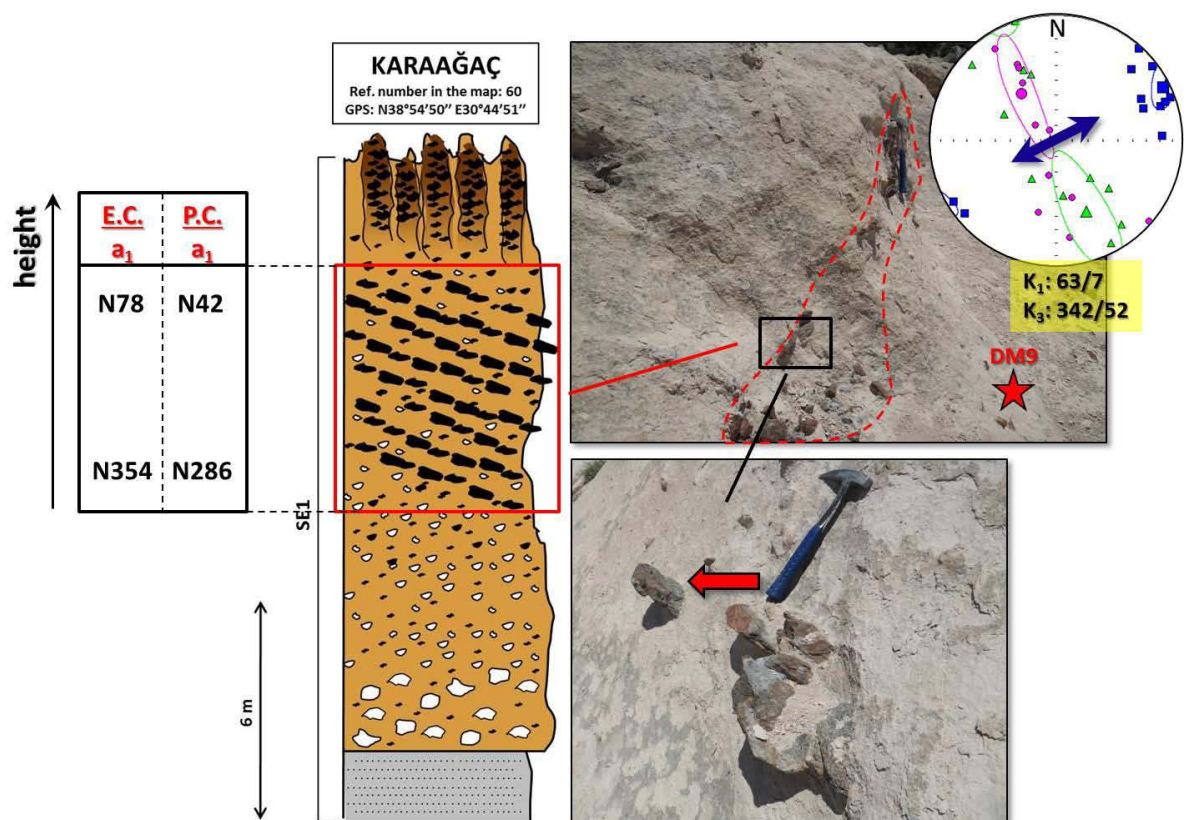


Figure 5.10 – Evidence of lithic clasts and AMS fabric consistence (site DM9, locality of Karaağaç). The AMS fabric, characterized by $L > F$, is consistent with lithic clasts lineation. E.C.: elongated clasts; P.C.; planar clasts; a_1 : maximum elongation axis.

Two examples are reported from the Seydiler ignimbrite at localities DM11 and DM9, where occurrence of well-developed grain fabric confers the same information of the magnetic fabric. Locality DM11 has been sampled at two sites lying at 3.5 m vertical distance each other (DM11-1 at the base, and DM11-2 at the top); the DM11-2 site has been further split into two blocks at the same stratigraphic level distant 4 m each other (fig. 5.9). A strong 3-dimensional pumice clasts imbrication occurring at the base near to the lower site gives the same directional information of the magnetic fabric, which is normal and characterized by a strong foliation prevailing on lineation ($F = 1.026$, $L = 1.004$) and oblate fabric ($T = 0.721$). Therefore, the clasts foliation plane is consistent with the magnetic one, such as their pole. Moreover, the magnetic fabric does not suffer any vertical variation through the stratigraphy, maintaining the same K_1 and K_3 directions. Locality DM9 has been sampled at one site, in the matrix portion of the deposit just below the breccia-like portion (fig. 5.10). Lithologies are represented by schists and quartzite, and clasts display a strong imbrication. It is possible to discriminate between two types of imbrications, given by different shaped-clasts. The first type of imbrication is given by elongated lithic clasts, mainly quartzite, which evidence a strong lineation (fig. 5.10); the second type of imbrication is given by planar clasts, mainly schists, which display foliation. In both cases the sense of flow is inferable from the imbricational structures, and in both cases the direction of maximum elongation axis (a_1) has been measured as proxy of flow direction. Data show that orientation of both elongated both planar clasts maximum axes display vertical variation, but in the case of elongated clasts (displaying lineation) it varies over a more restricted range of values (N78-N354) with respect to planar clasts (N42-N286). The AMS fabric is consistent with this observation: $L > F$ and the fabric is prolate ($T = -0.112$); therefore the AMS fabric mimics the clasts fabric. This evidence is also in according with the observations of Hughes and Druitt (1998) which, studying the vertical fabric of ignimbrite deposits of the Upper Laacher See Tephra at several sections, found that clasts lineation was always parallel to the flow direction and vertically constant through the sections, while in the of clasts foliation, the a - b planes dip upstream irrespective of axial ratio, but the a axes yield girdle fabrics. On the basis of these observations and of the absence of transverse to flow direction fabrics, they assumed that deposits were emplaced by laminar flow.

In the case of horizontal magnetic foliation it is not possible to infer a flow direction from K_3 mean direction; so the flow direction is always extrapolated from the direction of K_1 .

Figure 5.14 shows the AMS stereoplots of the sampled sites in the Incik, Sabuncu and Seydiler ignimbrites, with the inferred flow directions. AMS is considered to be the result of the preferential alignment of unequant Ti-magnetite grains, which are characterized by shape anisotropy. Distribution anisotropy is ruled out, as evidenced by R values greater than 0.5 in the crossover diagrams in fig. 4.11. It is detected the presence of 10 horizontal magnetic foliations for which $F > L$ at 9 out 10 sites and $L > F$ at DM10-2 site, where K_1 direction is considered to infer the flow

direction. The AMS fabric is usually well developed and characterized by small dispersion of the principal axes and well defined site mean directions, with the exception of some sites where low values of magnetic susceptibility causes a more dispersion of the data (e.g. DM10 locality and its sites, where the magnetic susceptibility is comprised between 57-83 μ SI). At some localities comprising more than one site, the magnetic fabric changes vertically. At AK5 locality, for example, K_3 direction varies from 262° at the lower site to 217° at the upper one; at DM13 locality K_1 direction varies of 120° passing from the lower to the upper site. Comparison between directional field evidence and AMS fabric point out that some sites are characterized by a good agreement between the two types of indicators and others by a slightly (e.g. AK6, DM4-1, DM4-2 sites) and strong discrepancy (e.g. AK7, DM15-1). One reason can arise from the cropping out conditions and quality of the sedimentary structure. In most of the cases sedimentary evidence are complex indicators to interpret because they appear as 2-dimensional structures exposed over one plane; their quality is less precise than ones exposed over two (or more) planes at different orientation giving the real 3-dimensional trend. Another cause is due to the statistical number of measured data. The AMS fabric of sites AK6 and AK10-1, for example, consist only of 5 specimens, and wide dispersion angles affect the mean susceptibility axes. Another reason is related to the type of directional structure detected in the field with respect to the emplacement mechanism which produced it. In the case of a pyroclastic flow moving counterslope which sediments for example a basal surge layer and a subsequent ignimbrite deposit, sedimentary structures preserved within the surge and ignimbrite deposit can give different information. The more diluted portion of the current may be able to surmount topographic reliefs and will produce sedimentary structures recording the real flow direction; the denser portion of the current may not be able to overcome the reliefs, it will move counterslope producing sedimentary structures which register an “opposite-to-flow” direction, so also the magnetic fabric. This is the case of the site DM8-2 which is characterized by a well-defined, even if horizontal, magnetic foliation ($F = 1.034$) with $K_1 = N195^\circ$, and a well preserved pumice clasts imbrication (dip direction/inclination = $218^\circ/20^\circ$). Both AMS and field indicators concur for a \approx NNE flow direction, but asymmetrical load cast structures preserved in the underlying surge layer indicate an opposite flow direction toward $N241^\circ$.

In order to test the applicability of the AMS data selection experimented in the Kızılkaya ignimbrite to enhance the AMS magnetic fabric, the same method has been exported also to the Afyon-Eskişehir ignimbrites. The procedure consists in discarding the specimens whose density values differ more than $\pm 1\sigma$ from the site mean value because considered inhomogeneous. Taking into account the θ angle comprised between the mean K_1 and K_3 site directions, three types of fabric can be identified (fig. 5.14; appendix 1):

1. Parallel ($\theta \leq 35^\circ$), in 14 out of 35 sites;

2. Oblique ($35^\circ < \theta \leq 55^\circ$), in 8 out of 35 sites;
3. Transverse ($\theta > 55^\circ$), in 13 out of 35 sites.

After having discarded the specimens with anomalous density, four types of variations are individuated (appendix 2):

1. changes in the type of fabric in terms of θ angle. The oblique fabric changes to parallel or transverse at 4 out of 8 sites (fig. 5.11, fig. 5.12 a). Two of them (DM8-1 and DM11-2a) contain Ti-magnetite as the only ferromagnetic mineral, the others (AK3 and DM5-1) contain also altered Ti-magnetite. Magnetic fabric of DM7 site changes from transverse to oblique (fig. 5.12 b). It is observed a net reduction of the oblique fabrics from 8 to 5. Plotting the θ angle in a graph for each site before and after the data selection (fig. 5.13) and taking into account the θ values comprised between $0^\circ < \theta < 15^\circ$ and $75^\circ < \theta < 90^\circ$, the number of sites falling within these two ranges increase from 14 to 18, testifying a greater amount of sites characterized by a “more parallel” and “more transverse” fabric component, with the consequent reduction of the number of sites characterized by intermediate situations;

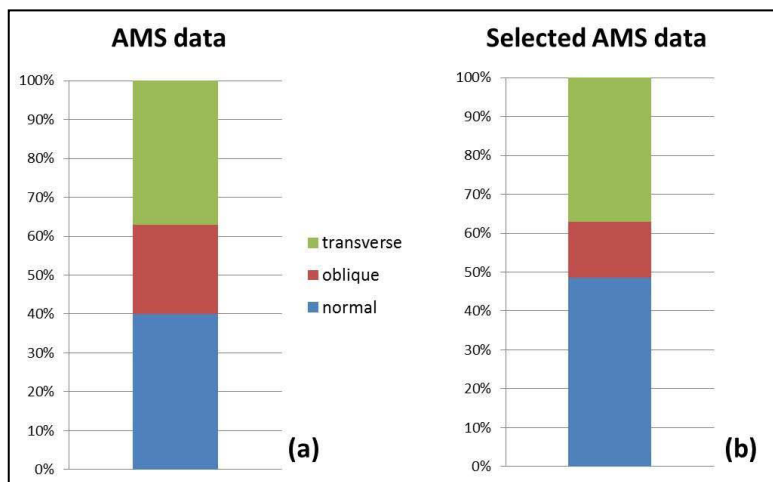


Figure 5.11 – Histogram graphs representing the amount of parallel, oblique and transverse fabric before (a) and after the data selection (b).

2. changes in the type of fabric in terms of F versus L. In the site DM4-1 the magnetic fabric is characterized by $F > L$ before data selection to $L > F$ after data selection; in the site DM8-1 the magnetic fabric passes from $F = L$ to $L > F$;
3. changes in the imbrication of the magnetic fabric. The horizontal magnetic fabric is reduced from 10 to 8 sites. Sites DM15-1 and DM6-1 change their magnetic foliation from horizontal to imbricated (fig. 5.12 c), then it is possible to infer a flow direction from the pole of the magnetic foliation plane;
4. general reduction of the dispersion angles associated to the main susceptibility axes (i.e. E_{1-2} , E_{1-3} , E_{3-2} , E_{3-1}), which contributes to the enhance the magnetic fabrics. This is clearly noticeable, for example, at localities DM7 (fig. 6.38 b), DM6-1, DM13-1, DM14-1, DM10-

1 (compare appendixes 1 and 2). In few cases, however, a slightly increase of the dispersion angles is observed, as in the case of the site DM14-2;

5. discard of specimens with anomalous densities leads to a general improvement of the AMS data. As a rule, two main considerations can be extrapolated from the application of this method to magnetic fabric enhancement. The first consideration concerns the improvement in the quality of the AMS fabrics which implies a major reliability of the inferred flow directions because of: (1) increase in the definition of magnetic fabric which confers a major degree of accuracy for the inferred flow direction; (2) presence of a greater number of normal fabrics where both K_3 both K_1 directions can be used as proxies for flow direction; (3) presence of a greater number of imbricated fabrics where it is possible to extrapolate the direction of K_3 , so to infer the sense of the flow. The second consideration concerns the relation between type of magnetic fabric and clasts concentration, highlighting that the occurrence of oblique fabrics is mainly related to the presence of anomalous concentrations of clasts which contribute to the creation of a microtopography able to deviate the flow at small scale, therefore to disperse the AMS data. In the Afyon-Eskişehir case, 5 sites characterized by oblique fabric are still detected after the data selection. Two of them (AK4 and DM7) contain low-to-high fraction of altered Ti-magnetite besides primary Ti-magnetite (table 4.1). In the sites DM2 and DM11-2b, the number of the remaining specimens after removal of the anomalous ones is too small to compute Fisher's statistics, which requires at least 5 data. To overcome this problem, more specimens with a density as close as possible to the considered density range limits were added, but they probably had a biasing effect in the resulting type of fabric (appendix 2). Therefore, just one site containing primary Ti-magnetite and characterized by oblique fabric still remains after the data selection, AK15-1.

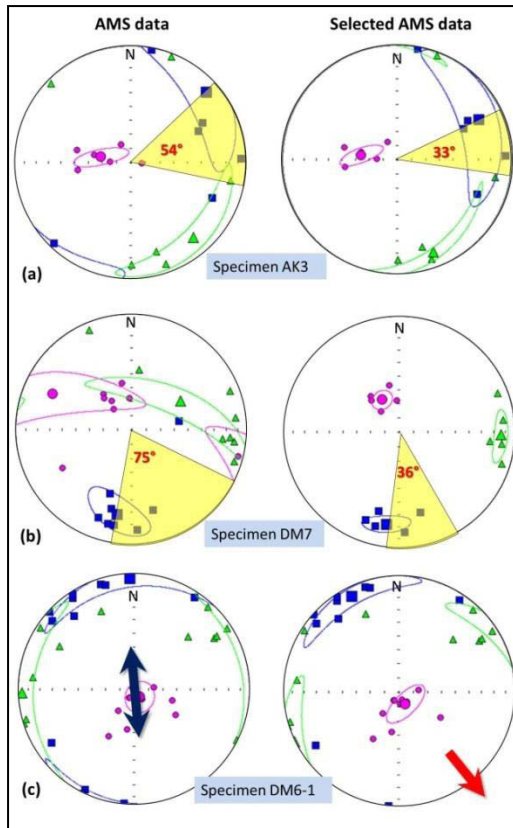


Figure 5.12 – Variations in the type of fabric before and after data selection. (a) Passage from oblique to parallel fabric; (b) passage from transverse to oblique fabric, with reduction of the dispersion angles associated to the main susceptibility axes; (c) passage from horizontal to imbricated fabric.

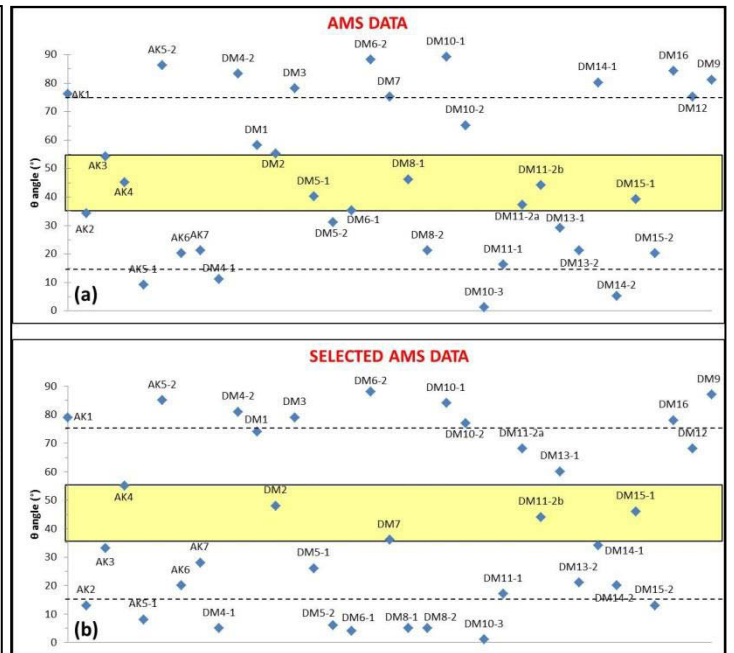
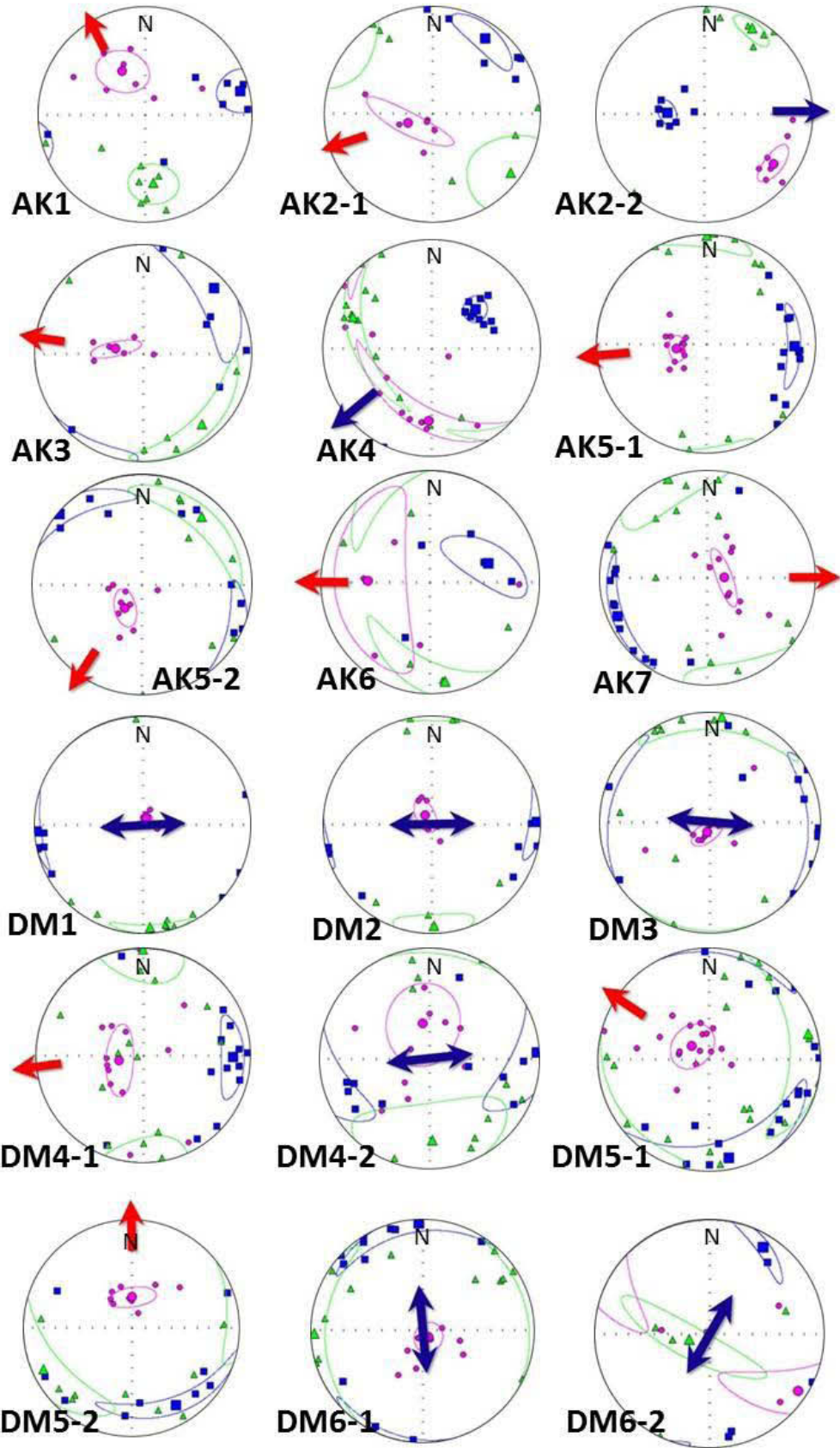


Figure 5.13 – θ angle values for each site before (a) and after data selection (b). After data selection it is noticeable the reduction of oblique fabrics and the increase of the number of “more parallel” and “more transverse” fabric component characterized respectively by $0^\circ < \theta < 15^\circ$ and $75^\circ < \theta < 90^\circ$.



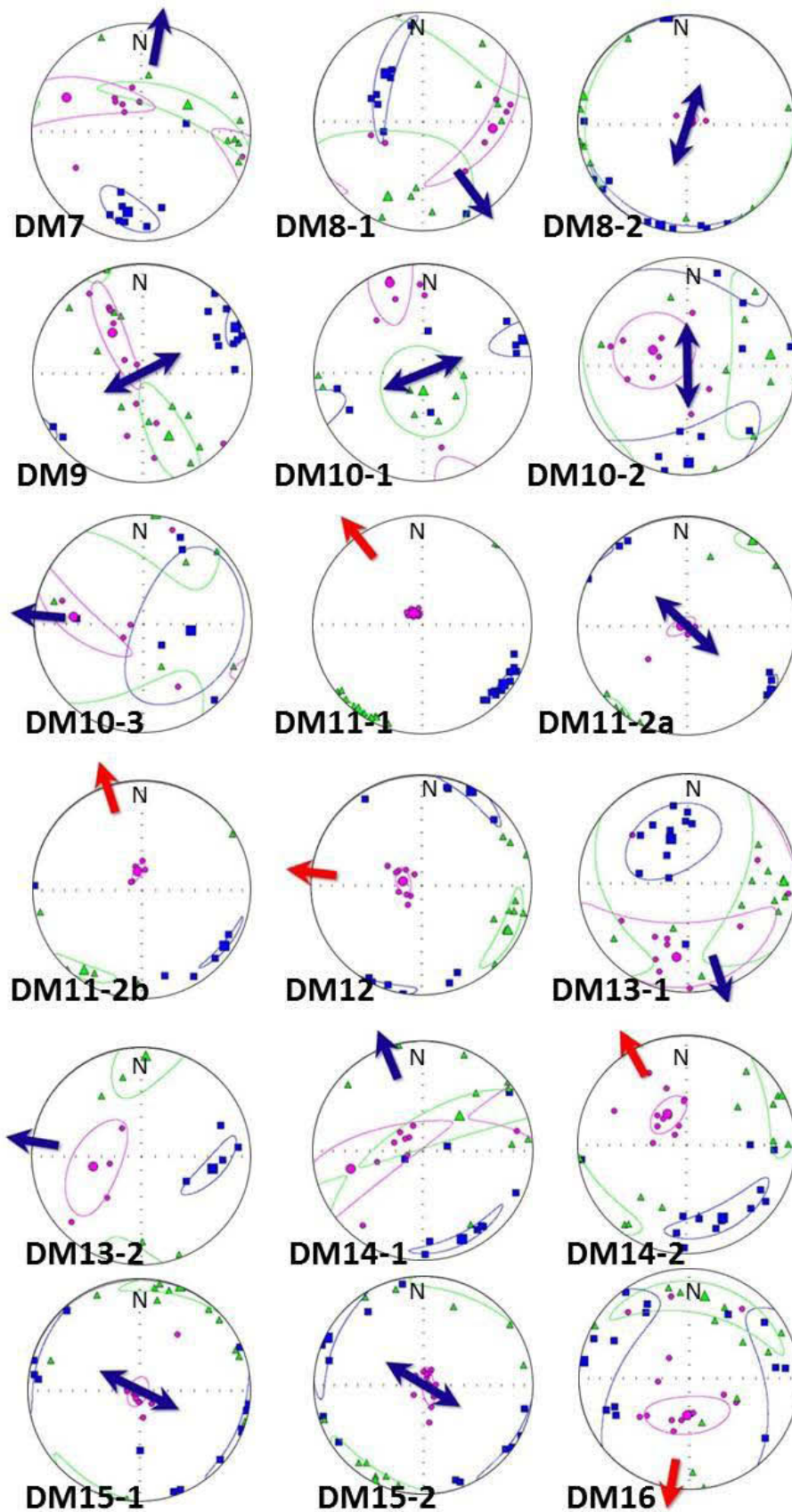
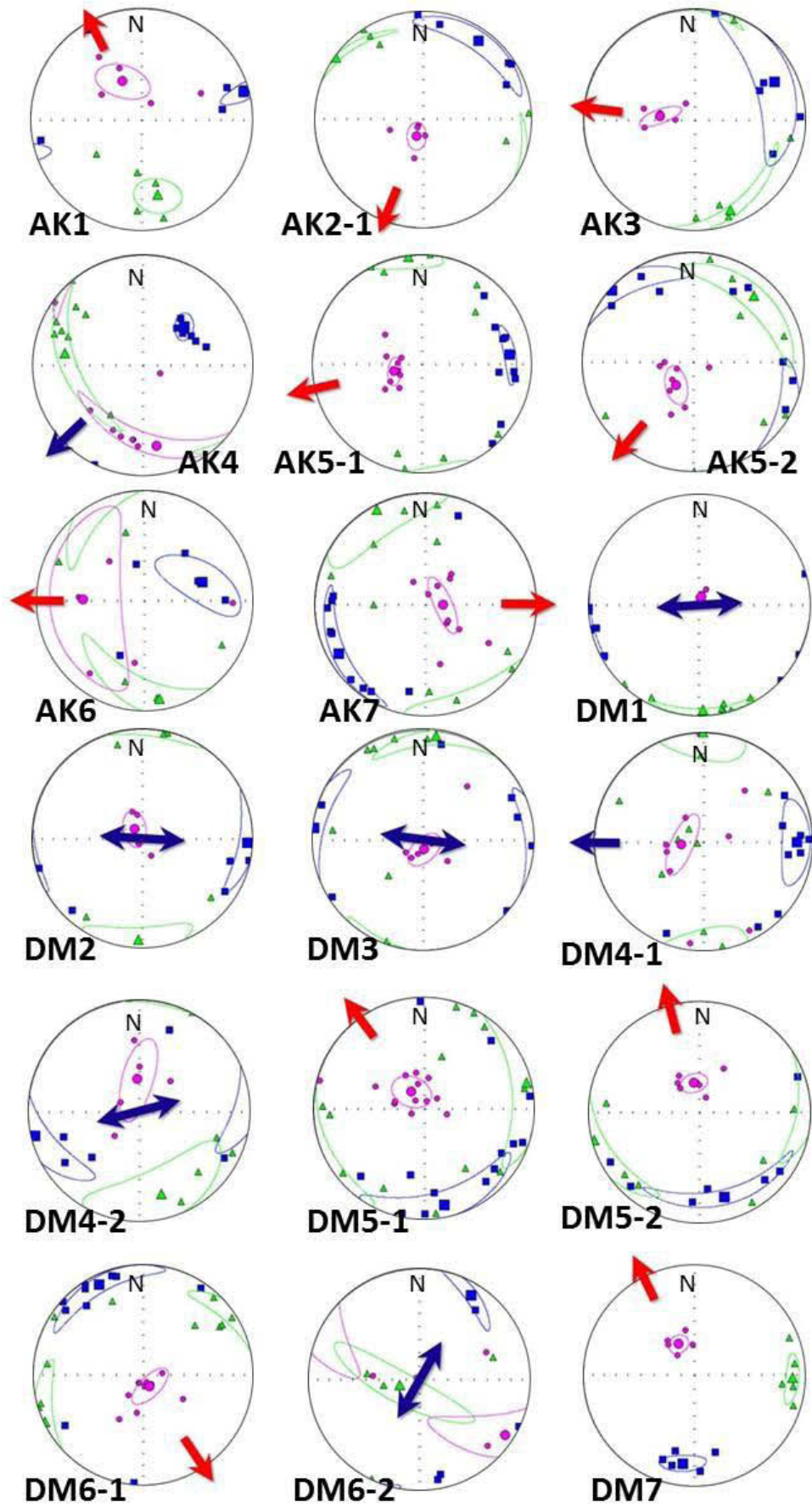


Figure 5.14 – AMS fabric stereoplots of the sampled sites before data selection (sampled sites and localities sections are shown in fig. 4.7). Symbols: squares = K_1 axes; triangles = K_2 axes; circles = K_3 axes; arrows: inferred flow direction. The ellipses show the dispersion angles.



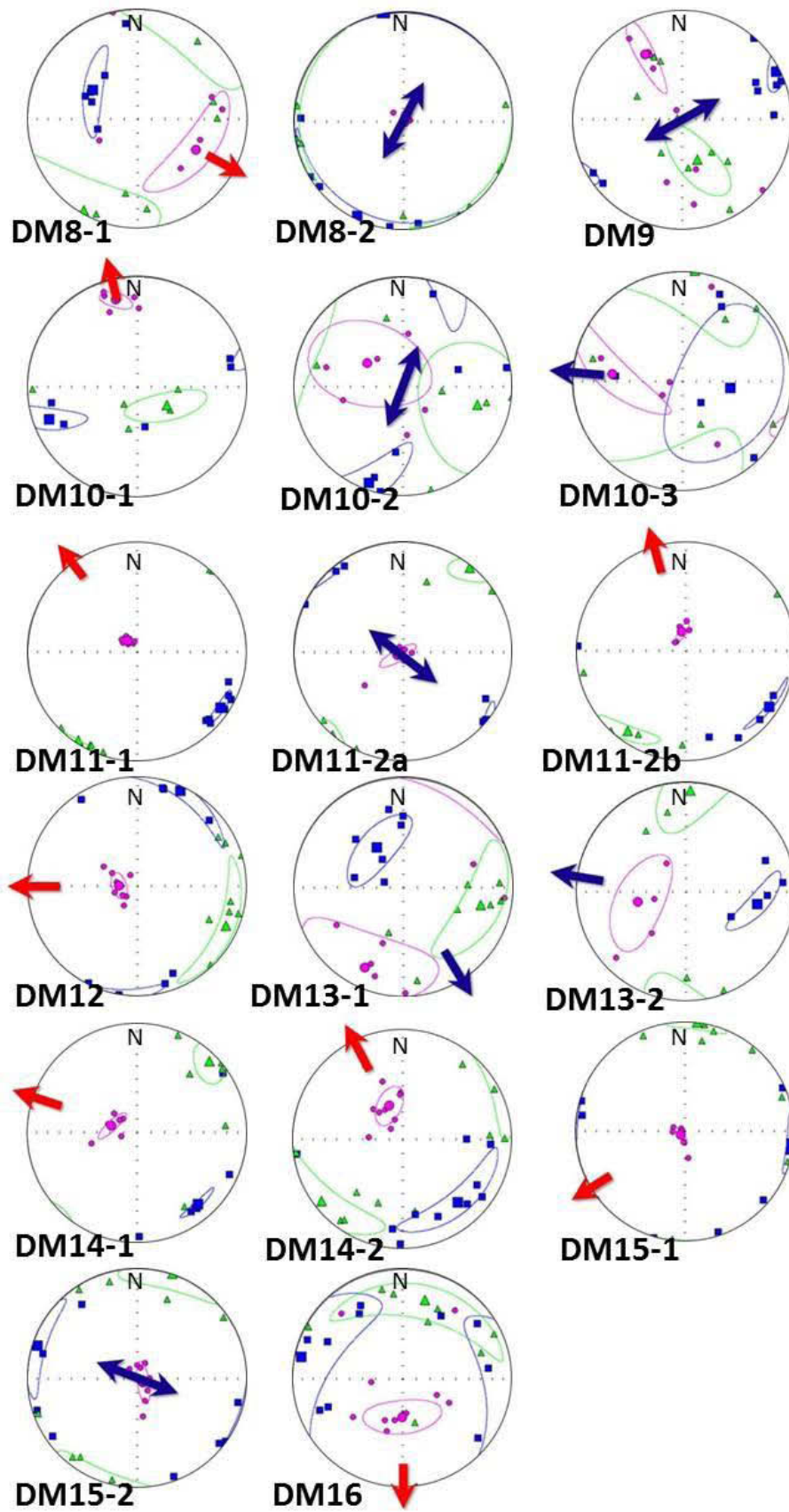


Figure 5.15 – AMS fabric stereoplots of the sampled sites after data selection. Symbols: as in fig. 5.14.

5.2.3 – AIRM and magnetic fabric

In order to investigate the contribution of the ferromagnetic minerals to the magnetic fabric, AIRM measurements were performed. Measurements were done on specimens with different magnetic mineralogy from 4 sites from the Incik and Sabuncu ignimbrites. In order to consider only the magnetic fabric related to the matrix, all the measured specimens densities fall within the range $\pm 1\sigma$ from the site mean value.

The magnetic fabric is well defined and oblate at 3 out 4 sites (appendix 3); at AK4 it is prolate. Degree of anisotropy P is higher than for susceptibility, and comprised between 1.177 and 1.355. The highest value occurs in the site AK4, which contains the greater fraction of altered Ti-magnetite (< 10%) among the others AIRM investigated sites. Comparison of AMS and AIRM fabrics (fig. 5.16) points out a fully consistence between the two types of fabric at AK5-2 and DM4-2, where the dispersion angles associated to the main AMS and AIRM axes intersect. The site AK1 shows a lower value of the AIRM K_3 axis with respect to the AMS one, even their dispersion angles intersect and then they are statistically indistinguishable. No inversions between other axes is observed. In AK4 site, the principal axes K_2 and K_3 exchange their direction. This could be related to a passage to strongly prolate fabric, with $K_1 > K_2 \approx K_3$. No exchange between K_1 and K_3 axes is observed, pointing out that AIRM is controlled by the low-coercivity ferromagnetic fraction, i.e. MD Ti-magnetite.

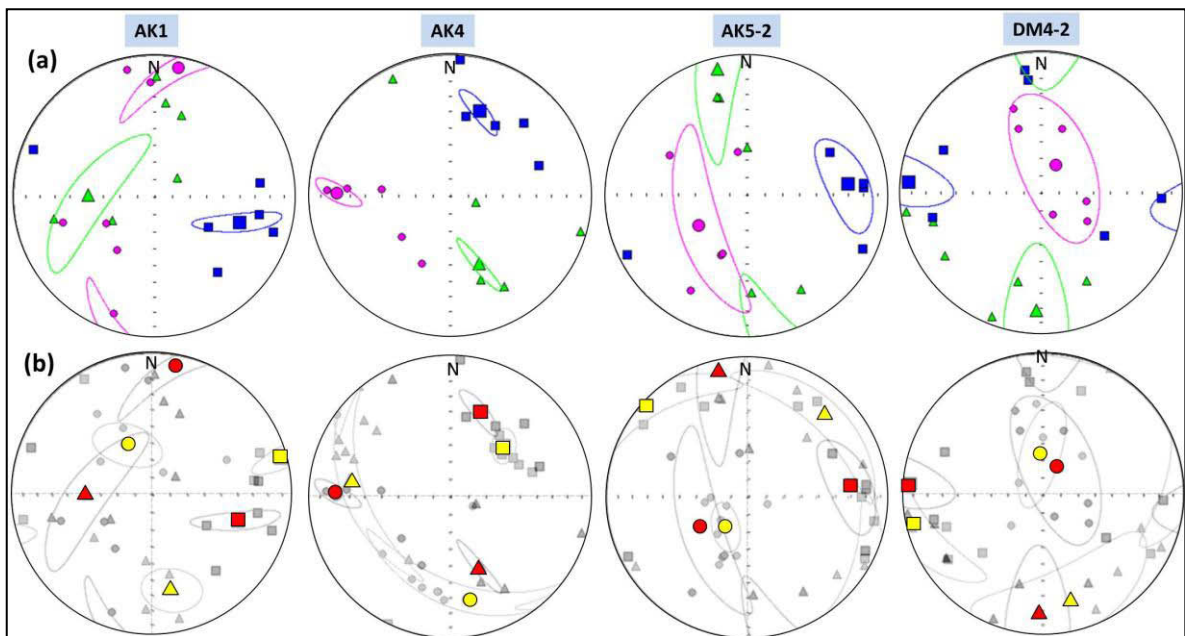


Figure 5.16 – (a) AIRM fabric stereoplots and (b) comparison with the AMS fabric ones. Symbols: (a) As fig. 6.38; (b) Square = K_1 , triangle = K_2 , circle = K_3 . Yellow symbols = AMS main axes; red symbols = AIRM main axes.

6 – Magnetic remanence

Most volcanic rocks contain ferro- and ferri-magnetic minerals that record past geomagnetic field in both direction and intensity. Lavas and indurated or welded pyroclastic rocks thus represent an invaluable material to obtain paleomagnetic information of utmost relevancy for volcanological and tectonic works. Ignimbrites have been widely used in previous paleomagnetic works (e.g. Black et al., 1996; Urrutia-Fucugauchi et al., 2000; Urrutia-Fucugauchi and Ferrusquia-Villafranca, 2001); however, while the input of paleomagnetic results based on the analysis of volcanic rocks is indisputable, little attention has been paid to sampling strategies and notably to the evaluation of the consistency and reliability of paleomagnetic data when results are obtained on a single volcanic unit with uneven magnetic mineralogy (McIntosh, 1991; Palmer et al., 1996; Paquereau-Lebti et al., 2008).

In the Kızılkaaya ignimbrite, NRM intensity varies over one order of magnitude in the range 0.2 – 2.4 A/m, and the highest values occur in the specimens from the most welded sites, e.g. at Ihlara. For most sites, during AF demagnetization, the direction changes very little in the first steps below 20 mT, and then does not change any more (fig. 6.1 a). Thermal demagnetization reveals two components: a high- T_b component, pointing to the origin (fig. 6.1 b) and a low- T_b component (20 – 400 °C). This shows a small angular deviation with respect to the high- T_b component, generally within 5° and it is deflected towards both E and W. These results show that the NRM consists of a negligible secondary component, likely viscous in origin, and a stable characteristic component (ChRM) of reverse polarity, which is well-defined, with maximum angular deviation (MAD) values typically lower than 4°. The ChRM directions are well clustered (fig. 6.2 a, b) and their site mean values, computed using Fisher's (1953) statistics, yield semi-angles of confidence α_{95} comprised mainly between 1.5° and 5° (table 6.1).

At some sites, the remanent magnetization is more complex, as evidenced in most specimens by no stable end-point direction reached during AF or thermal demagnetization, and the resulting remanence directions, measured after each demagnetization step, moving along a great circle (fig. 6.1 c, d). The NRM consists of two components with overlapping coercivity or unblocking temperature spectra. This is observed in figure 6.1 c, where the intensity decay of the specimen is rather slow and the Median Destructive Field (MDF) is very high. The unblocking temperature spectra of the two remanence components (fig. 6.1 d) apparently overlap completely.

For these sites, the site mean direction was computed using the great circle remagnetization paths and Fisher's statistics as modified by McFadden and McElhinny (1988). Also in this case, the ChRM directions are clustered and their site mean value well defined, with α_{95} below 5° (fig. 6.2 c, d; table 6.1).

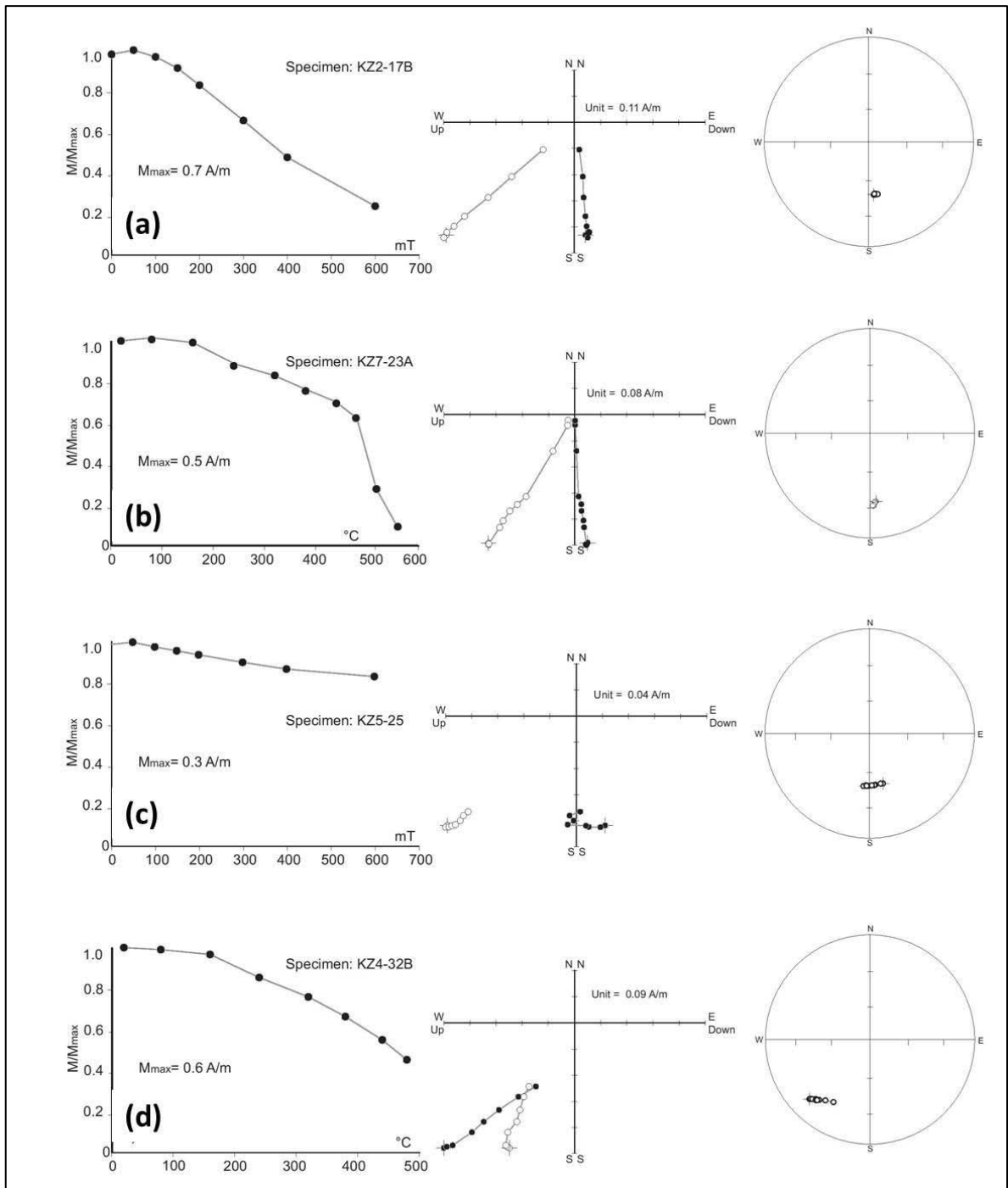
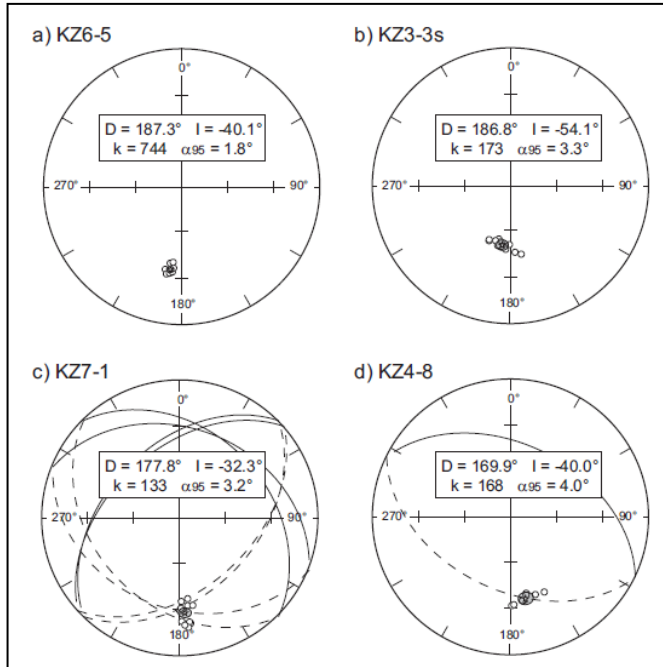


Figure 6.1 - Demagnetization results. Left: normalized intensity decay; middle: Zijderveld (1967) diagrams. Symbols: full/open dot = declination/apparent inclination; right: equal-area projection of demagnetization directions. Symbols: open dot = negative inclination.

A closer inspection in the arrangement of the ChRM directions at site level shows that their distribution is elongated (fig. 6.2 as well as in fig. 6.1 c, d) and the circular distribution, as assumed by Fisher's statistics, is rather uncommon. The eccentricity in the distribution was computed following Engebretson and Beck (1978). Its value is 0 for a circular distribution, 1 for an elliptical one. In 14 out of 33 sites, the eccentricity is higher than 0.80 and mostly in the range 0.90 – 0.95. Besides, directions appear to spread over a plane and it is possible to compute a best-fitting great

circle, whose pole is well-defined with a confidence limit below 15° (fig. 6.3). Samples from these sites hold two magnetization components, which are not resolved after the demagnetization treatment. For those sites, no mean site paleomagnetic direction is provided in table 6.1. Instead, the remagnetization circles were used. Thus the mean paleomagnetic direction for the Kızılkaya



ignimbrite is computed using both 19 mean site directions and 14 best-fitting great circles, as illustrated in fig. 6.4, yielding $D = 179.5^\circ$, $I = -42.9^\circ$, $k = 93$, $\alpha_{95} = 2.6^\circ$.

Figure 6.2 - Equal-area projection of the site mean paleomagnetic direction. Symbols: open dot = negative inclination; star = mean value and 95% confidence limit. In a) and b) the mean direction is computed by Fisher's (1953) statistics; in c) and d) by McFadden and McElhinny (1988) method; k = precision parameter; α_{95} = semi-angle of confidence.

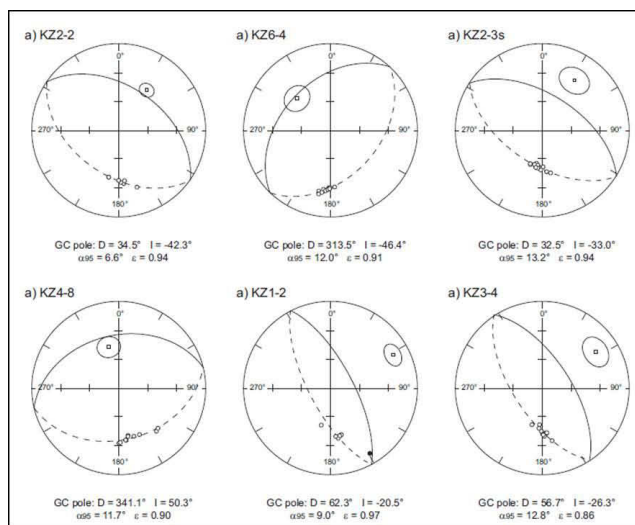


Figure 6.3 - Equal-areal projection of ChRM directions of representative sites (symbols as in figure 5) and the best-fit great circle and pole of the plane with confidence limit (McFadden and McElhinny, 1988). For each site the value of the pole direction and statistics parameters are indicated (Engebretson and Beck, 1978).

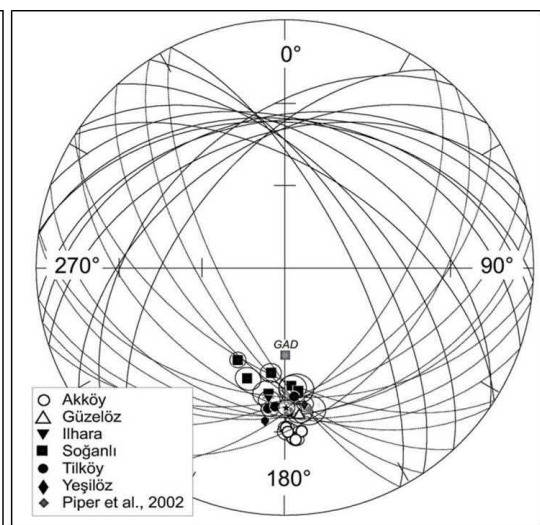


Figure 6.4 - Kizilkaya mean paleomagnetic direction (star and associated confidence limit) computed from site stable directions and site best-fitting circles. The direction of the GAD (grey square) and the directional value reported by Piper et al. (2002) (grey diamond), are drawn for comparison.

Locality	site	n/N	J _r	ChRM				Statistics
				A/m	D (°)	I (°)	k	
AKKÔY	KZ7-5	12/12	0,25	179,2	-34,5	438	2,1	M&M
	KZ7-4	12/12	0,40	179,8	-36,1	336	2,3	M&M
	KZ7-3	10/12	0,52	176,6	-31,5	377	2,3	M&M
	KZ7-2	12/12	0,47	171,6	-34,1	815	1,5	M&M
	KZ7-1	12/12	0,43	177,8	-32,3	133	3,2	M&M
GÜZELÔZ	KZ2-1	4/5	0,39	174,2	-40,7	558	3,9	F
	KZ2-2	7/7	0,43					
ILHARA	KZ6-1	6/6	0,88					
	KZ6-2	4/4	0,93					
	KZ6-3	4/5	2,43	186,7	-46,0	111	8,8	F
	KZ6-4	11/11	2,15					
	KZ6-5	10/12	2,10					
SOĞANLI	KZ5-7s	12/12	0,33	187,0	-46,6	148	4,7	M&M
	KZ5-6s	10/12	0,22	174,1	-48,4	292	5,4	F
	KZ5-5s	10/10	0,47	207,1	-55,4	337	2,6	F
	KZ5-4s	6/6	0,37	198,9	-50,7	280	4,0	F
	KZ2-3s	12/12	0,35					
	KZ2-2s	5/5	0,91	176,8	-50,1	458	4,3	F
	KZ2-1s	14/14	0,74	174,6	-49,4	789	1,4	F
TILKÖY	KZ4-9	11/11	0,64	178,5	-41,4	301	2,6	M&M
	KZ4-8	9/10	0,34					
	KZ4-7	13/13	0,50	175,8	-46,7	309	2,4	M&M
	KZ4-6	10/12	0,49	182,0	-42,6	283	3,2	F
	KZ3-5	9/13	0,47					
	KZ3-4	11/13	0,50					
	KZ3-3	12/12	0,41					
	KZ3-2	10/12	0,33	186,7	-42,2	243	2,7	F
YEŞİLÖZ	KZ1-1	5/6	1,71	173,7	-42,1	979	2,5	M&M
	KZ1-2	6/8	1,18					
	KZ1-3	11/15	1,61					
	KZ1-4	14/16	0,93	172,2	-43,3	266	2,6	M&M
	KZ1-5	7/11	0,89					

Table 6.1 - Paleomagnetic direction of the Kizilkaya ignimbrite. Symbols: n/N = number of specimens used for calculation/number of measured specimens; J_r = remanent magnetization intensity; D, I = magnetic declination and inclination; k) precision parameter; α₉₅ = semi-angle of confidence; Statistics: M&M = McFadden and McElhinny (1988); F = Fisher (1953).

7 – Data interpretation

7.1 – *Kızılkaya ignimbrite*

7.1.1 – Magnetic fabric

In the Kızılkaya ignimbrite, different processes affected the deposits and the magnetic mineralogy itself is complex. Ti-magnetite is the main magnetic mineral and occurs as both magmatic free grains and as inclusions in other phenocrysts and glass shards. At some sites, it is accompanied by an oxidized phase and/or hematite. Moreover, ferromagnetic minerals also occur in the embedded lithic and pumice clasts. The use of the magnetic fabric to infer the ignimbrite flow directions requires the capability to isolate the primary fabric, which is thought to be related to the flow dynamics, from all other effects, which can be regarded as noise sources. As suggested by Laberge et al. (2009), it is important to evaluate the primary or secondary origin of the magnetic fabric to locate the vent position.

Keeping in mind all of these factors in the magnetic fabric interpretation, as a first step, the definition of the AMS fabric was enhanced by discarding the specimens with anomalous densities. This resulted in the disappearance of all oblique fabrics. This has been interpreted as indicating a bias effect of the embedded clasts rather than a direct relation with the flow dynamics. As a second conservative step, only the normal fabrics were considered: consistency of the two directions, one derived from the magnetic foliation plunge and the other from the magnetic lineation, is a strong indication for the primary nature of the fabric. The results are shown in fig.7.1, where the arrows correspond to the foliation plunge and the white fans to the 95% confidence limit of the lineation.

According to the model (Hillhouse and Wells 1991, Le Pennec et al. 2000, Palmer and McDonald 2002), the convergence area of all these directions should locate the source area from which the pyroclastic current flowed. Inspection of figure 7.1 shows that the source area is not well defined: at some sites (Ovacık, Soğanlı, Guzelöz), the directions point to a source area in the southwest, in the Çiflik region, whereas those from the other sites are scattered.

The AIRM measurements were only done on the specimens with minor lithic fragment contents. The low value of the direct field (20 mT) stresses the contribution to the fabric of the Ti-magnetite grains of magmatic origin and has little effect on the very small grains included in the crystals of other minerals and glass shards. Preliminary data mostly point to the occurrence of MD Ti-magnetite as the main carrier of the fabric; thus magnetic fabric indicators may be considered as proxies of the flow directions. Figure 7.2 reports the AIRM fabric results in the same way as for AMS data in fig. 7.1. Most of the inferred flow directions point to a source area between the Derinkuyu Basin and the Göllü Dağ rhyolite massif (dashed area) and substantiate the location

proposed by Le Penec (2000) and Le Penec et al. (1998). The limited number of sites and their uneven geographical distribution prevent a closer definition of the source area.

These results show that AMS data may not be enough to define the primary fabric of an ignimbrite with a composite magnetic mineralogy. On the other hand, measurements of the anisotropy of remanent magnetization - AIRM in the present study - help separate the effect of the various minerals and thus possible overprints that mask the fabric derived from the emplacement dynamics.

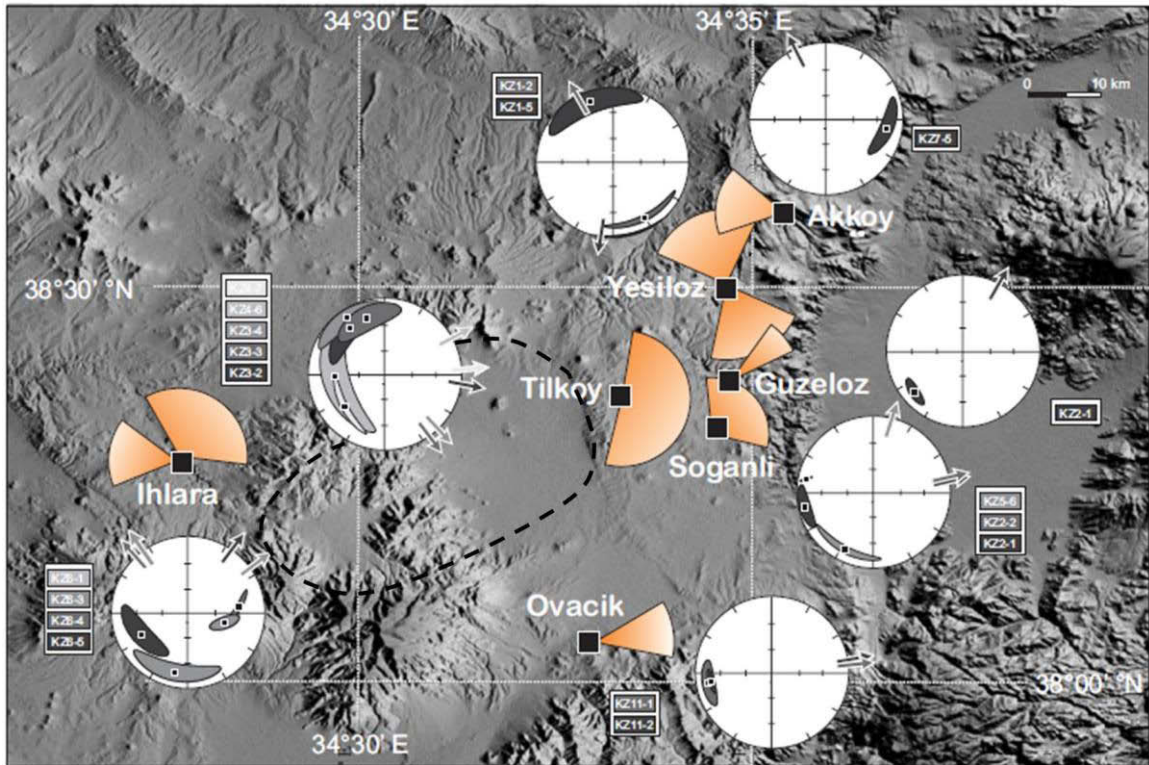


Figure 7.1 - Map of the flow directions inferred from the enhanced AMS data. Symbols: white fan = position of the magnetic lineation with associated 95% confidence limit; grey arrow = plunge of the magnetic foliation imbrication. The sequence of grey shades from dark to light corresponds to the stratigraphic order from the base to the top. Label indicates the site number.

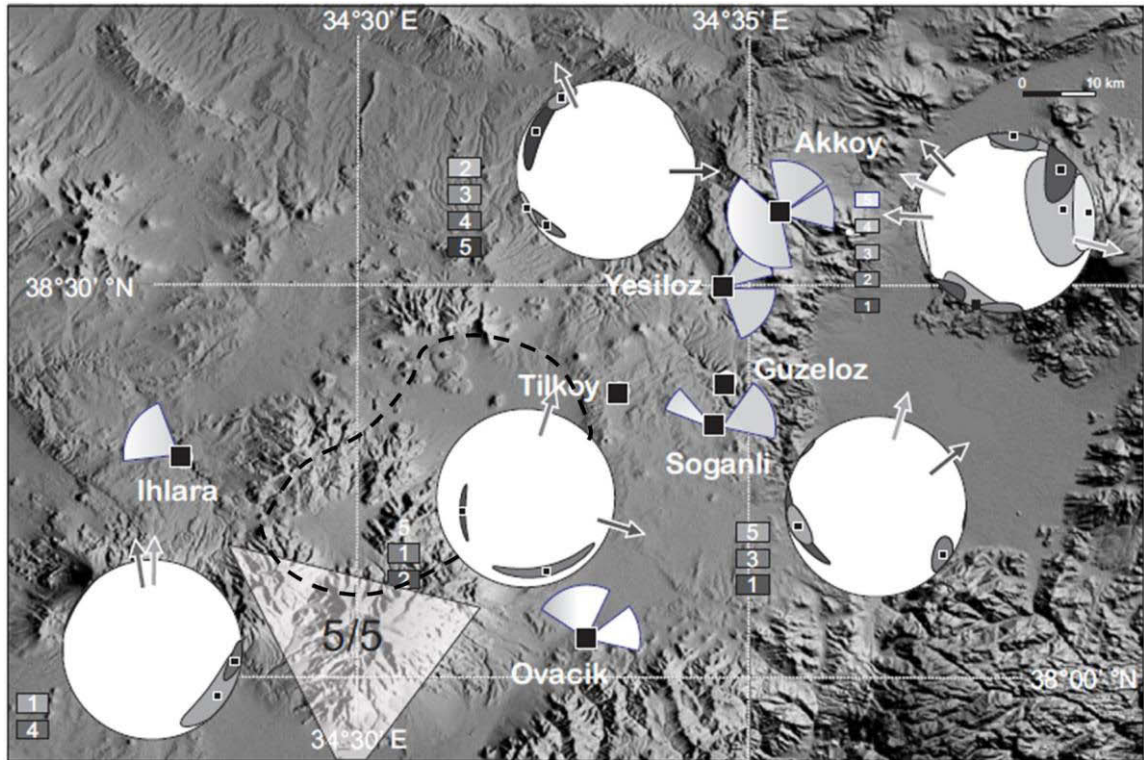


Figure 7.2 - Map of flow direction inferred from AIRM data. Symbols as in fig. 7.1. The dashed area represents the maximum overlapping zone after triangulation, regarded as the Kizilkaya ignimbrite source area.

7.1.2 – Magnetic remanence

The emplacement of large-volume ignimbrites and the deposition of accompanying plinian tephra fallout occur instantaneously at geological time scales. Widespread ignimbrite deposits might thus be considered as ideal stratigraphic marker horizons at the regional scale, as often reported in literature (Best et al., 1995; Bogue and Coe 1981; McIntosh 1991; Ort et al., 1999; Paquereau-Lebti et al., 2008). In these cases, the correlation is straightforwardly applied with little attention to the intrinsic characteristics of the deposit as well as the processes that acted at a specific locality.

Various processes have been proposed in the literature to explain lateral and vertical variations of the paleomagnetic direction recorded in an ignimbrite: reheating by an overlying hot flow deposit (Gose 1970); overprinting of the primary thermoremanence by a later chemical remanent magnetization (CRM) (Reynolds 1977); sub-blocking temperature plastic deformation (Rosenbaum 1986), but also welding compaction, anisotropy of magnetic susceptibility, geomagnetic secular variations, local magnetic anomalies, and tectonic tilting, as pointed out by Rosebaum (1986). Secondary alteration and formation of ferromagnetic grains with unblocking temperatures of ChRM above emplacement temperatures may occur during devitrification or vapor-phase crystallizations (Paquereau-Lebti et al., 2008).

Although The Kızılkaya ignimbrite is a single flow and cooling unit, its magnetic properties show notable variations within the deposit. In most places the magnetic mineralogy is not vertically homogeneous, as might be expected from a large-volume pyroclastic flow emplaced in a short time interval. Notably, the magnetic susceptibility values display considerable differences among sites in the same section, and at some locations the magnetic remanence varies significantly from lower to upper sites. The necessity of a stratigraphic sampling in order to obtain reliable data for paleomagnetic reconstructions is therefore of primary importance.

Figure 7.3 shows the variations of the site paleomagnetic direction throughout the section at each locality. At Akköy, Güzelöz, Tilköy and Yeşilöz, the directions show negligible variations. At Soğanlı, and to a minor extent at Ihlara, the paleomagnetic directions vary significantly with the stratigraphic height: declination ranges from 170° to 210° , inclination from -34° to -55° . Large deflections from the mean direction occur at sites characterized by the occurrence of oxidized magnetite and/or hematite. A partial to complete secondary magnetic overprint partially masks the primary remanence. These results suggest that at these sites the Kızılkaya ignimbrite acquired a thermal remanent magnetization during the emplacement and a chemical remanent magnetization, during the eventual cooling or a short time later. McClelland-Brown (1982), interpreted the T_b overlapping during thermal demagnetization as a clue for the occurrence of two probably contemporaneous thermal and chemical magnetizations; consistently, Piper et al. (2002) recognized in the Kızılkaya ignimbrite two magnetization components, thermal and thermo-chemical (TCRM) in origin. They interpreted the low-blocking temperature reverse component as primary TRM and the high-blocking temperature component as a secondary chemical (CRM) or thermochemical (TCRM) remanence acquired in younger geological times. This interpretation is supported by the angular difference between the two components, which would result from tectonic rotations which affected the area.

Data obtained in the present work show that the angular deviation is not systematic, because the low- T_b component in some cases is deviated towards E, in other towards W. Moreover, AF demagnetizations reveal only one well-defined component. In the case of Akköy, site KZ7-3, for example, the mean direction computed for AF directional data is $D = 176.8^\circ$, $I = -31.9^\circ$, $\alpha_{95} = 3.0^\circ$. The high- T_b component ($D = 177.3^\circ$, $I = -30.3^\circ$, fig. 6.1b) falls within the α_{95} semi-cone of confidence. It may therefore be reasonably assumed as the primary remanence. On the contrary, the low- T_b component ($D = 172.1^\circ$, $I = -34.4^\circ$) falls outside the confidence limit and the small angular deviation between the two remanences (ca 6°) is fully consistent with the effect of paleosecular variations. According to this interpretation, the low- T_b component would have been acquired a short time after the emplacement.

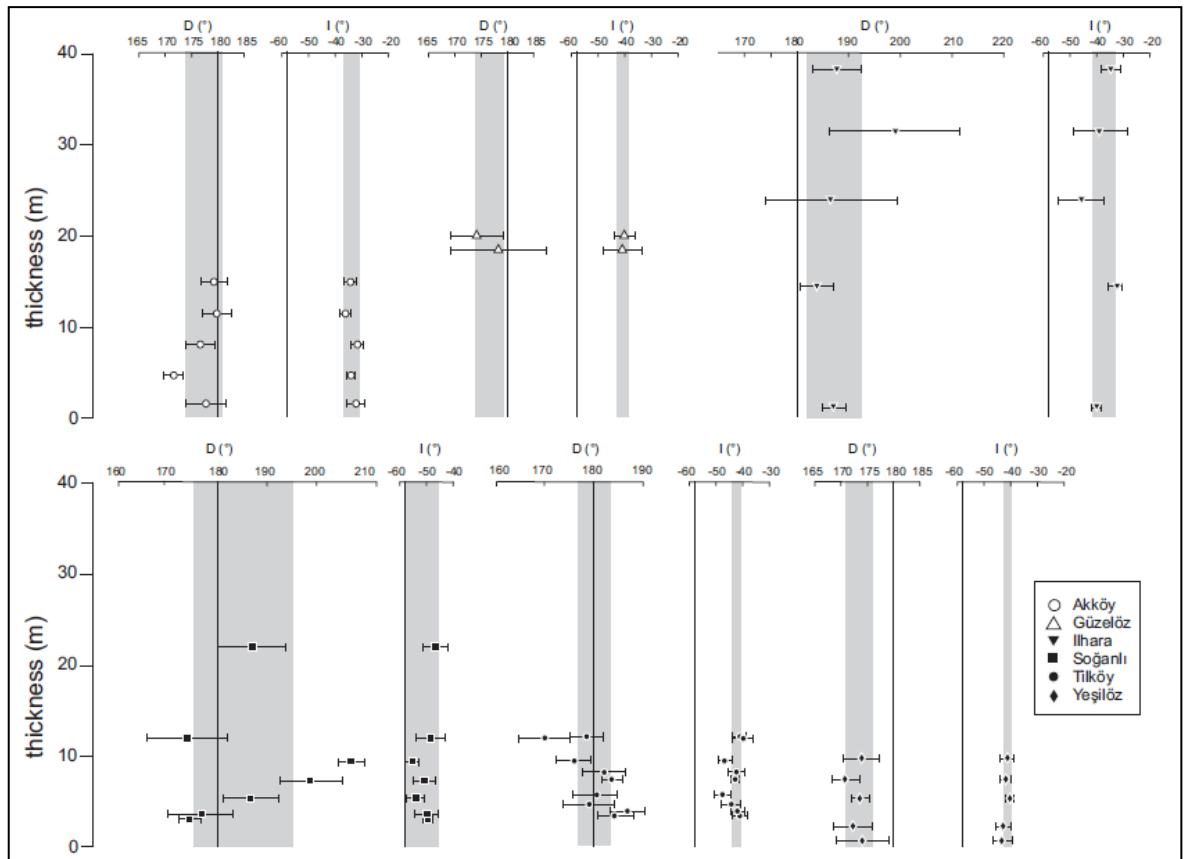


Figure 7.3 - Magnetic declination and inclination variation as a function of sites' stratigraphic position at each locality. Vertical axes: GAD values at the sampling region ($D = 0^\circ$, $I = 58^\circ$); grey areas: locality mean declination and inclination confidence limit; horizontal bar: ΔD and ΔI values for sampling sites.

Paleomagnetic directions recorded in the Kızılkaya ignimbrite at some localities are well defined and consistent with those of Piper et al. (2002). This is the case at Akköy, Güzelöz and Yeşilöz, where mean paleomagnetic directions ($n = 12$, $D = 175.2^\circ$, $I = -38.6^\circ$, $k = 249$, $\alpha_{95} = 2.7^\circ$) are statistically indistinguishable from literature data ($D = 170.9^\circ$, $I = -39.9^\circ$; $k = 211$, $\alpha_{95} = 5.3^\circ$), because their 95% ellipses intersect. In these cases, the Kızılkaya ignimbrite possesses a single and stable direction of thermal remanence, which from all evidence appears to be a reliable representation of the ambient field at the time of cooling (fig. 7.3).

A different behavior characterizes the remaining localities, where the remanent directions change systematically with stratigraphic height. In 14 out of 33 cases, the ignimbrite is characterized by two remanence components, as a result of the complex magnetic mineralogy (occurrence of Ti-magnetite, oxidized Ti-magnetite and hematite) and variations in the thermal cooling and alteration histories. Depending on the temperature and coercivity spectra of the magnetic carriers it is not always possible to resolve the magnetization components. If the secondary components are not completely erased, the paleomagnetic results are biased, as shown by the elliptical distribution of the ChRM directions (fig. 6.3). In these sites, ChRMs are arranged along a great circle and no mean direction was computed. Instead, the pole of the best-fitting circle was calculated for each of the 14

sites, and the resulting mean paleomagnetic direction for Kızılkaya ignimbrite was obtained combining both the stable directions and the best-fitting circles (fig. 6.4). Where present, the secondary overprint contributes to deflect the direction by a few degrees. The Kızılkaya mean paleomagnetic direction obtained here and by Piper et al. (2002) are 7.4° apart, even if their confidence ellipses intersect (fig. 6.4). The difference is smaller for the declination, but it should be treated with caution when interpreting tectonic rotations in young rocks, because the uncertainty associated to the rotation (ΔR) (Demarest 1983) may be higher than the rotation (R). Piper et al. (2002) identified a generalized anticlockwise rotation for the Cappadocian ignimbrites younger than 9 Ma with respect to Eurasian and African palaeofields. In the Cappadocian sector they estimated the rotation rate at $9 \pm 5^\circ$.

The inclination values are systematically lower than GAD for both this study and Piper et al. (2002). The difference with respect to GAD is -15° and -18° , respectively. The stable paleomagnetic direction inferred at Akköy, Güzelöz and Yeşilöz in the present work shows an inclination in agreement with that of Piper et al. (2002). These authors discussed some possibilities to explain the ΔI . They excluded experimental problems and imperfections in the references APWPs, but took into account the occurrence of a complex geomagnetic source during the rock's magnetization acquisition and a northwards movement of the region since the time of magnetization. In the sites where a complex magnetization is revealed and two components are recognized, inclination values are higher, up to -55° and closer to the GAD one: these higher values, therefore, can be likely associated with the secondary chemical remanence. Since the two components were acquired close in time, a hypothesis is that the inclination of the secondary component represents a reliable record of the Earth's magnetic field during emplacement/alteration. Yet, this component shows a low intensity, thus in the average the thermal remanence is prevalent and the result is characterized by a low inclination value. The latter may reveal the occurrence of some processes acting soon after emplacement that bias the recorded magnetic direction.

Magnetic anisotropy can affect the recorded field toward the plane of maximum alignment of the magnetic grains, and anisotropy of remanence may lead to apparent paleosecular variation (Gattacceca and Rochette 2002). To test the flattening effect, the anisotropy of isothermal remanent magnetization (AIRM) was measured for Soğanlı specimens. Data are preliminary; the anisotropy degree P_{AIRM} is around 1.200. Using the relation $\tan I_r = (1/P_{\text{AIRM}})\tan I_g$, where I_r and I_g are respectively the paleomagnetic inclination recorded by the rocks and the inclination of the paleofield during cooling, an inclination $I_r \sim 53^\circ$ is determined. This value is still lower (-5°) than the expected one, but it may explain part of the discrepancy. Possibly it may be added to other mechanisms as for example in Piper et al. (2002): a regional effect which affects the eastern Mediterranean, the northward movement of the Central Anatolian block.

7.2 – *Afyon-Eskişehir ignimbrites*

7.2.1 Considerations about eruption dynamics and paleogeography

The volcanic stratigraphy of the ≈ 18.87 Ma Incik ignimbrite deposits shows that the eruption consisted of two distinct phases: an initial Incik 1 phase of at least three fall and pyroclastic surge and flow episodes (Incik 1a, Incik 1b and Incik 1c; the latter comprising at least two pulses, as evidenced in the deposits exposed at Inli in fig. 3.8 d), and a subsequent Incik 2 phase comprising one single fall and pyroclastic surge and flow episode. The considerable thickness of Incik 1 fall deposits and the occurrence of many pumice-fall layers complicate the reconstruction of the number of events which produced the ignimbrite unit. At places where Incik 1 fall deposit is more condensed (e.g. area of Akkaya, Incik and Söğüt; for reference see the map of the measured stratigraphic sections in fig. 3.4), three fall deposits forming-events are detected, recognizable from three distinct sets of pumice fall layers, each one displaying normal grading. Occurrence of accretionary lapilli within the ash fall layers in the fall deposit indicate humid conditions, possibly due to rain, during deposition. The relatively fine clasts granulometry and the presence of abundant ash fall deposits even at proximal facies within the caldera system (e.g. Üçsaray and Göknebi; fig. 3.30) may indicate pauses in the eruption, as revealed by the occurrence of many distinct sets of pumice fall deposits with distinct grading underlying the outflow deposits. The transition from Plinian to surge and flow activity may have been caused by vent erosion which led to a condition of eruption column collapse with resulting pyroclastic flows and surges. Caldera collapse stage is marked by the occurrence of a lithic-rich concentration zone in the basal portion of the Incik 1c ignimbrite, composed by reddish, banded rhyolitic clasts deriving from the disruption of dome structures within the caldera system. Evidence of surficial interaction between ignimbrite flow and water is supported by the occurrence of lacustrine deposits (both limestone and silt) preceding the Incik 1c ignimbrite. From the west to the east it is detected a lateral passage from limestone (Karacaören, in the Porsuk paleo-valley) to silt deposits (Fındık and Inli), therefore the evidence of the existence of a lacustrine basin with a depocenter around the Porsuk paleo-valley and characterized by more shallow conditions toward the east. At Karacaören limestone deposits are followed by reworked fluvial deposits containing aphyric pumice clasts displaying oblique and convolute lamination, possibly deriving from the Incik 1a and/or Incik 1b deposits. The reworked deposits testify the progressive upfilling of the basin through the time. They represent high-energy events occurred soon after the eruption and revealing the establishment of hydrographic instability conditions originated as a consequence of the Plinian eruption which abruptly modified the hydrographic system of the region. Fluvial deposits preceding the Incik 1c ignimbrite are found only in this area, supporting the hypothesis of the presence of a paleo-valley with a flowing river. At localities where lacustrine deposits occur, fall deposits lack. Another evidence supporting that pyroclastic flow entered in a lake is the ubiquitous presence of the fine-poor zone, interpreted as a

fine-depleted zone, at the base of Incik 1c ignimbrite, testifying extensive interaction between pyroclastic flow and water. Sigurdsson and Carey (1989), investigating the volcanic stratigraphy of the 1815 eruption of Tambora volcano, also ascribe the occurrence of fine-depleted layers and pipes structures as the result of interaction between the pyroclastic flow and oceanic water, and explain the process of fines-depletion as due to flushing of steam through the flows upon entrance into the water. Finally, other features of the interaction with water include the occurrence of numerous steam pipes (fig. 3.11 b). In many exposures, flow deposits show varying degrees of fines-depletion. Both thickness both clasts granulometry increase from the east to the west: at Inli the fine-depleted layer it is 20-cm-thick and contains pumice clasts up to 5-6 cm, at Karacaören it is 3-m-thick and contains pumice clasts up to 13 cm. These evidence indicate a more intense interaction between pyroclastic flow and water in the area of Karacaören, as evidenced by deeper basin conditions. Also Yalçın (1990) recognized in its “Karaören Formation” two facies of ignimbrite deposits: lacustrine (identified with the Incik ignimbrite by the present research), which is generally more extended toward the south-eastern portion of the Kırka basin, and continental (identified with the Seydiler ignimbrite by the present research), mostly occurring in the area comprised between Kümbet and Afyon. This general westward gently dipping of the paleo-surface may had also important implication in the paleo-drainage and in the emplacement of pyroclastic flow, which was affected by the paleo-topography, leading the flow to converge toward the Porsuk paleo-valley. Dipping of the paleo-topograpy is considered to be pre-emplacment in time, or occurred between the emplacement of Incik 1 and Sabuncu ignimbrite, since the contact between Sabuncu ignimbrite and the overlain lava is everywhere horizontal. The occurrence of many pulses testifies PDC waxing and waning more than once during the main sustained eruption as evidenced by the presence of single thick proximal flow unit deposits splitting into two or more flow sub-units, as in the case of Inli (fig. 3.8 d). Several ignimbrite sheets have architectures with such characteristics: for example parts of the Bishop Tuff (Wilson and Hildreth, 1997) and parts of the Ata ignimbrite (Aramaki and Ui, 1966). Presence of reworked fluvial deposits separating the Incik 1 and Incik 2 fall deposits is detected at all localities but Haymana and Göçeri. They are stratigraphically higher with respect to the Incik 1c ignimbrite, representing the products of its erosion. Haymana and Göçeri may have represented structurally higher portions of the basin where the Incik 1c ignimbrite has not been completely eroded. Their higher position with respect to nearby areas may have represented a topographic barrier for the north-westward directed Seydiler pyroclastic flow, explaining the lacking of Seydiler ignimbrite deposits northern than Ovacık. Persistence of more bacinal condition to the west and more shallow condition toward the east has been continued also after the emplacement of Incik 1 ignimbrite. This is testified by the lateral passage from limestone facies at Çayca, through siltite followed by limestone facies at Seydiköy, siltite facies at Demirli, to sandstone facies at Yenisofça and Uluçayır.

Contact with the ≈ 9.43 Ma Sabuncu ignimbrite is only observed at Fındık and Göçeri; despite the

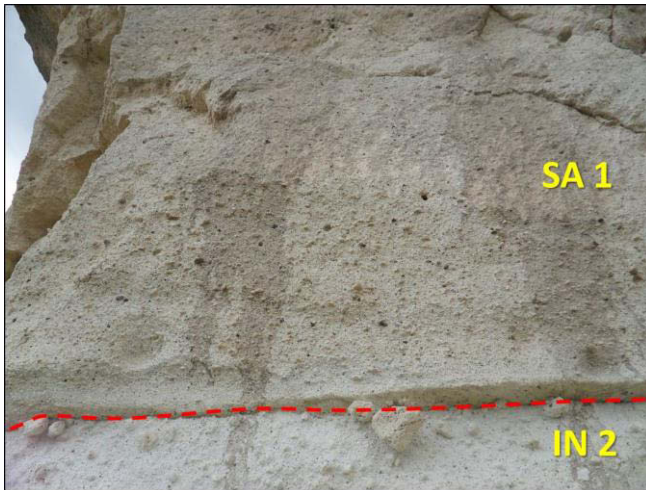


Figure 7.4 – Contact between Sabuncu 1 and Incik 2 ignimbrites at Göçeri. The base of Sabuncu 1 ignimbrite do not evidence any erosional structures.

wide gap in the time occurred between Incik and Sabuncu ignimbrites emplacement, at both locality nor volcanoclastic deposits nor paleosoil separate the Incik from Sabuncu ignimbrites. At Fındık the Sabuncu 1 fall layer occurs directly in contact with Incik 1c ignimbrite, at Göçeri the Sabuncu 1 ignimbrite is directly in contact with the Incik 2 ignimbrite (fig. 3.15; fig. 7.4). It is

possible that in the latter locality intense erosional processes have been occurred between the two ignimbrite eruptions,

explaining the relatively thin Incik 2 ignimbrite deposit (2.3 m) and lacking of any sedimentary deposits between Incik and Sabuncu units. Lacking of Sabuncu 1 fall deposit may be related to the main wind direction rather to removal from the emplacing pyroclastic flow, since the base of Sabuncu 1 ignimbrite does not evidence any erosional structures (fig. 7.4).

The > 14.8 Ma Seydiler ignimbrite deposits show that the eruption consisted of two distinct phases: an initial Seydiler 1 phase comprising at least one fall and pyroclastic flow episode, and a subsequent Seydiler 2 phase consisting of at least one fall and pyroclastic surge and flow episode. Both ignimbrite units have the same pumice mineralogy, as also reported by Keller and Villari (1972) who only noticed a variation in the An content of the plagioclase from the lower unit, ranging from An₂₃ and An₃₂, to the upper unit, ranging between An₂₂ and An₂₄. These elements suggest that eruption evolved with the same geochemical features through the time, and the emplacement span of the ignimbrites was relatively short, as also supported by lacking of volcanoclastic sediments between Seydiler 1 and Seydiler 2 units. Fall deposits of the Seydiler 1 unit display a normal grading of pumice clasts evidencing a paroxysmal event during the first phases of the eruption, while Seydiler 2 unit displays a general inverse grading of the pumice clasts contained in the fall deposit, pointing out that the paroxysmal event occurred during the last phases. Interaction between paleo-topography and pyroclastic flow is evidenced at many localities. Presence of two paleo-valleys are detected in the present-day Midas and Derbent valleys. Pumice clasts imbrication (fig. 7.10 and fig. 7.14 a) and AMS fabric at these places evidence an opposite-to-flow direction, considering a source area in proximity of Bayat village. Presence of topographic barriers was revealed in the area of Kayıhan (locality DM6; fig. 4.7) and Yeşilyayla (locality DM8; fig. 4.7). Here it is hypothesized the presence of a structurally higher relief, that pyroclastic flow may has not been able to surmount completely. This is evidenced by the presence of opposite-to-

flow directions inferred by ignimbrite pumice clasts imbrication (fig. 7.14 a) and AMS fabric (fig. 7.19 and fig. 7.20), that are discordant to flow directions inferred by load cast structures preserved in the underlain surge deposits. This may be explained by the different ability of distinct expanded- portions of the pyroclastic flow to overcome topographic barriers. Evidence of the interaction between pyroclastic flow and water is reported in the area of Ovacık, which delimitates the southern margin of the lacustrine basin of Kırka. In this locality the effects of pyroclastic flow entering into the lake resulted in the production of large pipe structures (fig. 3.25 a), besides the occurrence of limestone-derived clay chips. Occurrence of massive lithic breccia lens (mlBr) in the Seydiler 1 ignimbrite containing large lithic blocks up to 1 m within the area comprised among Olukpınar, Karaağaç and Karakaya, testifies proximal-to-medial lithofacies of the ignimbrite. According to Druitt (1985) and Druitt and Bacon (1986), such lithofacies can be found as far as 14 km from source. In the Seydiler ignimbrite, it generally occurs in the middle-upper portion of the ignimbrite sheet and is interstratified with massive lapilli-tuff lithofacies (mLT), which laterally pass to pumiceous mLT (as at Yeşilyayla and upper portions of Seydiler 1 ignimbrite more to the west). Contacts between mlBr and mLT is sharp at Karakaya (fig. 3.25 c), more gradational at Karaağaç (fig. 3.25 d). According to subdivisions proposed by Druitt and Sparks (1982), Walker (1985), Druitt and Bacon (1986), Roobol et al. (1987) and Scott et al. (1996), mlBr lithofacies is clast-supported fines-poor at Karakaya, clast-supported fines-rich and matrix-supported at Karaağaç. Blocks lithologies contained in mlBr portions are metamorphic, testifying erosion from the substrate by the PDC. Massive lithic breccia lithofacies have thickness and grain size variations from Karakaya (respectively ≈ 25 m; up to 1 m; ≈ 11 -km-far from the source area) to Karaağaç (≈ 7 m; up to 29 cm; ≈ 14 -km-far from the source area). This evidence, associated to the lateral passage from mlBr to pumiceous mLT at Yeşilyayla (≈ 28 -km-far from the source area) and at more distal facies, represents a down current transition from proximal mlBr into medial and distal pumiceous mLT, recording a depletive current that only in proximal regions was sufficiently competent to transport the lithic blocks. In addition to this interpretation, lenses of mlBr locally occurring within ignimbrites are reported where local topographic effects caused deposition of blocks (e.g. Freundt and Schmincke, 1985; Buesch, 1992; Bryan et al., 1998). The developed lithic clasts imbrication detected at Karaağaç, with most elongated *a* axis parallel to the flow direction and more dispersed foliation planes-dip directions, records laminar conditions of the emplacing pyroclastic flow (Hughes and Druitt, 1998).

7.2.2 Ignimbrites volume and eruption magnitude determination

Procedure used for area and volume determination is shown in fig. 7.5, taking as example the Incik ignimbrite. For each ignimbrite was firstly calculated the minimum area extension by considering the enveloped area of the cropping out pyroclastic deposits (fig. 7.5 a, fig. 7.6). The corresponding

volume was estimated by sub-dividing the enclosed area into several sub-areas characterized by a specific average thickness value inferred by the isopach map (7.5 b), then multiplying each sub-area for the relative average thickness value. After have determined the pre-erosional area extension (fig. 7.5 c), the corresponding pre-erosional volume was calculated as for the minimum volume. Minimum area extension areas of the Incik, Sabuncu and Seydiler ignimbrites are shown in fig. 7.6.

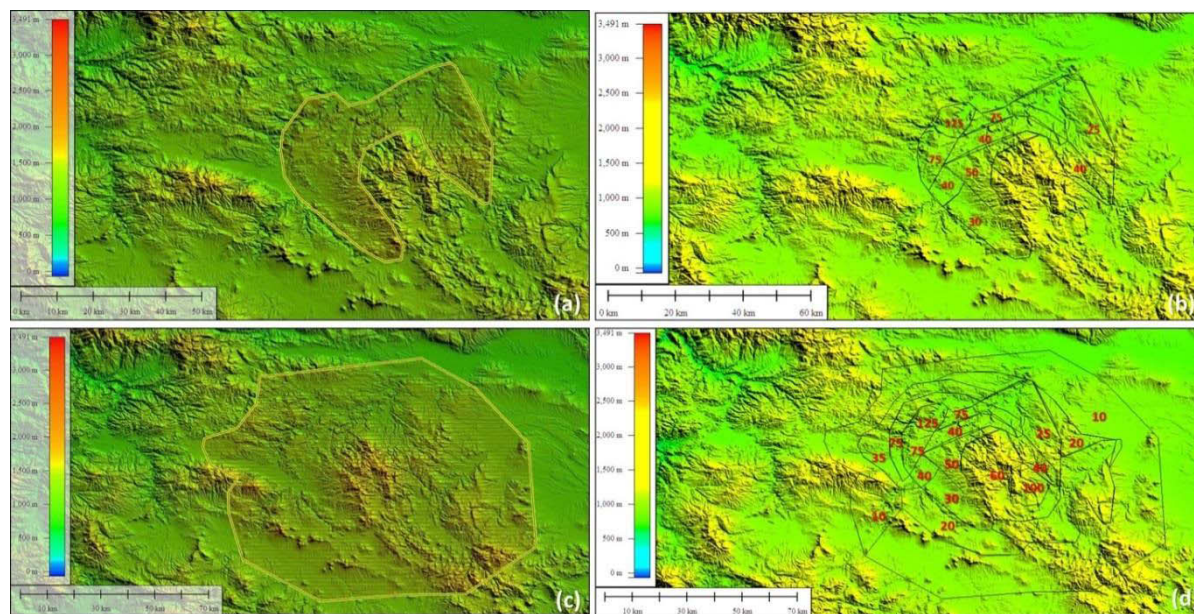


Figure 7.5 – Area extension and volume estimation procedure (Incik ignimbrite): a) Minimum area extension; b) Minimum volume, obtained by multiplying each sub-area for the relative average thickness value (in red); c) Pre-erosional area extension; d) Pre-erosional volume, obtained in the same way as in (b).

In order to draw the pre-erosion area extension maps (fig. 7.6), pre-erosional surface was deduced on the basis of stratigraphic correlations, lateral facies variation of the deposits and paleo-topography (e.g. evidence of paleo-valleys or topographic barriers). The Incik ignimbrite was originally more extended than present-day (fig. 7.5 a and c). Isopach maps of the Incik 1c ignimbrite (fig. 3.31), evidence that deposits are still considerably thick at the edges of the exposed area, as pointed out by thickness values of the more external isopach curves (20 m between Ayvacık and Karaalan, about 35 km from the source; more than 100 m in the area of Karacaören, about 55 km from the source; more than 40 m at Haymana, about 30 km from the source). Presence of a main paleo-valley has been detected between Çalca and Sofça (the Porsuk paleo-valley), where nowadays the Porsuk river flows. In this area ignimbrite deposits are considerably thick (up to 170 m at Karacaören and more than 65 m at Sofça) and so pumice dimension (MP up to 8.4 cm), if compared with nearby ignimbrite deposits. Thickness and clasts dimension decrease for about 5-10 km toward the south-east (i.e. toward the source), to increase again toward the source. The paleo-valley has a south-west – north-east direction, so it is presumable that the pyroclastic flow flowed

toward the north-east along the Porsuk paleo-valley, possibly arriving over the city of Eskişehir. A second \approx SSE-NNW-trended paleo-valley has been detected in the area comprised between Ayvacık and Yorükkırka (the Ayvacık paleo-valley), as evidenced by the shape of isopach and isopleth curves. In the area of Kırka ignimbrite deposits are not exposed because covered by lacustrine sediments (corresponding to the Sarıkaya Formation of Yalçın, 1990).

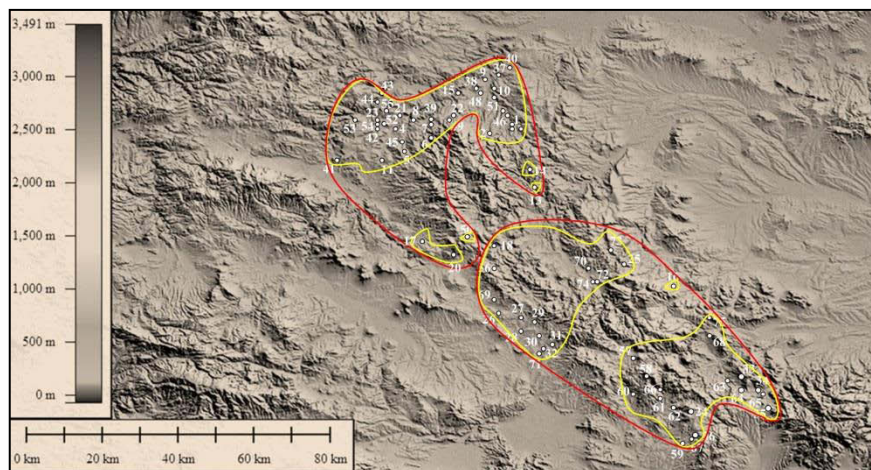


Figure 7.6 – Cropping out areas of the pyroclastic deposits (enclosed by yellow lines), and enclosed outcropping areas of Incik and Sabuncu ignimbrites (upper red line) and Seydiler ignimbrite (lower red line), used for minimum area and volume calculations. Numbers in the map as in fig. 3.4.

The Sabuncu ignimbrite is exposed over a more restricted area compared to Incik ignimbrite. Its thickness is greater than 30 m at the edges of the exposed area, and the trending of isopach and isopleth evidence the presence of a paleo-valley identifiable with the Porsuk paleo-valley as for Incik ignimbrite, even if Sabuncu ignimbrite (9.43 ± 0.09 Ma; U.Pb analyses on zircons) is much younger than Incik ignimbrite (18.866 ± 0.071 Ma; U-Pb analyses from zircons). Therefore the original area extension map of the Sabuncu ignimbrite has been considered to have a similar shape, even if more restricted, compared with the Incik one.

Isopach maps of Seydiler ignimbrite also display that deposits are still considerably thick at the edges of the exposed area, where deposits are 50 m-thick (e.g. > 65 m at Döğür, > 44 m at Yeşilyayla), pointing out that the pyroclastic flow had to travel for many kilometres more. Toward to the North, however, it is not clear until where the Seydiler ignimbrite arrived because lacking of exposures, and relationships between Seydiler and Incik ignimbrites are complicated because their contact is buried. The only section where both ignimbrites are exposed is Ovacık, where the Seydiler ignimbrite lies above limestone deposits (fig. 3.23 a), which overlain the Incik ignimbrite. Therefore, Seydiler deposits may be mostly eroded North from Kırka and Ovacık, or maybe this area was structurally higher and the pyroclastic flow could have not been able to surmount the topographic barrier. The shape of isopach and isopleth maps evidence the presence of two main paleo-valleys (fig. 3.38; fig. 3.40). The Midas paleo-valley corresponds to the present-day homonymous valley, which is SSE-NNW-trended and starts approximately from Yazılıkaya village. The Derbent paleo-valley starts few kilometres south-east from Bayat and ends around

Kurudere. Deposits exposures are lacking in the area north-east from Bayat because Quaternary deposits cover the ignimbrite succession.

IGNIMBRITE	AREA (km ²)		VOLUME (km ³)		Min. distance by source (km)	ASPECT RATIO		VEI index	M	DRE volume (km ³)
	Min.	P.-E.	Min.	P.-E.		P.-D.	P.-E.			
INCIK	1205	6674	59	185	55	1:1300	1:4700	7	>7	112
SABUNCU	538	3672	24	94	55	1:1100	1:3900	6	>7	53
SEYDILER	1745	4401	143	201	71	1:1100	1:2800	7	>7	135

Table 3.2 – Extensional and volumetric parameters of the Incik, Sabuncu and Seydiler ignimbrites. M = magnitude of the eruption (Pyle, 2000).

Taking into account the pre-erosional bulk volume estimations, which are 185 km³ for the Incik ignimbrite, 94 km³ for the Sabuncu ignimbrite and 201 km³ for the Seydiler ignimbrite, the VEI indexes are (table 3.2):

$$VEI_{INCIK} = 7;$$

$$VEI_{SABUNCU} = 6;$$

$$VEI_{SEYDILER} = 7,$$

which evidence Plinian eruptions. If the additional 35% of co-ignimbrite ash (Sparks and Walker, 1977) is also taken into account in the calculations, pre-erosional volumes would be roughly estimated at 250 km³ for the Incik ignimbrite, 127 km³ for the Sabuncu ignimbrite and 271 km³ for the Seydiler ignimbrite, and a corresponding VEI index = 7 for each ignimbrite. It has to be noticed that volume estimations are calculated without taking into account the underlying pumice fall and surge deposits because in many cases is eroded or not well preserved, therefore calculated volumes are underestimated.

The magnitude of the eruption M (Pyle, 2000) is calculated using the mean ignimbrite density values, obtained by the average of the specimens densities (appendix 1), and the pre-erosional bulk volume values. Assuming a mean density of 1390 kg/m³ for the Incik ignimbrite, 1290 kg/m³ for the Sabuncu ignimbrite and 1550 kg/m³ for the Seydiler ignimbrite, the M values are (table 3.2):

$$M_{INCIK} = \log_{10}[185 \cdot 10^9 \text{ m}^3 \cdot 1390 \text{ kg/m}^3] - 7 > 7;$$

$$M_{SABUNCU} = \log_{10}[94 \cdot 10^9 \text{ m}^3 \cdot 1290 \text{ kg/m}^3] - 7 > 7;$$

$$M_{SEYDILER} = \log_{10}[201 \cdot 10^9 \text{ m}^3 \cdot 1550 \text{ kg/m}^3] - 7 > 7.$$

DRE volumes are calculated assuming a density of the magma of 2300 kg/m^3 , which is usually applied for rhyolitic magmas (Crossweller et al., 2012) (table 3.2):

$$DRE_{\text{INCIK}} = (185 \text{ km}^3 \cdot 1390 \text{ kg/m}^3) / 2300 \text{ kg/m}^3 = \mathbf{112 \text{ km}^3};$$

$$DRE_{\text{SABUNCU}} = (94 \text{ km}^3 \cdot 1290 \text{ kg/m}^3) / 2300 \text{ kg/m}^3 = \mathbf{53 \text{ km}^3};$$

$$DRE_{\text{SEYDILER}} = (201 \text{ km}^3 \cdot 1550 \text{ kg/m}^3) / 2300 \text{ kg/m}^3 = \mathbf{135 \text{ km}^3}.$$

Minimum distances by the source are of 55 km for Incik and Sabuncu ignimbrites, 71 km for Seydiler ignimbrite (table 3.2). Data about Seydiler ignimbrite are sensibly different if compared to those reported by Aydar et al. (1998) for the same ignimbrite, who calculated an area extension of 1100 km^2 , a volume of 77 km^3 and a minimum traveled distance of 50 km.

The aspect ratio of each ignimbrite was calculated using the equation: $\text{aspect ratio} = H_m/d$, with H_m = average sheet thickness, and d = diameter of a circle that covers the same area as the sheet (Walker, 1983; Wilson et al., 1995). Both present-day both pre-erosional aspect ratio values were determined on the basis of minimum and original extensions of the deposits. Ignimbrite sheet average thickness was obtained through a weighted average of every sub-areas average thicknesses using the equation: $H_m = \frac{\sum_{i=1}^n (h_i \cdot A_i)}{\sum_{i=1}^n A_i}$, with H_m = ignimbrite sheet average thickness, h_i = sub-area average thickness, and A_i = sub-area extension. Present-day aspect-ratio values are in the order of 10^{-3} for each ignimbrite, so displaying a high aspect-ratio. However, if considering pre-erosional parameters, the aspect-ratio values for each ignimbrite is in the order of 10^{-4} , evidencing a low aspect-ratio. This discrepancy is due to the lacking of distal facies of the deposits, which is attributed to the occurrence of intense erosional processes and/or to the covering of pyroclastic deposits by younger deposits.

7.2.3 Locating the source of the Afyon-Eskişehir ignimbrites: reconciling field evidence with magnetic fabric data

Locating the source of the Afyon-Eskişehir ignimbrites was inferred by the exploitation and combination of several volcanologic and magnetic techniques, i.e.: (1) isopach and isopleth maps of the fall and ignimbrite deposits, (2) maps of the imbrication structures, welded and silicified facies of the ignimbrite deposits, and (3) AMS and AIRM magnetic fabrics.

7.2.3.1 Isopach and isopleth maps

Isopach and isopleth maps of the fall and ignimbrite units were used to infer the source area and flow directions. Specifically, source areas were constrained using the fall deposits maps since tephra dispersal is not affected by topography, which is not the case of ignimbrite deposits. The Incik 1c and Seydiler 2 fall deposits maps point out the presence of more than one dispersal axes (fig. 7.7; fig. 7.11). Large volcanic plumes that are injected into the atmosphere at mid and high latitudes, such as those of Incik and Seydiler, can be expected to show deep effects caused by the interaction of the eruptive column with the jetstreams, consisting in high speed geostrophic winds that span the globe at latitudes from 30° to 60°. Jetstream speed, that is average 40 m/s in winter, and 10 m/s in summer, can approach and even surpass local plume speeds, resulting in ingestion of unusual amounts of air during plume rise, bending over the plume in the windfield, and subsequent effects on maximum plume height and tephra dispersal. In the cases of Incik and Seydiler fall deposits, for each unit, the source area was found using the following procedure (fig. 7.7; fig. 7.11):

1. For each isopach, pumice isopleth and lithic isopleth map, the source area was get by intersecting the angle fans associated to the main dispersal axes;
2. the resulting inferred source area was then obtained according to the principle of maximum overlapping area, by intersecting the three source areas obtained in the point (1).

Isopach and isopleth maps of the Incik ignimbrite fall deposits concur for a source area located within the basin of Kırka, as clearly pointed out by the maps of Incik 1c (fig. 7.7). Data of Incik 2 (fig. 7.8) define a wider overlapping area because of less data, however it is consistent with the data of Incik 1c. Isopach and isopleth maps of the Incik ignimbrite flow deposits (fig. 3.31) evidence the interaction of the pyroclastic flow with the paleo-topography, pointing out the presence of the Porsuk paleo-valley, to the west, and the Ayvacık paleo-valley, to the east (fig. 7.9). The approximately east-to-west inferred flow directions represented in fig. 7.9 were deduced considering a westward dipping paleo-topography and paleo-drainage, as discussed in the paragraph 7.2.1, and because of the presence of the Porsuk paleo-valley, toward which the westward and part of the pyroclastic flow was directed to.

Data of Sabuncu ignimbrite are few because of the limited exposures of the deposits. However, isopach and isopleth maps of Sabuncu 1 fall deposits (fig. 3.34) display an increase of both thickness and grain size values toward the caldera system. Maps of Sabuncu 1 flow deposits (fig. 3.35) also evidence the existence of a paleo-valley identifiable with the Porsukpaleo-valley, characterized by higher thickness and clasts grain size values with respect the surrounding areas.

Isopach and isopleth maps of the Seydiler ignimbrite fall deposits concur for a source area located in the proximity of Bayat village, approximately in the same location of the Koroğlu caldera described by Aydar et al. (1998); the maximum overlapping area is centred in the locality of Bayat (fig. 7.11). Figure 7.10 shows the Seydiler ignimbrite isopach map, taking into account the contribute of both Seydiler 1 and Seydiler 2 ignimbrite deposits. In the map is well defined the external edges of Seydiler ignimbrite and is evidenced the interaction between paleo-topography and pyroclastic flow; moreover, it is detected the presence of two paleo-valleys (Midas, to the north, and Derbent, to the east). Places marked by both red both orange arrows, correspond to the areas where the presence of an opposite-to-flow direction has been detected by imbrication structures preserved in the ignimbrite deposit (orange arrows), while directional structures preserved in the underlain surge deposits (e.g. load cast) record a flow direction as expected to come from the inferred source area (thin red arrows).

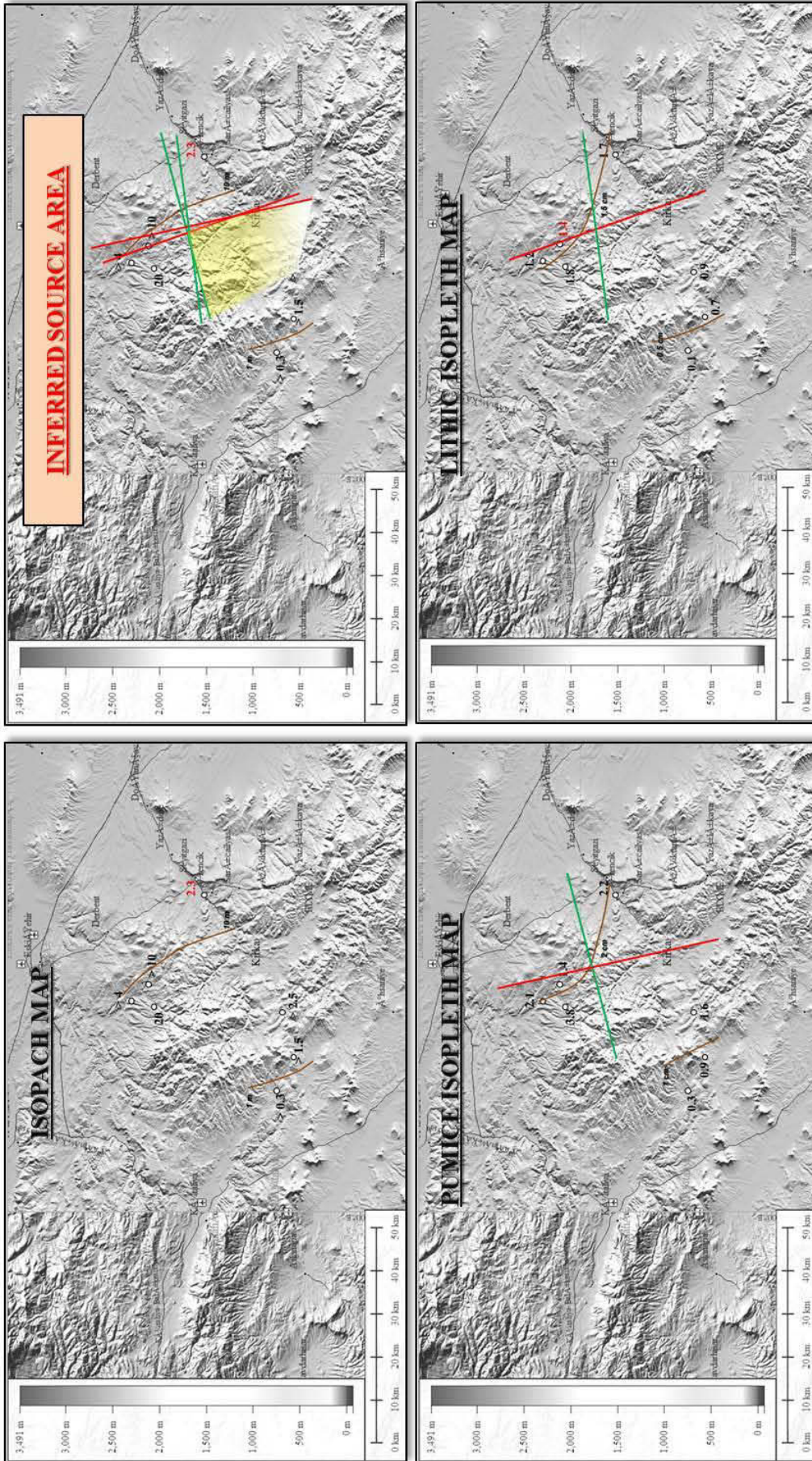


Figure 7.8 - Interpreted isopach, pumice isopleth and lithic isopleth maps of Incik 2 unit fall deposit. Symbols: as in fig. 7.7

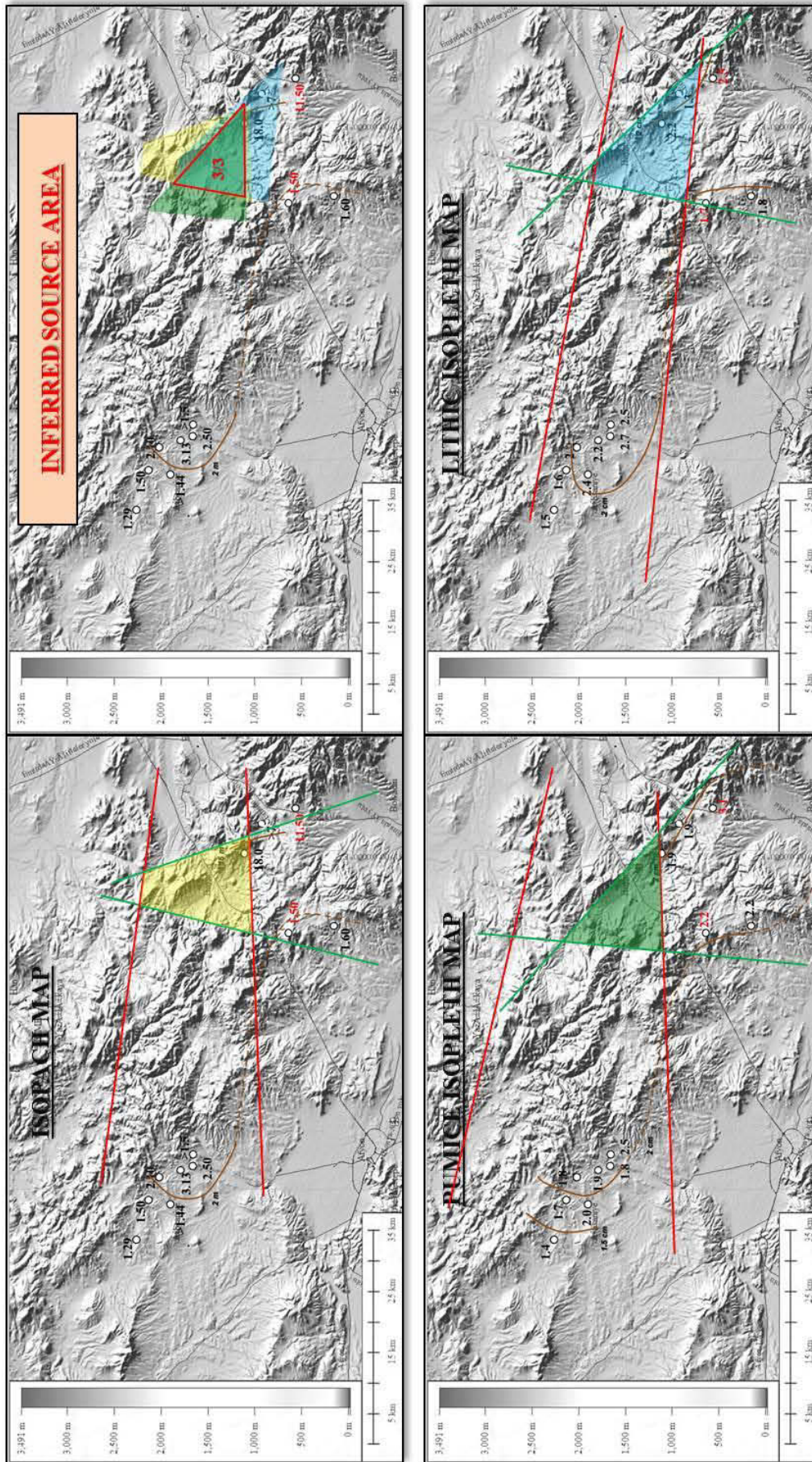


Figure 7.11 - Interpreted isopach, pumice isopleth and lithic isopleth maps of Seydiler 2 unit fall deposit. Symbols: as in fig. 7.7

7.2.3.2 Imbricational structures, welded and silicified facies maps

Maps of the imbrication structures were used to infer the source areas on the basis of directional field evidence. Moreover, maps of the welded and silicified facies were realized in order to help in the constraining of the source. Development of welding is essentially controlled by two factors (Streck and Grunder, 1995; Schumacher and Mues-Schumacher, 1996b; Le Penec, 2000; Branney and Kokelaar, 2002: (1) lithostatic load (welding is function of the thickness of the deposit), and (2) rheologic contrast of the hot pyroclasts (welding is independent from the thickness of the deposit).

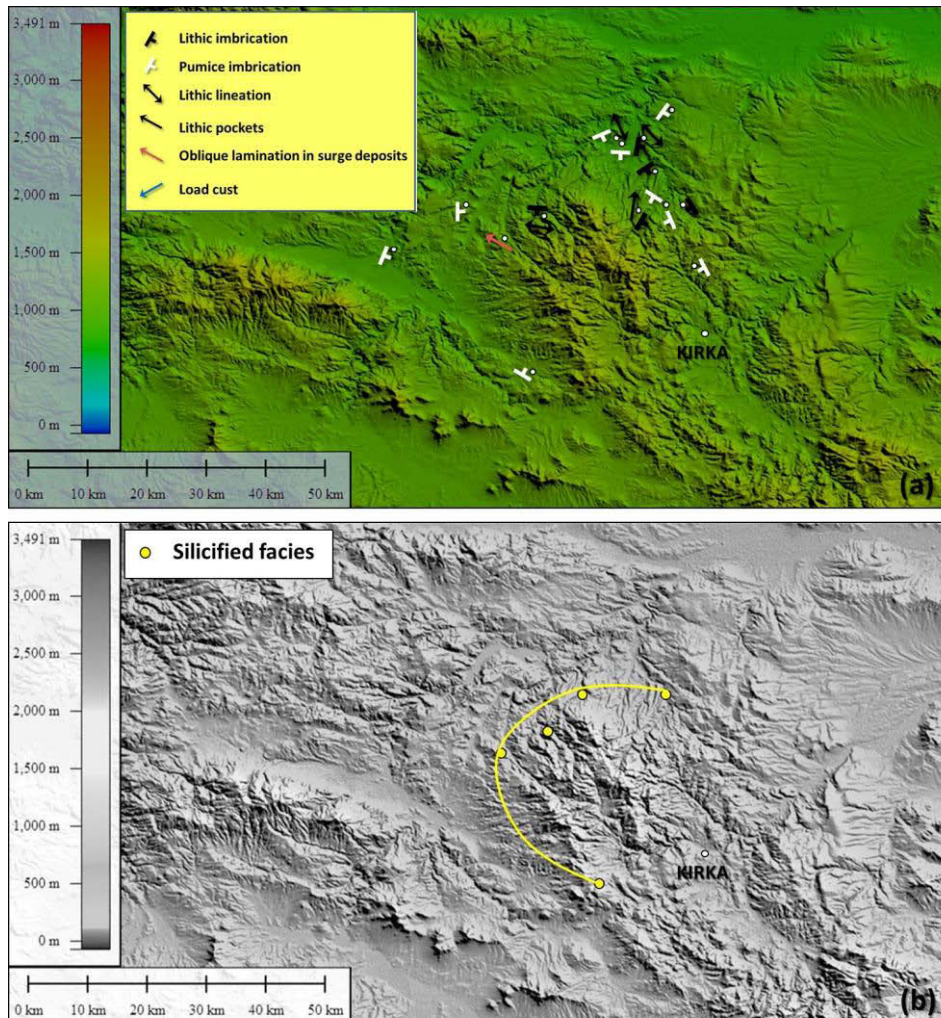


Figure 7.12 – Incik ignimbrite: a) Map of the imbrication structures; b) Map of the silicified facies.

Considering that ignimbrite deposits are thicker at proximal facies than medial and distal facies, provided that topography is uniform and without the presence of canyons or valleys where pyroclastic flow thickens even far from the source, welding would be more developed at proximal facies where lithostatic load is greater, and the map of the welded facies would circumscribe the source area. In paleo-valleys, ignimbrite deposit thickens and lithostatic load increases; therefore, welding may be enhanced even farther from proximal facies. Map of the silicified facies may reveal useful to constrain the caldera system. During hydrothermal activity and mineralisation of a caldera development, which may occur throughout the life of the caldera, but begins to dominate activity

during its late stages, silicification processes may be intense. Hydrothermal activity, leading to the origination of silicified facies, occurs through faults and fractures originated during the caldera development that are mostly related to the ring faults delimiting the edges of the caldera system.

Imbrication structures of the Incik ignimbrite (fig. 7.12 a) are mostly consistent with location of the source in the Kırka basin. Clasts imbrication and other directional structures such as lithic pockets evidence the presence of the Ayvacık paleo-valley, from where part of the flow travelled eastward probably through smaller canyons departing from the main paleo-valley. This hypothesis is supported by the fact that clasts imbrications east from the Ayvacık paleo-valley do not record a flow direction departing radially from the expected source, but record a flow direction which results to be affected by the paleo-topography. Silicified facies map (fig. 7.12 b) also support the Kırka basin as the source area of the Incik ignimbrite.

The only imbrication structures detected in the Sabuncu ignimbrite (fig. 7.13), at Göçeri, are also consistent with a source area located in the Kırka basin.

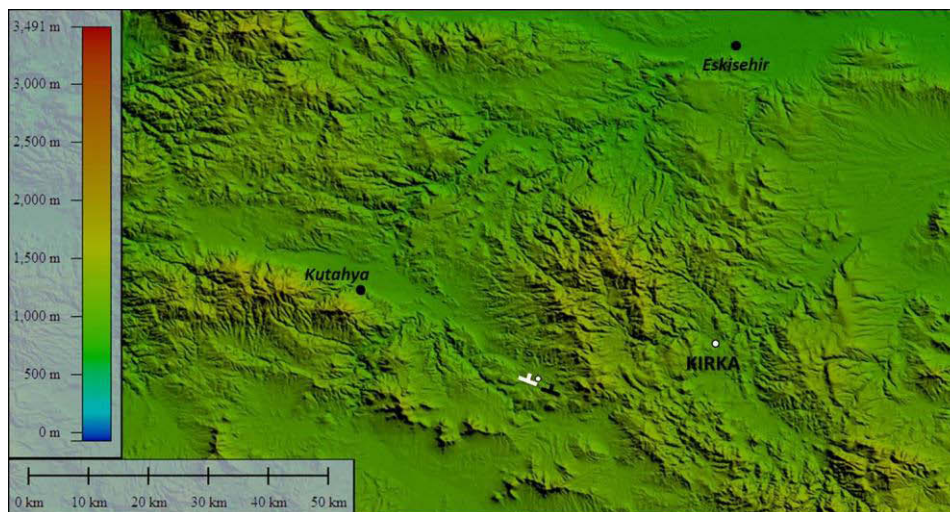


Figure 7.13 – Sabuncu ignimbrite: map of the imbrication. Symbols: as in fig. 7.12.

Imbrication structures of the Seydiler ignimbrite (fig. 7.14 a) are consistent with a source area in the proximity of Bayat village. Evidence of interaction between paleo-topography and pyroclastic flow is evidenced at localities marked by a dashed line. In this localities clasts imbrication preserved in the ignimbrite deposit gives an opposite-to-flow direction, while load cast structures preserved in the underlain surge deposit are consistent with the expected flow direction, because of the presence of topographic barriers. It is also noticeable opposite-to-flow directions recorded by pumice clasts imbrications in the Derbent and paleo-valley, possibly because of the flow travelling counter-slope. Medial-to-distal facies record flow directions always consistent with the inferred source area. Map of the welding and silicified facies also concurs to the same source area (fig. 7.14 b). Welding, ranging from incipient to moderate, occurs not only in the proximal facies near Bayat, but also in the Midas paleo-valley near to the locality of Yazılıkaya. This evidence would be

explained by the greater lithostatic load exerted where ignimbrite deposit is thicker (e.g. > 250 m around Bayat, > 57 m in the Midas paleo-valley; fig. 7.10).

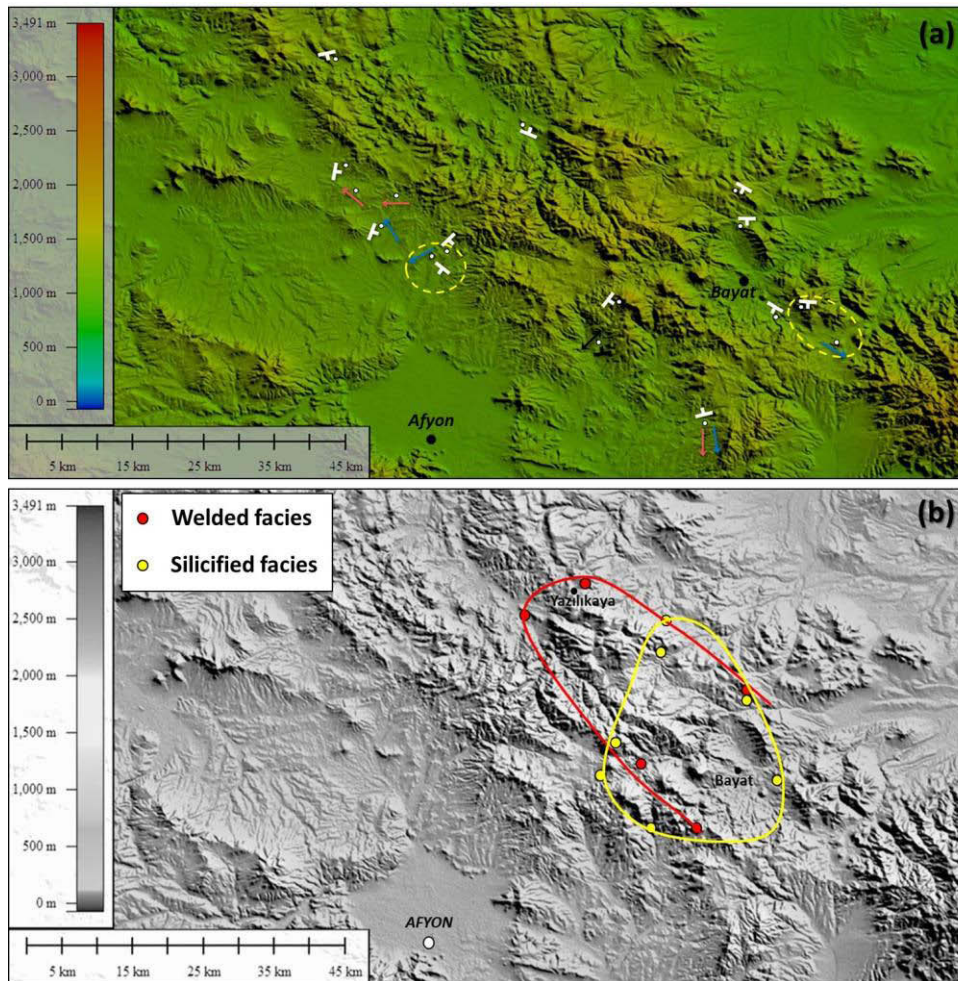


Figure 7.14 – Seydiler ignimbrite: a) Map of the imbrication structures. Dashed lines: localities where an opposite-to-flow direction has been detected by comparing clasts imbrication preserved in the ignimbrite deposit and load cast structures preserved in the underlain surge deposit; b) Map of the welded and silicified facies. Symbols: as in fig. 7.12.

7.2.3.3 Magnetic fabric

Flow directions inferred from AMS fabrics were used to constrain ignimbrites source area. In order to test the efficacy of the AMS fabric enhancing method described in paragraphs 5.1.2 and 5.2.2, for each ignimbrite the source area was found by using both flow directions obtained by AMS fabrics before the data selection (fig. 5.14) and those obtained by selected AMS fabrics (fig. 5.15). Moreover, AMS directional data were compared and integrated with AIRM ones.

Source areas were determined through the following procedure:

1. For each site, the AMS fabric stereoplots were reported in a map;
2. the inferred flow directions (obtained by K_3 AMS axis if $F > L$, or by K_1 magnetic axis if $L > F$) were reported together with their relative dispersion angle fans;

3. the source area was found through the method of maximum overlapping areas, by triangulating the dispersion angle fans of every site, eventually excluding sites considered affected by paleo-topography and therefore not representative to infer the source area. For Incik and Sabuncu ignimbrites it has been reported the maximum overlapping area included within the Kırka basin.

Source areas inferred by AMS fabric are consistent with those constrained by isopach and isopleth map of the fall deposits (fig. 7.7, 7.8 and 7.11) and with maps of the imbrication structures and of the welded of silicified facies (fig. 7.12, 7.13 and 7.14).

AMS directional data of Incik ignimbrite points to a maximum overlapping area localized near Kırka village (fig. 7.15 b; fig. 7.16 b). This result is slightly different from the inferred source area obtained by isopach maps of the Incik 1c fall deposits (fig. 7.7), that constrain the source area more to the north-west, but always within the Kırka basin. In the case of Incik ignimbrite, the latter result is more reliable because isopach and isopleth maps are obtained by more data (16 localities) with respect to the AMS map (6 localities, 8 sites). Moreover, for the triangulation of the flow directions inferred by the AMS, 3 localities were discarded (AK7, AK5 and AK4) because their flow directions are considered to be affected by paleo-topography, making reduce the considered sites for the triangulation to 3.

AMS directional data of Sabuncu ignimbrite consist just of DM4 and AK2 localities. The latter locality was discarded for the research of the source because considered to be affected by the paleo-topography, characterized, as for the Incik case, by approximately east-to-west paleo-drainage because of the westward tilting of the paleo-surface in this area. The dispersion angle fan defined by DM4 locality is however consistent with a source location that includes the Kırka basin (fig. 7.17 b; fig. 7.18 b). Both for Incik both for Sabuncu ignimbrites, AIRM flow directions (fig. 5.16) are in agreement with AMS ones, pointing out an east-to-west flow directions at AK4 and AK5, and a west-east flow direction at DM4-2.

The considered sites for the triangulation in the Seydiler ignimbrite are those not affected by paleo-topography (i.e. paleo-valleys and topographic barriers). The maximum overlapping area lies in a region slightly west from Bayat village (fig. 7.19 c; fig. 7.20 c), that is in accordance to that inferred by isopach and isopleth map of the Seydiler 2 fall deposits (fig. 7.11).

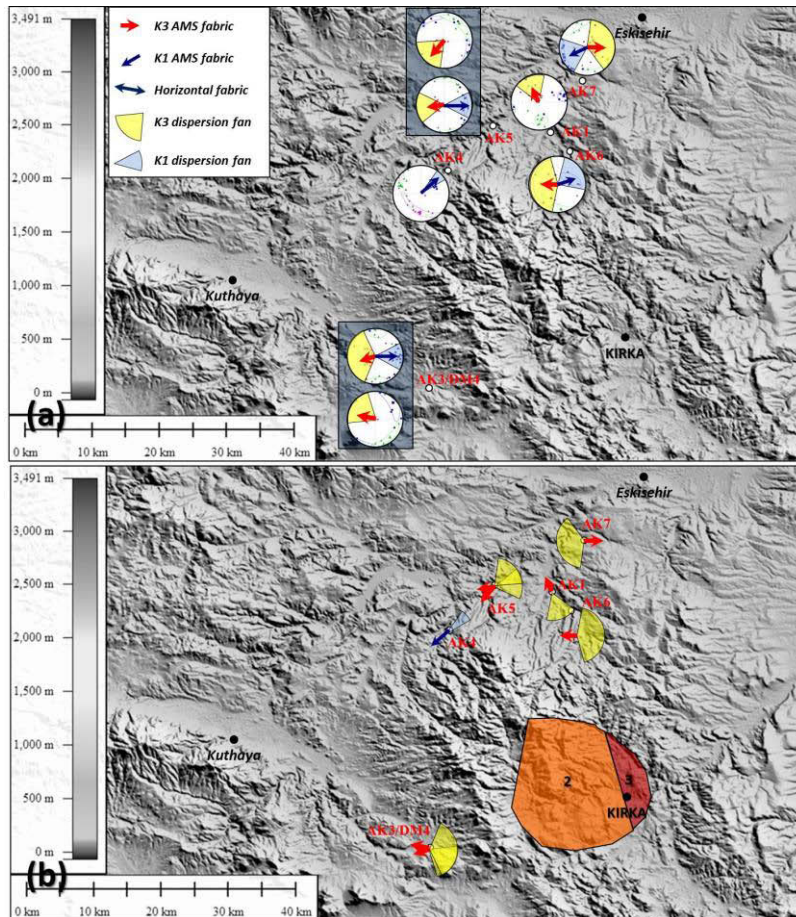


Figure 7.15 – Incik ignimbrite (not selected AMS data): a) AMS stereoplots; b) interpreted map of the inferred flow directions with their associated dispersion angle fans, and maximum overlapping areas included within the Kirka basin (colored areas). Numbers contained in the overlapping areas refer to the number of intersecting dispersion angle fans.

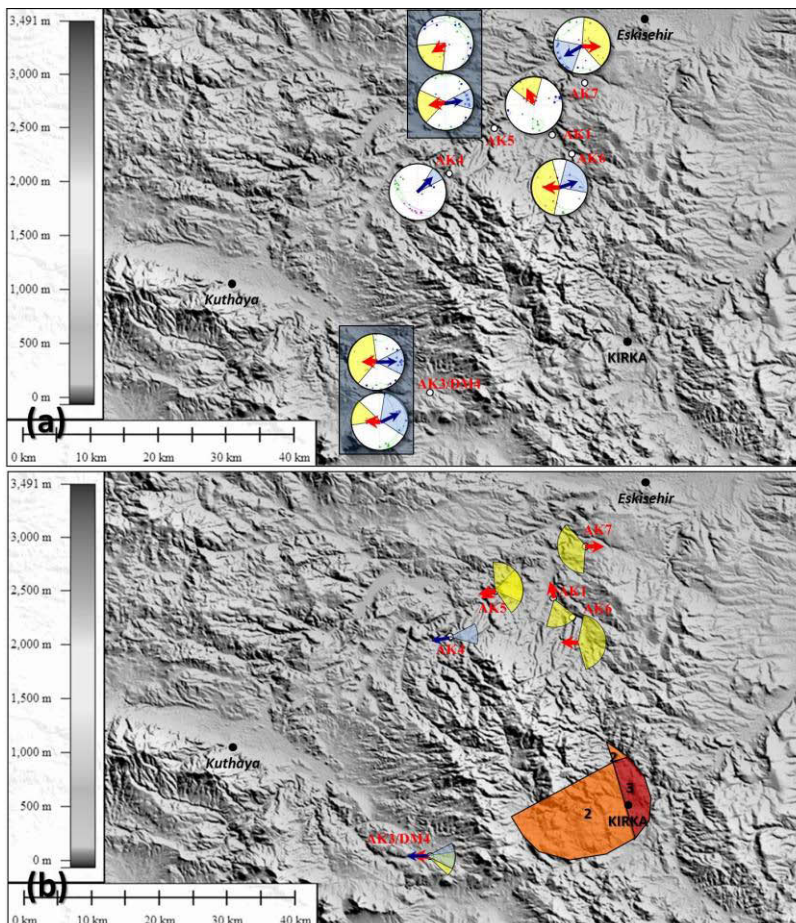


Figure 7.16 – Incik ignimbrite (selected AMS data): a) AMS stereoplots; b) interpreted map of the inferred flow directions with their associated dispersion angle fans, and maximum overlapping areas included within the Kirka basin (coloured areas). Numbers contained in the overlapping areas refer to the number of intersecting dispersion angle fans. Symbols: as in fig. 7.15 a.

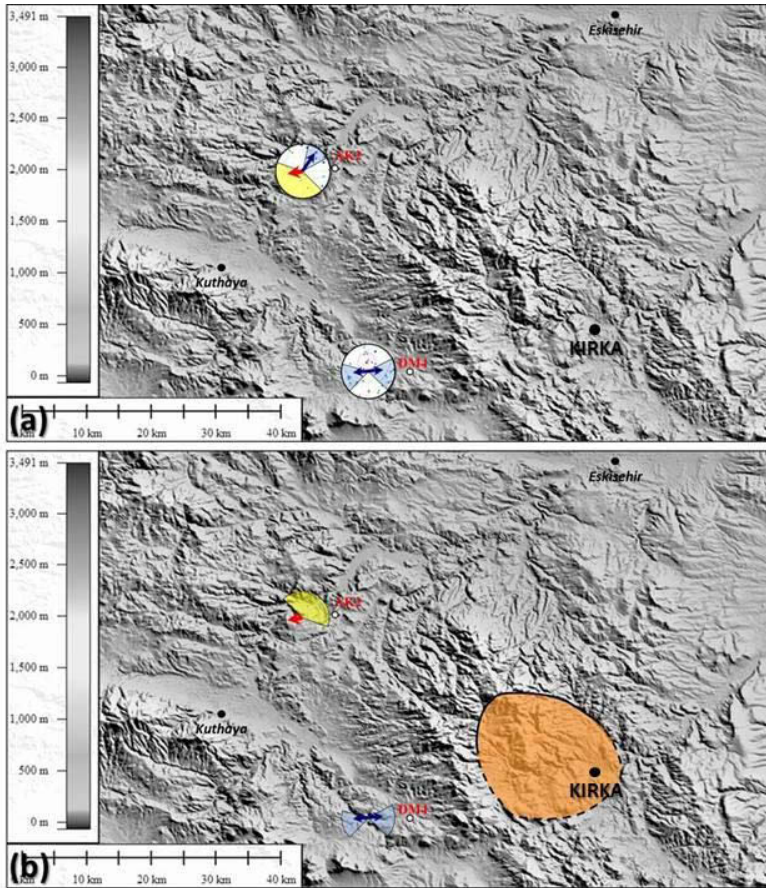


Figure 7.17 – Sabuncu ignimbrite (not selected AMS data): a) AMS stereoplots; b) interpreted map of the inferred flow directions with their associated dispersion angle fans. Maximum overlapping area includes the Kurka basin (coloured area). Symbols: as in fig. 7.15 a.

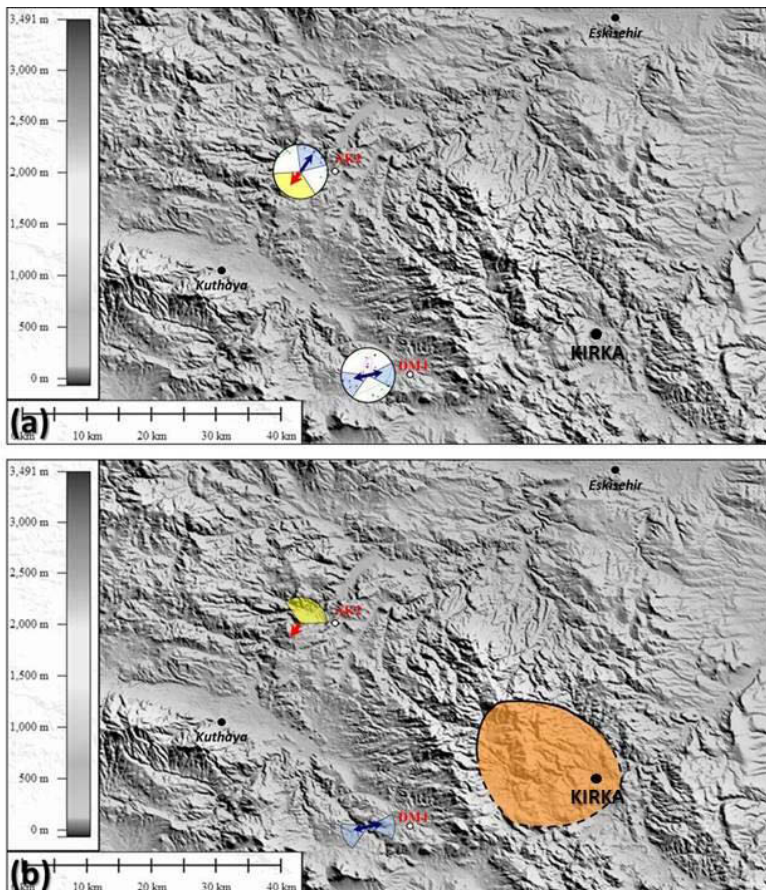


Figure 7.18 – Sabuncu ignimbrite (selected AMS data): a) AMS stereoplots; b) interpreted map of the inferred flow directions with their associated dispersion angle fans. Maximum overlapping area includes the Kurka basin (coloured area). Symbols: as in fig. 7.15 a.

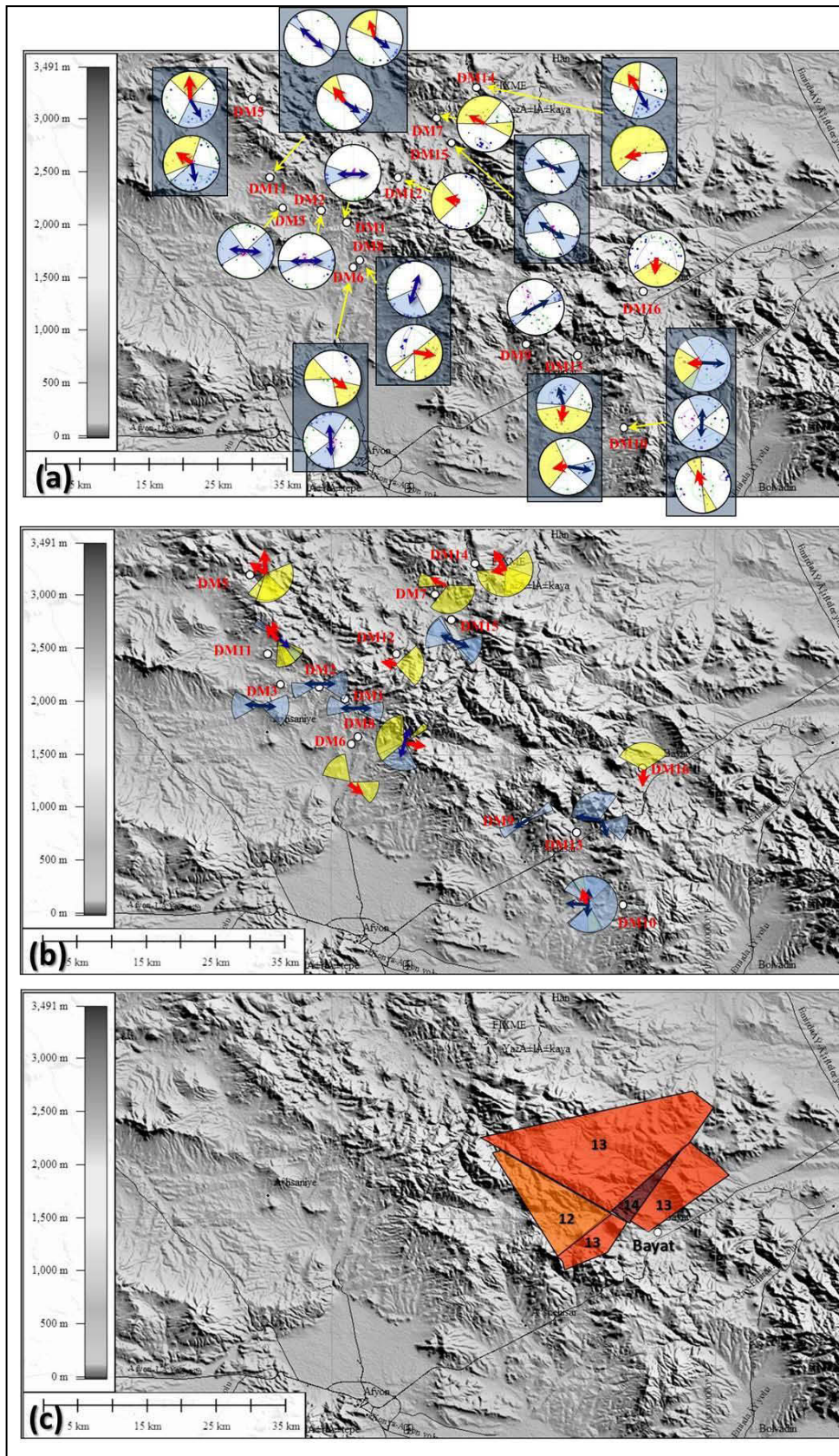


Figure 7.19 – Seydiler ignimbrite (not selected AMS data): a) AMS stereoplots; b) interpreted map of the inferred flow directions with their associated dispersion angle fans; c) maximum overlapping areas (coloured areas). Numbers contained in the overlapping areas refer to the number of intersecting dispersion angle fans. Symbols: as in fig. 7.15 a.

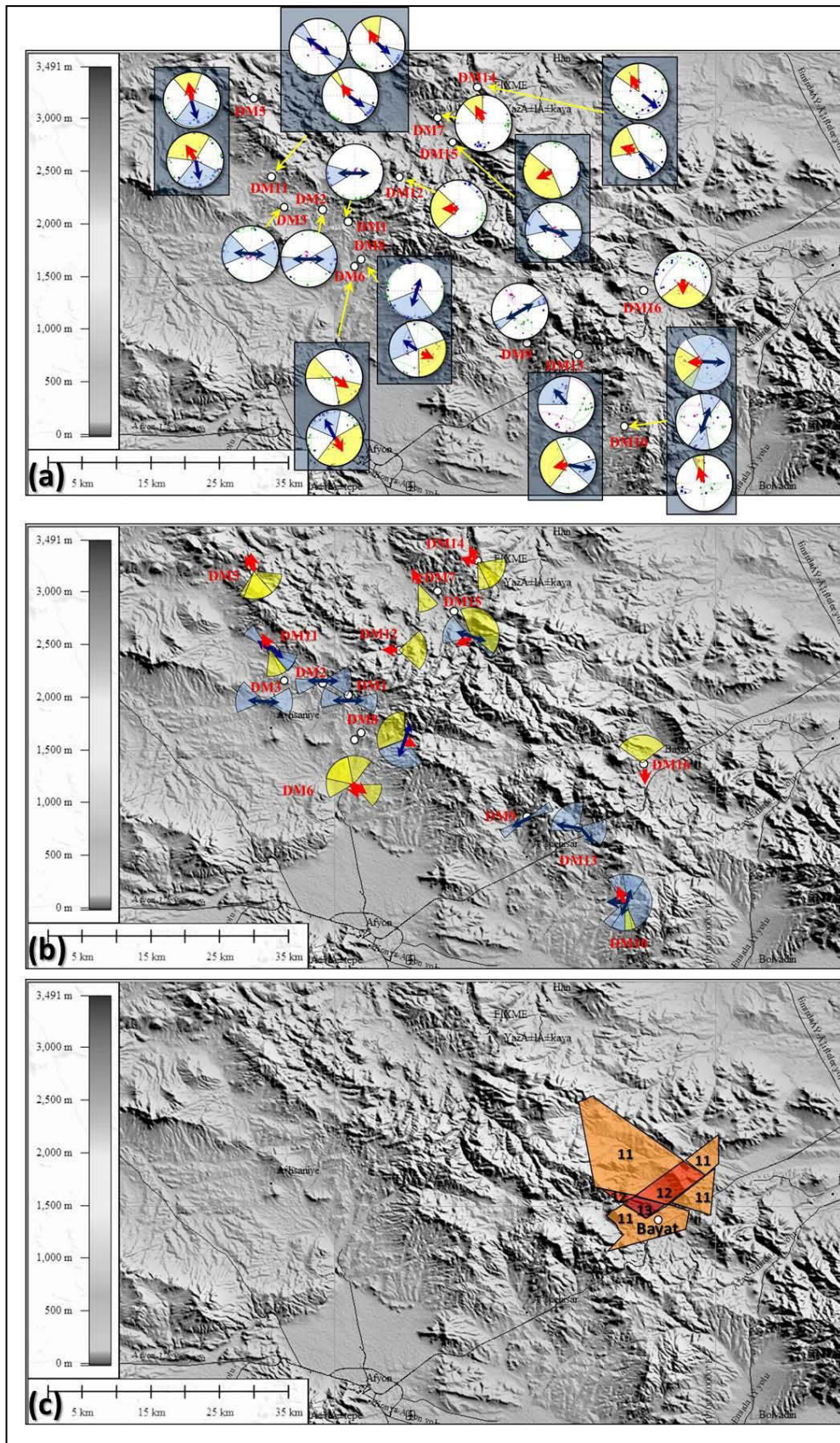


Figure 7.20 – Seydiler ignimbrite (selected AMS data): a) AMS stereoplots; b) interpreted map of the inferred flow directions with their associated dispersion angle fans; c) maximum overlapping areas (coloured areas). Numbers contained in the overlapping areas refer to the number of intersecting dispersion angle fans. Symbols: as in fig. 7.15 a.

Comparison of the maps of not selected AMS data and selected AMS data, evidences an improvement of the quality of the results, attesting the efficacy of this AMS fabric enhancing method to be used in order to constrain more precisely source areas. Both for Incik and for Seydiler ignimbrites the maximum overlapping area is more confined (compare figs. 7.15 b with 7.16 b, and 7.19 c with 7.20 c); in the Sabuncu ignimbrite the improvement in the quality of the result is not appreciable because of the presence of only a single site. In the case of Seydiler ignimbrite, the lower number of maximum overlapping areas for selected AMS data (13 sites) with respect to not selected AMS data (14 sites) is only apparent. In fact, the greater number of overlapping areas in the latter case is due to the occurrence of wider dispersion angle fans (compare as an example the sites DM7 and DM14-1 in figs. 7.19 b and 7.20 b) that intersect into a common area. Results obtained by selected AMS data evidence a higher quality because overlapping areas, even if including one site less than the former case, are more confined, and the maximum overlapping area is circumscribed over a more narrow zone west of Bayat.

7.2.3.4 Kırka caldera system

Both field data (i.e. isopach and isopleth maps, maps of the imbrication structures and maps of the welded and silicified facies) and magnetic fabric inferred-flow directions concur for a source area of the Incik and Sabuncu ignimbrites within the Kırka basin. This area has been identified and named as “Kırka caldera system” by this work. The caldera system is $\approx 20 \times 20$ km extended, and it preserves several structures that have been originating through the time during its development stages (fig. 7.21). Field evidence for the caldera system are several:

1. Presence of Incik ignimbrite proximal deposits along the caldera rims (Damlalıkaraağaç and Üçsaray) and within the caldera system (Göknebi). At Üçsaray is exposed the contact between magma chamber rocks and ignimbrite deposit, and is found the source of the clasts lithologies occurring in medial and distal facies of the deposit (red banded rhyolite clasts and greenish perlithic obsidian and pumices). Red banded rhyolitic clasts derive from the disruption of domes in the area of Üçsaray (fig. 3.10 k), while field evidence indicate that both greenish perlithic obsidian both pumice clasts derive from different expansion degrees of the green rock which constitutes the magma chamber, which also occurs together with the red banded rhyolite to form the ignimbrite intruding-dykes (fig. 3.10 c, e).
2. intra-caldera ignimbrite facies dipping at high angle inward the caldera system at the locality of Damlalıkaraağaç (dip direction/inclination: 30/70); on the contrary, outflow sheet facies gently dip outward the caldera system;

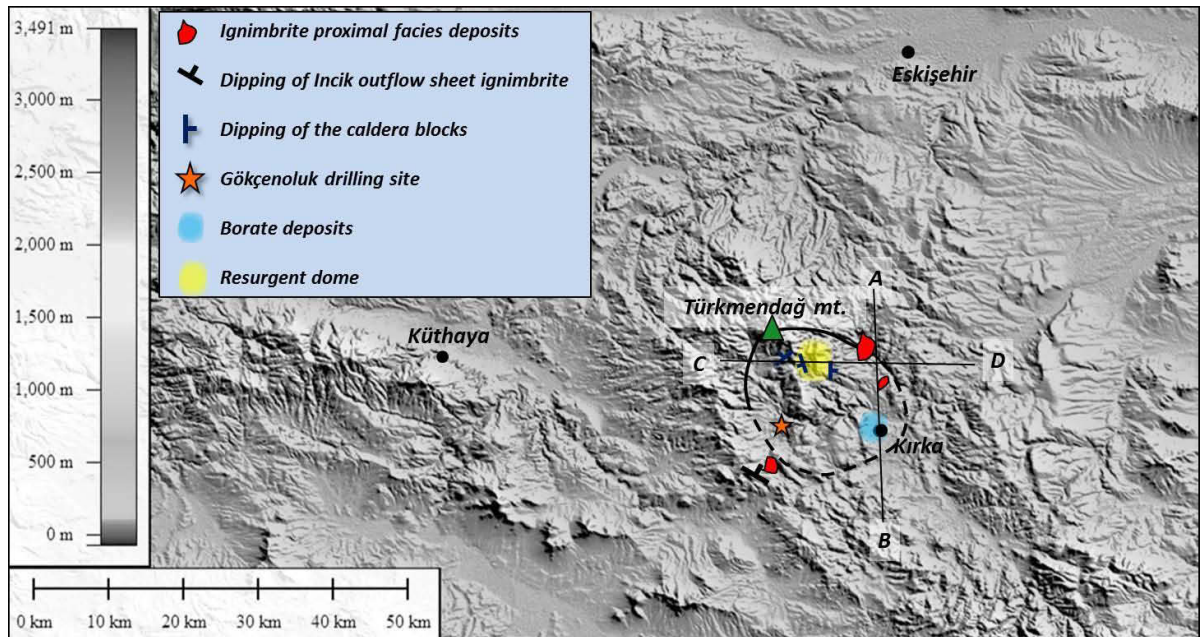


Figure 7.21 – Kirka caldera system and its peculiar structures. Bold line: preserved northern caldera rims; bold dashed line: buried southern caldera rims. A-B and C-D cross-section lines represent the profiles in fig. 7.23.

3. geology of the caldera system interior:
 - a. widespread presence of moat deposits (lacustrine and fluvial) filling the caldera basin. According to this interpretation, lacustrine deposits correspond to the Sarıkaya Formation of Yalçın (1990);
 - b. presence of rhyolitic dome extrusions near the caldera rims;
 - c. presence of several fault structures dislocating the ignimbrite deposit (fig. 3.10 i) along the margins of the caldera, possibly related to the main ring faults (fig. 7.23, profile A-B);
4. caldera rims preserved in the northern part of the caldera (fig. 7.22). Lacking of caldera rims in the southern part and around Kirka, associated to the occurrence of moat deposits, indicates that these areas were at lower altitude and progressive sedimentation within the basin buried the southern caldera rims;



Figure 7.22 – Panoramic view of the north-western rim of the caldera from the western block delimitating the apical graben near the village of Idrisyayla.

5. presence of borate deposits around Kırka, whose origin is genetically related to volcanic activity. Many studies state that borate deposits of western Turkey are closely associated in space and time with Miocene tuffs and lavas (Helvacı et al., 1993; Helvacı, 1995). The source of the boron is often linked to volcanic activity via the agency hydrothermally generated B-rich springs that mix with the lake waters and precipitate borates (e.g. Inan et al., 1973; Helvacı, 1995). Floyd et al. (1998) assert that ignimbritic calc-alkali volcanics of rhyolite composition are associated with the Kırka borate deposits, and the initial source of boron was in a subduction environment via the release of B-rich fluids caused by the progressive dehydration of the altered oceanic slab and a sediment component;

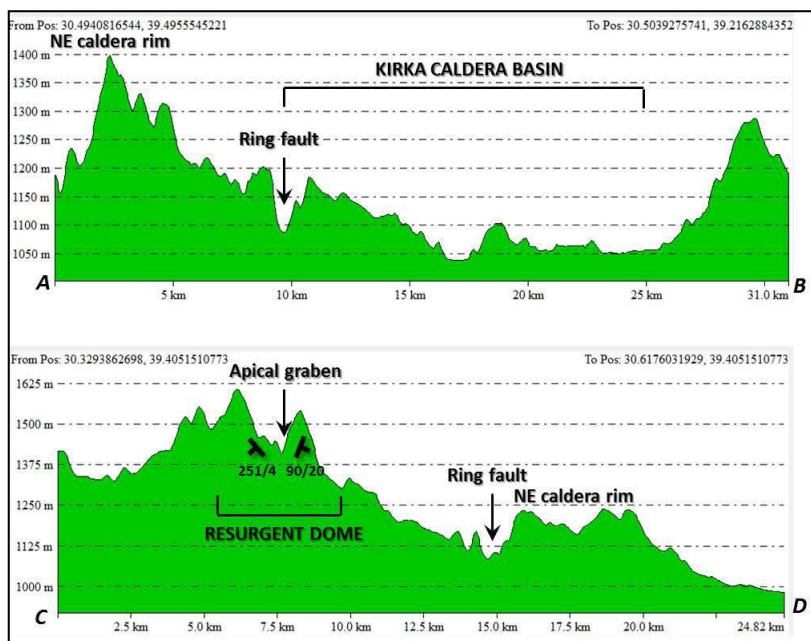


Figure 7.23 – Digital topographic profiles of the Kırka caldera interior obtained with the program Global Mapper (version 15.0.5). A-B and C-D cross-section lines are reported in fig. 7.21.

6. presence of ignimbrite deposits at 1000 m beneath the surface near the locality of Gökçenoluk, detected through a drilling survey (unpublished data);
7. Presence of a resurgent dome within the caldera system centred in the locality of Idrisyayla, formed by moat sediments overlying the intracaldera ignimbrite. Field evidence for the resurgent dome are:
 - a. preserved apical graben with a N-S axis (fig. 7.23, profile C-D);
 - b. symmetrically opposite tilted-blocks with respect to the apical graben (fig. 7.21; fig. 7.23, profile C-D);
 - c. evidence of normal faults delimitating tilted blocks;
8. Presence of the Türkmendağ basaltic complex along the north-western rim of the caldera, which is the result of post-caldera stage (fig. 7.21; fig. 7.22). According to whole-rock K-Ar dates performed on basaltic lava samples by Yalçın (1990), the age of Türkmendağ is 9.3 ± 1 Ma. This age is statistically indistinguishable from the one obtained for Sabuncu

ignimbrite in this work (9.43 ± 0.09 Ma; U-Pb dates both on whole rock and pumice clasts), attesting that both events are contemporary, and Sabuncu ignimbrites forming-eruption occurred during the post-caldera stage as well.

8 – Conclusions

The present research provides relevant results concerning the factors influencing the vertical variability of the magnetic signal and the stratigraphy and research of source area of two large silicic ignimbrites of Anatolia: the Kızılkaya ignimbrite (central Anatolia) and the Afyon-Eskişehir ignimbrites (western Anatolia). Results have been obtained by a combined stratigraphic-sedimentologic and paleomagnetic study, by developing a useful rock-magnetic method to the investigation of ignimbrites, exportable also to other large ignimbrite systems worldwide.

Specifically, the study performed on the Kızılkaya ignimbrite pointed out that:

1. Magnetic remanences are not vertically homogenous through the deposits. Two main cases are distinguished: (1) a stable and well-defined TRM, whose direction is consistent with previous literature data (Piper et al. 2002), that is detected at sites where Ti-magnetite (or weakly altered Ti-magnetite) is the only magnetic carrier; and (2) two magnetization components, with overlapping T_b and coercivity spectra. This case is typically found where magnetic mineralogy is given by Ti-magnetite, altered Ti-magnetite and hematite. Data suggest the occurrence of a primary TRM and a secondary CRM acquired a short time later, and their angular difference is consistent with the paleosecular variation. The Kızılkaya mean paleomagnetic direction shows a significant difference in the inclination value with that expected for GAD in the region, which is sensibly reduced when inclination value is re-calculated using the P_{AIRM} value. Therefore, part of this difference can be attributed to compaction processes which have been acted during ignimbrite cooling. The consideration of this factor, would reduce the considerable northwards movement of the region as proposed by Piper et al. (2002);
2. the AMS is mainly oblate and magnetic foliation is always well defined; shape anisotropy is the main factor controlling the AMS fabric.
3. AMS data only are not enough to attest the primary origin of magnetic fabric in ignimbrites with composite magnetic mineralogy, such as the Kızılkaya case. On the other hand, AIRM measurements help in separating the effect of the various minerals and thus possible overprints which mask the fabric derived from the emplacement dynamics. Correspondence between AMS and AIRM fabrics attested the primary origin of the magnetic fabric and the allowance to use the AMS indicators as proxies for flow direction;
4. the tested enhancing method on the AMS data resulted in a net improvement on the quality of magnetic fabrics in terms of improvement in the confidence values and reduction of horizontal magnetic fabrics, thus obtaining more accurate flow directions to constrain the source area;

5. thick ignimbrite units should not be considered as magnetically uniform rock bodies. Detailed and systematic sampling is required to evidence possible rock-magnetic inhomogeneity, avoiding local and inadequate sampling which may lead to unrepresentative paleomagnetic results.

The investigation carried out on the Afyon-Eskişehir ignimbrites revealed that:

1. The ignimbrite succession consists of at least three distinct eruptions that originated the Incik, Sabuncu and Seydiler ignimbrites, different for age, areal distribution, structure and textural features of the deposits. On the basis of volcanic stratigraphy, the lacustrine and continental facies of the Karaören Formation of Yalçın (1990) have been respectively identified with the distinct Incik and Seydiler ignimbrites;
2. U-Pb analyses on zircon crystals confer an age of 18.866 ± 0.071 Ma for the Incik ignimbrite and 9.43 ± 0.09 Ma for the Sabuncu ignimbrite. The Seydiler ignimbrite is considered to be older than 14.8 Ma, as revealed from Ar-Ar dating on the lava overlying the pyroclastic deposits, but younger than the Incik ignimbrite, as pointed out from their stratigraphic relationship;
3. both field data and magnetic fabric results concur for two source areas. The source area of the Incik and Sabuncu ignimbrites is identified with the Kırka caldera; more specifically, isopach maps better constrain the source in the proximity of the resurgent dome. The source area of the Seydiler ignimbrite is identified in the proximity of the village of Bayat, which is consistent with the Koroğlu caldera described by Aydar et al. (1998). From isopach and AMS data, the source area has been more accurately constrained in a restricted area north-west from Bayat;
4. the AMS fabric enhancing method has been revealed to be efficacy also in this case, allowing to constrain the source over a more restricted area;
5. field evidence and AMS results point out a strong topographic control on the Afyon-Eskişehir ignimbrites, highlighting an irregular paleo-topography characterized by the presence of many paleo-valleys and a westward paleo-drainage in the southern region of Eskişehir;
6. considering the pre-erosional volumes of the Incik (185 km^3), Sabuncu (94 km^3) and Seydiler ignimbrite (201 km^3), the resulting VEI index is respectively: 7, 6 and 7, evidencing Plinian eruptions, and the calculated magnitude M (Pyle, 2000) is greater than 7 for each ignimbrite. Areal and volumetric data, together with minimum traveled distance of the Seydiler ignimbrite, result to be greater if compared with the previous estimations of Aydar et al. (1998), pointing out a larger-scale eruption.

References

- Acocella, V., Funicello, R., 1999. *The interaction between regional and local tectonics during resurgent doming: the case of the Island of Ischia, Italy*. Journ. Volcanol. Geotherm. Res.; 88, 109-123.
- Acocella, V., Cifelli, F., Funicello, R., 2000. *Analogue models of collapse calderas and resurgent domes*. Journ. Geotherm. Res.; 104, 81-96.
- Acocella, V., Cifelli, F., Funicello, R., 2001. *The control of overburden thickness on resurgent domes: insights from analogue models*. Journ. Volcanol. Geotherm. Res.; 111, 137-153.
- Allen, J.R.L., 1982. *Development in sedimentology* Vol. 30 A and B, *Sedimentary structures. Their character and Physical basis*. Elsevier, Amsterdam.
- Altunkaynak, Ş.; Dilek, Y., 2006. *Timing and nature of postcollisional volcanism in western Anatolia and geodynamic implications*. Geol. Soc. Am, Special Paper; 409, 321-351.
- Alva-Valdivia, L.M., Rosas-E, J., Bravo-M, T., Urrutia-F, J., Henry, C., Caballero, M., Rivas-S, L., Goguitchaichvili, A., Lopez, H., 2005. *Paleomagnetic and magnetic fabrics studies of the San Gaspar ignimbrite, western Mexico-constraints on emplacement mode and source vents*. Journ. Volcanol. Geoph. Res.; 147, 68-80.
- Anilkumar, A.V., Sparks, R.S.J., Sturtevant, B., 1993. *Geological implications and applications of high velocity two-phase flow experiments*. Journ. Volcanol. Geoth. Res.; 56, 145-160.
- Aramaki, S., Ui, T., 1966. *The Aira and Ata pyroclastic flows and related caldera depressions in southern Kyushu, Japan*. Bulletin Volcanologique; 29, 29-47
- Aydar, E., Bayhan, H., Gourgaud, A., 1998. *Koroğlu caldera, mid-west Anatolia, Turkey: volcanological and magmatological evolution*. Journ. Volcanol. Geoth. Res.; 85, 83-98.
- Aydar, E., Schmitt, A.K., Çubukçu, H. E., Akin, L., Ersoy, O., Sen, E., Duncan, R. A., Atici, G. 2012. *Correlation of ignimbrites in the central Anatolian volcanic province using zircon and plagioclase ages and zircon compositions*. Journ. Volcanol. Geoth. Res.; 213-214, 83-97.
- Baas, J.H., Hailwood, E.A., McCaffrey, W.D., Kay, M., Jones, R. 2007. *Directional petrological characterisation of deep-marine sandstones using grain fabric and permeability anisotropy: Methodologies, theory, application and suggestions for integration*. Earth-Sci. Rev.; 82, 101-142.
- Bacon, C.R., 1983. *Eruptive history of Mount Mazama and Crater Lake Caldera, Cascade Range, USA*. Journ. Volcanol. Geotherm. Res.; 18, 57-115.

- Baer, E.M., Fisher, R.V., Fuller, M., Valentine, G., 1997. *Turbulent transport and deposition of the Ito pyroclastic flow: Determinations using anisotropy of magnetic susceptibility*. Journ. Geophys. Res.; 102, 22565-22586.
- Baker, P.E., Harris, P.G., Reay, A., 1971. *The geology of Tofua Islands, Tonga*. Bull. R. Soc., N.Z., 8, 67-79.
- Bardintzeff, J.M., 1984. *Merapi volcano (Java, Indonesia) and Merapi-type nuée ardent*. Bull. of Volcanol.; 47, 433-446.
- Barka, A.A., Reilinger, R., 1997. *Active tectonics of the Mediterranean region: deduced from GPS, neotectonic and seismicity data*. Ann. Geophys.; XI, 587-610.
- Beekman, P.H., 1966. *The Pliocene and Quaternary volcanism in the Hasan Dağ Melendiz Dağ region*. Bull. Gen. Director. Min. Res. & Esplorat. (MTA); 66, 90-105.
- Beresford, S.W., Cole, J.W., 2000. *Kaingaroa Ignimbrite, Taupo Volcanic Zone, New Zealand: evidence for asymmetric caldera subsidence of the Reporoa Caldera*. N.Z. Journ. Geol. Geophys.; 43, 471-481.
- Besang, C., Eckhart, F.J., Harre, W., Kreuzer, H., Müller, P., 1977. *Radiometrische altersbestimmungen an neogenen eruptivgesteinen der Türkei*. Geol. Jahrb.; B25, 3-36.
- Best, M.G., Christiansen, E.H., Deino, A.L., Grommé, C.S., Tingey, D.G., 1995. *Correlation and emplacement of a large, zoned, discontinuously exposed ash flow sheet: The $^{40}\text{Ar}/^{39}\text{Ar}$ chronology, paleomagnetism, and petrology of the Pahranaagat Formation, Nevada*. Journ. Geophys. Res.; 100, 24593-24609.
- Bibby, H.M., Caldwell, T.G., Davey, F.J., Webb, T.H., 1995. *Geophysical evidence on the structure of the Taupo Volcanic Zone and its hydrothermal circulation*. Journ. Volcanol. Geotherm. Res.; 68, 29-58.
- Black, T.M., Shane, P.A.R., Westgate, J.A. & Froggatt, P.C., 1996. *Chronological and paleomagnetic constraints on widespread welded ignimbrites of the Taupo Volcanic Zone, New Zealand*. Bull. Volcanol.; 58, 226-238.
- Bogue, S.W., Coe, R.S., 1981. *Paleomagnetic correlation of Columbia River Basalt Flow using secular variation*. Journ. Geophys. Res.; 86, 11883-11897.
- Bonadonna, C., Houghton, B.F., 2005. *Total grain-size distribution and volume of tephra-fall deposits*. Bull. Volcanol.; 67, 441-456.

- Bonadonna, C., Costa, A., 2012. *Estimating the volume of tephra deposits: A new simple strategy*. *Geology*; 40, 415-418.
- Branney, M.J., Kokelaar, P., 1992. *A reappraisal of ignimbrite emplacement: progressive aggradation and particulate to non-particulate flow transitions during emplacement of high grade ignimbrite*. *Bull. Volcanol.*; 54, 504-520
- Branney, M.J., Kokelaar, P., 2002. *Pyroclastic density currents and the sedimentation of ignimbrites*. The Geolog. Soc. Of London; 143 pp.
- Bryan, S.E., Cas, R.A.F., Marti, J., 1998. *Lithic breccias in intermediate volume phonolitic ignimbrites, Tenerife (canary Islands): constraints on pyroclastic flow depositional processes*. *Journ. Volcanol. Geotherm. Res.*; 81, 269-296.
- Buesch, D.C., 1992. *Incorporation and redistribution of locally-derived lithic fragments within a pyroclastic flow*. *Geol. Soc. Am. Bull.*; 104, 1193-1207.
- Burgissier, A., Bergantz, G.W., 2002. *Reconciling pyroclastic flow and surge: the multiphase physics of pyroclastic density currents*. *Earth Plan. Sci. Lett.*; 202, 405-418
- Caballero-Miranda, C.I., Torres-Hernandez, J.R., Alva-Valdivia, L.M., 2009. *Anisotropy of magnetic susceptibility analysis of the Cantera Ignimbrite, San Luis Potosi, Mexico: flow source recognition*. *Earth Plan. Sp.*; 61, 173-182.
- Campbell, C.S., Cleary, P.W., Hopkins, M., 1995. *Large-scale landslide simulations: global deformation, velocities and basal friction*. *Journ. Geophys. Res.*; 100, 8267-8283.
- Cagnoli, B., Tarling, D.H., 1997. *The reliability of anisotropy of magnetic susceptibility (AMS) data as flow direction indicators in friable base surge and ignimbrite deposits: Italian examples*. *Journ. Volcanol. Geoth. Res.*; 75, 309-320.
- Canon-Tapia, E., 1996. *Single-grain versus distribution anisotropy: a simple three-dimensional model*. *Phys. Of the Earth and Plan. Int.*; 94, 149-158.
- Capaccioni, B., Nappi, G., Valentini, L., 2001. *Directional fabric measurements: an investigative approach to transport and depositional mechanisms in pyroclastic flows*. *Journ. of Volcanol. and Geoth. Res.*; 107, 275-292.
- Carey, S.N., Sparks, R.S.J., 1986. *Quantitative models of the fallout and dispersal of tephra from volcanic eruptions*. *Bull. Volcanol.*; 48, 109-126.
- Carey, S.N., Sigurdsson, H., 1989. *The Intensity of Plinian Eruptions*. *Bull. Volcanol.*; 51, 28-40.

- Cas, R.A.F., Wright, J.W., 1987. *Volcanic Successions, modern and ancient*. Allen & Unwin London; 528 pp.
- Cerling, T.E., Brown, F.H., Bowman, J.R., 1985. *Low-temperature alteration of volcanic glass – hydration, Na, K, ¹⁸O and Ar mobility*. *Chemical Geology*; 52 (3-4), 281-293.
- Channell, J.E.T., Tüysüz, O., Bektaş, O., Şengör, A.M.C., 1996. *Jurassic-Cretaceous paleomagnetism and palaeogeography of the Pontides (Turkey)*. *Tectonics*; 15, 201-212.
- Chaput, E., 1936. *Voyages d'études géologiques et géomorphologiques en Turquie*. Mém. Inst. Fr. D'Archeéologique de Stamboul; 2, 312 pp.
- Cisowski, S., 1981. *Interacting vs. non-interacting single domain behaviour in natural and synthetic samples*. *Phys. Earth planet. Inter.*; 26, 56–62.
- Claoué-Long, J., Compston, W., Roberts, J., Fanning, C.M., 1995. *Two Carboniferous ages: A comparison of SHRIMP zircon dating with conventional zircon ages and ⁴⁰Ar/³⁹Ar analysis*. In: Berggren, W.A., et al., eds., *Geochronology, time scales, and global stratigraphic correlation: SEPM (Soc. Sedim. Geol.), Special Publication*; 54, 1-22.
- Cole, J.W., Milner, D.M., Spinks, K.D., 2005. *Calderas and caldera structures: a review*. *Earth Sci. Rev.*; 69, 1-26.
- Cole, P.D., Calder, E.S., Druitt, T.H., Hoblitt, R., Robertson, R., Sparks, R.S.J., Young, S.R., 1998. *Pyroclastic flows generated by gravitational instability of the 1996-97 lava dome of Soufriere Hills Volcano, Montserrat*. *Geophys. Res. Lett.*; 25, 3425-3428.
- Cole, P.D., Calder, E.S., Sparks, R.S.J., Clarke, A.B., Druitt, T.H., Young, S.R., Herd, R.A., Harford, C.L., Norton, G.E., 2002. *Deposits from dome-collapse and fountain-collapse pyroclastic flows at Soufriere Hills Volcano, Montserrat*. In: Druitt, T.H., Kokelaar, B.P. (eds) *The Eruption of Soufriere Hills Volcano, Montserrat, From 1995 to 1999*. *Geol. Soc. London, Memoirs*; 21, 231-262.
- Crossweller, H.S., Arora, B., Brown, S.K., Cottrell, E., Deligne, N.I., Guerrero, N.O., Hobbs, L., Kiyosugi, K., Loughlin, S.C., Lowndes, J., Nayembil, M., Siebert, L., Sparks, R.S.J., Takarada, S., Venzke, E., 2012. *Global database on large magnitude explosive volcanic eruptions (LaMEVE)*. *Journ. Appl. Volcanol.*; 1, 1-13.
- Davies, D.K., Quearry, M.W., Bonis, S.B., 1978. *Glowing avalanches from the 1974 eruption of volcano Fuego, Guatemala*. *Geolog. Soc. Of America Bull.*; 89, 369-384.

- Dedzo, M.G., Nedelec, A., Nono, A., Njanko, T., Font, E., Kamgang, P., Njonfang, E., Launeau, P., 2011. *Magnetic fabrics of the Miocene ignimbrites from West-Cameroon: Implications for pyroclastic flow source and sedimentation*. *Journ. Volcanol. Geoth. Res.*; 203, 113-132.
- Dewey, J.F., Pitman, W.C., Ryan, W.B.F., Bonnin, J., 1973. *Plate tectonics and evolution of the Alpine system*. *Geol. Soc. Am. Bull.*; 84, 3137-3180.
- Dewey, J.F., Hempton, M.R., Kidd, W.S., Şaroğlu, F., Şengör, A.M.C., 1986. *Shortening of continental lithosphere: the neotectonics of eastern Anatolia – a young collision zone*. In: Coward, M.P., Reis, A.C (Eds.). *Collision Tectonics*, Geol. Soc. London, Special Publication; 19, 2-36.
- Dilek, Y., Altunkaynak, Ş., 2010. *Geochemistry of Neogene-Quaternary alkaline volcanism on western Anatolia, Turkey, and implications for the Aegean mantle*. *Int. Geol. Rev.*; 52, 631-655.
- Dirik, K., 2001. *Neotectonic evolution of the northwestward arched segment of the Central Anatolian fault zone, Central Anatolia, Turkey*. *Geodinamica Acta.*; 14, 147-158.
- Druitt, T.H., 1985. *Vent evolution and lag breccia formation during the Cape Riva Eruption of Santorini, Greece*. *Journ. Geol.*; 93, 439-454.
- Druitt, T.H., Bacon, C.R., 1986. *Lithic breccia and ignimbrite erupted during the collapse of Crater Lake Caldera, Oregon*. *Journ. Volcanol. Geoth. Res.*; 29, 1-32.
- Druitt, T.H., Sparks, R.S.J., 1982. *A proximal ignimbrite breccias facies on Santorini, Greece*. *Journ. Volcanol. Geoth. Res.*; 13, 147-171.
- Druitt, T.H., Sparks, R.S.J., 1984. *On the Formation of Calderas during Ignimbrite Eruptions*. *Nature*; 54, 638-645.
- Dungan, M.A., Lipman, P.W., Colucci, M., Ferguson, K., Balsey, S., 1989. *Southeastern (Platoro) Caldera Complex*, In: Chapin, C.E., Zidek, J. (Eds.), *Field Excursion to Volcanic Terranes in the Western United States*. Volume 1 Southern Rocky Mountains Region. *Mem. N. M. Bur. Mines. Miner. Resour.*; 46, 305-329.
- Eaton, P.C., Setterfield, T.N., 1993. *The relationship between epithermal and porphyry hydrothermal systems within the Tavua Caldera, Fiji*. *Econ. Geol.*; 88, 1053-1083.
- Elitok, Ö., Dolmaz, M.N., 2008. *Mantle flow-induced crustal thinning in the area between the easternmost part of the Anatolian plate and the Arabian Foreland (E. Turkey) deduced from the geological and geophysical data*. *Gondwana Res.*; 13 (3), 302-318.

- Ellwood, B.B., 1982. *Estimates of flow direction for calc-alkaline welded tuffs and paleomagnetic data reliability from anisotropy of magnetic susceptibility measurements: central San Juan Mountains, southwest Colorado*. Earth Planet. Sci. Lett.; 59, 303-314.
- Elston, W.E., 1984. *Mid-Tertiary ash-flow cauldrons, southwestern New Mexico*. Journ. Geophys. Res.; 89B, 8733-8750.
- Elston, W.E., Smith, E.I., 1970. *Determination of flow direction of rhyolitic ash-flow tuffs from fluidal textures*. Geol. Soc. Am. Bull.; 81, 3393-3406.
- Engebretson, D.C., Beck, M.E., 1978. *On the shape of directional data sets*. Journ. Geophys. Res.; 83, 5979-5982.
- Erkan, Y., Bayhan, H., Tolluoğlu, A.U., Aydar, E., 1996. *Geologica, Petrographical and Geochemical Investigations of Afyon Metamorphic and Volcanic Rock Suites*. Project report of TÜBITAK-YBAG-0044/DPT; 206 pp (in Turkish).
- Fierstein, J., Nathenson, M., 1992. *Another look at the calculation of fallout tephra volumes*. Bull. Volcanol.; 54, 156.
- Fisher, R.A., 1953. *Dispersion on a sphere*, Proc. R. Soc.; 217, 295-305.
- Fisher, R.V., 1966. *Mechanism of deposition from pyroclastic flows*. Amer. Journ. Sc.; 264, 350-363.
- Fisher, R.V., 1979. *Models for pyroclastic surges and pyroclastic flows*. Jour. Volc. and Geoth. Res; 6, 305-318.
- Fisher, R.V., 1983. *Flow transformations in sediment gravity flows*. Geology; 11, 273-274.
- Fisher, R.V., 1995. *Decoupling of pyroclastic currents: hazard assessments*. Journ. Volcanol. Geoth. Res.; 66, 257-263.
- Fisher, R.V., Waters, A.C., 1970. *Base surge bedforms in maar volcanoes*. Am. Journ. Sc.; 268, 157-180.
- Fisher, R.V., Schmincke, H.U., 1984. *Pyroclastic Rocks*. Springer-Verlag Berlin; 472 pp.
- Fisher, R.V., Orsi, G., Ort, M., Heiken G. 1993. *Mobility of a large-volume pyroclastic flow-emplacment of the Campanian Ignimbrite, Italy*. Journ. Volcanol. Geotherm. Res.; 56, 205-220.
- Fisher, R.V., Heiken, G., Hulen, J.B., 1997. *Volcanoes: Crucibles of Change*. Princeton Univ. Press, Princeton, NJ, USA; 371 pp.

- Floyd, P.A., Helvacı, C., Mittwede, S.K., 1998. *Geochemical discrimination of volcanic rocks associated with borate deposit: an explanation tool?* Journ. Geochem. Expl.; 60, 185-205.
- Françalanci, L., Civetta, L., Innocenti, F., Manetti, P., 1990. *Tertiary-Quaternary alkaline magmatism of the Aegean-Western Anatolian area: a petrological study in the light of new geochemical and isotopic data.* Proc. Int. Earth Sci. Coll. On the Aegean Region 1990, Izmir; 2, 385-396.
- Françalanci, L., Innocenti, F., Manetti, P., Savaşçın, M.Y., 2000. *Neogene alkaline volcanism of the Afyon-Isparta area, Turkey: petrogenesis and geodynamic implications.* Min. and Petr.; 70, 285-312.
- Francis, P.W., Roobol, M.J., Walker, G.P.L., Cobbold, P.R., Coward, M., 1974. *The San Pedro and San Pablo volcanoes and their hot avalanche deposits.* Geologische Rundschau; 63, 357-388.
- Freundt, A., Schmincke, H.U., 1985. *Lithic-enriched segregation bodies in pyroclastic flow deposits of Laacher See Volcano (East Eifel, Germany).* Journ. Volcan. Geoth. Res.; 25, 193-224.
- Fridrich, C.J., Smith, R.P., DeWitt, E., McKee, E.H., 1991. *Structural, eruptive and intrusive evolution of the Grizzly Peak caldera, Sawatch Range, Colorado.* Geol. Soc. Am. Bull.; 103, 1160-1177.
- Froger, J.L., Lenat, J.F., Chorowicz, J., Le Pennec, J.L., Bourdier, J.L., Köse, O., Zimitoğlu, O., Gündoğdu, N.M., Gourgaud, A., 1998. *Hidden calderas evidenced by multisource geophysical data: example of Cappadocian Calderas, Central Anatolia.* Journ. Volcanol. Geoth. Res.; 185, 99-128.
- Fuji, T., Nakada, S., 1999. *The 15 September 1991 pyroclastic flows at Unzen Volcano (Japan): a flow model for associated ash-cloud surges.* Journal of Volc. and Geoth. Res; 89, 159-172.
- Gaillot, P., Saint-Blanquat (de), M., Bouchez, J.L., 2006. *Effects of magnetic interactions in anisotropy of magnetic susceptibility: Models, experiments and implications for igneous rock fabric quantification.* Tectonophys.; 418, 3-19.
- Gattacceca, J., Rochette, P., 2002. *Pseudopaleosecular variation due to remanence anisotropy in a pyroclastic flow succession.* Geophys. Res. Lett.; 29, 10.1029/2002GL014697
- Gaziry, A.W., 1976. *Jungtertiäre Mastodonten aus Anatolien (Turkei).* Geol. Jahrb.; B22, 1-143.
- Goff, F., Gardner, J.N., 1994. *Evolution of a mineralized geothermal system, Valles Caldera, New Mexico.* Econ. Geol.; 89, 1803-1832.

- Görür, N., Okay, F.Y., Seymen, J., Şengör, A.M.C., 1984. *Palaeotectonic evolution of the Tuzgolu Basin complex, central Turkey: sedimentary record of a Neo-Tethyan closure*. Geol. Soc. Spec. Publ.; 17, 467-482.
- Gose, W.A., 1970. *Paleomagnetic studies of Miocene ignimbrites from Nevada*. Geophys. J. R. Astron. Soc.; 20, 241-252.
- Govers, R., Wortel, M.J.R., 2005. *Lithosphere tearing at STEP faults: Response to edges of subduction zones*. Earth Plan. Sci. Lett.; 236, 505-523.
- Granar, L., 1958. *Magnetic measurements on Swedish varved sediments*. Ark. Geofys.; 3, 1-40.
- Grégoire, V., Saint Blanquat (de), M., Nédélec, A., Bouchez, J.L., 1995. *Shape anisotropy versus magnetic interactions of magnetite grains: experiments and application to AMS in granitic rocks*. Geophys. Res. Lett.; 22, 2765-2768.
- Grégoire, V., Darrozes, J., Gaillot, P., Nédélec, A., 1998. *Magnetite grain shape fabric and distribution anisotropy vs rock magnetic fabric: a three-dimensional case study*. Journ. of Struct. Geol.; 20, 937-944.
- Gudmundsson, A., 1995. *Infrastructure and mechanism of volcanic systems in Iceland*. Journ. Volcanol. Geotherm. Res.; 64, 1-22.
- Gudmundsson, A., 1998. *Formation and development of normal-fault calderas and the initiation of large explosive eruptions*. Bull. Volcanol.; 60, 160-170.
- Gurioli, L., Pareschi, M.T., Zanella, E., Lanza, R., Deluca, E., Bisson, M. 2005. *Interaction of pyroclastic density currents with human settlements: Evidence from ancient Pompeii*. Geology; 33, 441-444.
- Gürsoy, H., Temiz, H., Poisson, A.M., 1992. *Recent faulting in the Sivas area (Sivas Basin), Central Anatolia*. Türkiye Cumhuriyet univ., J.Engeneer. Fac., Serie A, Earth Sci. 9, 1-11.
- Gürsoy, H., Piper, J.D.A., Tatar, O., 2003. *Neotectonic deformation in the western sector of tectonic escape in Anatolia: paleomagnetic study of the Afyon region, central Turkey*. Tectonophysics; 374, 57-79.
- Hargraves, R.B., Johnson, D., Chan, C.Y., 1991. *Distribution anisotropy: the cause of AMS in igneous rocks?* Geophys. Res. Lett.; 18, 2193-2196.
- Heiken, G., Goff, F., Stix, J., Tamanyu, S., Shafiqullah, M., Garcia, S., 1986. *Intracaldera volcanic activity, Toledo Caldera and embayment, Jemez Mountains, New Mexico*. Journ. Geophys. Res.; 91B, 1799-1815.

- Heiken, G., Goff, F., Gardner, J.N., Balridge, W.S., 1990. *The Valles/Toledo Caldera Complex, Jemez Volcanic Field, New Mexico*. *Annu. Rev. Earth Planet. Sci.*; 18, 27-53.
- Helvacı, C., 1995. *Stratigraphy, mineralogy, and genesis of the Bigadic borate deposits*. *Mercian Geol.*; 6, 257-270.
- Helvacı, C., Stamatakis, M.G., Zagouroglou, C., Kanaris, J., 1993. *Borate minerals and related authigenic silicates in northeastern Mediterranean late Miocene continental basins*. *Explor. Min. Geol.*; 2, 171-178.
- Hildreth, W., Christiansen, R.L., O'Neil, J.R., 1984. *Catastrophic isotopic modification of rhyolitic magma at times of caldera subsidence, Yellowstone plateau volcanic field*. *Journ. Geophys. Res.*; 89B, 8339-8369.
- Hildreth, W., Mahood, G.A., 1985. *Correlation of ash-flow tuffs*. *Geol. Soc. Amer. Bull.*; 96, 968-974.
- Hillhouse, J.W., Wells, R.E. 1991. *Magnetic fabric, flow directions and source area of the Lower Miocene Peach Spring Tuff in Arizona, California and Nevada*. *Journ. Geophys. Res.*; 96, 12443-12460.
- Hoblitt, R.P., 1986. *Observations of the eruptions of July 22 and August 7, 1980, at Mount St. Helens, Washington*. US Geological Survey, Professional Paper; 1335, 1-44.
- Hora, J.M., Singer, B.S., Jicha, B.R., Beard, B.L., Johnson, C.M., de Silva, S., Salisbury, M., 2010. *Volcanic biotite-sanidine $^{40}\text{Ar}/^{39}\text{Ar}$ age discordances reflect Ar partitioning and pre-eruption closure in biotite*. *Geology*; 38 (10), 923-926.
- Houghton, B.F., Weaver, S.D., Wilson, C.J.N., Lanphere, M.A., 1992. *Evolution of a Quaternary pralkaline volcano: Mayor Island, New Zeland*. *Journ. Volcanol. Geotherm. Res.*; 51, 217-236.
- Hrouda, F., 1982. *Magnetic anisotropy of rocks and its application in geology and geophysics*. *Geophys. Surv.*; 5, 37-82.
- Hughes, S.R., Druitt, T.H., 1998. *Particle fabric in a small, type-2 ignimbrite flow unit (Laacher See, Germany) and implications for emplacement dynamics*. *Bull. Volcanol.*; 60, 125-136.
- Inan, K., Dunham, A.C., Esson, J., 1973. *Mineralogy, chemistry and origin of Kirka borate deposit, Eskisehir Province, Turkey*. *Inst. Min. Metall. Appl. Earth Sci.*; B82, 114-123.
- Innocenti, F., Mazzuoli, R., Pasquarè, G., Radicati di Brozolo, F., Villari, L., 1975. *The Neogene calc-alkaline volcanism of Central Anatolia: geochronological data on Kayseri-Nigde area*. *Geol. Mag.*; 112, 349-360.

- Innocenti, F., Manetti, P., Mazzuoli, R., Pasquarè, G., Villari, L., 1982. *Anatolia and Northern Iran*. In: Thorpe, R.S., (Ed.), *Andesites, Orogenic Andesites and Related Rocks*. The Open University, Department of Earth Sciences, Milton Keynes; 327-349.
- Jackson, M., Tauxe, L., 1991. *Anisotropy of magnetic susceptibility and remanence: developments in the characterization of tectonic, sedimentary and igneous fabrics*. Rev. Geophys. Suppl.; 29, 371-376.
- Jackson, S.E., Pearson, N.J., Griffin, W.L., Belousova, E.A., 2004. *The application of laser ablation-inductively coupled plasma-mass spectrometry to in situ U-Pb zircon geochronology*. Chemical Geology; 211, 47-69.
- Jelinek, V. 1977. *The Statistical Theory of Measuring Anisotropy of Magnetic Susceptibility of Rocks and Its Application*. Geofyzika, Brno, Czech Republic; 88 pp.
- Kamata, H., Mimura, K., 1983. *Flow directions inferred from imbrications in the Handa pyroclastic flow deposit in Japan*. Bull. Volcanol.; 46, 277-292.
- Karaoğlu, Ö., Özdemir, Y., Tolluoğlu, A.Ü., Karabıyıkoglu, M., Köse, O., Froger, J.L., 2005. *Stratigraphy of the Volcanic Products Around Nemrut Caldera: Implications for Reconstruction of the Caldera Formation*. Turk. Journ. Earth Sci.; 14, 123-143.
- Karig, D.E., Kozlu, H., 1990. *Late Paleogene evolution of the triple junction region near Maraş, south-central Turkey*. T. Geol. Soc.; London 147, 1023-1034.
- Keller, J., 1983. *Potassic lavas in the orogenic volcanism of the Mediterranean area*. Journ. Volcanol. Geoth. Res.; 18, 321-335.
- Keller, J., Villari, L., 1972. *Rhyolitic ignimbrites in the region of Afyon (Central Anatolia)*. Bull. Volcanol.; 36, 342-358.
- Kelling, G., Gökçen, S.L., Floyd, P.A., Gökçen, N.D., 1987. *Neogene tectonics and plate convergence in the eastern Mediterranean: new data from southern Turkey*. Geology; 14, 425-429.
- Kissel, C., Laj, C., Poisson, A., Görür, N., 2002. *Palaeomagnetic reconstruction of the Cenozoic evolution of the Eastern Mediterranean*. Tectonophysics; 362, 199-217.
- Knight, M.D., Walker, G.P.L., Ellwood, B.B., Diehl, J.F., 1986. *Stratigraphy, paleomagnetism, and magnetic fabric of the Toba Tuff: constraints on the sources and eruptive styles*. Journ. Geophys. Res.; 91, 10355-10382.

- Kruiver, P.P., Dekkers, M.J., Heslop, D., 2001. *Quantification of magnetic coercivity components by the analysis of acquisition curves of isothermal remanent magnetisation*. Earth Planet. Sci. Lett.; 189, 269-276.
- Kürkçüoğlu, B., Şen, E., Aydar, E., Gourgaud, A., Gündoğdu, N., 1998. *Geochemical approach to magmatic evolution of the Mt. Erciyes stratovolcano, Central Anatolia, Turkey*. Journ. Volcanol. Geoth. Res.; 85, 473-494.
- LaBerge, R.D., Porreca, M., Mattei, M., Giordano, G., Cas, R.A.F., 2009. *Meandering flow of a pyroclastic density current documented by the anisotropy of magnetic susceptibility (AMS) in the quartz latite ignimbrite of the Pleistocene Monte Cimino volcanic centre (central Italy)*. Tectonophysics; 466, 64-78.
- Larsen, G., 2010. *3 Katla: Tephrocronology and Eruption History*. Develop. In Quat. Sci.; 13, 23-49.
- Le Pennec, J.L., 2000. *Identifying ash flow sources with directional data: An application to the Kizilkaya ignimbrite, central Anatolia*. Journ. Geophys. Res.; 105, 28427-28441.
- Le Pennec, J.L., Bourdier, J.L., Froger, J.L., Temel, A., Camus, G., Gourgaud, A., 1994. *Neogene ignimbrites of the Nevşehir plateau (central Turkey): Stratigraphy, distribution and source constraints*. Journ. Volcanol. Geoth. Res.; 63, 59-87.
- Le Pennec, J.L., Chen Y., Diot, H., Froger, J.L., Gourgaud, A., 1998. *Interpretation of anisotropy of magnetic susceptibility fabric of ignimbrites in term of kinematic and sedimentological mechanism: An Anatolian case-study*. Earth Planet. Sci. Lett.; 157, 105-127.
- Le Pennec, J.L., Temel, A., Froger, J.L., Sen, S., Gourgaud, A., Bourdier, J.L., 2005. *Stratigraphy and age of the Cappadocian ignimbrites, Turkey: Reconciling field constraints with paleontologic, radiochronologic, geochemical and paleomagnetic data*. Journ. Volcanol. Geoth. Res.; 141, 45-64.
- Lepetit, P., Viereck-Goette, L., Gürel, A., 2007. *Neogene Stratigraphy of the Nevşehir Plateau, Cappadocia, Turkey: Geological Background*. In: *Field Guide to the Excursion on the Geology of the Nevşehir Plateau and the Historical Cultural Site of the Göreme Open Air Museum* (Guides: P. Lepetit, L. Viereck-Goette, A. Gürel, and M. Şener): Niğde Üniversitesi. Symposium on the Geology of the Kapadokya Region, 17-20 October 2007, in the framework of the International Year of Planet Earth; 18 pp.
- Lepetit, P., Viereck-Goette, L., Schumacher, R., Mues-Schumacher, U., Abratis, M., 2009. *Parameters controlling the density of welded ignimbrites-A case study on the Incesu Ignimbrite, Cappadocia, Central Anatolia*. Chemie der Erde; 69, 341-357.

- Lindsay, J.M., de Silva, S., Trumbull, R., Emmermann, R., Wemmer, K., 2001. *La Pacana caldera, N. Chile: a re-evaluation of the stratigraphy and volcanology of one of the world's largest resurgent calderas*. Journ. Volcanol. Geotherm. Res.; 106, 145-173.
- Lipman, P.W., 1984. *The roots of ash flow calderas in western North America; windows into the tops of granitic batholiths*. Journ. Geophys. Res.; 89B, 8801-8841.
- Lipman, P.W., 1992. *Ash-flow calderas as structural controls of ore deposits-recent work and future problems*. U.S. Geol. Surv. Bull. 2012; L1-L12.
- Lipman, P.W., 1995. *Subsidence of ash-flow calderas; role of magma chamber geometry*. IUGG Ge. Asem. 21 (Week A); 452.
- Lipman, P.W., 1997. *Subsidence of ash-flow calderas: relation to caldera size and magma chamber geometry*. Bull. Volcanol.; 59, 198-218.
- Lipman, P.W., 2000a. *The central san Juan caldera cluster: regional volcanic framework*. Spec. Pap. Geol. Soc. Am.; 346, 9-71.
- Lipman, P.W., 2000b. *Calderas*. In: Sigurdsson, H. (Eds.), *Encyclopedia of Volcanoes*. Academic Press, San Francisco; 643-662.
- Lipman, P.W., Sawyer, D.A., 1985. *Mesozoic ash-flow caldera fragments in southeastern Arizona and their relation to porphyry copper deposits*. Geology, 13; 652-656.
- Lipman, P.W., Dungan, M.A., Brown, L.L., Deino, A., 1996. *Recurrent eruption and subsidence at the Platoro caldera complex, southeastern San Juan volcanic field, Colorado: new tales from old tuffs*. Geol. Soc. Amer. Bull.; 108, 1039-1055.
- Lowrie, W., 1990. *Identification of ferromagnetic minerals in a rock by coercitivity and unblocking properties*. Geophys. Res. Lett. 17; 159-162.
- Ludwig, K.R., 2001. *User's manual for Isoplot/Ex version 2.49: A geochronological toolkit for Microsoft Excel*. Berkeley, California, Berkeley Geochronological Center, Special Publication; 1a, 55 pp.
- MacDonald, W.D., Palmer, H.C., 1990. *Flow directions in ash-flow tuffs: a comparison of geological and magnetic susceptibility measurements, Tshirege member (upper Bandelier Tuff), Valles caldera, New Mexico, USA*. Bull. Volcanol.; 53, 45-59.
- Marti, J., Gudmundsson, A., 2000. *The Las Canadas caldera (Tenerife, Canary Islands): an overlapping collapse caldera generated by magma-chamber migration*. Journ. Volcanol. Geotherm. Res.; 103, 161-173.

- Marti, J., Ablay, G.J., Redshaw, L.T., Sparks, R.S.J., 1994. *Experimental studies of caldera collapse*. Journ. Geol. Soc. (Lond.); 151, 919-929.
- McClelland-Brown, E., 1982. *Discrimination of TRM and CRM by blockin-temperature spectrum analysis*. Phys. Earth Planet. Int.; 30, 405-414.
- McFadden, P.L., McElhinny, M.W., 1988. *The combined analysis of remagnetization circles and direct observations in palaeomagnetism*. Earth Planet. Sci. Lett.; 87, 161-172.
- McIntosh, C.W., 1991. *Evaluation of paleomagnetism as a correlation criterion for Mogollon-Datil Ignimbrites, Southwestern New Mexico*. Journ. Geophys. Res.; 96, 13459-13483.
- McKenzie, D.P., 1978. *Active tectonics of the Alpine-Himalayan belt: the Aegean Sea and surrounding regions*. Geophys. Journ. Roy. Astron. Soc.; 55, 217-254.
- Middleton, G.V., Southard, J.B., 1989. *Mechanics of sediment movements*. SEPM, Tulsa, OK, 401 pp.
- Miller, T.P., Smith, R.L., 1977. *Spectacular mobility of ash flows around Aniakchak and Fisher calderas, Alaska*. Geology; 5, 173-176.
- Mills, B.A., Boden, D.R., Sander, M.V., 1988. *Alteration and precious metal mineralization associated with the Toquima caldera complex, Nye County, Nevada*. In: Schafer, R.W., Cooper, J.J., Vikre, P.G. (Eds.), *Bulk-Mineable Precious Metals Deposits of the Western United States*. Symposium Proceedings. Geol. Soc, Nevada; 303-332.
- Milner, D.M., Cole, J.W., Wood, C.P., 2002. *Asymmetric, multiple-block collapse at Rotorua Caldera, Taupo Volcanic Zone, New Zealand*. Bull. Volcanol.; 64, 134-149.
- Moore, I., Kokelaar, P., 1997. *Tectonic influences in piecemeal caldera collapse and Glencoe volcano, Scotland*. Journ. Geol. Soc. (Lond.); 154, 765-768.
- Mueller, W.U., Stix, J., Corcoran, P.L., Daigneault, R., 2009. *Subaqueous calderas in the Archean Abitibi greenstone belt: An overview and new ideas*. Ore Geol. Rev.; 35, 4-46.
- Mues-Schumacher, U., Schumacher, R., 1996. *Problems of stratigraphic correlation and new K-Ar data for ignimbrites from Cappadocia, central Turkey*. Int. Geol. Rev.; 38, 737-746.
- Mues-Schumacher, U., Schumacher, R., Viereck-Goette, L., Lepetit, P., 2004. *Areal distribution and bulk rock density variations of the welded Incesu ignimbrite, Central Anatolia, Turkey*. Turk. Journ. Earth Sci.; 13, 249-276.

- Newhall, C.G., Self, S., 1982. *The Volcanic Explosivity Index (VEI): an estimate of the explosive magnitude for historical volcanism*. Journ. Geophys. Res.; 87©, 1231-1238.
- Oral, M.B., Reilinger, R.E., Toksöz, M.N., Kong, R.W., Barka, A.A., Kınık, I., Lenk, O., 1995. *Global positioning system offers evidence of plate motions in eastern Mediterranean*. EOS transact.; 76 (9).
- Ort, M., 1993. *Eruptive processes and caldera formation in a nested downsag-collapse caldera: Cerro Panizos, central Andes Mountains*. Journ. Volcanol. Geother. Res.; 56, 221-252.
- Ort, M.H., Fisher, R.V., Orsi, G., 1993. *AMS evidence for complex interactions between topography and pyroclastic flows: Campanian Ignimbrite, Italy*. IAVCEI General Assembly, Canverra, Abstract.
- Ort, M.H., Rosi, M., Anderson, C.A., 1999. *Correlation of deposits and vent locations of the proximal Campanian Ignimbrite deposits, Campi Flegrei, Italy, based on natural remanent magnetization and anisotropy of magnetic susceptibility characteristics*. Journ. Volcanol. Geoth. Res.; 91, 167-178.
- Ort, M.H., Orsi, G., Pappalardo, L., Fisher, R.V., 2003. *Anisotropy of magnetic susceptibility studies of depositional processes in the Campanian Ignimbrite, Italy*. Bull. Volcanol.; 65, 55-72.
- Ozansoy, F., 1962. *Unité chronostratigraphique du Néogène Continental de Turquie en particulier d'Anatolie Centrale et Occidentale*. Cool. Ist. CNRS, Paris; 104, 5 pp.
- Palmer, H.C., MacDonald, W.D., Hayatsu, A. 1991. *Magnetic, structural and geochronologic evidence bearing on volcanic sources and Oligocene deformation of ash flow tuffs, Northeast Nevada*. Journ. Geophys. Res.; 96, 2185-2202.
- Palmer, H.C., McDonald, W.D., Gromme, C.S., Ellwood, B.B., 1996. *Magnetic properties and emplacement of the Bishop Tuff, California*. Bull. Volcanol.; 58, 101-116.
- Palmer, H.C. and MacDonald, W.D., 1999. *Anisotropy of magnetic susceptibility in relation to source vent of ignimbrites: empirical observations*. Tectonophys.; 307, 207-218.
- Palmer, H.C., MacDonald, W.D. 2002. *The Northeast Nevada Volcanic Field: Magnetic properties and source implications*. Journal of Geophysical Research; 107, 2298.
- Paquereau-Lebti, P., Fornari, M., Roperch, P., Thouret, J.C., Macedo, O., 2008. *Paleomagnetism, magnetic fabric, and $^{40}\text{Ar}/^{39}\text{Ar}$ dating of Pliocene and Quaternary ignimbrites in the Arequipa area, southern Peru*. Bull. Volcanol.; 70, 977-997.

- Paquette, J.L., Le Pennec, J.L., 2012. *3.8 Ga zircons sampled by Neogene ignimbrite eruptions in Central Anatolia*. *Geology*; 40, 239-242.
- Parejas, E., 1943. *Le substratum ancien du Taurus occidental au sud de Afyonkarahisar (Anatolie)*. *C. R. Séances Soc. Phys. Et Hist. Nat., Genève*; 60, 110-114.
- Pasquarè, G., 1968. *Geology of the Cenozoic volcanic area of central Anatolia*. *Atti Accad. Naz. Lincei*; 9, 55-204.
- Pasquarè, G., 1971. *Cenozoic volcanic of the Erzurum area (Turkish Armenia)*. *Geol. Rundsch.*; 60, 900-911.
- Pasquarè, G., Poli, S., Vezzoli, L., Zanchi, A., 1988. *Continental arc volcanism and tectonic setting in Central Anatolia, Turkey*. *Tectonophysics*; 146, 217-230.
- Pearce, J.A., Bender, J.F., Long, S.E., Kidd, W.S.F., Low, P.J., Güner, Y., Saroğlu, F., Yılmaz, Y., Moorbat, S., Mitchell, J.G., 1990. *Genesis of collision volcanism in Eastern Anatolia, Turkey*. *Journ. Volcanol. Geoth. Res.*; 44, 189-229.
- Petronis, M.S., Geissman, J.W., 2009. *Anisotropy of magnetic susceptibility data bearing on the transport direction of mid-tertiary regional ignimbrites, Candelaria Hills area, West-Central Nevada*. *Bull. Volcanol.*; 71, 121-151.
- Piper, J.D.A., Gürsoy, H., Tatar, O., 2002. *Paleomagnetism and magnetic properties of the Cappadocian ignimbrite succession, central Turkey, and neogene tectonics of the Anatolian collage*. *Journ. Volcanol. Geoth. Res.*; 117, 237-262.
- Piper, J.D.A., Tatar, O., Gürsoy, H., Koçbulut, F., Mesci, B.L., 2006. *Paleomagnetic Analysis of Neotectonic Deformation in the Anatolian accretionary collage, Turkey*. In: Dilek, Y., Pavlides, S. (Eds.), *Post-Collisional Tectonics and Magmatism in the Eastern Mediterranean Region*. *Geol. Soc. Am., Special Paper*; 409, 417-440.
- Piper, J.D.A., Gürsoy, H., Tatar, O., Beck, M.E., Rao, A., Koçbulut, F., Mesci, B.L., 2010. *Distributed neotectonic deformation in the Anatolides of Turkey: A palaeomagnetic analysis*. *Tectonophysics*; 488, 31-50.
- Platzman, E.S., Tapirdamaz, C., Sanver, M., 1998. *Neogene anticlockwise rotation of central Anatolia (Turkey): preliminary paleomagnetic and geochronological results*. *Tectonophysics*; 299 (3), 175-189.

- Porreca, M., Mattei, M., Giordano, G., De Rita, D., Funicello, R. 2003. *Magnetic fabric and implications for pyroclastic flow and lahar emplacement, Albano maar, Italy*. Journ. Geophys. Res.; 108, 2264, doi:10.1029/2002JB002102.
- Postma, G., Nemeč, W., Kleinspehn, K.L., 1988. *Large floating clasts in turbidites: a mechanism for their emplacement*. Sediment. Geol.; 58. 47-61.
- Potter, D.B., 1983. *Flow directions and possible sources of the Otowi ash-flows, Jemez Mountains, New Mexico*. Geol. Soc. Am. Abstr. Programs; 15, 389.
- Potter, D.B., Oberthal, C.M., 1987. *Vent sites and flow directions of the Otowi ash flows (lower Bandelier Tuff), New Mexico*. Geol. Soc. Am. Bull.; 98, 66-76.
- Potter, D.K., Stephenson, A., 1988. *Single-domain particles in rocks and magnetic fabric analysis*. Geophys. Res. Lett.; 15, 1097-1100.
- Pyle, D.M., 1989. *The thickness, volume and grain size of tephra fall deposits*. Bull. Volcanol.; 51, 1-15.
- Pyle, D.M., 2000. *Sizes of volcanic eruptions*. In: Sigurdsson, H., Houghton, B.F., McNutt, S.R., Rymer, H., Stix, J., (eds) Encyclopedia of Volcanoes. Academic Press, London.
- Ragan, D.H., Sheridan, M.F., 1972. *Compaction of the Bishop Tuff*. Geol. Soc. Am. Bull.; 83, 95-106.
- Rees, A.I., 1983. *Experiments on the production of transverse grain alignment in a sheared dispersion*. Sedimentology; 30, 437-448.
- Reilinger, R.E., McClusky, S.C., Oral, M.B., King, W., Toksöz, M.M., 1997. *Global Positioning System measurements of present-day crustal movements in the Arabian-Africa-Eurasia plate collision zone*. Journ. Geophys. Res.; 102, 9983-9999.
- Reynolds, R.L., 1977. *Paleomagnetism of Welded Tuffs of the Yellowstone Group*. J. Geophys. Res.; 82, 3677-3693.
- Rhodes, R.C., Smith, E.I., 1972. *Distribution and directional fabric of ash-flow sheets in the north-western Mogollon Plateau, New Mexico*. Geol. Soc. Am. Bull.; 83, 1863-1869.
- Roche, O., Druitt, T.H., Merle, O., 2000. *Experimental study of caldera formation*. Journ. Geophys. Res.; 105B, 395-416.
- Rochette, P., Jackson, M., Aubourg, C., 1992. *Rock magnetism and the interpretation of the anisotropy of magnetic susceptibility*. Rev. Geophys.; 30, 209-226.

- Rochette, P., Aubourg, C., Perrin, M., 1999. *Is this fabric normal? A review and case studies in volcanic formations*. Tectonophys.; 307, 219-234.
- Roobol, M.J., Smith, A.L., Wright, J.V., 1987. *Lithic breccias in pyroclastic flow deposits on St. Kitts, West Indies*. Bull. Volcanol.; 49, 694-707.
- Rosenbaum, J.G., 1986. *Paleomagnetic directional dispersion produced by plastic deformation in a thick Miocene welded tuff, Southern Nevada: Implications for welding temperatures*. J. Geophys. Res.; 91, 12817-12834.
- Savaşçın, M.Y., Oyman, T., 1998. *Tectono-Magmatic Evolution of Alkaline Volcanics at the Kirka-Afyon-Isparta Structural Trend, SW Turkey*. Tr. Journ. Earth Sci.; 7, 201-214.
- Scandone, R., Giacomelli, L., 2004. *Vulcanologia Principi fisici e metodi d'infagine*. Liguori editore; 642 pp.
- Schlenger, C.M., Veblen, D.R. & Rosenbaum, J.G., 1991. *Magnetism and Magnetic Mineralogy of Ash Flow Tuffs from Yucca Mountain, Nevada*. J. Geophys. Res.; 96, 6035-6052.
- Schischwani, E., 1974. *Mineralbestand, Chemische und Petrographische Zusammensetzung Ignimbritischer Gesteine zwischen Aksaray und Kayseri (Zentralanatolien, Türkei)* [Ph.D. thesis]: Freiburg, Germany. Universität Freiburg; 115 pp.
- Schmincke, H.U., Swanson, D.A., 1967. *Laminar viscous flowage structures in ash-flow tuffs from Gran Canaria, Canary Islands*. Journ. of Geol.; 75, 641-664.
- Schumacher, R., Mues-Schumacher, U., 1996a. *Depositional characteristics of ignimbrites in Cappadocia, central Anatolia, Turkey*. In: Savaşçın, M.Y., Eronat, A.H., (Eds.), Proceedings of the International Earth Science Congress on Aegean Regions (IESCA 1990); 2, 435-449.
- Schumacher, R., Mues-Schumacher, U., 1996b. *The Kizilkaya ignimbrite – an unusual low-aspect-ratio ignimbrite from Cappadocia, central Turkey*. Journ. Volcanol. Geoth. Res.; 70, 107-121.
- Scott, W.E., Hoblitt, R.P., Torres, R.C., Self, S., Martinez, M.L., Nillos, T.J., 1996. *Pyroclastic flows of the June 15, 1991, climatic eruption of Mount Pinatubo*. In: Newhall, C.C., Punongbayan, S. (eds) *Fire and Mud: Eruptions of Mount Pinatubo, Philippines*. Philippine Institute Volcanology and Seismology, Quezon City & University of Washington Press, Seattle; 545-570.
- Seaman, S.J., Williams, M.L., 1992. *Center-to-center analysis and flow fanric characterization in ash-flow tuffs*. Bull. Volcanol.; 54, 319-328.

- Seaman, S.J., McIntosh, W.C., Geissman, J.W., Williams, M.L., Elston, W.E., 1991. *Magnetic fabrics of the Bloodgood Canyon and Shelley Peak tuffs, southwestern New Mexico: Implications for emplacement and alteration processes*. Bull. Volcanol.; 53, 460-470.
- Self, S., Goff, F., Gardner, J.N., Wright, J.V., William, M.K., 1986. *Explosive Rhyolitic Volcanism in the Jemez Mountains: Vent Locations, Caldera Development and Relation to Regional Structure*. Journ. of Geophys. Res.; 91, 1779-1798.
- Self, S., Wolff, J.A., Spell, T.L., Skuba, C.E., Morrissey, M.M., 1991. *Revisions to the stratigraphy and Volcanology of the Post-0.5 Ma Units and the Volcanic Section of VC-1 Core Hole, Valles Caldera, New Mexico*. Journ. Geophys. Res.; 96 (B3), 4107-4116.
- Şen, E., Kürkçüoğlu, B., Aydar, E., Gourgaud, A., Vincent, P.M., 2003. *Volcanological evolution of Mount Erciyes stratovolcano and origin of the Valibaba Tepe Ignimbrite (Central Anatolia, Turkey)*. Journ. Volcanol. Geoth. Res.; 125, 225-246.
- Şen, S., Seyitoğlu, G., Karadenizli, L., Kazancı, N., Varol, B., Araz, H., 1998. *Mammalian biochronology of Neogene deposits and its correlation with the lithostratigraphy in the Çankırı-Çorum Basin, central Anatolia, Turkey*. Eclogae Geol. Helv.; Basel, 91, 307-320.
- Şengör, A.M.C., Kidd, W.S.F., 1979. *Post-collisional tectonics of the Turkish-Iranian plateau and a comparison with Tibet*. Tectonophysics; 55, 361-376.
- Şengör, A.M.C., Yılmaz, Y., 1981. *Tethyan evolution of Turkey: a plate tectonic approach*. Tectonophysics; 75, 181-241.
- Şengör, A.M.C., Görür, N., Şaroğlu, F., 1985. *Strike slip faulting and related basin formation in zones of tectonic escape: Turkey as a case study*. In: Biddle, K.T., Christie-Blick, N. (Eds.), *Strike Slip Deformation, Basin Formation and Sedimentation*. Soc. Econ. Paleontol. Mineral. Spec. Publ.; 37, 227-264.
- Şenyürek, M.S., 1954. *A Study of the Remains of Samotherium found in Taskinpaşa*. Rev. Fac. Lan. His.Geogr. Univ. Ankara; 12, 32 pp.
- Seyitoğlu, G., Scott, B.C., 1996. *The cause of N-S extensional tectonics in western Turkey: tectonic escape vs back-arc spreading vs orogenic collapse*. Journ. Geodyn.; 22, 145-153.
- Shemeta, J.E., Weaver, C.S., 1986. *Seismicity Accompanying the May 18, 1980 Eruption of Mount St. Helens, Washington*. In: Keller S.A.C., Editor, *Mt. St. Helens: five years later*. Eastern Washington University Press, Cheney, WA.; 44-58.

- Sheridan, M.F., Updike, R.G., 1975. *Sugarloaf Mountain Tephra- a Pleistocene rhyolitic deposit of base surge origin in northern Arizona*. Geol. Soc. of Am. Bull.; 86, 571-581.
- Sickenberg, O., Becker-Platen, J.D., Benda, L., Berg, D., Engesser, B., Gaziry, W., Hessig, K., Hünemann, K.A., Sondaar, P.Y., Schmidt-Kitter, N., Staesche, K., Staesche, U., Steffens, P.Y., Tobien, H., 1975. *Die Gliederung des höheren Jungtertiärs und Altquartärs in der Turkey nach Vertebraten und ihre Bedeutung für die internationale neogen-Stratigraphie*. Geol. Jahrb.; B15, 1-167.
- Sigurdsson, H., Carey, S., 1989. *Plinian and co-ignimbrite tephra fall from the 1815 eruption of Tambora volcano*. Bull. Volcanol.; 51, 243-270.
- Smith, R.L., 1960. *Zones and zonal variations in welded ash flow tuffs*. SGS Prof. Pap.; 354F, 149-159.
- Smith, R.L., 1979. *Ash-flow magmatism*. Geol. Soc. Am. Spec. Pap.; 180, 5-27.
- Smith, R.L., Bailey, R.A., 1968. *Resurgent cauldrons*. Geol. Soc. Am. Mem.; 116, 153-210.
- Smith, R.L., Bailey, R.A., Ross, C.S., 1961. *Structural evolution of the Valles Caldera, New Mexico, and its bearing on the emplacement of ring dikes*. U.S Geol. Surv. Prof. Paper; 424, 145-149.
- Sparks, R.S.J., 1976. *Grain size variations in ignimbrites and implications for the transport of pyroclastic flow*. Sedimentology; 23, 147-188.
- Sparks, R.S.J., 1978. *The Dynamics of Bubble formation and Growth in Magmas: A review and Analysis*. Journ. Volcanol. Geoth. Res.; 3, 1-37.
- Sparks, R.S.J., Walker, G.P.L., 1977. *The significance of vitric-enriched air-fall ashes associated with crystal-enriched ignimbrites*. Journ. Volcan. and Geoth. Res.; 2, 329-341.
- Sparks, R.S.J., Self, S., Walker, G.P.L., 1973. *Products of Ignimbrite eruptions*. Geology; 1, 115-118.
- Sparks, R.S.J., Wilson, L., Hulme, G., 1978. *Theoretical modeling of the generation, movement and emplacement of pyroclastic flows by column collapse*. Journ. Geophys. Res.; 83, 1727-1739.
- Sparks, R.S.J., Bursik, M.I., Carey, S.M., Gilbert, J.S., Glaze, L.S., Sigurdsson, H., Woods, A.W., 1997. *Volcanic Plumes*. Wiley, Chichester.
- Stephenson, A., 1994. *Distribution anisotropy: two simple models for magnetic lineation and foliation*. Phys. of the Earth and Plan. Int.; 82, 49-53.

- Streck, M.J., Grunder, A.L., 1995. *Crystallization and welding variations in a widespread ignimbrite sheet – the Rattlesnake Tuff, Eastern Oregon, USA*. Bull. Volcanol.; 57, 151-169.
- Sulpizio, R., Dellino, P., 2008. *Sedimentology, Depositional Mechanism and Pulsating Behaviour of Pyroclastic Density Currents*. Develop. Volcanol.; 10; 57-96.
- Sulpizio, R., Mele, D., Dellino, P., La Volpe, L., 2007. *High variability of sedimentology and physical properties of pyroclastic density currents during complex Subplinian eruptions: the example of the AD 472 (Pollena) eruption of Somma-Vesuvius, Italy*. Sedimentology; 54, 607-635.
- Sulpizio, R., De Rosa, R., Donato, P., 2008. *The influence of variable substrate morphology on sedimentology of pyroclastic density currents: the example of Upper Pollara eruption (Salina Island, southern Italy)*. Journ. Volcanol. Geotherm. Res.; Submitted for publication.
- Sunder, M., 1982. *Kırka (Eskişehir) çvresinin jeolojisi ve Sarıkaya borat yataklarının oluşumu*. TÜBİTAK VII, Bilim Kongresi Tebliğleri; 105-117 (in Turkish).
- Suzuki, K., Ui, T., 1982. *Grain orientation and depositional ramps as flow direction indicators of large-scale pyroclastic flow deposits, Japan*. Geology; 10, 429-432.
- Suzuki, K., Ui, T., 1988. *Depositional ramps: asymmetrical distribution structure in the Ata pyroclastic flow deposit, Japan*. Bull. Volcanol.; 50, 26-34.
- Sweetkind, D.S., Reynolds, R.L., Sawyer D.A., Rosenbaum, J.G., 1993. *Effects of hydrothermal alteration on the magnetization of the Oligocene Carpenter Ridge Tuff, Bachelor Caldera, San Juan Mountains, Colorado*. Journ. Geophys. Res. ; 98, 6255-6266.
- Tarling, D.H., Hrouda, F., 1993. *The magnetic anisotropy of rocks*. Chapman and Hall; London.
- Tatar, O., Gürsoy, H., Piper, J.D.A., 2002. *Differential neotectonic rotations in Anatolia and the Tauride Arc: paleomagnetic investigation of the Erenlerdağı Complex and Isparta volcanic district, south-central Turkey*. Journ. Geol. Soc. London; 159, 281-294.
- Temel, A., 1992. *Kapadokya eksplozif volkanizmasının petrolojik ve jeokimyasal özellikleri*. PhD thesis, Hacettepe University, 208 pp (in Turkish).
- Tera, F., Wasserburg, G., 1972. *U-Th-Pb systematics in three Apollo 14 basalts and the problem of initial Pb in lunar rocks*. Earth and Planet. Sci. Lett.; 14, 281-304.
- Temel, A., Gündoğdu, M.N., Gourgaud, A., Le Penned, J.L., 1998. *Ignimbrites of Cappadocia (Central Anatolia, Turkey): petrology and geochemistry*. Journ. Volcanol. Geith. Res.; 85, 447-471.
- Thompson, R., Oldfield, F., 1986. *Environmental magnetism*. Allen & Unwin, London; 227 pp.

- Toprak, V., Keller, J., Schumacher, R., 1994. *Volcano-tectonic features of the Cappadocian volcanic province*. Int. Volcanol. Congr. Excurs. Guide; Ankara, 58 pp.
- Ui, T., Matsuwo, N., Sumita, M., Fujinawa, A., 1999. *Generation of block and ash flows during the 1990-1995 eruption of Unzen volcano, Japan*. Journ. Volcanol. Geoth. Res; 89, 123-137.
- Ui, T., Suzuki-Kamata, K., Matsusue, R., Fujita, K., Metsugi, H., Araki, M., 1989. *Flow behavior of large-scale flows. Evidence obtained from petrofabric analysis*. Bull. Volcanol.; 51, 115-122.
- Urrutia-Fucugauchi, J., Alva Valdivia, L.M., J. Rosas Elguera, J., Campos Enríquez, O., Goguitchaichvili, A., Soler Arechalde, A.M., C. Caballero Miranda, C., Venegas Salgado, S., Sánchez Reyes, S., 2000. *Magnetostratigraphy of the volcanic sequence of Río Grande de Santiago-Sierra de la Primavera region, Jalisco, western Mexico*. Geofisica International.; 39, 247-265.
- Urrutia-Fucugauchi, J., Ferrusquia-Villafranca, I., 2001. *Paleomagnetic results for the Middle-Miocene continental Suchilquitongo Formation, Valley of Oaxaca, southeastern Mexico*. Geofisica International.; 40, 191-205.
- Valentine, G.A., 1987. *Stratified flow in pyroclastic surges*. Bull. Volcanol.; 49, 616-630.
- Valentine, G.A., Fisher, R.V., 1986. *Origin of layer 1 deposits in ignimbrites*. Geology; 1, 146-148.
- Valentine, G.A., Fisher, R.V., 2000. *Pyroclastic surges and blasts*. In: Sigurdsson, H. (Ed.), *Encyclopedia of Volcanoes*. Academic Press, New York; 571-580.
- Viereck-Goette, L., Gürel, A., Ganskow, G., Çopuroğlu, I., Abratis, M., 2010. *Revised volcanostratigraphy of the Upper Miocene to Lower Pliocene Ügüp Formation, Central Anatolian volcanic province, Turkey*. Geol. Soc. Am., Special Paper; 464, 85-112.
- Walker, G.P.L., 1973. *Explosive volcanic eruptions, a new classification scheme*. Geol. Rund.; 62, 431-446.
- Walker, G.P.L., 1980. *The Taupo Pumice: Product of the most powerful known ultraplinian eruption*. Journ. Volcanol. Geoth. Res.; 8, 69-94.
- Walker, G.P.L., 1981a. *Generation and dispersal of fine ash and dust by volcanic eruptions*. Journ. Volcanolog. Geath. Res.; 11, 81-92.
- Walker, G.P.L., 1981b. *Plinian eruptions and their products*. Bull. Volcanol.; 44, 223-240.
- Walker, G.P.L., 1983. *Ignimbrite types and ignimbrite problems*. Journ. Volcan. and Geoth. Res.; 17, 65-88.

- Walker, G.P.L., 1984. *Downsag calderas, ring faults, caldera sizes, and incremental caldera growth*. Journ. Geophys. Res.; 89B, 8407-8416.
- Walker, G.P.L., 1985. *Origin of coarse lithic breccias near ignimbrite source vents*. Journ. Volcanol. Geoth. Res.; 25, 157-171.
- Walker, G.P.L., 1988. *Three Hawaiian calderas: an origin through loading by shallow intrusion?* Journ. Geophys. Res.; 93B, 14773-14784.
- Walker, G.P.L., Hayashi, J.N., Self, S., 1995. *Travel of pyroclastic flows as transient waves: implications for the energy line concept and particle-concentration assessment*. Journ. Volcanol. Geoth. Res.; 66, 265-282.
- Wang, X., Roberts, J., Schmidt, P. 2001. *Flow directions of Carboniferous ignimbrites, southern New England Oregon, Australia, using anisotropy of magnetic susceptibility*. Journ. Volcanol. Geotherm. Res.; 110, 1-25.
- Waters, A.C., Fisher, R.V., 1971. *Base surges and their deposits: Capelinos and Taal volcanoes*. Journ. Geophys. Res.; 76, 5596-5614.
- Wiedenmann, A., Regnard, J.R., Fillion, G., Hafner, S., 1986. *Magnetic properties and magnetic ordering of the orthopyroxenes*. Journ. Phys.; C19, 3683-3695.
- Williams, H., 1941. *Calderas and their origin*. Un. Calif. Pub. Pull. Dep. Geol. Sci.; 25, 239-346.
- Williams, H., McBirney, A.R., 1979. *Volcanology*. Freeman, Cooper and Co, San Francisco Publ., Berkeley, CA; 397 pp.
- Wilson, C.J.N., 1980. *The role of fluidization in the emplacement of pyroclastic flows: an experimental approach*. Journ. Volcanol. and Geoth. Res.; 8, 231-249.
- Wilson, C.J.N., 1985. *The Taupo eruption, New Zealand II. The Taupo ignimbrite*. Phil. Trans. R. Soc. London; A314, 229-310.
- Wilson, C.J.N., Walker, G.P.L., 1982. *Ignimbrite depositional facies: the anatomy of a pyroclastic flow*. Journ. Geol. Soc. Lond.; 139, 581-592.
- Wilson, C.J.N., Hildreth, W., 1997. *The Bishop Tuff: new insights from eruptive stratigraphy*. Journ. of Geol.; 105, 407-439.
- Wilson, C.J.N., Houghton, B.F., McWilliams, M.O., Lanphere, M.A., Weaver, S.D., Briggs, R.M., 1995. *Volcanic and structural evolution of Taupo Volcanic Zone, New Zealand: a review*. Journ. Volcanol. Geotherm. Res.; 68, 1-28.

- Wilson, L., Sparks, R.S.J., Walker, G.P.L., 1980. *Explosive Volcanic Eruptions – IV. The control of Magma Properties and Conduit Geometry on Eruption Column Behaviour*. Geophys. Journ. Roy. Astr. Soc.; 63, 117-148.
- Wohlfarth, E.P., 1958. *Relations between different modes of acquisition of remanent magnetization of ferromagnetic particles*. Journ. appl. Phys.; 99(8).
- Wolff, J.A., Wright, J.V., 1981. *Rheomorphism of welded tuffs*. Journ. Volcanol. and Geoth. Res.; 10, 13-34.
- Wright, I.C., Gamble, J.A., Shane, P.A.R., 2003. *Submarine silicic volcanism of the Healy caldera, southern Kermadec arc (SW Pacific): 1-Volcanology and eruption mechanism*. Bull. Volcanol.; 65, 15-29.
- Wright, J.V., Walker, G.P.L., 1977. *The ignimbrite source problem: Significance of a co-ignimbrite lag-fall deposit*. Geology; 5, 729-732.
- Wright, J.V., Walker, G.P.L., 1981. *Eruption transport and deposition of ignimbrite: A case study from Mexico*. Journ. Volc. Geoth. Res.; 9, 111-131.
- Wright, J.V., Self, S., Fisher, R.V., 1979. *Eruption transport and deposition of ignimbrites: A case study from Mexico*. Journ. Volcanol. Geoth. Res.; 9, 111-131.
- Yalçın, H., 1990. *Neojen yaşlı Kırka (Eskişehir) volkanosedimanter gölssel basenin stratigrafik ve tektonik özellikleri*. PhD thesis, Hacettepe Univ.; 209 pp (in Turkish).
- Yokoyama, I., 1956. *Energetics in active volcanoes: Activities of Volcano Mihara, Oshima Island during 1953-54*. Bull. Earth. Res.; 34, 185-195.

Appendix 1 - Magnetic susceptibility and AMS data of the Incik, Sabuncu and Seydiler ignimbrites before data selection. Symbols: k = bulk susceptibility, L , F = magnetic lineation, foliation; P = degree of anisotropy; Magnetic lineation: D , I = declination, inclination of the K_1 axis with angles of the 95% confidence ellipse (E_1-2 , E_1-3); Magnetic foliation pole: D , I = declination, inclination of the K_3 axis with angles of the 95% confidence ellipse (E_3-1 , E_3-2).

Locality	Ignimbrite unit	Site	Specimen	Density (g/cm ³)	k (SI)	L (K ₁ /K ₂)	F (K ₂ /K ₃)	P (K ₁ /K ₃)	T	Magnetic lineation (K ₁)				Magnetic foliation pole (K ₃)				Θ angle (°)			
										D (°)	I (°)	E ₁₋₂ (°)	E ₁₋₃ (°)	D (°)	I (°)	E ₃₋₂ (°)	E ₃₋₁ (°)				
AKCAKAYA	IN2	AK1	AK1-6	1,51	1,11E-03			1,022	-0,250												
			AK1-7	1,40	8,74E-04			1,019	0,510												
			AK1-5	1,60	1,05E-03			1,019	-0,140												
			AK1-1	1,49	1,28E-03			1,012	0,740												
			AK1-9	1,55	1,02E-03			1,015	-0,470												
			AK1-4	1,52	9,70E-04			1,034	0,070												
			AK1-2	1,32	9,69E-04			1,027	-0,090												
			AK1-3	1,56	1,14E-03			1,028	0,160												
			average	1,49	1,05E-03	1,010	1,011	1,022	0,066	75,9	10,4	21,8	12,4	332,2	52,2	20,6	15,4	76			
SEYDIKOY	SA2	AK2-1	AK2-3	1,07	5,98E-04			1,024	0,180												
			AK2-1	1,11	5,62E-04			1,024	0,550												
			AK2-6	1,18	5,12E-04			1,014	0,040												
			AK2-2	1,05	6,08E-04			1,028	0,060												
			AK2-5	0,97	7,06E-04			1,044	0,390												
			AK2-4	1,13	6,36E-04			1,020	-0,270												
			average	1,09	6,04E-04	1,010	1,015	1,026	0,158	34,8	16,6	24,6	11,0	248,9	70,1	36,8	8,3	34			
	Lava flow	AK2-2	AK2-12	2,87	-6,70E-06			1,045	-0,420												
			AK2-7	2,74	-6,00E-06			1,043	-0,610												
			AK2-9	2,71	-2,30E-06			1,106	-0,140												
			AK2-10	2,78	-4,20E-06			1,051	0,090												
AK2-8			2,69	-5,30E-06			1,060	-0,260													

			AK2-11	2,74	-4,20E-06			1,065	0,170												
			AK2-13	2,74	-4,20E-06			1,080	-0,080												
			average	2,75	-4,70E-06	1,036	1,027	1,064	-0,179	272,6	62,1	9,6	6,4	125,5	24,0	13,8	8,1	33			
INCIK	IN1a	AK4	AK4-2B	1,58	3,48E-05			1,008	-0,450												
			AK4-8B	1,54	3,29E-05			1,005	-0,740												
			AK4-1A	1,49	3,39E-05			1,009	-0,180												
			AK4-3A	1,48	3,65E-05			1,008	-0,400												
			AK4-7B	1,62	4,02E-05			1,005	-0,370												
			AK4-5A	1,57	3,72E-05			1,010	-0,690												
			AK4-10C	1,56	3,71E-05			1,004	0,160												
			AK4-4A	1,63	3,90E-05			1,005	-0,210												
			AK4-7A	1,51	3,57E-05			1,013	0,250												
			AK4-2C	1,54	3,21E-05			1,010	-0,590												
			AK4-9A	1,58	4,14E-05			1,005	0,680												
			AK4-9B	1,55	3,81E-05			1,006	-0,100												
						average	1,55	3,65E-05	1,005	1,003	1,007	-0,210	47,4	45,4	10,2	8,4	182,5	34,9	75,7	9,1	45
AKKAYA	IN1c	AK5-1	AK5-6A	1,18	9,81E-04			1,011	0,050												
			AK5-7A	1,25	9,31E-04			1,014	0,480												
			AK5-8	1,20	9,20E-04			1,018	0,280												
			AK5-9	1,15	8,51E-04			1,016	0,760												
			AK5-10A	1,23	9,01E-04			1,016	0,720												
			AK5-11B	1,19	9,21E-04			1,016	-0,210												
			AK5-13A	1,19	9,58E-04			1,021	0,630												
			AK5-14A	1,34	9,64E-04			1,018	0,070												
			AK5-10B	1,23	1,20E-03			1,015	0,790												
			AK5-6B	1,22	9,42E-04			1,015	0,650												
			AK5-7B	1,28	9,12E-04			1,016	0,540												

			AK5-11A	1,25	9,40E-04			1,017	0,120									
			average	1,22	9,52E-04	1,005	1,011	1,016	0,413	91,2	22,1	26,9	5,9	262,2	67,7	9,7	6,1	9
		AK5-2	AK5-19A	1,24	1,09E-03			1,015	-0,100									
			AK5-16	1,16	1,01E-03			1,020	0,560									
			AK5-17	1,27	1,04E-03			1,013	0,200									
			AK5-21	1,10	8,83E-04			1,007	0,820									
			AK5-18	1,18	8,50E-04			1,012	0,590									
			AK5-25	1,14	9,75E-04			1,016	0,210									
			AK5-19B	1,25	9,35E-04			1,019	-0,210									
			AK5-20	1,26	1,00E-03			1,015	0,740									
			AK5-23	1,26	1,13E-03			1,011	0,390									
			average	1,21	9,90E-04	1,005	1,009	1,014	0,360	311,0	1,7	48,4	9,5	216,5	69,0	14,2	7,9	86
ASAGI KALABAK	IN1c	AK6	AK6-5	1,45	9,74E-04			1,014	0,270									
			AK6-8	1,48	1,16E-03			1,012	-0,340									
			AK6-11	1,38	1,00E-03			1,007	0,730									
			AK6-6	1,36	1,09E-03			1,006	-0,180									
			AK6-7	1,43	1,03E-03			1,008	-0,450									
			average	1,42	1,05E-03	1,005	1,005	1,009	0,017	71,4	44,5	36,3	14,6	271,4	43,8	68,5	28,6	20
ASAGI CAGLAN	IN1c	AK7	AK7-3B	1,53	1,22E-03			1,018	0,600									
			AK7-12A	1,46	1,00E-03			1,008	0,830									
			AK7-5	1,45	8,69E-04			1,015	-0,220									
			AK7-10A	1,60	1,12E-03			1,023	-0,240									
			AK7-2B	1,45	1,01E-03			1,019	0,790									
			AK7-4B	1,39	8,86E-04			1,020	-0,220									
			AK7-11	1,43	8,97E-04			1,018	0,320									
			AK7-10B	1,48	1,11E-03			1,017	-0,240									

			AK7-8	1,54	1,12E-03			1,018	-0,120											
			AK7-1A	1,44	1,05E-03			1,012	0,810											
			AK7-2C	1,52	9,95E-04			1,017	-0,380											
			AK7-9A	1,41	1,11E-03			1,020	-0,510											
			average	1,47	1,03E-03	1,008	1,009	1,017	0,121	247,0	11,7	37,2	5,4	88,2	77,4	23,2	5,8	21		
GOCERI	IN1c	AK3	AK3-6	1,39	8,31E-04			1,011	0,750											
			AK3-10B	1,43	9,17E-04			1,021	0,270											
			AK3-1	1,28	6,95E-04			1,016	0,350											
			AK3-7	1,45	7,71E-04			1,014	0,630											
			AK3-10A	1,17	7,21E-04			1,016	0,160											
			AK3-8	1,40	8,33E-04			1,015	0,140											
			average	1,35	7,95E-04	1,005	1,010	1,016	0,383	46,8	13,1	47,7	16,5	280,5	68,6	19,9	5,3	54		
		IN2	DM4-1	DM4-9A	1,41	2,68E-04			1,022	0,730										
	DM4-6			1,52	3,20E-04			1,013	-0,040											
	DM4-1B			1,46	3,15E-04			1,016	-0,290											
	DM4-9B			1,53	3,37E-04			1,037	0,610											
	DM4-7			1,23	3,31E-04			1,029	0,670											
	DM4-2A			1,37	2,63E-04			1,028	-0,240											
	DM4-4			1,47	3,40E-04			1,027	-0,130											
	DM4-3			1,49	3,26E-04			1,031	0,470											
	DM4-1A			1,45	3,38E-04			1,033	-0,550											
	DM4-5			1,47	3,81E-04			1,025	-0,240											
	DM4-2B			1,48	2,84E-04			1,015	-0,840											
	DM4-8A			1,31	2,55E-04			1,022	0,280											
DM4-8B	1,26			3,05E-04			1,009	0,130												
			average	1,42	3,12E-04	1,011	1,013	1,024	0,043	90,6	18,3	26,4	10,6	259,5	71,4	27,4	10,5	11		

			DM2-7	1,46	1,33E-03			1,012	0,260											
			average	1,36	1,22E-03	1,005	1,008	1,014	0,199	88,4	4,9	23,4	6,9	323,0	81,6	13,2	7,1	55		
UCLERKAYASI	SE2	DM3	DM3-1	1,76	2,98E-04			1,010	0,450											
			DM3-2	1,61	2,82E-04			1,011	0,730											
			DM3-3	1,82	3,76E-04			1,013	-0,130											
			DM3-4	1,66	2,89E-04			1,009	0,680											
			DM3-5	1,58	2,88E-04			1,011	0,730											
			DM3-6	1,88	3,63E-04			1,012	0,640											
			DM3-7	1,83	3,67E-04			1,019	0,000											
			DM3-8	1,81	4,41E-04			1,012	0,860											
			DM3-9	1,85	4,40E-04			1,021	0,550											
			DM3-10	2,01	5,62E-04			1,037	0,700											
						average	1,78	3,70E-04	1,004	1,012	1,016	0,521	96,3	1,5	48,5	11,0	198,2	82,7	13,8	6,9
OVACIK	SE1	DM5-1	DM5-8	1,39	1,57E-04			1,032	0,000											
			DM5-5	1,34	2,08E-04			1,005	0,070											
			DM5-11A	1,25	3,65E-04			1,033	0,560											
			DM5-9A	1,41	1,84E-04			1,032	0,450											
			DM5-10	1,40	1,34E-04			1,025	0,740											
			DM5-11B	1,30	1,65E-04			1,028	0,500											
			DM5-2	1,34	4,69E-05			1,010	-0,160											
			DM5-9B	1,26	1,59E-04			1,038	0,580											
			DM5-4	1,39	7,00E-05			1,014	0,100											
			DM5-3B	1,25	4,39E-05			1,015	0,220											
			DM5-1B	1,38	6,80E-05			1,019	0,460											
			DM5-1A	1,48	7,61E-05			1,012	0,590											
			DM5-3A	1,42	4,69E-05			1,019	-0,740											
			DM5-6B	1,28	1,41E-04			1,019	0,890											

			DM5-6A	1,28	1,30E-04			1,018	0,260											
			DM5-7A	1,17	9,72E-05			1,019	0,820											
			DM5-7B	1,28	1,82E-04			1,046	0,430											
			average	1,33	1,34E-04	1,007	1,016	1,023	0,339	168,6	12,3	65,3	15,5	308,2	74,0	17,6	14,4	40		
		DM5-2	DM5-16	1,41	6,01E-04			1,049	0,420											
			DM5-17	1,40	5,55E-04			1,041	0,490											
			DM5-19	1,47	5,97E-04			1,036	0,310											
			DM5-20	1,55	5,77E-04			1,031	0,770											
			DM5-18	1,28	4,85E-04			1,030	0,810											
			DM5-13	1,48	5,38E-04			1,032	0,920											
			DM5-14	1,38	5,39E-04			1,038	0,000											
			DM5-12	1,37	6,37E-04			1,046	-0,150											
			DM5-15	1,17	9,05E-04			1,043	0,050											
			average	1,39	6,04E-04	1,012	1,026	1,038	0,402	150,2	20,4	51,4	7,3	0,7	66,7	17,7	7,4	31		
KAYIHAN	SE1	DM6-1	DM6-8	1,62	6,86E-04			1,021	0,920											
			DM6-9	1,66	8,06E-04			1,016	0,860											
			DM6-7	1,69	9,41E-04			1,044	0,440											
			DM6-2B	1,41	3,59E-04			1,008	0,430											
			DM6-4	1,58	6,73E-04			1,020	0,600											
			DM6-1	1,56	8,21E-04			1,016	-0,160											
			DM6-2A	1,68	5,59E-04			1,018	0,190											
			DM6-6A	1,59	4,85E-04			1,011	0,000											
			DM6-5	1,63	5,48E-04			1,009	-0,040											
			DM6-6B	1,54	5,86E-04			1,012	0,100											
			DM6-10	1,56	7,04E-04			1,016	-0,170											
			DM6-3	1,74	8,86E-04			1,090	0,520											

			average	1,61	6,71E-04	1,006	1,017	1,023	0,308	357,7	5,2	55,3	8,0	142,9	83,6	11,1	10,1	35	
		DM6-2	DM6-14	1,71	2,54E-04			1,098	0,273										
			DM6-13	1,55	1,49E-04			1,017	-0,007										
			DM6-11	1,62	3,62E-04			1,037	0,346										
			DM6-12	1,65	1,79E-04			1,013	0,510										
			average	1,63	2,36E-04	1,015	1,026	1,041	0,280	31,0	12,2	25,8	5,3	123,1	9,6	60,9	14,0	88	
KUMBET	SE2	DM7	DM7-8	1,63	2,85E-03			1,035	0,600										
			DM7-5	1,70	3,31E-03			1,075	0,290										
			DM7-6	1,56	2,41E-03			1,030	0,660										
			DM7-7	1,62	2,81E-03			1,033	0,660										
			DM7-1	1,60	2,47E-03			1,047	0,840										
			DM7-4	1,61	2,48E-03			1,031	0,920										
			DM7-2	1,70	5,72E-03			1,326	0,270										
			DM7-3	1,59	2,36E-03			1,038	0,460										
			average	1,62	3,05E-03	1,021	1,052	1,077	0,588	189,9	27,3	23,7	12,0	294,6	26,1	67,1	13,7	75	
YESILYAYLA	SE1	DM8-1	DM8-3A	1,19	4,01E-05			1,011	-0,550										
			DM8-3B	1,21	4,13E-05			1,011	0,900										
			DM8-4	1,10	3,68E-05			1,014	0,520										
			DM8-5	1,17	3,85E-05			1,008	-0,750										
			DM8-6	1,23	4,40E-05			1,012	-0,370										
			DM8-7	1,15	3,77E-05			1,008	-0,200										
			DM8-8	1,13	3,64E-05			1,009	-0,100										
			DM8-9	1,29	4,59E-05			1,005	-0,100										
			average	1,18	4,01E-05	1,005	1,005	1,010	-0,075	321,6	43,5	49,8	6,7	95,5	36,2	62,3	8,9	46	
	SE2	DM8-2	DM8-11	1,55	4,64E-04			1,041	0,730										

			DM8-12	1,68	4,65E-04			1,045	0,750										
			DM8-13	1,70	4,63E-04			1,042	0,860										
			DM8-14	1,77	4,94E-04			1,041	0,750										
			DM8-15	1,76	4,64E-04			1,037	0,890										
			DM8-16A	1,59	4,66E-04			1,039	0,840										
			DM8-17A	1,74	5,02E-04			1,032	0,900										
			DM8-18A	1,65	5,17E-04			1,031	0,910										
			DM8-18B	1,64	4,66E-04			1,032	0,940										
			DM8-19A	1,57	5,85E-04			1,036	0,610										
			DM8-19B	1,52	5,31E-04			1,042	0,690										
			average	1,65	4,92E-04	1,004	1,034	1,038	0,805	195,0	4,9	52,2	4,4	36,3	84,8	5,4	4,1	21	
KALE	SE1	DM10-1	DM10-1	1,31	5,84E-05			1,040	0,660										
			DM10-2	1,43	6,52E-05			1,030	0,290										
			DM10-3	1,48	6,64E-05			1,018	0,560										
			DM10-4	1,33	6,34E-05			1,023	0,420										
			DM10-5	1,37	5,91E-05			1,017	0,640										
			DM10-6	1,38	6,27E-05			1,018	0,430										
			DM10-7	1,49	7,20E-05			1,041	0,570										
			average	1,40	6,39E-05	1,006	1,020	1,027	0,513	71,0	4,8	31,6	9,7	339,9	13,2	35,6	13,0	89	
	SE2	DM10-2	DM10-9A	1,21	5,78E-05			1,014	0,740										
			DM10-9B	1,31	5,92E-05			1,009	0,440										
			DM10-9C	1,23	5,38E-05			1,013	-0,560										
			DM10-9D	1,25	6,29E-05			1,021	-0,290										
			DM10-9E	1,28	5,74E-05			1,005	0,570										
			DM10-9F	1,23	5,60E-05			1,014	-0,540										
DM10-9G			1,21	5,31E-05			1,014	-0,220											

			DM10-9H	1,16	5,27E-05			1,023	-0,480											
			DM10-9I	1,31	5,68E-05			1,006	0,150											
			average	1,24	5,66E-05	1,008	1,006	1,013	-0,015	179,3	13,2	58,1	27,0	294,8	61,5	31,4	27,6	65		
		DM10-3	DM10-10A	1,43	7,51E-05			1,009	0,800											
			DM10-10B	1,41	1,18E-04			1,005	0,610											
			DM10-10C	1,11	6,88E-05			1,031	-0,580											
			DM10-10D	1,36	7,70E-05			1,011	0,200											
			DM10-10E	1,23	7,45E-05			1,015	-0,370											
			average	1,31	8,27E-05	1,008	1,006	1,014	0,132	97,2	54,1	62,7	41,0	275,8	35,9	51,3	11,3	1		
DOGER	SE2	DM11-1	DM11-2	1,50	2,63E-03			1,026	0,680											
			DM11-10	1,52	2,65E-03			1,033	0,820											
			DM11-6	1,64	2,75E-03			1,035	0,620											
			DM11-9	1,55	2,64E-03			1,031	0,720											
			DM11-3	1,59	2,89E-03			1,031	0,710											
			DM11-4B	1,63	2,77E-03			1,027	0,710											
			DM11-4A	1,61	2,69E-03			1,027	0,810											
			DM11-5B	1,60	2,66E-03			1,027	0,670											
			DM11-7	1,63	2,83E-03			1,032	0,580											
			DM11-8B	1,55	2,69E-03			1,035	0,680											
			DM11-11	1,57	2,56E-03			1,030	0,890											
			DM11-8A	1,52	2,66E-03			1,036	0,800											
					average	1,57	2,70E-03	1,004	1,026	1,031	0,721	126,2	10,4	11,0	3,0	322,0	79,2	3,2	2,1	16
				DM11-2a	DM11-14	1,55	2,99E-03			1,031	0,000									
			DM11-15B	1,56	2,48E-03			1,027	0,690											
			DM11-13	1,59	2,53E-03			1,027	0,450											

			DM11-12	1,45	2,36E-03			1,029	0,570											
			DM11-17A	1,51	2,44E-03			1,022	0,380											
			DM11-16	1,47	2,31E-03			1,030	0,440											
			DM11-18B	1,55	2,49E-03			1,026	0,570											
			average	1,53	2,51E-03	1,008	1,020	1,027	0,442	127,7	3,7	10,9	3,6	270,6	85,3	11,7	5,1	37		
		DM11-2b	DM11-21	1,48	2,43E-03			1,023	0,670											
			DM11-23	1,42	2,35E-03			1,023	0,480											
			DM11-19	1,47	2,47E-03			1,031	0,670											
			DM11-20	1,54	2,65E-03			1,031	0,960											
			DM11-22	1,42	2,36E-03			1,029	0,730											
			average	1,47	2,45E-03	1,004	1,023	1,027	0,705E	123,8	10,3	19,6	2,8	348,0	75,7	8,4	2,8	44		
KARAKAYA	SE1	DM13-1	DM13-1	1,68	5,55E-05			1,009	-0,690											
			DM13-2	1,86	5,69E-05			1,004	0,250											
			DM13-3	1,75	7,41E-05			1,006	0,460											
			DM13-4	1,70	6,35E-05			1,004	-0,590											
			DM13-5A	1,63	8,54E-05			1,004	0,090											
			DM13-5B	1,60	6,64E-05			1,006	0,040											
			DM13-6	1,72	6,90E-05			1,004	-0,040											
			DM13-7A	1,72	7,46E-05			1,002	-0,180											
			DM13-7B	1,95	7,49E-05			1,004	-0,520											
			DM13-8	1,93	6,59E-05			1,008	0,580											
			DM13-9A	1,76	6,25E-05			1,004	-0,800											
					average	1,75	6,80E-05	1,003	1,002	1,005	-0,123	339,5	53,9	37,1	25,7	188,5	32,5	73,8	27,3	29
				DM13-2	DM13-11	1,29	8,54E-05			1,005	0,097									
			DM13-12	1,44	8,36E-05			1,005	0,411											

			DM13-13	1,35	8,03E-05			1,007	-0,120												
			DM13-14	1,28	7,73E-05			1,012	-0,517												
			average	1,34	8,17E-05	1,004	1,003	1,007	-0,032	99,4	34,9	28,2	7,5	258,6	53,3	38,7	18,2	21			
CUKURCA	SE2	DM14-1	DM14-1	1,17	5,61E-04			1,023	0,390												
			DM14-3	1,40	2,83E-03			1,119	0,750												
			DM14-4	1,41	5,61E-04			1,032	0,570												
			DM14-5	1,33	7,60E-04			1,026	0,390												
			DM14-6	1,33	7,25E-04			1,025	0,730												
			DM14-7	1,27	6,47E-04			1,027	0,850												
			DM14-8	1,32	6,18E-04			1,022	0,430												
			DM14-9	1,31	1,02E-03			1,056	-0,020												
			DM14-10	1,39	9,87E-04			1,015	-0,440												
			average	1,33	9,66E-04	1,009	1,028	1,038	0,408	156,4	14,3	31,4	4,9	256,1	33,5	83,8	18,4	80			
				DM14-2	DM14-11	1,23	2,37E-04			1,036	0,860										
					DM14-12	1,19	5,41E-04			1,019	0,270										
					DM14-13A	1,05	2,97E-04			1,024	-0,030										
					DM14-13B	1,24	7,61E-04			1,030	0,620										
					DM14-14	1,26	2,92E-04			1,024	0,230										
					DM14-15	1,20	3,69E-04			1,024	0,770										
					DM14-16	1,30	5,23E-04			1,022	0,170										
					DM14-17	1,16	6,27E-04			1,013	0,100										
					DM14-18	1,31	7,18E-04			1,017	-0,060										
					DM14-19	1,37	1,15E-03			1,063	0,690										
					DM14-20	1,25	6,84E-04			1,055	0,670										
		DM14-21	1,27	8,38E-04			1,017	0,140													
		average	1,24	5,85E-04	1,007	1,021	1,028	0,368	153,7	27,0	38,1	11,1	328,9	63,0	16,5	9,9	5				

YAPILDAK	SE2	DM15-1	DM15-12A	1,51	2,61E-03			1,030	0,770													
			DM15-10C	1,50	2,56E-03			1,038	0,840													
			DM15-11	1,54	2,66E-03			1,039	0,910													
			DM15-4	1,58	3,04E-03			1,028	-0,140													
			DM15-6B	1,51	2,63E-03			1,031	0,920													
			DM15-2	1,56	2,63E-03			1,033	0,640													
			DM15-13	1,73	2,86E-03			1,032	0,730													
			DM15-7A	1,56	2,84E-03			1,033	0,730													
			DM15-3A	1,54	2,72E-03			1,031	0,740													
			DM15-14	1,68	2,72E-03			1,029	0,920													
			DM15-5A	1,59	2,75E-03			1,033	0,460													
			DM15-13	1,73	2,99E-03			1,025	0,730													
			average	1,59	2,75E-03	1,005	1,027	1,032	0,688	111,1	1,2	32,4	6,6	252,2	88,4	11,4	7,0	39				
				DM15-2	DM15-25B	1,88	2,49E-04			1,017	0,320											
					DM15-22B	1,84	2,69E-04			1,011	0,580											
					DM15-23	1,92	2,95E-04			1,012	0,920											
					DM15-21	1,86	2,85E-04			1,012	0,570											
					DM15-24A	1,85	2,54E-04			1,015	0,530											
					DM15-20A	1,74	2,72E-04			1,010	0,510											
					DM15-25A	2,00	3,22E-04			1,013	0,630											
					DM15-20B	1,76	2,80E-04			1,008	0,270											
					DM15-16A	1,97	2,86E-04			1,010	0,480											
					DM15-22A	1,90	2,86E-04			1,013	0,830											
					DM15-18	1,84	2,92E-04			1,011	0,410											
					DM15-17	1,84	2,69E-04			1,010	0,470											
		average	1,87	2,80E-04	1,003	1,009	1,012	0,547	296,6	2,9	34,4	7,9	97,0	86,9	14,3	4,7	20					

BAYAT	SE1	DM16	DM16-7B	1,48	1,07E-04			1,008	0,450											
			DM16-8B	1,52	1,39E-04			1,010	0,000											
			DM16-14B	1,49	1,39E-04			1,006	0,450											
			DM16-12B	1,57	1,56E-04			1,007	0,130											
			DM16-12A	1,61	1,52E-04			1,004	0,090											
			DM16-2A	1,71	1,52E-04			1,005	-0,700											
			DM16-4A	1,64	1,20E-04			1,002	-0,270											
			DM16-10A	1,52	1,36E-04			1,007	-0,040											
			DM16-9A	1,43	1,32E-04			1,008	0,640											
			DM16-3	1,47	1,12E-04			1,010	-0,020											
			DM16-1B	1,53	1,13E-04			1,004	0,270											
			DM16-14A	1,60	1,41E-04			1,007	0,130											
			DM16-13A	1,53	1,40E-04			1,011	-0,900											
			average	1,55	1,34E-04	1,003	1,003	1,007	0,018	279,2	2,9	61,8	30,0	183,6	62,7	31,0	14,1	84		
			GOKBAHCE	SE2	DM12	DM12-2A	2,50	1,95E-04			1,012	0,740								
DM12-2B	2,54	1,88E-04						1,011	0,800											
DM12-2C	2,56	1,81E-04						1,015	0,740											
DM12-2D	2,68	2,09E-04						1,014	0,920											
DM12-2E	2,44	1,92E-04						1,013	0,920											
DM12-2F	2,68	2,02E-04						1,015	0,910											
DM12-2G	2,87	2,18E-04						1,013	0,930											
DM12-2H	3,06	2,54E-04						1,021	0,500											
DM12-2I	2,82	2,22E-04						1,016	0,770											
DM12-2L	2,80	2,05E-04						1,013	0,970											
average	2,70	2,07E-04				1,001	1,013	1,014	0,820	27,4	3,6	26,6	7,0	282,6	76,0	9,9	5,3	75		
KARAAGAC	SE1	DM9	DM9-1A	1,25	2,54E-04			1,013	0,440											
			DM9-1C	1,44	2,45E-04			1,026	0,400											

		DM9-1E	1,34	2,51E-04		1,006	0,370										
		DM9-1H	1,57	2,59E-04		1,009	-0,060										
		DM9-1I	1,48	2,30E-04		1,013	-0,200										
		DM9-1N	1,50	2,93E-04		1,014	-0,870										
		DM9-1P	1,50	2,80E-04		1,008	0,170										
		DM9-1Q	1,48	3,23E-04		1,023	-0,650										
		DM9-1R	1,53	2,90E-04		1,011	-0,500										
		DM9-1S	1,43	3,10E-04		1,011	-0,380										
		DM9-1T	1,53	3,13E-04		1,007	-0,170										
		DM9-1Z	1,54	2,77E-04		1,009	0,110										
		average	1,47	2,77E-04	1,007	1,005	1,013	-0,112	62,9	6,9	14,5	7,2	324,2	51,8	46,4	8,3	81

Appendix 2 - Magnetic susceptibility and AMS data of the Incik, Sabuncu and Seydiler ignimbrites after data selection. Highlighted specimens are those whose density value does not fall within the range $-\sigma \leq \text{mean density} \leq +\sigma$, but have been anyway included to compute the statistics. Symbols: as in appendix 1.

Locality	Ignimbrite unit	Site	Specimen	Density (g/cm ³)	k (SI)	L (K ₁ /K ₂)	F (K ₂ /K ₃)	P (K ₁ /K ₃)	T	Magnetic lineation (K ₁)				Magnetic foliation pole (K ₃)				Θ angle (°)
										D (°)	I (°)	E ₁₋₂ (°)	E ₁₋₃ (°)	D (°)	I (°)	E ₃₋₂ (°)	E ₃₋₁ (°)	
AKCAKAYA	IN2	AK1	AK1-6	1,51	1,11E-03			1,022	-0,250									
			AK1-1	1,49	1,28E-03			1,012	0,740									
			AK1-9	1,55	1,02E-03			1,015	-0,470									
			AK1-4	1,52	9,70E-04			1,034	0,070									
			AK1-3	1,56	1,14E-03			1,028	0,160									
			average		1,11E-03	1,011	1,011	1,022	0,050	74,4	6,6	22,3	4,6	333,7	57,9	20,6	11,6	79
SEYDIKOY	SA2	AK2-1	AK2-3	1,07	5,98E-04			1,024	0,180									
			AK2-1	1,11	5,62E-04			1,024	0,550									
			AK2-6	1,18	5,12E-04			1,014	0,040									
			AK2-2	1,05	6,08E-04			1,028	0,060									
			AK2-4	1,13	6,36E-04			1,020	-0,270									
			average		5,83E-04	1,009	1,012	1,022	0,112	35,1	13,3	40,6	9,5	202,6	76,4	10,5	7,1	13
INCIK	IN1a	AK4	AK4-2B	1,58	3,48E-05			1,008	-0,450									
			AK4-8B	1,54	3,29E-05			1,005	-0,740									
			AK4-5A	1,57	3,72E-05			1,010	-0,690									
			AK4-10C	1,56	3,71E-05			1,004	0,160									
			AK4-7A	1,51	3,57E-05			1,013	0,250									
			AK4-2C	1,54	3,21E-05			1,010	-0,590									
			AK4-9A	1,58	4,14E-05			1,005	0,680									
			AK4-9B	1,55	3,81E-05			1,006	-0,100									
average		3,61E-05	1,005	1,003	1,008	-0,182	46,0	47,7	10,4	6,7	170,6	27,3	64,9	7,8	55			
AKKAYA	IN1c	AK5-1	AK5-6A	1,18	9,81E-04			1,011	0,050									
			AK5-7A	1,25	9,31E-04			1,014	0,480									

			AK5-8	1,20	9,20E-04			1,018	0,280									
			AK5-10A	1,23	9,01E-04			1,016	0,720									
			AK5-11B	1,19	9,21E-04			1,016	-0,210									
			AK5-13A	1,19	9,58E-04			1,021	0,630									
			AK5-10B	1,23	1,20E-03			1,015	0,790									
			AK5-6B	1,22	9,42E-04			1,015	0,650									
			AK5-11A	1,25	9,40E-04			1,017	0,120									
			average		9,66E-04	1,005	1,011	1,016	0,398	83,5	21,3	18,9	5,2	255,8	68,5	10,6	4,9	8
		AK5-2	AK5-19A	1,24	1,09E-03			1,015	-0,100									
			AK5-16	1,16	1,01E-03			1,020	0,560									
			AK5-17	1,27	1,04E-03			1,013	0,200									
			AK5-18	1,18	8,50E-04			1,012	0,590									
			AK5-25	1,14	9,75E-04			1,016	0,210									
			AK5-19B	1,25	9,35E-04			1,019	-0,210									
			AK5-20	1,26	1,00E-03			1,015	0,740									
			AK5-23	1,26	1,13E-03			1,011	0,390									
			average		1,00E-03	1,005	1,010	1,015	0,304	311,8	1,9	48,5	10,0	216,9	68,7	14,4	7,9	85
ASAGI KALABAK	IN1c	AK6	AK6-5	1,45	9,74E-04			1,014	0,270									
			AK6-8	1,48	1,16E-03			1,012	-0,340									
			AK6-11	1,38	1,00E-03			1,007	0,730									
			AK6-6	1,36	1,09E-03			1,006	-0,180									
			AK6-7	1,43	1,03E-03			1,008	-0,450									
			average	1,42	1,05E-03	1,005	1,005	1,009	0,017	71,4	44,5	36,3	14,6	271,4	43,8	68,5	28,6	20
ASAGI CAGLAN	IN1c	AK7	AK7-3B	1,53	1,22E-03			1,018	0,600									
			AK7-12A	1,46	1,00E-03			1,008	0,830									
			AK7-5	1,45	8,69E-04			1,015	-0,220									

			AK7-2B	1,45	1,01E-03				1,019	0,790											
			AK7-11	1,43	8,97E-04				1,018	0,320											
			AK7-10B	1,48	1,11E-03				1,017	-0,240											
			AK7-8	1,54	1,12E-03				1,018	-0,120											
			AK7-1A	1,44	1,05E-03				1,012	0,810											
			AK7-2C	1,52	9,95E-04				1,017	-0,380											
			AK7-9A	1,41	1,11E-03				1,020	-0,510											
			average		1,04E-03	1,007	1,009		1,016	0,192	241,0	11,2	40,0	6,5	88,9	77,4	22,3	6,6	28		
GOCERI	IN1c	AK3	AK3-6	1,39	8,31E-04				1,011	0,750											
			AK3-10B	1,43	9,17E-04					1,021	0,270										
			AK3-1	1,28	6,95E-04					1,016	0,350										
			AK3-7	1,45	7,71E-04					1,014	0,630										
			AK3-8	1,40	8,33E-04					1,015	0,140										
			average		8,09E-04	1,005	1,011			1,015	0,428	63,8	22,1	53,0	16,3	277,2	64,0	16,4	5,0	33	
	IN2	DM4-1	DM4-9A	1,41	2,68E-04				1,022	0,730											
			DM4-6	1,52	3,20E-04					1,013	-0,040										
			DM4-1B	1,46	3,15E-04					1,016	-0,290										
			DM4-2A	1,37	2,63E-04					1,028	-0,240										
			DM4-4	1,47	3,40E-04					1,027	-0,130										
			DM4-3	1,49	3,26E-04					1,031	0,470										
			DM4-1A	1,45	3,38E-04					1,033	-0,550										
			DM4-5	1,47	3,81E-04					1,025	-0,240										
			DM4-2B	1,48	2,84E-04					1,015	-0,840										
			average		3,15E-04	1,013	1,010			1,023	-0,126	90,0	16,3	26,2	13,0	264,6	73,6	24,6	8,5	5	
	SA1	DM4-2	DM4-14B	1,52	2,10E-04				1,023	0,510											

			DM4-13	1,41	2,15E-04			1,026	0,500										
			DM4-16	1,54	2,61E-04			1,020	-0,110										
			DM4-17	1,43	3,49E-04			1,029	0,170										
			DM4-19	1,58	3,04E-04			1,041	0,210										
			average		2,68E-04	1,010	1,017	1,028	0,256	257,4	4,0	48,1	11,6	356,4	65,6	32,1	11,1	81	
DEMIRLI	SE2	DM1	DM1-1A	1,98	2,33E-03			1,018	0,260										
			DM1-1B	2,00	2,09E-03			1,022	0,320										
			DM1-2	1,82	2,31E-03			1,018	0,770										
			DM1-3A	1,95	2,52E-03			1,017	0,560										
			DM1-4	1,97	2,99E-03			1,022	0,730										
			DM1-5A	1,96	2,90E-03			1,021	0,700										
			DM1-5B	1,90	2,97E-03			1,016	0,680										
			average		2,59E-03	1,004	1,015	1,019	0,574	268,1	1,7	29,0	2,8	14,2	83,9	4,3	0,9	74	
UCLERKAYASI	SE2	DM3	DM3-1	1,76	2,98E-04			1,010	0,450										
			DM3-3	1,82	3,76E-04			1,013	-0,130										
			DM3-4	1,66	2,89E-04			1,009	0,680										
			DM3-6	1,88	3,63E-04			1,012	0,640										
			DM3-7	1,83	3,67E-04			1,019	0,000										
			DM3-8	1,81	4,41E-04			1,012	0,860										
			DM3-9	1,85	4,40E-04			1,021	0,550										
			average		3,67E-04	1,004	1,010	1,014	0,436	276,8	1,3	38,3	9,5	175,3	83,3	14,4	8,7	79	
BAYRAMALILER	SE2	DM2	DM2-1	1,34	1,12E-03			1,013	0,080										
			DM2-2	1,49	1,13E-03			1,010	0,090										
			DM2-4	1,22	1,09E-03			1,015	0,350										
			DM2-5	1,27	1,17E-03			1,013	0,310										
			DM2-7	1,46	1,33E-03			1,012	0,260										
			average		1,17E-03	1,005	1,008	1,013	0,218	91,9	6,5	32,0	7,5	320,2	80,3	13,7	8,4	48	

OVACIK	SE1	DM5-1	DM5-8	1,39	1,57E-04			1,032	0,000												
			DM5-5	1,34	2,08E-04			1,005	0,070												
			DM5-9A	1,41	1,84E-04			1,032	0,450												
			DM5-10	1,40	1,34E-04			1,025	0,740												
			DM5-11B	1,30	1,65E-04			1,028	0,500												
			DM5-2	1,34	4,69E-05			1,010	-0,160												
			DM5-9B	1,26	1,59E-04			1,038	0,580												
			DM5-4	1,39	7,00E-05			1,014	0,100												
			DM5-3B	1,25	4,39E-05			1,015	0,220												
			DM5-1B	1,38	6,80E-05			1,019	0,460												
			DM5-6B	1,28	1,41E-04			1,019	0,890												
			DM5-6A	1,28	1,30E-04			1,018	0,260												
			DM5-7B	1,28	1,82E-04			1,046	0,430												
			average		1,30E-04	1,007	1,016	1,023	0,349	168,3	14,4	49,5	12,3	322,2	74,0	15,1	10,8	26			
		SE1	DM5-2	DM5-16	1,41	6,01E-04			1,049	0,420											
	DM5-17			1,40	5,55E-04			1,041	0,490												
	DM5-19			1,47	5,97E-04			1,036	0,310												
	DM5-20			1,55	5,77E-04			1,031	0,770												
	DM5-13			1,48	5,38E-04			1,032	0,920												
DM5-14	1,38			5,39E-04			1,038	0,000													
DM5-12	1,37			6,37E-04			1,046	-0,150													
average				5,77E-04	1,012	1,026	1,039	0,394	163,6	22,2	50,3	6,5	349,2	67,7	10,0	6,9	6				
KAYIHAN	SE1	DM6-1	DM6-8	1,62	6,86E-04			1,021	0,920												
			DM6-9	1,66	8,06E-04			1,016	0,860												
			DM6-7	1,69	9,41E-04			1,044	0,440												
			DM6-4	1,58	6,73E-04			1,020	0,600												

			DM6-1	1,56	8,21E-04			1,016	-0,160									
			DM6-2A	1,68	5,59E-04			1,018	0,190									
			DM6-6A	1,59	4,85E-04			1,011	0,000									
			DM6-5	1,63	5,48E-04			1,009	-0,040									
			DM6-6B	1,54	5,86E-04			1,012	0,100									
			DM6-10	1,56	7,04E-04			1,016	-0,170									
			average		6,81E-04	1,005	1,013	1,018	0,274	334,0	9,4	37,9	7,8	149,9	80,6	17,3	7,4	4
		DM6-2																
			DM6-14	1,71	2,54E-04			1,098	0,273									
			DM6-13	1,55	1,49E-04			1,017	-0,007									
			DM6-11	1,62	3,62E-04			1,037	0,346									
			DM6-12	1,65	1,79E-04			1,013	0,510									
			average	1,63	2,36E-04	1,015	1,026	1,041	0,280	31,0	12,2	25,8	5,3	123,1	9,6	60,9	14,0	88
KUMBET	SE2	DM7	DM7-8	1,63	2,85E-03			1,035	0,600									
			DM7-7	1,62	2,81E-03			1,033	0,660									
			DM7-1	1,60	2,47E-03			1,047	0,840									
			DM7-4	1,61	2,48E-03			1,031	0,920									
			DM7-3	1,59	2,36E-03			1,038	0,460									
			average		2,60E-03	1,006	1,030	1,037	0,696	187,8	21,3	14,5	6,9	332,1	64,4	7,5	6,5	36
YESILYAYLA	SE1	DM8-1	DM8-3A	1,19	4,01E-05			1,011	-0,550									
			DM8-3B	1,21	4,13E-05			1,011	0,900									
			DM8-5	1,17	3,85E-05			1,008	-0,750									
			DM8-6	1,23	4,40E-05			1,012	-0,370									
			DM8-7	1,15	3,77E-05			1,008	-0,200									
			DM8-8	1,13	3,64E-05			1,009	-0,100									
			average		3,97E-05	1,006	1,004	1,010	-0,172	303,1	49,9	33,8	7,2	117,9	40,0	44,5	13,4	5

KALE	SE2	DM8-2	DM8-12	1,68	4,65E-04			1,045	0,750											
			DM8-13	1,70	4,63E-04			1,042	0,860											
			DM8-16A	1,59	4,66E-04			1,039	0,840											
			DM8-17A	1,74	5,02E-04			1,032	0,900											
			DM8-18A	1,65	5,17E-04			1,031	0,910											
			DM8-18B	1,64	4,66E-04			1,032	0,940											
			DM8-19A	1,57	5,85E-04			1,036	0,610											
			average		4,95E-04	1,003	1,033	1,037	0,830	206,3	4,7	60,6	5,7	21,8	85,3	5,9	3,9	5		
	SE1	DM10-1	DM10-2	1,43	6,52E-05			1,030	0,290											
			DM10-3	1,48	6,64E-05			1,018	0,560											
			DM10-4	1,33	6,34E-05			1,023	0,420											
			DM10-5	1,37	5,91E-05			1,017	0,640											
			DM10-6	1,38	6,27E-05			1,018	0,430											
			average		6,33E-05	1,006	1,015	1,021	0,470	250,1	16,0	31,2	6,7	346,1	19,9	11,9	5,6	84		
	SE2	DM10-2	DM10-9A	1,21	5,78E-05			1,014	0,740											
			DM10-9C	1,23	5,38E-05			1,013	-0,560											
			DM10-9D	1,25	6,29E-05			1,021	-0,290											
			DM10-9E	1,28	5,74E-05			1,005	0,570											
			DM10-9F	1,23	5,60E-05			1,014	-0,540											
			DM10-9G	1,21	5,31E-05			1,014	-0,220											
		average		5,68E-05	1,008	1,006	1,014	-0,185	199,9	8,1	45,7	10,6	303,1	57,9	49,8	30,1	77			
DM10-3		DM10-10A	1,43	7,51E-05			1,009	0,800												
		DM10-10B	1,41	1,18E-04			1,005	0,610												
		DM10-10C	1,11	6,88E-05			1,031	-0,580												
	DM10-10D	1,36	7,70E-05			1,011	0,200													

			DM10-10E	1,23	7,45E-05			1,015	-0,370											
			average		8,27E-05	1,008	1,006	1,014	0,132	97,2	54,1	62,7	41,0	275,8	35,9	51,3	11,3	1		
DOGER	SE2	DM11-1	DM11-6	1,64	2,75E-03			1,035	0,620											
			DM11-9	1,55	2,64E-03			1,031	0,720											
			DM11-3	1,59	2,89E-03			1,031	0,710											
			DM11-4A	1,61	2,69E-03			1,027	0,810											
			DM11-5B	1,60	2,66E-03			1,027	0,670											
			DM11-8B	1,55	2,69E-03			1,035	0,680											
			DM11-11	1,57	2,56E-03			1,030	0,890											
			average		2,70E-03	1,004	1,026	1,031	0,724	123,2	10,3	11,1	3,7	319,7	79,3	3,9	2,0	17		
				DM11-2a	DM11-14	1,55	2,99E-03			1,031	0,000									
					DM11-15B	1,56	2,48E-03			1,027	0,690									
					DM11-17A	1,51	2,44E-03			1,022	0,380									
					DM11-16	1,47	2,31E-03			1,030	0,440									
					DM11-18B	1,55	2,49E-03			1,026	0,570									
					average		2,54E-03	1,008	1,019	1,027	0,413	129,0	1,9	12,5	3,8	241,3	85,0	15,5	4,2	68
				DM11-2b	DM11-21	1,48	2,43E-03			1,023	0,670									
					DM11-23	1,42	2,35E-03			1,023	0,480									
					DM11-19	1,47	2,47E-03			1,031	0,670									
					DM11-20	1,54	2,65E-03			1,031	0,960									
					DM11-22	1,42	2,36E-03			1,029	0,730									
		average	1,47		2,45E-03	1,004	1,023	1,027	0,705E	123,8	10,3	19,6	2,8	348,0	75,7	8,4	2,8	44		
KARAKAYA	SE1	DM13-1	DM13-1	1,68	5,55E-05			1,009	-0,690											
			DM13-2	1,86	5,69E-05			1,004	0,250											
			DM13-3	1,75	7,41E-05			1,006	0,460											

			DM13-4	1,70	6,35E-05			1,004	-0,590										
			DM13-6	1,72	6,90E-05			1,004	-0,040										
			DM13-7A	1,72	7,46E-05			1,002	-0,180										
			DM13-9A	1,76	6,25E-05			1,004	-0,800										
			average		6,51E-05	1,003	1,002	1,005	-0,224	326,1	53,7	32,3	13,6	205,8	20,4	45,9	28,7	60	
		DM13-2	DM13-11	1,29	8,54E-05			1,005	0,097										
			DM13-12	1,44	8,36E-05			1,005	0,411										
			DM13-13	1,35	8,03E-05			1,007	-0,120										
			DM13-14	1,28	7,73E-05			1,012	-0,517										
			average	1,34	8,17E-05	1,004	1,003	1,007	-0,032	99,4	34,9	28,2	7,5	258,6	53,3	38,7	18,2	21	
CUKURCA	SE2	DM14-1	DM14-5	1,33	7,60E-04			1,026	0,390										
			DM14-6	1,33	7,25E-04			1,025	0,730										
			DM14-7	1,27	6,47E-04			1,027	0,850										
			DM14-8	1,32	6,18E-04			1,022	0,430										
			DM14-9	1,31	1,02E-03			1,056	-0,020										
			DM14-10	1,39	9,87E-04			1,015	-0,440										
			average		7,89E-04	1,010	1,018	1,028	0,325	139,4	16,3	13,1	2,8	285,1	70,6	13,7	3,5	34	
		DM14-2	DM14-11	1,23	2,37E-04			1,036	0,860										
			DM14-12	1,19	5,41E-04			1,019	0,270										
			DM14-13B	1,24	7,61E-04			1,030	0,620										
			DM14-14	1,26	2,92E-04			1,024	0,230										
			DM14-15	1,20	3,69E-04			1,024	0,770										
			DM14-16	1,30	5,23E-04			1,022	0,170										
			DM14-17	1,16	6,27E-04			1,013	0,100										
			DM14-18	1,31	7,18E-04			1,017	-0,060										

			DM14-20	1,25	6,84E-04			1,055	0,670										
			DM14-21	1,27	8,38E-04			1,017	0,140										
			average		5,58E-04	1,007	1,019	1,026	0,376	138,5	25,6	41,6	10,0	338,0	63,1	15,3	8,9	20	
YAPILDAK	SE2	DM15-1	DM15-12A	1,51	2,61E-03			1,030	0,770										
			DM15-11	1,54	2,66E-03			1,039	0,910										
			DM15-4	1,58	3,04E-03			1,028	-0,140										
			DM15-6B	1,51	2,63E-03			1,031	0,920										
			DM15-2	1,56	2,63E-03			1,033	0,640										
			DM15-7A	1,56	2,84E-03			1,033	0,730										
			DM15-3A	1,54	2,72E-03			1,031	0,740										
			DM15-5A	1,59	2,75E-03			1,033	0,460										
			average		2,73E-03	1,006	1,026	1,032	0,629	96,6	2,9	16,6	4,7	231,1	85,8	6,7	2,1	46	
		DM15-2	DM15-25B	1,88	2,49E-04			1,017	0,320										
			DM15-22B	1,84	2,69E-04			1,011	0,580										
			DM15-23	1,92	2,95E-04			1,012	0,920										
			DM15-21	1,86	2,85E-04			1,012	0,570										
			DM15-24A	1,85	2,54E-04			1,015	0,530										
			DM15-22A	1,90	2,86E-04			1,013	0,830										
DM15-18	1,84		2,92E-04			1,011	0,410												
DM15-17	1,84		2,69E-04			1,010	0,470												
average		2,75E-04	1,003	1,010	1,013	0,579	288,5	4,9	29,5	8,0	121,9	85,0	15,7	4,5	13				
BAYAT	SE1	DM16	DM16-7B	1,48	1,07E-04			1,008	0,450										
			DM16-8B	1,52	1,39E-04			1,010	0,000										
			DM16-14B	1,49	1,39E-04			1,006	0,450										
			DM16-12B	1,57	1,56E-04			1,007	0,130										
			DM16-12A	1,61	1,52E-04			1,004	0,090										

			DM16-10A	1,52	1,36E-04			1,007	-0,040										
			DM16-3	1,47	1,12E-04			1,010	-0,020										
			DM16-1B	1,53	1,13E-04			1,004	0,270										
			DM16-14A	1,60	1,41E-04			1,007	0,130										
			DM16-13A	1,53	1,40E-04			1,011	-0,900										
			average		1,33E-04	1,004	1,004	1,007	0,055	282,6	6,6	62,4	26,6	180,3	61,5	28,6	12,8	78	
GOKBAHCE	SE2	DM12	DM12-2A	2,50	1,95E-04			1,012	0,740										
			DM12-2B	2,54	1,88E-04			1,011	0,800										
			DM12-2C	2,56	1,81E-04			1,015	0,740										
			DM12-2D	2,68	2,09E-04			1,014	0,920										
			DM12-2F	2,68	2,02E-04			1,015	0,910										
			DM12-2G	2,87	2,18E-04			1,013	0,930										
			DM12-2I	2,82	2,22E-04			1,016	0,770										
			DM12-2L	2,80	2,05E-04			1,013	0,970										
			average		2,02E-04	1,001	1,013	1,014	0,847	24,0	5,3	42,5	6,4	271,6	76,2	10,1	5,4	68	
KARAAGAC	SE1	DM9	DM9-1C	1,44	2,45E-04			1,026	0,400										
			DM9-1I	1,48	2,30E-04			1,013	-0,200										
			DM9-1N	1,50	2,93E-04			1,014	-0,870										
			DM9-1P	1,50	2,80E-04			1,008	0,170										
			DM9-1Q	1,48	3,23E-04			1,023	-0,650										
			DM9-1R	1,53	2,90E-04			1,011	-0,500										
			DM9-1S	1,43	3,10E-04			1,011	-0,380										
			DM9-1T	1,53	3,13E-04			1,007	-0,170										
			DM9-1Z	1,54	2,77E-04			1,009	0,110										
			average		2,85E-04	1,008	1,005	1,014	-0,232	63,2	5,0	15,2	6,5	329,9	32,8	34,4	5,9	87	

Appendix 3 - Magnetic susceptibility and AIRM data of the Incik and Sabuncu ignimbrites. Symbols: as in annex 1

Locality	Ignimbrite unit	Site	Specimen	k (SI)	L (K ₁ /K ₂)	F (K ₂ /K ₃)	P (K ₁ /K ₃)	T	Magnetic lineation (K ₁)				Magnetic foliation pole (K ₃)							
									D (°)	I (°)	E ₁₋₂ (°)	E ₁₋₃ (°)	D (°)	I (°)	E ₃₋₂ (°)	E ₃₋₁ (°)				
AKCAKAYA	IN2	AK1	AK1-1	1.76E-04			1.223	0.210												
			AK1-2	1.24E-04			1.243	0.156												
			AK1-5	1.39E-04			1.165	0.409												
			AK1-6	1.19E-04			2.172	0.198												
			AK1-7	1.34E-04			1.092	0.328												
			AK1-9	1.36E-04			1.089	-0.617												
			average	1.38E-04	1.115	1.174	1.331	0.114	106.9	37.8	28.4	4.8	10.3	8.4	45.7	5.7				
INCIK	IN1a	AK4	AK4-10C	1.62E-06			2.363	0.926												
			AK4-2B	1.65E-06			1.121	-0.327												
			AK4-2C	2.93E-03			1.070	-0.365												
			AK4-9A	1.97E-06			1.109	0.321												
			AK4-9B	1.71E-06			1.111	0.236												
			average	5.88E-04	1.047	1.298	1.355	0.158	18.5	36.6	16.0	4.4	271.6	21.4	17.0	4.1				
AKKAYA	IN1c	AK5-2	AK5-16	1.29E-04			1.173	-0.724												
			AK5-17	1.31E-04			1.026	-0.734												
			AK5-19B	1.15E-04			1.198	0.344												
			AK5-20	1.19E-04			1.330	0.482												
			AK5-25	1.24E-04			1.155	0.558												
			average	1.24E-04	1.068	1.102	1.177	-0.015	83.3	30.2	26.4	13.2	237.4	57.1	56.7	12.1				
GOCERI	SA1	DM4-2	DM4-11	3.40E-05			1.090	0.976												
			DM4-13	2.93E-05			1.171	0.376												
			DM4-14A	3.60E-05			1.261	0.659												
			DM4-15A	3.69E-05			1.204	-0.248												

			DM4-16	3.62E-05			1.297	0.479											
			DM4-18	3.64E-05			1.212	-0.439											

Acknowledgements

Foremost, I would like to express my sincere gratitude to my tutor Elena Zanella, who offered her continuous advices and encouragements throughout the course of this thesis, and worked to stimulate the international aspect of the project. I am thankful to her professionalism and extreme patience in explaining the arduous concepts in a very clear way, training me in the scientific field... As well to her providential energetic breaks of “*focaccia ligure*”!

My sincere thanks go to my co-tutor Jean-Luc Le Pennec, who introduced me into the exciting and challenging world of volcanology and kept on carrying me through it during these three years. I won't never forget his extraordinary ability to transmit preparation and passion for this subject, as well his constant presence and availability to share and compare scientific ideas in order to improve my formation. The field work performed during these years represented for me not only a merely high quality-science formative experience, but also an unforgettable experience of life made up by many moments of conversation, confrontation and smiles.

Special thanks to Abidin Temel, who helped in the organization of the field work and gave a strong effort in the good result of the project with his experience in geochemical topics and his precious contacts with many universities in Turkey.

I am very thankful to Michael Ort and Roberto Sulpizio for the time they spent to revise my thesis and for their precious suggestions which have been useful to improve the quality of my research.

I want to thank everyone who collaborated to help me in the laboratory: Jean-Louis Paquette in Clermont-Ferrand and Hervé Guillou in Paris for the geochronologic datings, and Evdokia Tema in Torino for the magnetic analyses.

A special thank goes also to my Turkish friends who supported me during the whole time spent for the field work, treating me much more than a guest. Thanks to Ahmet, Turgut, Derya and Canan from the Çakmak Marble hotel in Afyon; Ahmet and Saffet from the Otel Sultan in Eskişehir and especially Ali, Esra, Elif, Emine and Fatih from Papağan restaurant in Eskişehir because their hospitality really made me feel like at home: *çok teşekkürler!*

Thanks to Giulia for her continuous support and for the time spent together which has always the power to turn me happy in every moment!

Tanks to my friend Niccolò who has been like a brother during these years. Our crazy out-of-route trips during these years gave me the needful energy to go ahead with the thesis!

A special thanks to Moreno and Sara, whose friendship has been very precious and their presence made me smile many times!

Many thanks also to my special university friends Erica and Loretta, my cousin Gabriele and all my friends who supported me through these years.

Last but not the least, I would like to thank my parents for their continuous support and encouragement throughout my life.

Riassunto

Tale ricerca ha come oggetto la correlazione e la localizzazione delle aree sorgenti di diverse unità ignimbriche attraverso uno studio di terreno, paleomagnetico e di magnetismo delle rocce sui depositi ignimbrici appartenenti a due grandi complessi silicici ubicati in due diverse regioni della Turchia: la regione della Cappadocia (Anatolia centrale), ove sono stati effettuati numerosi studi precedenti, e la regione di Afyon-Eskişehir, finora poco studiata circa la stratigrafia dei depositi piroclastici.

La ricerca effettuata sull'ignimbrite di Kızılkaya (regione della Cappadocia), di età tardo miocenica, è consistita in uno studio stratigrafico del segnale magnetico all'interno dell'unità ignimbrica, considerata essere un'unica unità di messa in posto e di raffreddamento. La magnetizzazione rimanente, il fabric magnetico (AMS, AIRM e AARM) e la mineralogia magnetica sono stati investigati presso 35 siti appartenenti a 7 località ubicate a diversa distanza dalla presunta area sorgente secondo Le Pennec et al. (1998) e a differenti altezze stratigrafiche, per un totale di 444 provini. La magnetizzazione rimanente non si presenta verticalmente omogenea all'interno del deposito. Sono stati riconosciuti due diversi casi: (1) la presenza di una TRM stabile, la cui direzione è consistente con quella riscontrata precedentemente in letteratura (Piper et al., 2002) e (2) la presenza di due componenti di magnetizzazione caratterizzate da temperature di blocco e spettri di coercitività sovrapposti. Tali situazioni sono state imputate rispettivamente alla presenza di sola Ti-magnetite primaria, e alla presenza contemporanea di Ti-magnetite e fasi magnetiche secondarie (Ti-magnetite alterata e/o ematite). Anche il fabric dell'AMS varia verticalmente all'interno del deposito; tenendo in considerazione l'angolo formato tra la direzione della lineazione magnetica K1 ed il polo della foliazione magnetica K3, sono stati riscontrati tre diversi tipi di fabric: normale, obliquo e trasversale. In seguito ad aver verificato l'origine primaria del fabric magnetico, i fabric dell'AMS sono stati selezionati, al fine di migliorarne la qualità, scartando i provini le cui densità ricadessero al di fuori dell'intervallo $\pm 1\sigma$ dal valore di densità medio del sito. Ciò ha comportato la scomparsa dei fabric obliqui, la cui origine è stata imputata all'orientazione dovuta alla presenza locale di concentrazioni anomale di clasti di pomice e litici all'interno del provino. Le misure di AIRM e AARM hanno evidenziato che la Ti-magnetite di tipo MD è la fase magnetica principale che origina il fabric, confermando quindi che il fabric magnetico può essere utilizzato come elemento per la determinazione delle direzioni di flusso.

L'investigazione della successione ignimbrica esposta nella regione di Afyon-Eskişehir, di età compresa tra il Miocene inferiore e Miocene superiore, è consistita in uno studio stratigrafico-sedimentologico e di magnetismo delle rocce dei depositi ignimbrici su un'area di circa 14,300 km², al fine di localizzare l'area sorgente attraverso la combinazione delle direzioni di flusso ottenute dai dati di terreno e magnetici. Le misure stratigrafiche, effettuate presso 76 località, hanno permesso la realizzazione di mappe delle isopache ed isoplete e la correlazione delle varie unità ignimbriche. La successione ignimbrica è costituita dai prodotti di almeno tre eruzioni (ignimbriti di Incik, Sabuncu e Seydiler), distinti per età, distribuzione areale, struttura e tessitura dei depositi. Lo studio magnetico è consistito in analisi di mineralogia magnetica e di fabric magnetico (AMS e AIRM). Il campionamento è stato effettuato presso 22 località in 36 siti ubicati a diverse altezze stratigrafiche, per un totale di 600 provini. Sia i dati di terreno che quelli derivanti dall'analisi di fabric magnetico, indicano la presenza di due diverse aree sorgenti. Quella relativa alle ignimbriti di Incik e Sabuncu è stata identificata con la caldera di Kırka, un'area vasta circa 20 x 20 km in cui è stata riscontrata la presenza di un duomo risorgente; l'area sorgente delle ignimbriti di Seydiler, invece, è stata individuata in prossimità del villaggio di Bayat. Il volume dei depositi è stato calcolato sulla base dei dati di terreno. L'indice VEI è 7 per le ignimbriti di Incik e Seydiler, 6 per l'ignimbrite di Sabuncu; tali valori sono indice di eruzioni di tipi pliniano. I corrispondenti valori della magnitudo M (Pyle, 2000) sono 7 per tutte e tre le ignimbriti.

Résumé

Cette recherche exploite une combinaison de techniques de terrain, paléomagnétiques et de magnétisme des roches pour corréler et localiser la source de plusieurs ignimbrites de deux régions de Turquie qui appartiennent à deux grands systèmes acides: la région du Cappadoce (Anatolie centrale), qui a été précédemment étudiée par plusieurs auteurs, et la région de Afyon-Eskişehir (Anatolie occidentale), jusqu'à présent peu étudiée.

L'examen de l'ignimbrite de Kızılkaya (région du Cappadoce), d'âge Miocène supérieur, a consisté en une étude stratigraphique et de magnétisme des roches de l'unité ignimbritique, qui est considérée comme une seule unité d'écoulement et de refroidissement. La magnétisation rémanente, la fabrique magnétique (AMS, AIRM et AARM) et la minéralogie magnétique ont été analysées pour 35 sites de 7 localités situées à des distances différentes de la source supposée par Le Pennec et al. (1998) et à différentes hauteurs stratigraphiques, pour un total de 444 spécimens. La signature magnétique rémanente n'est pas verticalement homogène dans les dépôts. Deux cas sont distingués: (1) une TRM stable, dont la direction est conforme aux données de la littérature précédente (Piper et al., 2002) et (2) deux composantes de magnétisation caractérisées par une température de blocage et des spectres de coercivité se recouvrant. Ces situations ont été enregistrées respectivement en présence d'un Ti-magnétite primaire, et en présence simultanée de Ti-magnétite et de phases magnétiques secondaires (Ti-magnétite altérée et/ou hématite). La fabrique AMS varie verticalement dans le dépôt, en fonction de l'angle entre la direction de la linéation magnétique K1 et du pôle de la foliation magnétique K3, trois types de fabriques ont été caractérisées: normale, oblique et transversale. Après avoir démontré l'origine primaire de la fabrique magnétique, l'AMS a été accentuée par élimination des échantillons caractérisés par des valeurs de densité différentes de plus de $\pm 1\sigma$ de la valeur moyenne du site. Cette opération s'est traduite par l'élimination des fabriques obliques, qui sont interprétées par la présence locale de fragments de ponces et clastes lithiques dans les échantillons. Les données d'AIRM et AARM indiquent que la Ti-magnétite MD est le principal minéral magnétique porteur de la fabrique, ce que suggère que la fabrique magnétique peut être utilisée pour déterminer les directions d'écoulement.

L'examen de la succession ignimbritique d'âge Miocène précoce-Miocène supérieur, exposée sur une zone de $\approx 14\ 300$ km² dans la région d'Afyon-Eskişehir, a consisté en une étude stratigraphique-sédimentologique et de magnétisme des roches, afin de localiser la source des ignimbrites en combinant les données du terrain avec les directions de fabrique magnétique. La mesure des sections stratigraphiques, qui ont été réalisées pour 76 localités, conduit aux corrélations stratigraphiques et à la production de cartes d'isopaques et d'isoplètes. La succession ignimbritique est constituée d'au moins trois éruptions majeures distinctes qui ont produit les ignimbrites de Incik, Sabuncu et Seydiler, différentes en âge, distribution, structure et caractéristiques texturales des dépôts. L'étude magnétique consistait en analyses de la minéralogie magnétique et de la fabrique magnétique (AMS et AIRM), qui a été déterminée pour 22 localités sur un total de 36 sites à différentes hauteurs stratigraphiques, soit 600 spécimens. Les données de terrain et les résultats de la fabrique magnétique indiquent deux zones sources. La source des ignimbrites de Incik et Sabuncu est identifiée dans la caldeira de Kırka, une vaste zone de $\approx 20 \times 20$ km de diamètre, où la présence d'un dôme résurgent a été détectée. La source de l'ignimbrite de Seydiler est identifiée à proximité du village de Bayat. Les calculs de volume, réalisés sur la base de données de terrain, révèlent un indice de VEI 7 pour les ignimbrites de Incik et Seydiler, et un indice VEI 6 pour l'ignimbrite de Sabuncu, caractérisant les éruptions pliniennes au sens large. La magnitude correspondante M (Pyle, 2000) est supérieure à 7 pour toutes les ignimbrites étudiées.

Abstract

This research exploits a combination of field, paleomagnetic and rock-magnetic techniques to correlate and locate the source and investigate several ignimbrites from two selected regions of Turkey, belonging to two large silicic ignimbrite systems: the well-investigated Cappadocia region (central Anatolia) and the poorly studied Afyon-Eskişehir region (western Anatolia).

Investigation of the Upper Miocene Kızılıkaya ignimbrite (Cappadocia region) consisted in a stratigraphic rock-magnetic study of the ignimbrite unit, which is considered to be a single flow and cooling unit. Remanent magnetization, magnetic fabric (AMS, AIRM and AARM) and magnetic mineralogy investigations were performed at 35 sites in 7 areal distributed localities at different distance from the vent position inferred by Le Pennec et al. (1998) and different stratigraphic heights, for a total of 444 specimens. Magnetic remanences are not vertically homogenous through the deposits. Two cases are distinguished: (1) a stable TRM, whose direction is consistent with previous literature data (Piper et al., 2002) and (2) two magnetization components with overlapping blocking temperature and coercivity spectra. These situations have been referred respectively to the occurrence of only primary Ti-magnetite, and primary Ti-magnetite plus secondary magnetic phases (altered Ti-magnetite and/or hematite). The AMS fabric varies vertically throughout the deposit; based on the angle between the direction of the magnetic lineation K_1 and that of the foliation plunge K_3 , three types of fabric are evidenced: normal, oblique and transverse. After having attested a primary origin of the magnetic fabric, the AMS was firstly enhanced by discarding all specimens whose density values differ more than $\pm 1\sigma$ from the site mean value. This resulted in the elimination of the oblique fabrics, which are interpreted as an orientation disturbance due to local occurrence of pumices and lithic clasts in the specimens. Measurement of the AIRM and AARM pointed out that MD Ti-magnetite is the main carrier of the fabric, which suggests that the magnetic fabric is a reliable proxy for flow directions.

Investigation of the Early-Upper Miocene ignimbrite succession exposed in the region of Afyon-Eskişehir consisted in a stratigraphic-sedimentologic and rock-magnetic study of the ignimbrite deposits over a $\approx 14,300$ km² extended area, in order to locate the source by combining field data and magnetic fabric flow directions. Measurement of the stratigraphic sections, performed at 76 distributed localities, led to ignimbrite correlations and production of isopach and isopleth maps. The ignimbrite succession consists of at least three distinct eruptions that originated the Incik, Sabuncu and Seydiler ignimbrites, different for age, areal distribution, structure and textural features of the deposits. Magnetic investigation consisted in magnetic mineralogy and magnetic fabric analyses (AMS and AIRM), was performed at 22 distributed localities for a total of 36 sites at different stratigraphic heights and 600 specimens. Both field data and magnetic fabric results concur for two source areas. The source area of the Incik and Sabuncu ignimbrites is identified with the Kırka caldera, a $\approx 20 \times 20$ km extended area where the presence of a resurgent dome has been detected; source area of the Seydiler ignimbrite is identified in the proximity of the village of Bayat. Volume calculations based on field data pointed out a VEI index of 7 for the Incik and Seydiler ignimbrite, 6 for Sabuncu ignimbrite, evidencing Plinian eruptions; the correspondent magnitude M (Pyle, 2000) is greater than 7 for each ignimbrite.